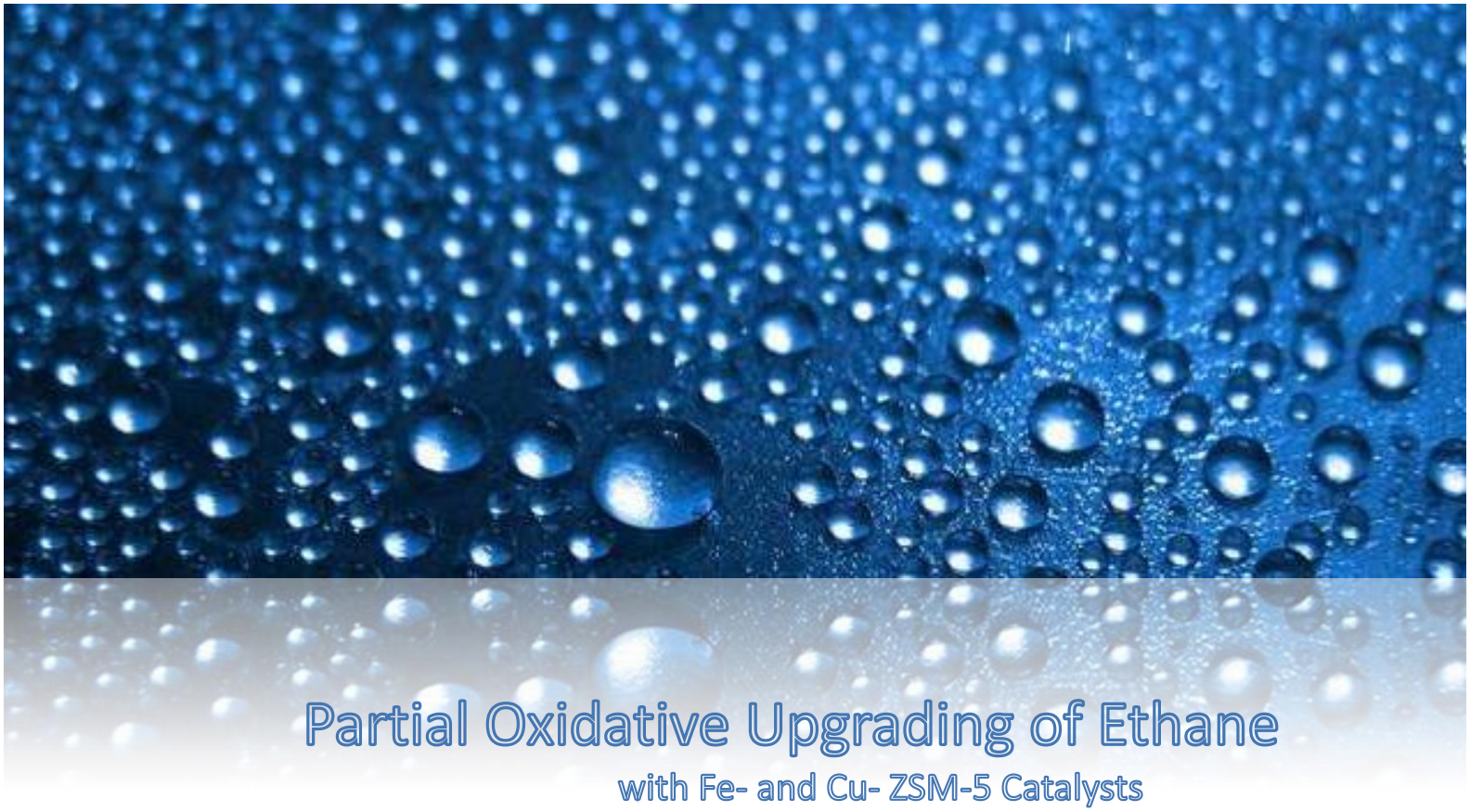

Partial Oxidative Upgrading of Ethane

with Fe- and Cu- ZSM-5 Catalysts

Robert David Armstrong, 2013

Prof. G. J. Hutchings

For Mike & Catherine

Dorothy & Frank

Madonna & Brian

& David

''Building a sustainable world- a world where today's society meets its needs while preserving the ability of future generations to meet their own- is the single most important challenge of our time.''

Paul Anastas May 2010

DECLARATION

This work has not been submitted in substance for any other degree or award at this or any other university or place of learning, nor is being submitted concurrently in candidature for any degree or other award.

Signed …… (candidate) Date ……...

STATEMENT 1
This thesis is being submitted in partial fulfillment of the requirements for the degree of ……(insert MCh, MD, MPhil, PhD etc, as appropriate)

Signed …… (candidate) Date ……...

STATEMENT 2
This thesis is the result of my own independent work/investigation, except where otherwise stated.
Other sources are acknowledged by explicit references. The views expressed are my own.

Signed …… (candidate) Date ……...

STATEMENT 3
I hereby give consent for my thesis, if accepted, to be available for photocopying and for inter-library loan, and for the title and summary to be made available to outside organisations.

Signed …… (candidate) Date ……...

STATEMENT 4: PREVIOUSLY APPROVED BAR ON ACCESS
I hereby give consent for my thesis, if accepted, to be available for photocopying and for inter-library loans **after expiry of a bar on access previously approved by the Academic Standards & Quality Committee.**

Signed …… (candidate) Date ……...

ACKNOWLEDGEMENTS

Upon completing this PhD, I would like to extent my gratitude to a number of people, through whose support this was made possible.

Firstly, I wish to thank my supervisor Prof. Graham Hutchings for giving me the opportunity to work towards this PhD, and also for his guidance and support. A most sincere thank you also goes to Prof. Stuart Taylor and Drs. Nikolaos Dimitratos, Michael Forde, Simon Freakley and Robert Jenkins for their continued encouragement, support and counsel.

A special thank you goes to Steven Morris for his continued technical assistance and advice throughout the 3 years of my PhD.

Thanks also to Drs. Thomas Davies and Simon Kondrat, whose knowledge and advice has helped me to progress my work.

For their patience and guidance, I would like to thank Drs. Nikolaos Dimitratos, Simon Freakley, Greg Shaw and Michael Forde for taking the time to read and correct this thesis.

It goes without saying that without funding this research wouldn't have been possible, and so I extend my gratitude to Cardiff University for their financial support.

Finally I would like to thank my family and loved ones for their constant support, encouragement and patience throughout the past 3 years.

ABSTRACT

The selective oxidation of lower alkane components of natural gas, such as ethane, to partial oxygenates remains a major challenge for both industry and academia. At present 60% of industry's 7.8 Mt annual acetic acid demand is met through the carbonylation of methane, the operation of which is highly energy intensive, leads to formation of corrosive iodide by-products and requires high pressures of CO. Meanwhile ethene, a feedstock of great industrial importance, is produced via steam cracking of alkanes such as ethane, a process which is typically operated at > 800 ^{o}C and accounts for *ca.* 40% of the petrochemical industry's annual energy consumption. The development of an atom efficient, low temperature, environmentally benign process for the direct conversion of ethane to either of these molecules would circumvent the need for current practices and thereby represent an important milestone in the valorisation of natural gas.

The heterogeneous catalyst system explored in this thesis is based upon zeolite (ZSM-5) catalysts, which may be modified via post synthesis deposition of either or both of iron and copper and are shown to selectively transform ethane to a variety of higher value products including but not limited to ethanol, acetaldehyde, acetic acid and ethene under mild, environmentally benign conditions (H_2O_2 as oxidant, water as solvent, temperatures of < 90^{o}C). C-C scission of C_2 products led to formation of carbon centred radicals and yielded C_1 products including methylhydroperoxide, methanol and formic acid, whilst deep oxidation yielded CO_2, typically at selectivities of < 5%. The method by which catalysts were prepared was shown to impact significantly upon catalyst performance, with chemical vapour impregnation, a novel vapour deposition technique being shown to yield highly active catalysts. Investigations of reaction conditions such as ethane pressure, ethane partial pressure, temperature, oxidant concentration and catalyst mass

were conducted in a batch reaction system. All parameters were found to impact significantly upon both catalytic activity and product distributions allowing for directed selectivity to either ethanol or acetic acid as major product. Through extensive mechanistic studies, it was shown that a complex reaction scheme operates with these catalysts, which results in the primary C_2 products ethanol, ethylhydroperoxide and ethene. Of these the former two were shown to undergo consecutive oxidation to acetaldehyde and acetic acid, whilst ethene was shown to react under test conditions to yield acetic acid. Additionally, upon deposition of Cu^{2+} onto ZSM-5 catalysts ethene was shown to become the major reaction product, with selectivities of 45.5% at 1.15% conversion.

Following development under batch reaction conditions, the ZSM-5 catalysts were then applied under a continuous flow regime through co-feeding of an aqueous hydrogen peroxide solution and mixed ethane/ argon feed through a custom built fixed bed trickle bed reactor system. Through optimisation of reaction conditions 23% ethane conversion to acetic acid (73% selectivity) was observed. Through varying the catalyst bed makeup, turnover frequencies equal to those observed at comparable conditions under batch reaction conditions were observed, thereby showing the viability for translating this catalyst system to a more industrially viable continuous flow system. High ethene and acetic acid selectivities of 37.8% and 43.0% were observed, respectively at 3.3% ethane conversion upon testing of 1.25% Fe 1.25% Cu/ZSM-5 (30) within this regime at 50 ^{o}C.

Subsequent studies focused upon elucidating the role played by aluminium sites within the zeolite framework in catalyst activity and determining product selectivities. This has led to the development of Cu/ZSM-5 and FeCu/ZSM-5 catalysts which are not only highly active for the activation of ethane, but also highly selective for the formation of ethene, with productivity to ethene alone shown to reach 25.6 mol (ethene) kg^{-1} (catalyst)

h^{-1} (at 50% ethene selectivity). Through studies of ZSM-5 catalysts of varying support composition, headway has been made in decoupling the effects which increased exchange capacity (aluminium content) has upon catalyst performance, thereby paving the way for future development of more active, selective catalysts for the transformation of ethane to higher value products, specifically ethene. An interesting aspect of this work was the discovery that copper oxide particle size and size distribution may be controlled through varying of the ZSM-5 support's SiO_2/Al_2O_3 ratio due to a metal support interaction.

GLOSSARY

Å	Angstrom (10^{-10} meters)
a.u	Arbitrary units
BET	Brauner, Emmet and Teller
cm	Centimetre
cm^{-1}	Reciprocal Centimetre
^{o}C	Degrees Celsius
CVI	Catalyst prepared by Chemical Vapour Impregnation
DRIFTS	Diffuse Reflectance Infrared Fourier Transform Spectroscopy
eV	Electron Volts
FID	Flame ionisation detector
g	Gram
GC	Gas Chromatography
h	Hours
ICP-MS	Inductively Coupled Plasma Mass Spectroscopy
IE	Catalyst prepared by Ion Exchange
IMP	Catalyst prepared by Impregnation
M	Molar
mol	Moles
min	Minutes
nm	Nanometre (10^{-9} m)
NADH	Nicotinamide adenine dinucleotide
NMR	Nuclear Magnetic Resonance
rpm	Revolutions per minute
SiO_2/Al_2O_3	Molar ratio of SiO_2 to Al_2O_3 in a zeolite
TCD	Thermal conductivity detector
TEM	Transmission electron microscopy
Temp	Temperature
TOF	Turnover frequency
NH_3-TPD	Temperature programmed ammonia desoprtion
UV-Vis	Ultraviolet- Visible spectroscopy
wt%	Weight percent
XPS	X-ray photoelectron spectroscopy
XRD	X-ray diffraction
ZSM-5	Zeolite ZSM-5
µmol	Micromoles (10^{-6} moles)

TABLE OF CONTENTS

1

Introduction

1.1 Introduction

The increasing exploitation of traditional fossil fuels, coupled with their declining reserves has led to sharp increasing in the price of crude oil within recent years. Modern society is heavily dependent upon such finite hydrocarbon reserves, not only for utilisation as an energy source, but also as a feedstock for both bulk and fine chemicals. At the same time added emphasis is being given within the developed world to environmental conscience, with legislation emerging which seeks to curtail the environmental impact associated with CO_2 and methane emissions. An example of such legislation is the UK Climate Change Act (2008) which targets an 80% reduction in carbon emissions by 2050 relative to 1990 values. Burgeoning demand, coupled with dwindling oil reserves and more effective control of emissions has incentivized research into the exploitation of alternate energy sources, with a major field of scientific research being the valorisation/ upgrading of natural gas.

With estimated global reserves of 190 trillion cubic meters, natural gas is as yet an underutilised resource.[1] Although the exact composition of natural gas varies according to its source, a representative breakdown is; methane (70- 90%), ethane (1-10%), propane/ butane (1- 10 %), CO_2 (0- 8%), nitrogen (0-5%), hydrogen sulphide (0- 5%) and oxygen (0- 0.02%).[2] Due to the high abundance of methane (70-90% composition of natural gas), and realised uses for methanol as; a fuel additive, coolant, hydrogen carrier for fuels cells and chemical feedstock for bulk chemicals such as formaldehyde and acetic acid (via the

Monsanto process)[3] the direct oxidation of methane to methanol has captivated the scientific community for over three decades.

Meanwhile, ethane (1-10% natural gas) is primarily utilised in the production of ethene (through steam cracking)[4] which can in turn be used in the production of polyethylene, acetic acid, ethylene oxide, acetaldehyde, vinyl chloride and ethanol.[5, 6]

On-site oxidation of the aliphatic hydrocarbons present within natural gas circumvents the key limitation to their global distribution and utilisation; specifically that the transportation of large volumes of said flammable, volatile gases from their sources, which are nucleated in isolated regions of the world, incurs significant financial expense. Although developments have been made in the liquefaction and transportation of natural gas (LNG), the high energy requirements, low efficiency and associated safety concerns hinder its viability for application on a global scale. Natural gas has been proposed as a transitional fuel for the 21st century, allowing for continued dependence upon fossil fuels whilst reducing green house gas emissions when compared with oil of coal.[7, 8]

Unfortunately, in spite of the significant impetus to selectively oxidise methane and ethane under mild conditions, progress has been hampered due to their chemical inertness, which results from high C-H bond strengths of 439.57 kJ mol^{-1} and 423.29 kJ mol^{-1} respectively.[9] Another crucial limitation arises due to the fact that the partial oxidation products of methane and ethane are inherently more reactive than their respective alkane, with deep oxidation to CO_x (CO and CO_2) a limiting factor in the viability of catalytic systems. As such, there are few reports of selective oxidation of ethane at low temperatures using heterogeneous catalysts.

1.2 Industrial routes for ethene, ethanol and acetic acid synthesis

An overview of the industrial processes for the upgrading of ethane which are considered in this section (Section 1.2) is shown in Scheme 1.1.

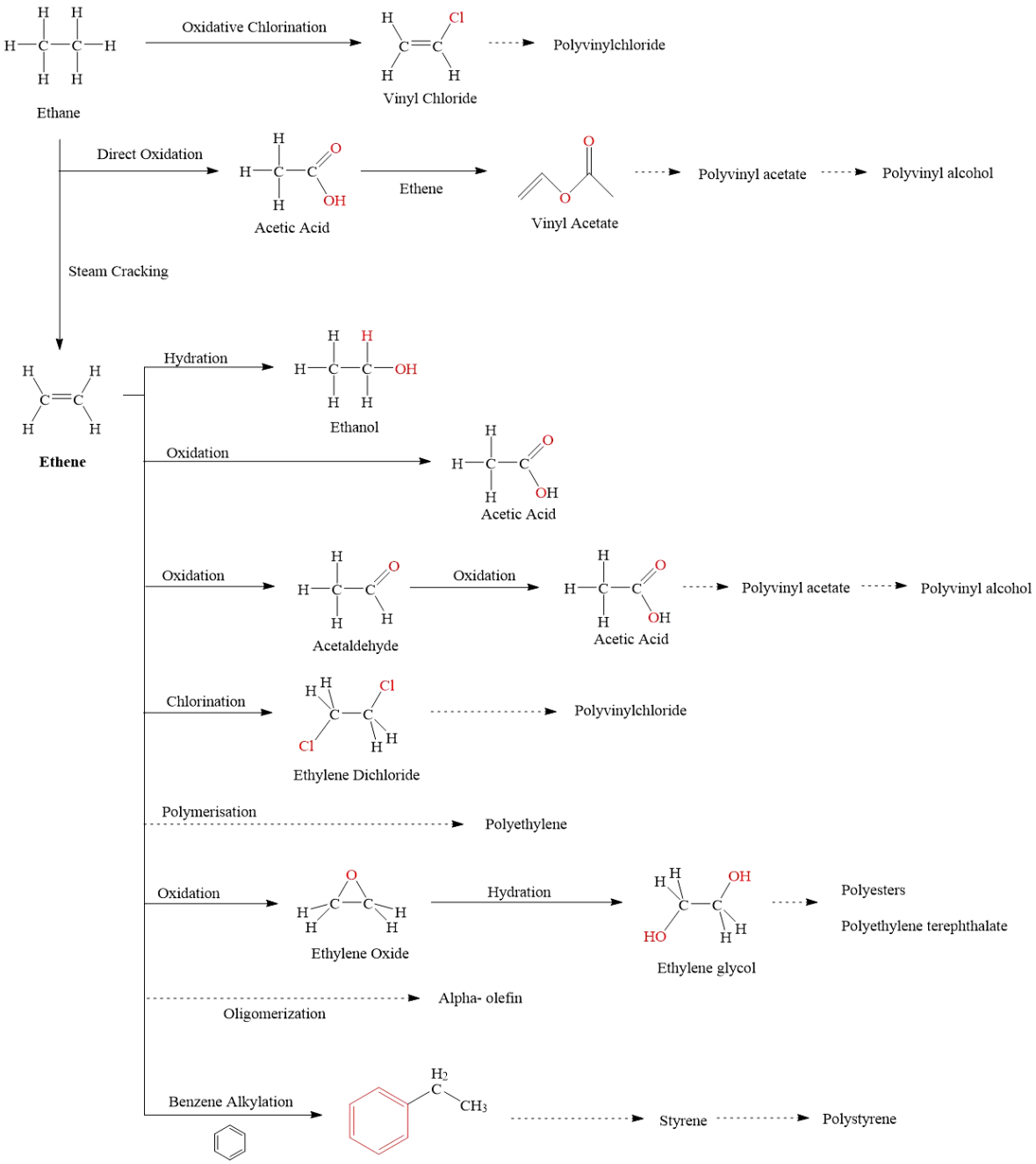

Scheme 1.1 A scheme showing key industrial ethane- derived products

1.2.1 Industrial processes for transformation of ethane to ethene

As mentioned previously, the main industrial use of ethane is in the production of ethene through steam cracking over zeolite catalysts.[4] Said process is the most energy intensive process in the petrochemical industry, requiring temperatures of between 500 and 880 ^{o}C (typically > 800 ^{o}C), and accounts for around 40% of the industry's annual energy consumption as well as a major portion of its CO_2 emissions, whilst affording yields of 24-55% depending on the gas feed. Of the commercially realised uses of ethene the most important perhaps is in production of polyethylene (*ca*. 78 Mt/annum).[10, 11] Other uses include the production of ethylene oxide (*ca*. 21 Mt/ annum)[12] and ethylene glycol (from ethylene oxide) (*ca*. 18 Mt/annum)[13], preparation of ethylene dichloride (*ca*. 43 Mt/ annum)[14] (a precursor to vinyl chloride monomer used in PVC production), and in the preparation of ethylbenzene (*ca*. 36 Mt/ annum)[15], 99% of which is used in the preparation of styrene.[16] Ethene oliomerization to α- Olefins (3.4 Mt/annum)[17].

A breakdown of global ethene production for 2013 by region is shown in Figure 1.1.[18] With global production predicted to exceed 143 million tonnes in 2013,[19] making it the most widely produced organic compound, and further growth forecasted in coming years, [16] the development of a less energy intensive route to ethene production from ethane would represent an important step in reducing the environmental impact associated with the production of ethene and its associated products.

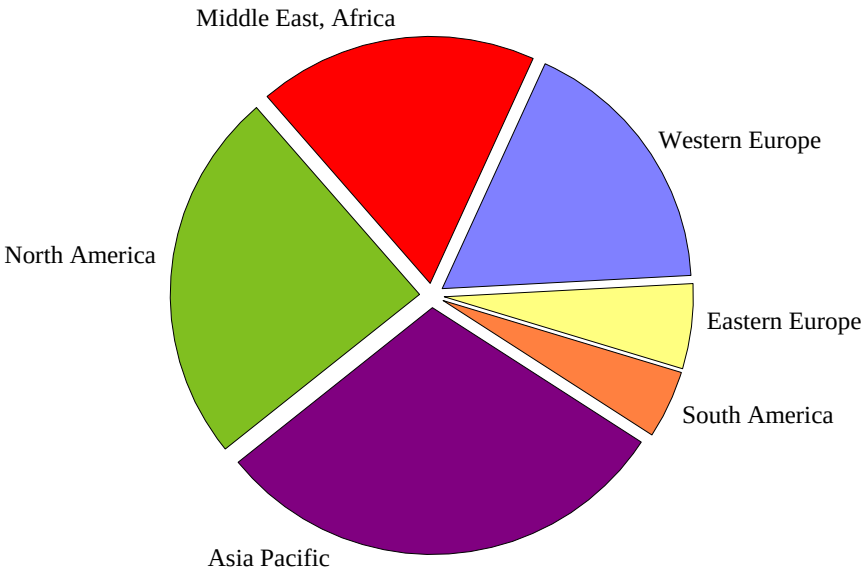

Figure 1.1 Global productivity of Ethene in 2013 according to region (adapted from reference [18])

1.2.2 Industrial routes to acetic acid synthesis

Global demand for acetic acid currently equals around 7.8 Mt/ annum, at 3.5 – 4.5% annual growth.[20, 21] Acetic acid is primarily used as a raw material in the production of vinyl acetate monomer (*ca.* 6.2 Mt / annum)[22], acetic anhydride and as a solvent for the synthesis of purified terephthalic acid (PTA).[21] Historically, acetic acid has been produced via alcohol fermentation in order to produce vinegar. Acetic acid production was first commercialised in 1916 in Germany whereby acetylene was converted to acetaldehyde and subsequently oxidised through to acetic acid.[21] A number of industrial processes are currently on line to produce acetic acid through synthetic and enzymatic routes. Principal amongst said processes are the BP Cativa Process (*ca.* 1.2 Mt/ annum) which proceeds through methanol carbonylation using a robust Iridium catalyst (Scheme 1.2) and the Rh- catalysed Monsanto- type process run by Celanese (*ca.* 2.1 Mt/annum).[3, 23]

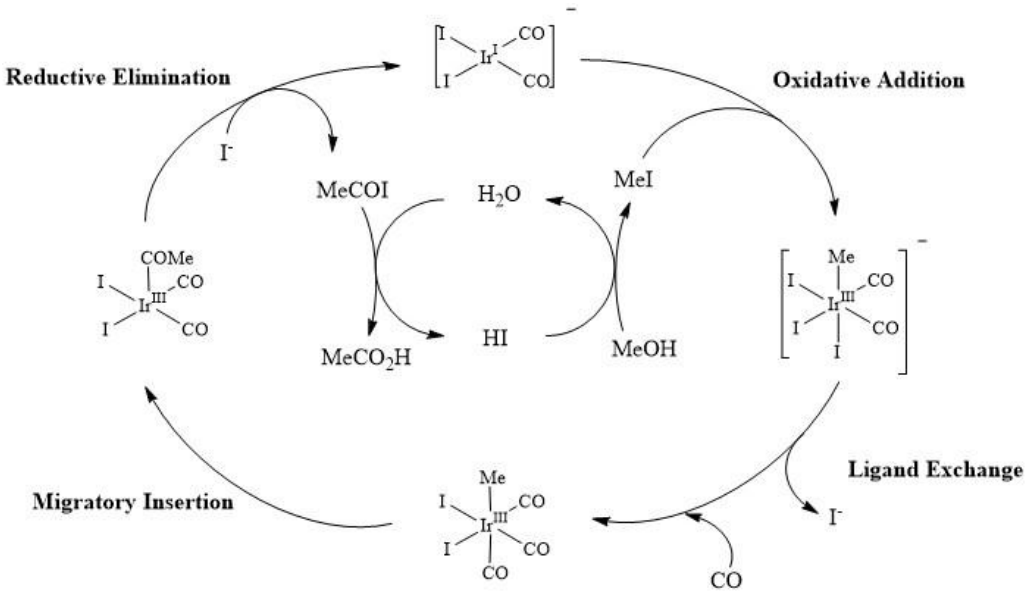

Scheme 1.2 Catalytic cycle for BP Cativa methanol carbonylation process using an Ir catalyst

To begin with, the square planar coordinate iridium (I) centre inserts into the C-I bond of methyl iodide to form an octahedral Ir (III) complex. This is followed by a ligand exchange of CO for iodide, after which the migratory insertion of CO into the Ir-C bond leads to formation of a square pyramidal Ir species with a bound acetyl ligand. Finally reductive elimination of acetyl iodide, which is hydrolysed to acetic acid, reforms the Ir (I) catalyst and allows for the generation of hydroiodic acid, which feeds back into the cycle.[3] Methanol carbonylation currently accounts for around 60% of global acetic acid production (2013).[20, 21]

Prior to the advent of the Cativa process, acetic acid was produced through the Monsanto process (Scheme 1.3), however due to the expense of the rhodium catalyst used ($5200 per ounce for Rh vs $300 for Ir), its shorter lifetime, reduced solubility and lower activity which resulted from an oxidative MeI addition which was 150 times slower than that for the Cativa process, many plants have been shifted to the latter catalytic system.[24]

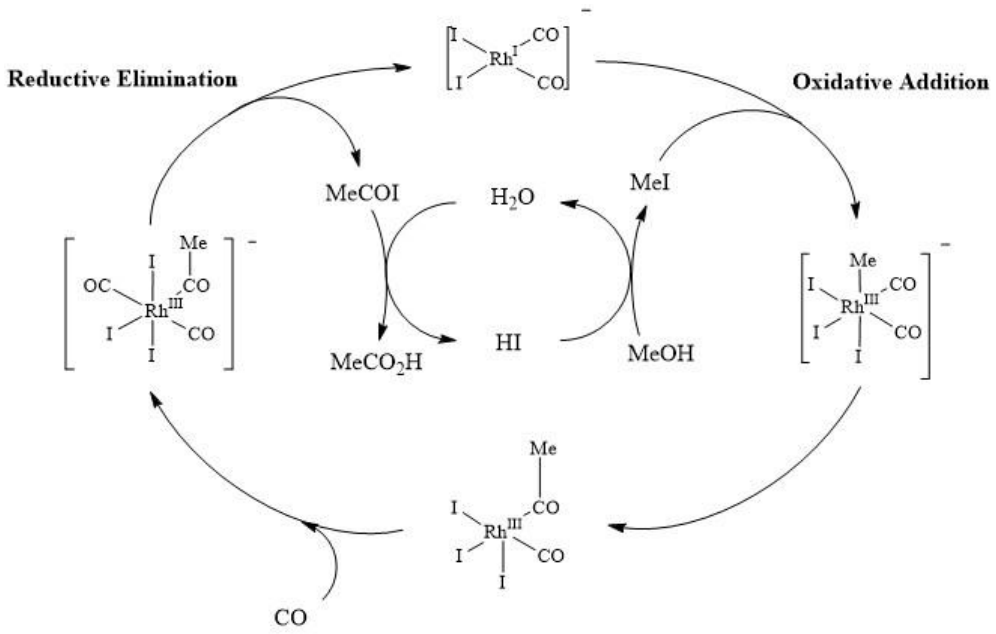

Scheme 1.3 Catalytic cycle for Monsanto methanol carbonylation process using a Rh catalyst

Use of the Cativa Ir castalyst allowed operation of the process in low water concentrations (8% versus 14-15% for the Monsanto process), thereby reducing side water gas shift reactions, and lowering downstream separation costs.[21] Owing to the presense of iodide species which are both toxic and corrosive, their dependence on expensive noble metals, for which recovery is difficult, and safety considerations regarding the high pressures of CO required, alternate routes for synthesis of acetic acid have been sought, though such a process is still used by Celanese.[23]

A number of attempts have been made to imobilise the Rh catalyst of the Monsanto process, to allow for gas phase operation, thereby negating the solubility issues associated with the Monsanto catalyst, with activated carbon,[25] inorganic oxides[26] and zeolites[27] having been studied as potential supports. However these showed rates which were lower by 1 or 3 orders of magnitude when compared with the homogeneous cycle. Some headway has been made by Chiyoda however, with the development of the Acetica process.[28-30] Through complexation of Rh with a poly-vinyl pyridine ion exchange resin, operation at 160-200 ^{o}C and 30 – 60 bar, with low water concentrations of 3-7% has been achieved. Said catalyst has been shown to be more stable than the homogeneous anologue, with steady state stability over 7000 h and negligible loss of Rh.

Aside from the homogeneous Cativa and Monsanto systems, acetic acid may also be derived from acetaldehyde at 150-160 ^{o}C, 80 bar over either cobalt or manganese acetates.[21] Recently, a process for the direct conversion of ethane to acetic acid with O_2 using molybdenum – mixed metal oxide catalysts has also been described, following Equation 1.1.[31, 32]

$$CH_3CH_3 + O_2 \xrightarrow{Cat} CH_3COOH + \text{by products} \qquad \text{(Equation 1.1)}$$

In 2001 SABIC announced their plans to build a 30,000 tonne/annum plant in Saudi Arabia, claiming to have a multicomponent oxide catalyst of formula Mo-V-Ln-Nb-Pd-X (X= Al, Ga, Ge and/or Si) catalysed system (typically $Mo_1V_{0.398}La_{7.08e-6}Pd_{0.0003}Nb_{0.125}Al_{0.226}$) which is active for the oxidation of ethane to acetic acid under continuous flow conditions in O_2 or air at operating temperatures of between 150 and 450 ^{o}C. Their patent claims the ability to oxidise ethane (C_2H_6: O_2 : N_2: H_2O (40:8:32:20) P(total) = 13.8 bar, T = 280^{o}C)[33] at 10% conversion, with 85% selectivity to acetic acid.

SABIC later patented a process for the co- production of ethene and acetic acid from ethane using a phosphorus- containing molybdenum-niobium vanadate ($Mo_{2.5}V_{1.0}Nb_{0.32}P_x$ where x = 0.01- 0.06) following Equation1.2.[34] It was claimed that at 260^{o}C, 13.8 bar ethane/air (15:85 by volume) 53.3% conversion to ethene (10.5% selectivity) and acetic acid (49.9% selectivty).

$$CH_3CH_3 + O_2 \xrightarrow{Cat} CH_2{=}\ CH_2 + CH_3COOH + H_2O \quad \text{(Equation 1.2)}$$

Acetic acid may also be produced through the one step oxidation of ethene to acetic acid, using a mixed ethene, water and O_2 feed at 140-250 ^{o}C. This process has been commercialised by *Showa Denko* in Oita, Japan with a capacity of 100,000 tonnes per annum.[35, 36] The catalyst employed comprises of three components; metallic palladium (0.1 – 2% wt), a heteropolyacid and its salt (silicotungstic acid salts of lithium, sodium and copper for example Pd-$Cu_{0.05}H_{3.9}SiW_{12}O_{40}$)[36] and one of; copper, silver, tin, lead, antimony, bismuth selenium or tellurium (typically tellurium is used) and operates at 150-160 ^{o}C, at 8 bar.[37, 38] The gas feed contains; ethene, steam, oxygen and nitrogen. Acetic acid selectivity is *ca* 86%, CO_2 5.2% with side reactions producing water and acetaldehyde according to Scheme 1.4.[21]

$$C_2H_4 + O_2 \xrightarrow{Cat} CH_3COOH \quad \text{(Main reaction)}$$
$$C_2H_4 + 3O_2 \xrightarrow{Cat} 2CO_2 + 2H_2O \quad \text{(Side reaction)}$$
$$C_2H_4 + ½\ O_2 \xrightarrow{Cat} CH_3CHO \quad \text{(Side reaction)}$$

Scheme 1.4 Main and side reactions occurring within the Showa Denko reactor system.[36]

Finally, the direct oxidation of ethane (EDO) to acetic acid has been shown to be an economically and energetically viable alternative to methanol carbonylation as an

industrial route to acetic acid production, with feasibility increasing from 50 kt to 200 kt/ annum.[39] A cost analysis based upon a model 76.1% acetic acid selectivity (C_2H_6: O_2: CO_2 of 0.73: 0.12: 0.15, 16 bar total, 242 ^oC) showed the direct oxidation process to be favourable to current industrial practices as; the feedstocks are cheaper, the product stream requires fewer separation steps and capitals costs are lower as methanol carbonylation reactors must me composed of Hastelloy to avoid corrosion, whereas EDO may be run in stainless steel systems.[39] These benefits offset the costs resulting from the need to re-cycle the ethane/CO_2 effluent from EDO back through the reactor system.

1.2.3 Industrial Routes to Ethanol Synthesis

Ethanol is a commodity chemical which is produced both synthetically, through the hydration of ethene[40] and enzymatically through the fermentation of sugars with yeast. Its investigation as a fuel additive or fuel source in its own right has been heightened in recent years due to government regulations, environmental incentives and the drive to reduce oil dependency.[41]

For the past five decades, the synthesis of ethanol on an industrial scale has proceeded through the gas phase hydration of ethene in the presence of silica-supported phosphoric acid (at 300 ^oC, 60 – 70 atm) and liquid phase synthesis using H_2SO_4 (Equation 1.3).[40]

$$C_2H_4 + H_2O \xrightarrow{Cat} CH_3CH_2OH \qquad \text{(Equation 1.3)}$$

The phosphoric acid/ silica catalysed process is favourable as it avoids the need for liquid acids, however in its current system, the commercial supported phosphoric acid does yield phosphoric acid vapours during operation. This acidic vapour leads to reduced catalytic activity and apparatus corrosion. As such, significant research has focused upon the development of alternate solid acids for the hydration of ethene to ethanol, with

systems based on; mixed zinc oxide- titanium dioxide,[42] mixed tungsten- phosphorus oxides,[43] mixed tungsten trioxide- zirconium dioxide,[40] tungstosilicic acid/ silica gel,[36, 44] zeolites,[45] niobium pentoxide,[46] and metal phosphates[47] reported.

Over the past decade, interest has grown worldwide regarding the development of viable biofuels in order to reduce our dependency of oil derived gasoline, with Brazil, the EU, USA, Canada, Japan, India, China and Europe seeking to establish biofuel markets.[41, 48] Ethanol is considered a clean, green fuel alternative to current crude oil derived fuels as its combustion releases 80% less CO_2 emissions than the latter, and avoids the release of sulphur dioxide, a major contributor to acid rain.[41, 49] Agricultural-product derived ethanol accounts for around 95% of global production, which is estimated at around 80 million tonnes per annum, through the enzymatic fermentation of sugar beets (40%) or starch crops (60%).[41] The USA and Brazil currently account for the majority of world biofuel-ethanol production (Figure 1.2).

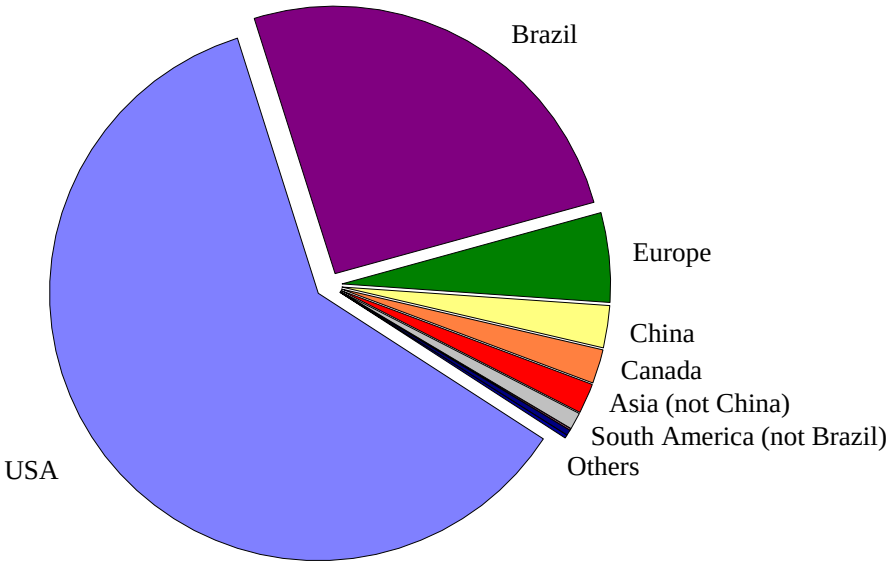

Figure 1.2 Global productivity of fuel ethanol in 2012 according to region

(data adapted from reference[50])

The key underlying controversy surrounding use of bioethanol as a fuel arises from the use of either food stuffs (such as sugarcane[51], sugar beets[52], corn, maize[53] and wheat[54]) as feed stocks for the fermentation process, or through the use of potential agricultural land to grow crops for the sole purpose of growing non-food 'energy crops.' The so- called food versus fuels debate is hotly contested, particularly in light of rising world populations. As a result, routes to the production of non- food derived bioethanol have been explored, for example the enzyme catalysed production of ethanol from syn gas using the bacterium *Clostridium Ijunjdahlii*, with algae and non-edible grasses as the feedstock.[55] This technology, which lends itself to a variety of feed stocks, has been developed on a commercialised scale by BRI Energy (USA) who have taken an integrated approach whereby municipal organic waste is utilised as a feedstock, with the heat generated by the fermentation used to drive electrical turbines.[56, 57]

1.3 Academic approaches to the selective oxidation of ethane and methane

The low reactivity and high stability of the C-H bond in ethane, second only to that of methane has hindered development of a viable process for the partial oxidation of ethane under mild conditions. This is further complicated by the fact that one must not only find a system capable of activating such inert molecules, but which also avoids further oxidation of desirable products to deep oxidation products such as formic acid and CO_2. There is great disparity within academic approaches which have been taken to ethane oxidation, however systems may be categorised as either gas phase, or liquid phase systems. The latter group may be further subdivided into; synthetic homogeneous catalyst systems, enzyme catalysed liquid phase systems, biomimetic liquid phase systems and liquid phase systems catalysed by solid heterogeneous catalysts.

1.3.1 Direct gas phase oxidation of ethane

A number of gaseous phase, solid catalyst- ethane oxidation systems have been described within the literature. Use of a mixed substrate- oxidant (typically oxygen) gas feed negates the substrate / oxygen solubility issues associated with liquid phase reactions, thereby maximising substrate-oxygen-catalyst interaction. Additionally, the lack of a solvent reduces downstream purification steps. In order to activate not only ethane, but also oxygen, high temperatures are typically employed in such systems.

Following the pioneering work of Thorsteinson *et al* the use of a Mo-V-Nb catalyst,[58] specifically $Mo_{0.61}V_{0.31}Nb_{0.08}$ and variations thereof have been reported as active for the selective oxidation of ethane to ethene and acetic acid using diatomic oxygen.[33, 59-68] This work was the basis for the SABIC process for oxidising ethane the acetic acid which was described in 1.2.2.

Through a number of studies, a system was developed whereby; $Mo_{0.61}V_{0.31}Nb_{0.08}O_x$/ TiO_2 afforded 5.4% ethane conversion to ethene (58%), acetic acid (35%) and CO_x (7%) whilst addition of 0.01wt % Pd led to slightly lower ethane conversion (5.1%) to ethene (1%), acetic acid (82%) and CO_2 (17%). In the latter system, an unprecedented acetic acid productivity of 13.8 (mol (acetic acid) kg $(cat)^{-1}h^{-1}$) was achieved.[68] Due to the array of phases present within such Mo-V-Nb oxides, the elucidation of the specific function of each component has limited the systems development.[67] Kinetic studies showed that the C-H bond activation in ethane by the oxygen-saturated surfaces present is the rate limiting step[67]. The initial step, that of ethane to ethene arises due to the interaction of ethane with lattice oxygen, which is associated with an oxidation state change in the vanadium component, which acts as a redox centre.[62] Through precipitation with TiO_2, leading to increased dispersion of the active mixed oxide component, a 10 fold increase in

reaction rate was reported. Niobium promotes the formation and stabilisation of Mo_5O_{14} and VMo_4O_{14} in preference to MoO_3, which can catalyse total oxidation to CO_2 when present.[66] It has been shown that ethene inhibits ethane oxidation through depletion of lattice oxygen (O*). The consecutive oxidation of ethene to acetic acid is itself catalysed by the palladium oxide in a heterogeneous analogue of the Wacker process.[62] The Pd(II) is purported to gain hydroxyl groups, thereby activating it for the ethene to acetic acid conversion.[62] Water is also believed to increase the acetic acid selectivity by promoting the desorption of acetate species as acetic acid.[67] To date, a number of patents have been filed for this family of catalysts, for application in direct ethane oxidation. [33, 63, 64, 69, 70] One such reported that an oxygen: ethene: ethane: nitrogen (6.5: 8: 79: 6.5) feed could be oxidised to acetic acid (63%) and ethene (14%) at 3% ethane conversion, over a vanadium, molybdenum, niobium, antimony, calcium catalyst ($Mo_{0.7}V_{0.25}Nb_{0.02}Sb_{0.01}Ca_{0.01}$) supported on an LZ-105 molecular sieve at 255 ^oC. Said system showed bifunctionality to (a) partially oxidise the methyl group and (b) hydrate the ethene to ethanol or acetaldehyde[70] as shown in Scheme 1.5.

$$CH_3CH_3 + O_2 \xrightarrow{Cat} CH_3COOH + C_2H_4 + \text{byproducts}$$

$$CH_2{=}CH_2 + \tfrac{1}{2}\, O_2 \xrightarrow{Cat} CH_3CHO$$

$$CH_3CHO + \tfrac{1}{2}\, O_2 \xrightarrow{Cat} CH_3COOH + H_2O$$

Scheme 1.5 Dual function oxidation and oxidative dehydrogenation system for converting ethane to oxygenates

Whilst the productivities shown by the Pd/Mo-V-Nb for acetic acid are impressive, the high CO_2 selectivities shown and lack of true understanding of the active sites present is a key limitation, as are the high temperatures employed (>500/k) at which primary oxidation products (ethylhydroperoxide, ethanol and acetaldehyde) observed under homogeneous conditions are rapidly oxidised to acetic acid and CO_x.

Numerous other solid catalysts have been reported as active for the direct oxidation of ethane (EDO) in gas phase. Unsupported heteropoly compounds (both free acids and caesium salts) containing molybdenum and vanadium anions have been reported for oxydehydrogenation of ethane to ethene (60%) and CO_x.[71] Oxidation of ethane to acetaldehyde (*ca* 25%), in addition to ethene (47%) and CO_x (18%) was reported by Moffat *et al* using silica- supported HPMo at 540 ^oC, however conversion was limited to 3% and no acetic acid was observed.[72] Sopa *et al* furthered this work by supporting Keggin molybdo (vanado) phosphoric heteropolyacid ($HPMoV_x$) on oxide supports (SiO_2, TiO_2 and Al_2O_3).[73] Activity was shown at 250-400 ^oC under atmospheric pressure (C_2H_6: O_2: H_2O: N_2 of 2: 1: 8: 4). Alumina, silica and titania supported HPAs showed acetic acid selectivities of 28%, 22% and 25% respectively at 250 ^oC. However the alumina and silica supported catalysts gave low conversions (0.4%) with titania-supported HPA showing 3% ethane conversion. HPA/SiO_2 showed high selectivity to ethene (67%) leaving acetic acid (22%) and CO_2 (11%) as minor products.[73] Higher conversions (22%) were attainable at higher temperatures (400 ^oC) however this was associated with reduced acetic acid selectivity (5%) compared with ethene (50%) and CO_2 (45%). Vanadium ions were shown to be integral for ethane conversion, with acetic acid selectivity limited to < 5 % in their absence. Silica and titania were shown to preserve the Keggin structure *in situ*, due to their acidic OH surface functionality, whilst the basic centres present in alumina led to the decay of the Keggin structure thereby reducing activity.[73]

Partial oxidation systems based upon silica-supported vanadium oxide catalysts were reported by Erdöhelyi *et al* who reported low ethane conversion (3%) but high selectivity towards acetaldehyde (45%) at 550 ^oC using $RbVO_3/SiO_2$ with N_2O as oxidant.[74] The same group later showed Rb_2MoO_4/SiO_2 to give higher conversion (8.9%) under the same

conditions, this time affording high ethene selectivity (45.7%) and lower acetaldehyde selectivity (7.3%).[75]

Bodke *et al* reported impressive ethane conversion (73%) to ethene (83%) using a Pt-Sn/ alumina catalyst at 900 – 950 ^{o}C.[76] By introducing H_2 into the gas feed to give 2: 1: 2 ratio for C_2H_6: O_2: H_2, deep oxidation to CO_x was reduced dramatically (20% to 5% seletivity) as H_2 is preferentially oxidised, to H_2O. Unfortunately, safety considerations limited said system's viability upon scale up.

1.3.2 Homogeneous liquid phase systems for ethane oxidation

Whilst a number of systems have been reported for the activation of methane, the transformation of ethane under homogeneous conditions has rarely been studied.[77-92]

Fujiwara *et al* showed the conversion of ethane to *N,N*- dimethylpropylamine through reaction with *N,N* – trimethylamine and N-oxide, catalysed by $Cu(OAc)_2$. Though not the desirable ethane to ethanol transformation, this system was seen as a major development in the C-H activation of ethane as it avoided the use of highly acidic, environmentally non-benign media often associated with electrophilic methane activation. Shortly thereafter Süss-Fink *et al* reported the selective oxidation of ethane in acetonitrile using $[PMo_{11}VO_{40}]^{4-}$ and $[PMo_6V_5O_{39}]^{4-}$ in their tetra-*n*-butylammonium salts using H_2O_2. They reported TOFs of 1.4 h^{-1} for the former at 60 ^{o}C, with selectivity favouring ethylhydroperoxide (CH_3CH_2OOH) as major product and ethanol and acetaldehyde as minor products.[93] Analogous tests under aqueous conditions afforded productivities towards ethanol, acetaldehyde and acetic acid which failed to exceed those of blank reactions. It was concluded that this process proceeds through formation of hydroxyl radicals upon interaction with a V (V) species as shown in Scheme 1.6.

$$V(V) + H_2O_2 \longrightarrow V(V) \cdots\cdots H_2O_2$$
$$V(V) \cdots\cdots H_2O_2 \longrightarrow V(IV) + HOO\cdot + H^+$$
$$V(IV) + H_2O_2 \longrightarrow V(V) + HO\cdot + HO^-$$

Scheme 1.6 Activation of H_2O_2 by the V(V) species[93]

It was then postulated that the radical species then went on to activate ethane, and a range of substrates, to form their alkylperoxide product as shown in Scheme 1.7.

$$HO\cdot + RH \longrightarrow H_2O + R\cdot$$
$$R\cdot + O_2 \longrightarrow ROO\cdot$$
$$ROO\cdot + e^- + H^+ \longrightarrow ROOH$$
$$2HOO\cdot \longrightarrow H_2O_2 + O_2$$
$$ROO\cdot + HOO\cdot \longrightarrow ROOH + O_2$$

Scheme 1.7 ROOH formation through free radical processes[93]

In spite of the selectivity shown, this system was limited by its low activity and its dependency on complex organic salts. That said, it was an important development in low temperature activation of ethane, given its 60 ^oC operating temperature, though the lack of analysis of the gas phase products for CO_x raises questions as to the true selectivity of the reaction.

Shul'pin *et al* later reported the efficient low temperature hydroperoxidation of ethane using H_2O_2 or ^{t}BuOOH in acetonitrile, catalysed by the complex manganese (IV) salt $[L_2Mn_2O_3](PF_6)_2$ where (L= 1,4,7-trimethyl-1,4,7-triazacyclononane).[94] The activity of the system was dependent upon addition of a carboxylic acid (typically acetic acid) to the

reaction solution, with only non-productive H_2O_2 decomposition to O_2 observed in the absence of homogeneous acid. As with the vanadium salt catalysed system described by Süss-Fink, the primary product was believed to be ethylhydroperoxide with acetaldehyde and ethanol shown to be secondary oxidation products. For 2 h tests a TOF of 180 h^{-1} was observed at 20 bar ethane, 25 ^oC, 1 M H_2O_2 with propionic acid additive (0.25 M). Under these conditions, selectivities to ethylhydroperoxide (39%), acetaldehyde (33%) and ethanol (28%) were claimed. At reduced temperatures (5^oC) and longer reaction times (75 h) the ethylhydroperoxide selectivity reached 65% with TOFs of 5.3 h^{-1}.[94] As with previous studies, selectivity towards CO_2 was not reported. Whether this is the due to the lack of deep oxidation, or of gas analysis is not stated, however the latter is most likely given the precedent for CO_2 formation in systems containing H_2O_2.[6, 95]

Shu'pin *et al* later reported that a range of iron (III) species are active for the activation of ethane with H_2O_2 using acetonitrile as solvent. These include iron (III) chloride, iron (III) perchlorate and iron (III) acetate,[96] with the latter two showing TOFs of 23 h^{-1} and 6 h^{-1} respectively, at 27 bar ethane and 25 ^oC with H_2O_2 (0.6 M). The most active catalyst Iron (III) perchlorate afforded high selectivitiy towards ethylhydroperoxide (88%) with minor products ethanol (3%) and acetaldehyde (9%). The reactions for iron perchlorate and iron acetate were shown to proceed through a hydroxyl radical oxidant, whereas the iron (III) chloride catalysed process's activity was attributed at least partially to the formation of a ferryl ion $(Fe^{IV}=O)^{2+}$.[96] Such ferryl species may arise as a result of interactions between H_2O_2, hydroperoxy radicals (·OOH) which are formed according to equations 1.4 and 1.5[97]

$$Fe^{2+} + H_2O_2 \longrightarrow \cdot OH + OH^- + Fe^{3+} \quad \text{(Equation 1.4)}$$

$$Fe^{3+} + H_2O_2 \longrightarrow \cdot OOH + H^+ + Fe^{2+} \quad \text{(Equation 1.5)}$$

More recently Yuan *et al* have shown a variety of transition metal chlorides to be active for the selective oxidation of ethane to oxygenates with H_2O_2 in aqueous conditions.[98] A broad range of metal chlorides were evaluated with activity for ethane oxidation following the order; H_2PtCl_6 < $PdCl_2$ < $FeCl_3$ <$HAuCl_4$ <$OsCl_3$. Of these, the most active ($OsCl_3$) showed a TOF of 40.8 h^{-1} for ethane oxidation at 30 bar ethane, 0.5 M H_2O_2, 90 ^oC. Of the homogeneous systems referenced thusfar, this was the first to quantify CO_2, with selectivities to ethanol, acetaldehyde and CO_2 of 21%, 64% and 15% respectively, at 0.56% conversion.[98] Through mechanistic studies with radical scavengers the mechanism for ethane oxidation was shown to proceed via the formation of hydroxyl and hydperoxy radical species through contact between the H_2O_2 and catalyst as opposed to electrophilic activation of ethane. An interesting observation which was made in said study was that despite increased system productivity at higher pressures of ethane, a proportional increase in H_2O_2 decomposition was not observed. Such a phenomenon is also discussed in Chapter 3 of this thesis.

Whilst homogeneous catalysts have been shown to be active for the selective oxidation of ethane to oxygenated products under mild, aqueous conditions, a general dependence upon additives coupled with low turnover frequencies and the inherent disadvantages of homogeneous catalysts render heterogeneous catalysts more favourable for downstream industrial applications.

1.3.3 Enzymatic activation of ethane in liquid phase systems

Methane mono-oxygenase of *Methylococcus capsulatus* (MMO) is a nonspecific oxygenase found in the Roman Baths, Bath, UK which is capable of catalysing the oxidation of a range of C_1-C_8 *n*- alkanes to corresponding primary and secondary alcohols in air at ambient conditions.[99] Colby *et al* showed that the soluble form (sMMO) (2 mg)

in a solution of KCN (0.5 nM) was active for the selective oxidation of ethane to ethanol yielding ethanol (1.64 μmol) in the presence of NADH cofactor over 12 min.[99] Tonge *et al* later showed that purified *Methylosinus trichosporium* could catalyse the stoichiometric oxidation of ethane to ethanol at productivities of 50 μmol (ethanol) min^{-1} mg (protein)$^{-1}$ lending it the descriptor '*monooxygenase*.'[100] Crucially, sMMO was able to avoid production of deeper oxidation products acetic acid and CO_2. Key to the activity of sMMO is the proposed diiron μ-oxo active site (Figure 1.3) of MMO.[101]

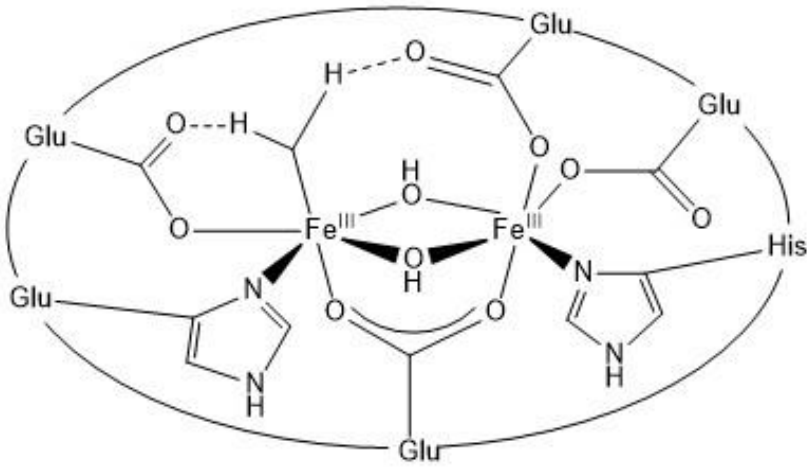

Figure 1.3 The active site for methane monoooxygenase[101]

More recently Meinhold *et al* have shown engineered variants of P450 BM3 to be active for the fast oxidation of ethane to ethanol, with turnover frequencies mol (ethanol) mol (protein)$^{-1}$ h^{-1} of 500 reported, at an NADPH oxidation rate of 31,200 h^{-1}.[102] The active site for P450 is shown in Figure 1.4.

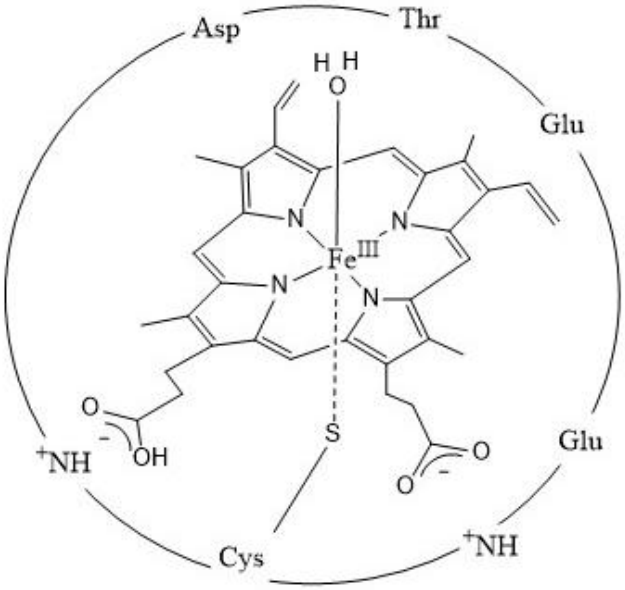

Figure 1.4 The active site of P450[101]

In such systems, catalysed by heme- dependent monooxygenase P450 enzymes, the cofactor (NADPH) is required to donate two electrons to activate oxygen in order to generate a [(Porphyrin)$^{+}$ Fe^{IV}=O] intermediate which attacks the C-H bonds (Scheme 1.3).[103] Feng *et al* also showed selective oxidation of ethane to ethanol exclusively, with H_2O_2 and NADH at higher turnover frequencies of up to 4962 h^{-1} at an NADH oxidation rate of 44,460 h^{-1} reported.[92, 103] The catalytic cycle proposed for P450 catalysed alkane oxidation, with O_2 is shown in Scheme 1.8.

Firstly the substrate (RH) coordinates to iron (III) centre. The iron (III) is then reduced and subsequently an O_2 molecule is coordinated, to form an iron (II) peroxo species. This species is then oxidised by the enzyme system to form an oxoiron (IV) radical cation [(Porphyrin)(RH) Fe^{IV}=O]$^{+\cdot}$ The C-H bond in RH is then cleaved, and oxygen extracted out of the iron oxo species, thereby reforming P450 and generating ROH.[92]

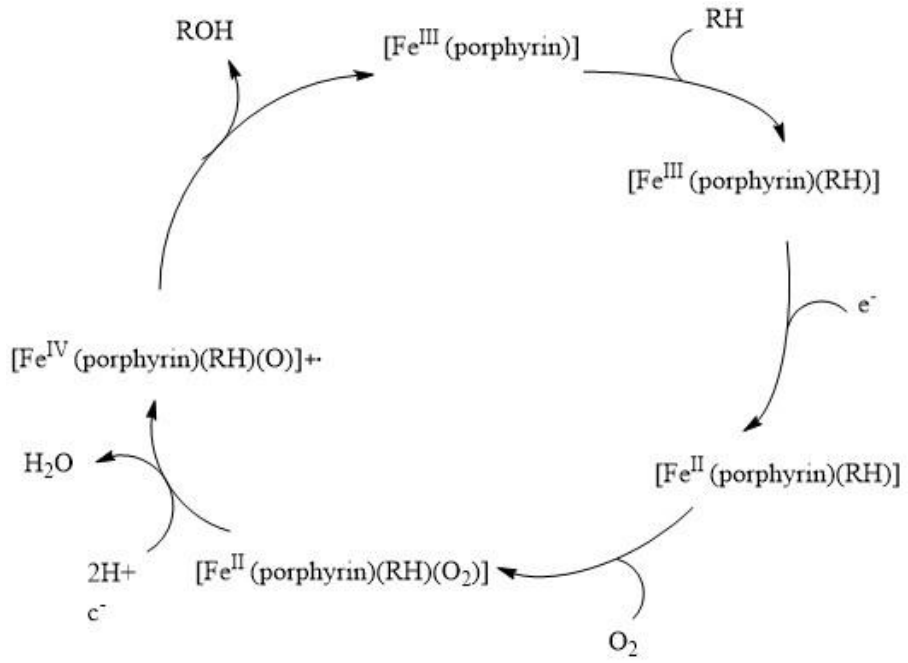

Scheme 1.8 The proposed catalytic cycle for alkane oxidation by O_2 catalysed by P450

Whilst the selective oxidation of ethane to ethanol under ambient conditions with air is an attractive prospect, the dependency on highly dilute aqueous environments, need for expensive cofactors and sensitivity to higher temperatures limits enzyme catalysed ethane oxidation's feasibility as an industrial process. Unfortunately, synthetic homologues of these structurally complex active enzymes and their active sites have not yet been realised, and a suitable organism for an optimised commercially applicable biocatalytic process has not yet been found.

1.3.4 Biomimetic approaches to the liquid phase oxidation of ethane

Due to the expense of NADH cofactors and difficulties associated with its isolation, MMO is not considered to be a viable commercial catalytic process. Therefore, in light of the high selectivity towards primary oxidation products for ethane oxidation, afforded by such enzyme catalysts as described previously, a number of approaches have been taken

in order to synthesise biomimetic catalysts often seeking to mimic the binuclear Fe^{III} active site ($Fe_2(\mu\text{-}O)_2$) found within methane monoxygenase (Figure 1.3).

Otsuka *et al* reported that $FePO_4$ catalysed the oxidation of ethane in a C_2H_6: H_2: O_2 feed to yield ethanol (22.5%) at a productivity of 0.059 mol (ethanol) kg $(cat)^{-1}$ h^{-1} at 350 ^oC via a redox mechanism involving a diferric active site (Scheme 1.9).[104] Whilst higher productivity (9.8 h^{-1}) was attainable upon increasing temperature to 422 ^oC, this led to a decrease in ethanol selectivity to 8.7%, suggesting that lower temperature systems may further favour ethanol selectivity.[104]

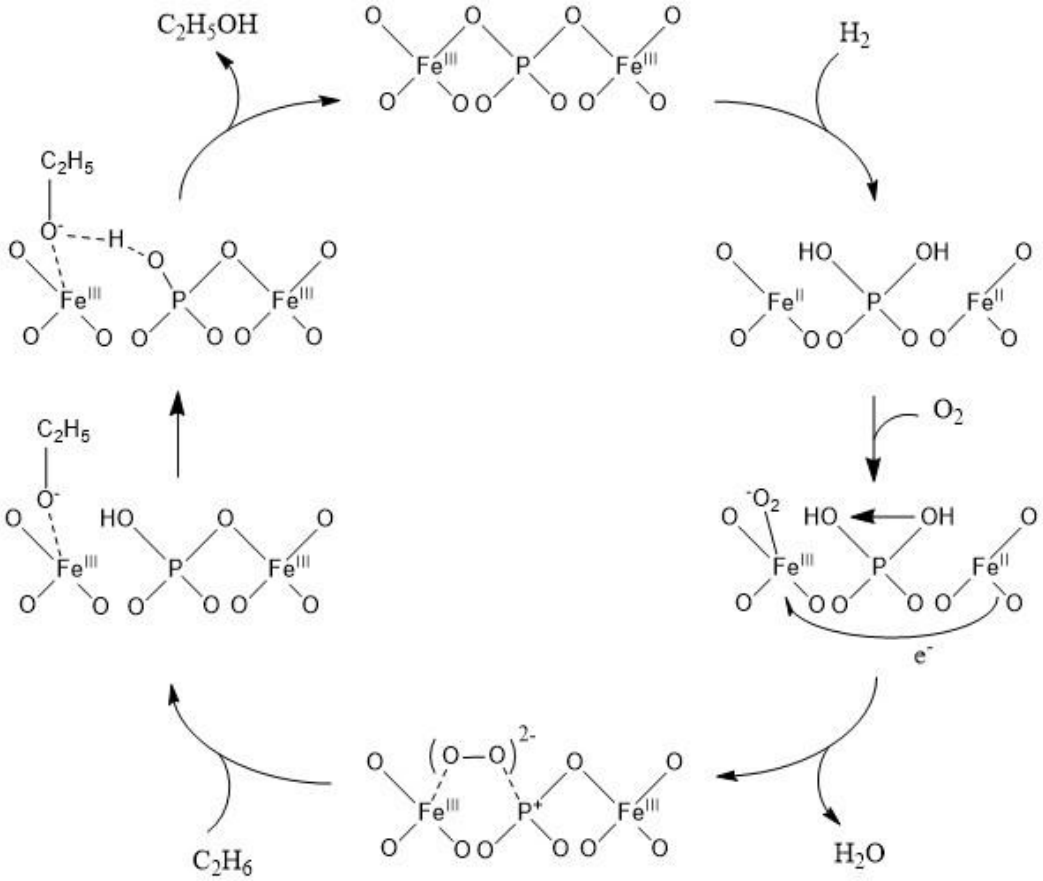

Scheme 1.9 Mechanism for the ethane oxidation proposed by Otsuka *et al*

Hydrogen was shown to reduce the catalyst surface to generate Fe (II) and H^+ which is absorbed by a neighbouring phosphate group. Oxygen is activated by accepting electrons from Fe (III) to form a peroxide species. This adsorbed peroxide may be formed using a gas feed comprising of either H_2-O_2 or N_2O. Formation of ethanol from the ethoxide intermediate occurs due to the proximity of the iron sites to acidic phosphate groups which allows rapid protonation of the ethoxide, thereby preventing decomposition to CO_x.[104] When compared with earlier studies whereby the same conditions and catalyst were used in methane oxidation, rates were determined to be 7-8 times higher.[104, 105]

Structural models of the binuclear iron active site present within MMO have also been tested for activity in ethane (and generic hydrocarbon oxidation reactions). For example Shul'pin *et al* showed iron (III) complexed with 1,4,7-triazacyclononane (shown in Figure 1.5) to be active for the oxidation of cyclohexane to cyclohexanone and cyclohexanol via a cyclohexyl hydroperoxide with H_2O_2 in acetonitrile under ambient conditions (TOF 10 h^{-1}) via formation of hydroxyl radicals.[96]

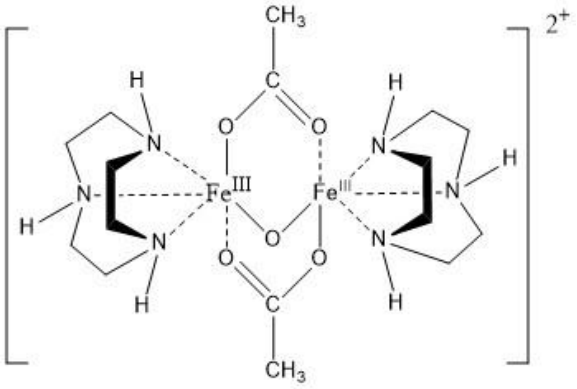

Figure 1.5 Shul'pin binuclear iron (III) complex with 1,4,7-triazacyclononane

Another biomimetic system for alkane oxidation was reported by Panov *et al* [106] who found that Fe- containing zeolites of MFI structure (ZSM-5) heat treated in N_2O at 250 ^oC

lead to the formation of an α-oxygen species upon interaction of N_2O with binuclear irom α-sites following Equation 1.6. Said α-oxygen was shown to be similar to the active oxygen of methane monooxygenase.

$$N_2O + (\ )_\alpha \longrightarrow N_2 + (O)_\alpha \qquad \text{(Equation 1.6)}$$

Following activation, the catalyst was shown to be able to form a chemisorbed methoxy species upon interaction with methane under ambient conditions.[106] Unfortunately the reaction is not catalytic, as the bound methoxy must be removed through extraction with acetonitrile, thereby causing the destruction of the active species.

1.3.5 Heterogeneous approaches to the liquid phase oxidation of ethane

Despite the significant interest shown within the scientific community towards the oxidation of lower alkanes, there are few reports regarding the low temperature, heterogeneously catalysed selective oxidation of ethane. That I am aware of, the earliest such report came in 1992 when Lin reported to have successfully oxidised ethane over 5% Pd/Carbon and 5% Pt/Carbon catalysts.[107] They reported that yields of 0.54 M acetic acid with 0.05M mmol acetaldehyde (1.81 % ethane conversion) were achievable in 20-24 h at 100 ^oC with 40 mg catalyst in 5 ml 0.1 M DCl under an ethane (35 bar), oxygen (7 bar) and oxygen (7 bar) feed. The proposed reaction scheme is shown in Scheme 1.10.

As shown in Scheme 1.10 the reaction proceeds through three catalytic steps and requires an acidic medium (DCl) and water due to the initial water gas shift. It was also shown that through charging the system with H_2 (7 bar) and O_2 (7 bar) and ethane (34 bar), a 0.002 M concentration of H_2O_2 could be prepared *in situ,* in a non-aqueous environment comprising of methylnitrate and trifluoroacetic acid, with acetic acid (0.1 M) and acetaldehyde (0.05 M) formed after 12 h at 85^oC. During the course of said work, the

oxidation of ethane to ethanol and subsequent oxidation to acetic acid, formic acid and CO_2 (deep oxidation) in the presence of H_2O_2 was reported.[107]

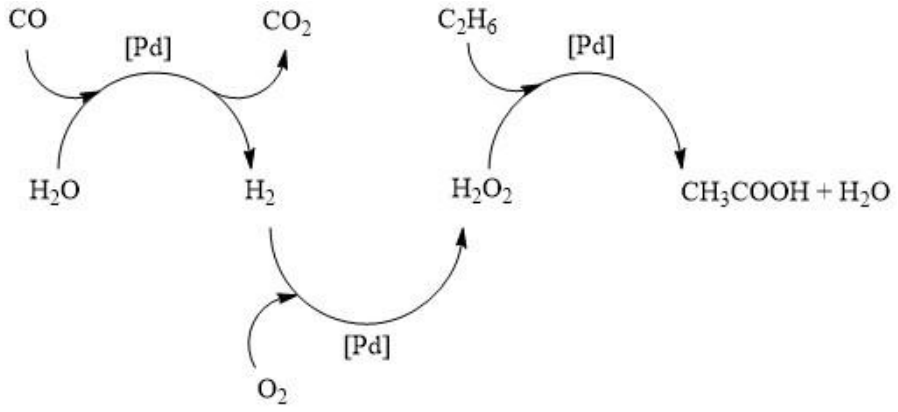

Scheme 1.10 Partial oxidation over Pd/C[107]

Shul'pin *et al* later reported the partial oxidation of ethane with H_2O_2, this time catalysed by titanosilicalite – 1 (TS-1) which formed a Ti-OOH reactive species.[108] They reported partial oxidation to a 0.028 M acetaldehyde, 0.017 M ethanol solution (0.025 % ethane conversion) using a 1 ml aqueous H_2O_2 solution, at 30 bar ethane, 12 h, 60 ^oC.[108]

Aside from the two systems described, above the only other heterogeneous low temperature systems for the partial oxidation of ethane which have been reported use ZSM-5[95] and Fe- and Cu- containing ZSM-5[6] catalysts and H_2O_2 as oxidant. This author's contribution to the latter report (Forde, M.; Armstrong, R *et al*. *JACS*. **2013**) forms a portion of Chapter 3 of this thesis.

Rahman *et al* reported the direct oxidation of ethane to acetic acid and formic acid using ZSM-5 (1.5 g), aqueous H_2O_2 (4 M), 30 bar ethane, 120 ^oC, 2 h with 0.3 g of PPh_3 as an additive. Under said conditions they showed 35.1% ethane conversion with major product selectivities of acetic acid (48.5%) formic acid (36.3%) and CO_2 (11.9%).[95] A positive

effect upon ethane conversion and acetic acid selectivity was reported at increasing SiO_2/ Al_2O_3 ratios, with a ratio of 23.8 shown to be the most active catalyst. This relationship is further explored in Chapter 5.

A summary of product selectivities (major) and catalyst productivities for the heterogeneous liquid phase oxidation systems described is shown in Table 1.1

Table 1.1 Product selectivities and productivities for reported heterogeneous liquid phase ethane oxidation systems

Catalyst	% Product Selectivities							Productivity[d]	ref
	CH_3COOH	CH_3CHO	CH_3CH_2OH	CH_3OH	HCOOH	C_2H_4	CO_2		
TS-1[a]	-	**94.27**	5.72	-	-	-	-	0.248	108
5% Pd/C[b]	**78.10**	21.90	-	-	-	-	-	3.40	107
H-ZSM-5 (23.7)[c]	**48.51**	2.07	1.12	0.26	36.31	-	11.93	6.81	95

[a] 10 mg TS-1, 1 ml H_2O_2 (35 wt%, 11,000 µmol), 60 ^oC, 12 h, P (C_2H_6) = 30 bar (0.120 mol)
[b] 40 mg 5% Pd/Carbon, 85 ^oC, 24 h, P (C_2H_6) = 34.47 bar (0.180 mol), P (CO) = 6.89 bar P (O_1) = 6.89 bar.
[c] 1500 mg H-ZSM-5 (23.7), 120 ^oC, [H_2O_2] = 4 M (279 mmol), 5 h, P (C_2H_6) = 30 bar (0.145 mol)
[d] Productivity measured as mol (2C in products) kg^{-1} (catalyst) h^{-1}

1.3.6 Summary of ethane oxidation

Though significant advances have been made in the fields of direct oxidation of ethane to oxygenates and oxidative dehydrogenation to ethene, with further hydration to oxygenated products, overoxidation to CO_x results due to the high temperatures required (> 150 ^oC). Thus far a highly productive low temperature heterogeneous approach to ethane oxidation has not been found; in fact few such systems have been reported. It is clear that ZSM-5, and Fe/Cu modified variants are highly active for the selective oxidation of methane, a more inert aliphatic hydrocarbon, to its corresponding alcohol. Avoidance of highly acidic media and additives used in homogeneous systems, and use of water and hydrogen peroxide as green solvent and oxidant would lead to the development of a more environmentally friendly, sustainable process for the oxidative upgrading of ethane to higher value, more energy dense products.

1.4 The Dow Methane Challenge

The work which is described in the following results chapters was completed as a follow up to the DOW methane challenge.

It has recently been reported that Fe – and Cu- containing ZSM-5 (30) are active for the selective oxidation of methane to methanol with H_2O_2 at temperatures as low as 30 ^oC.[109, 110, 111] Following high temperature calcination, ZSM-5 was shown to be active for the selective partial oxidation of methane with high selectivity to oxygenated products (95%) and limited selectivity to deep oxidation products (selectivity to CO_2 of 5.4%) following the oxidative pathway shown in Scheme 1.11.

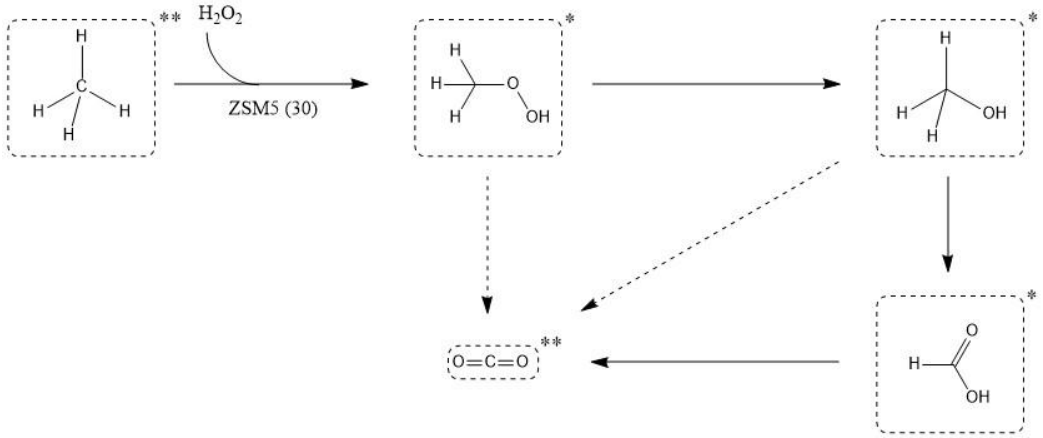

*** Quantified by ^{1}H-NMR, ** Quantified by GC-FID**

Scheme 1.11 Proposed pathway for ZSM-5 catalysed oxidation of methane with H_2O_2

Addition of extra framework iron post synthesis (2.5 wt %), through ion exchange techniques, was reported to lead to an increase in conversion (0.7% compared with 0.3% for ZSM-5). 2.5% Fe/ZSM-5 (30) yielded formic acid as major product (72%) with methanol (10%), methylhydroperoxide (1%) and CO_2 (17%) also formed. Addition of extra framework or homogeneous Cu^{2+} (2.5 wt%), in addition to iron (2.5 wt %) enabled the ‘’shutting off’’ of the methanol – formic acid transformation without affecting conversion, such that methanol became the major product (85%), with methylhydroperoxide (0.2%) and CO_2 (15%) also observed. Through EPR studies Cu^{2+} was shown to be scavenging ·OH radicals which were otherwise shown to play a role in the overoxidation of methanol to formic acid and CO_2. Through EXAFS investigations of the extra framework species present in Fe/ZSM-5 catalysts, and comparison of Fe-Fe (2.97 ± 0.04 Å) and Fe-O (2.04 ± 0.02 Å) separations, coupled with a low Fe-Fe coordination number of 1.6,[109] a DFT model allowed simulation of a likely active site **(1)**(Scheme 1.12) and closed catalytic cycle (Scheme 1.12).

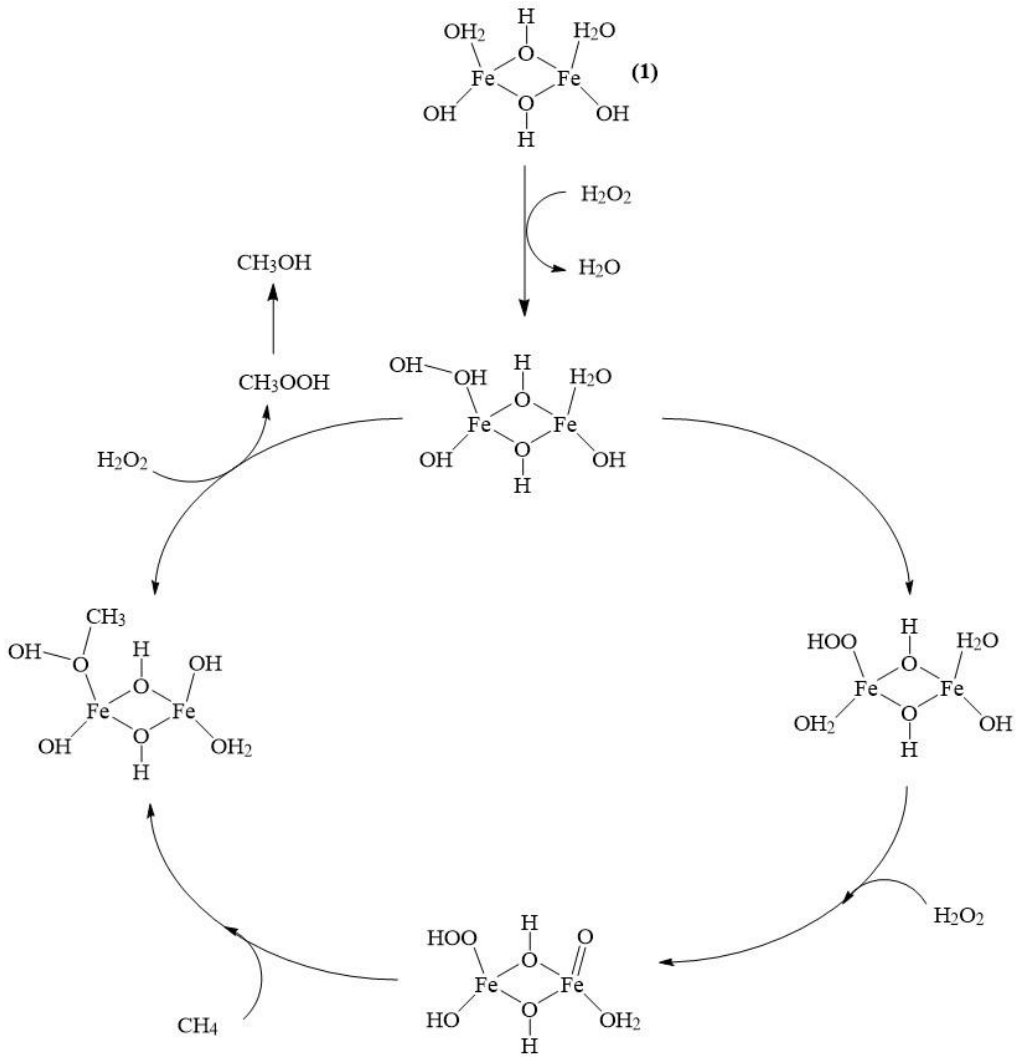

Scheme 1.12 Proposed catalytic cycle for methane oxidation on iron sites in ZSM-5

Given the similarity of the proposed diiron complex $[Fe_2(\mu_2\text{-}OH)_2(OH)_2(H_2O)_2]^{2+}$ with its coupled high spin octahedral Fe^{3+} pair and the active site of sMMO (Figure 1.3) it was perhaps surprising to note that catalysts were found to be inactive for the oxidation of methane with diatomic oxygen.[109] Given that Fe was shown to be the catalytically active component for C-H activation, comparison of TOFs for ZSM-5 (30) (2278 h^{-1}), 2.5% Cu/ZSM-5 (30) (2113 h^{-1}) and sMMO (95 h^{-1}) was enabled. Whilst sMMO shows 100% selectivity towards methanol using O_2, with no deep oxidation to CO_2, the 83% methanol

selectivity and activity expressed by 2.5% Cu/ZSM-5 (SiO_2/Al_2O_3 = 30) was deemed to be a significant result.[109]

Whilst an important academic study and major development in the field of low temperature heterogeneous methane activation, and C-H activation on the whole, the work of Hammond *et al* had limited commercial significance due to its use of hydrogen peroxide as terminal oxidant.

1.5 Zeolites

1.5.1 Structure

Zeolites are microporous crystalline aluminosilicalites composed of TO_4 tetrahedra (where T = Si, Al) which are connected via corner sharing of oxygen atoms. Uncharged, purely siliceous structures composed of SiO_4 units are highly crystalline, three dimensional analogues of silica.[112, 113] Upon isomorphous substitution of Al^{3+} (as AlO_4^- tetrahedra) for framework Si^{4+} sites, the framework acquires a negative charge, which requires the presence of extraframework exchanged cations within the channels or cages of the structure in order to render the structure charge neutral.[112] When the charge compensating cation is a proton (H^+), Brønsted acidity is induced, with acidity comparable to that of H_2SO_4,[114] whilst high temperature heat treatment of zeolites leads to migration of Al from the framework to extra framework sites, thereby affording zeolites a degree of Lewis acidity and reducing the Brønsted acidity due to loss of structural charge (AlO_4^-).

A wide range of Al contents are possible, with Si/Al = 1 - ∞, the purely siliceous polymorph of silica (silicalite). Thermal stability is dependent upon this ratio, with low Si/Al materials stable to *ca* 700 ^oC and silicalite stable to 1300 ^oC. At present 200

different zeolite structures have been reported, differing in shape, size and connectivity of their channels.[115] A lower limit of Si/Al = 1 was determined by Lowenstein, who proposed that, due to electrostatic repulsions between negative charges, adjacent AlO_4^- are disfavoured.[112, 116] The crystalline nature of the zeolite framework ensures that pore openings are uniform in size, enabling discrimination of molecules on the basis of their sizes (molecular sieving). Within catalysis this is often known as shape selectivity,[117] one industrial application of which is in catalytic hydrocarbon cracking over MFI- type catalysts, whereby the zeolite pores discriminate against branched molecules, thereby permitting access to the acid sites only by linear molecules.[118]

Zeolite synthesis occurs through a hydrothermal process with a silica source, an alumina source, a mineralising agent (OH^- or F^-) and an organic structure- directing agent. Tetravalent transition metal ions may also be substituted for Si^{4+} or Al^{3+} during zeolite synthesis, allowing for their incorporation into the zeolite lattice, often at low % compositions.[113] Fe^{3+} incorporated into the framework of Silicalite-1 and ZSM-5 has been shown to be active for both the conversion of benzene to phenol[119] and methane to methanol with H_2O_2.[120] Whilst zeolites of non MFI zeolites have been shown to be active catalysts for methane oxidation with H_2O_2, these showed significantly lower activity when compared with ZSM-5 (30). This was attributed to a combination of the confinement effect, imparted by the specific pore size, alumina content, residual framework Fe^{3+} and formation of extra framework iron and aluminium species upon high temperature activation of ZSM-5.[120]

1.5.2 MFI type zeolite ZSM-5

The crystallization of ZSM-5 was first reported by Argauer *et al* in 1978.[121] Such MFI-type zeolites (ZSM-5 and Silicalite-1 both feature in this thesis) comprise of 5- membered

pentasil units, five of which form the secondary building unit (SBU) shown in Figure 1.6. The porous network of ZSM-5 is composed of two channel systems; a straight channel which runs parallel to the (010) plane, with 10-ring openings of dimensions 5.4 x 5.6 Å, and a sinusoidal channel which is parallel to the (100) axis with 10- ring openings of dimensions 5.1 x 5.4 Å.[112, 122]

(a) (b)

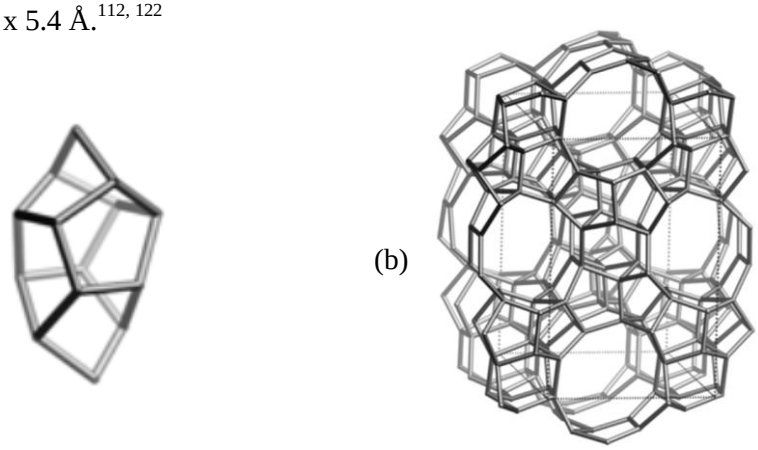

Figure 1.6 MFI SBU (a) and Framework viewed along [010] (b)[122]

1.5.3 Post synthesis incorporation of transition metal ions (TMI)

As mentioned previously, isomorphous substitution of Al^{3+} for framework Si^{4+} induces a negative charge to the zeolite framework. This negative charge is then compensated by cationic extraframework species to restore the charge neutral state.[113] In their proton form, with charge compensating H^+ in exchange sites, zeolites such as H-ZSM-5 are highly Brønsted acidic (Figure 1.7).

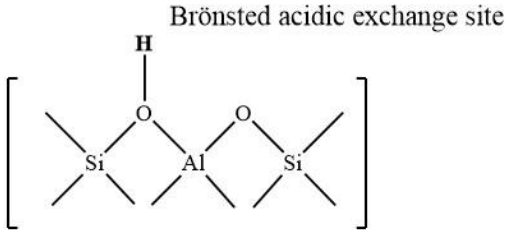

Figure 1.7 Structural representation of Al- site induced Brønsted acidity

As these cations are non framework, they can be exchanged with a range of cations such as Fe^{3+} and Cu^{2+}. Exchanged cationic species are effectively grafted to the Al- associated negatively charged exchange sites, thereby inhibiting both sintering and leaching.[123]

Of the methods used to prepare zeolites with transition metal ions in exchange sites, which include aqueous ion exchange, solid state ion exchange, sublimation deposition, chemical vapour impregnation and impregnation, aqueous ion exchange is the most commonly used.[112, 113, 123] Common to these preparation techniques is a high temperature post deposition heat treatment, which removes water and leads transition metal ions to coordinate to the surface oxygens at exchange sites. [123] The specific location of exchanged ions is dependent upon the zeolite's Si/Al ratio, the total amount of exchanged ions, the cation charge, the method of exchange and the conditions employed in the exchange, such as pH and temperature.[113] In MFI zeolites such as ZSM-5 the exchanged ions are located in the 10- membered ring (10 MR) channels or channel intersections, they are coordinated to 6 MR which contain either one or two Al tetrahedra but 5 MR with one Al cannot be excluded.[113] Wichterlova *et al* discerned three distinct exchange sites for Co ions exchanged into ZSM-5, these were denoted as α, β and γ exchange sites (Figure 1.8).[124]

This observation was extended by Lobree *et al*, to include exchanged Fe and Cu species, with spectroscopic studies suggesting that upon exchange of copper and iron ions onto ZSM-5, γ sites are filled preferentially, with β and the least energetically favourable α sites also filled as the M/Al ratio is increased. M^{n+} exchanged at α sites were shown to reduce (to M^{+}) more readily than those at β or γ sites.[125]

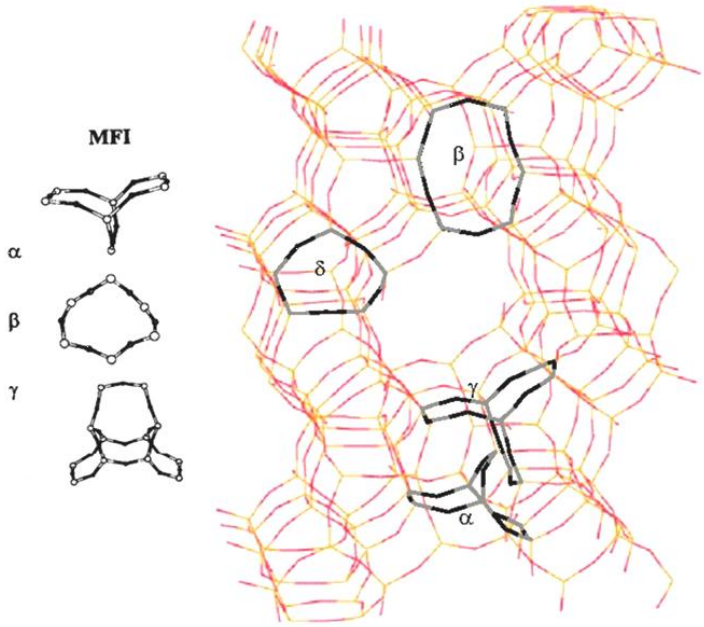

Figure 1.8 Local framework structures of α, β and γ sites in MFI zeolites and their crystallographic positions in ZSM-5 (Adapted from references[113, 126]).

A pictorial representation of the iron species formed upon high temperature heat treatment following deposition of iron onto ZSM-5 is shown in Figure 1.9.

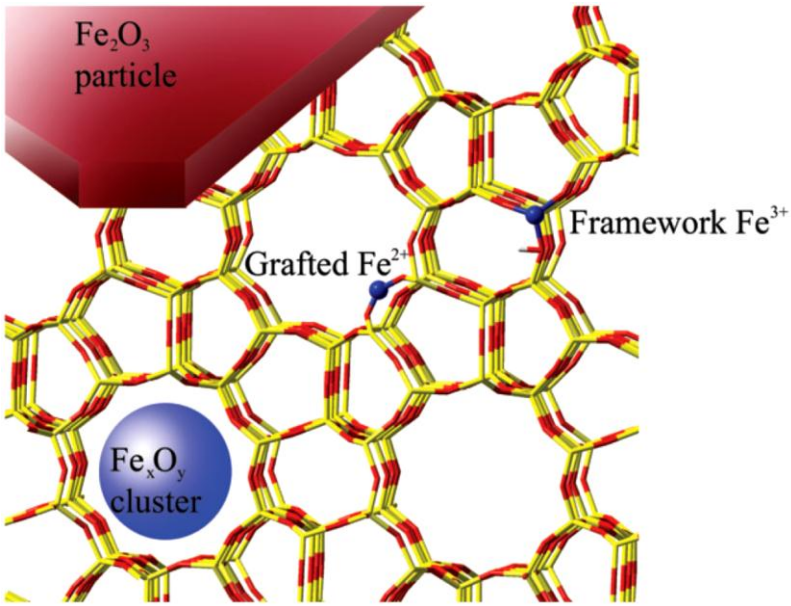

Figure 1.9 Pictorial representations of Fe_2O_3 particles, Fe_xO_y clusters, grafter Fe^{2+} and Fe^{3+} in framework position (from reference[123]).

Fe^{n+} species which result from deposition of iron onto ZSM-5 form a distribution of isolated, dimeric and clustered iron sites, as well as Fe_2O_3. As shown in figure 1.15, iron species on ZSM-5 may present as isolated Fe^{2+} and Fe^{3+} chemically grafted to the zeolite surface via SiOFe and AlOFe bridges. Dinuclear iron sites also form as Fe^{3+} OFe^{3+},Fe^{2+} OFe^{2+} and Fe^{3+} OFe^{2+} sites in oligomeric, clustered sites and Fe_2O_3 particles which are grafted to the framework via SiOFe and AlOFe bridges. The distribution of total iron present in these species depends upon metal loading and the temperature at which materials are heat treated (activated).[123]

1.6 Research objectives

- Development of heterogeneous catalysts for the liquid phase partial oxidation of ethane to oxygenated products using an environmentally benign oxidant (H_2O_2 or, ideally, diatomic oxygen) and solvent (H_2O) at low temperatures (<90^oC).
- Systematic study of the effect of reaction conditions; ethane pressure and partial pressure, temperature, oxidant concentration, reaction duration and both catalyst mass and metal loading upon catalyst performance and product distributions.
- Elucidation of reaction scheme to determine source of products and enable catalyst development to enhance product selectivities, though product stability studies both experimental and analytical such as use of time resolved ^1H NMR studies to monitor catalytic transformations.
- Translation of batch systems to a continuous flow system with system optimisation though investigation of reaction parameters and catalyst loadings.
- Elucidation of catalytically active sites for development of novel catalysts, to yield enhanced product selectivities.

1.7 References

1 Degirmenci, V.; Uner, D.; Yilmaz, A. *Catalysis Today* **2005**, *106*, 252.

2 In *What is Natural Gas?*, http://www.naturalgas.org/overview/background.asp, 2011.

3 Jones, J. H. *Platinum Metals Rev* **2000**, *44*, 94.

4 Rahimi, N.; Karimzadeh, R. *Applied Catalysis A: General* **2011**, *398*, 1.

5 Kosaric, N.; Duvnjak, Z.; Farkas, A.; Sahm, H.; Bringer-Meyer, S.; Goebel, O.; Mayer, D. In *Ethanol*; Wiley-VCH Verlag GmbH & Co. KGaA, 2000.

6 Forde, M. M.; Armstrong, R. D.; Hammond, C.; He, Q.; Jenkins, R. L.; Kondrat, S. A.; Dimitratos, N.; Lopez-Sanchez, J. A.; Taylor, S. H.; Willock, D.; Kiely, C. J.; Hutchings, G. J. *Journal of the American Chemical Society* **2013**, *135*, 11087.

7 Pacala, S.; Socolow, R. *Science* **2004**, *305*, 968.

8 Olah, G. A. *Angewandte Chemie International Edition* **2005**, *44*, 2636.

9 Blanksby, S. J.; Ellison, G. B. *Accounts of Chemical Research* **2003**, *36*, 255.

10 Cossee, P. *Journal of Catalysis* **1964**, *3*, 80.

11 Sagel, E. In *Polyethylene Global Overview*, 2012.

12 Global, S. In *Ethylene oxide/ethylene glycol (EO/EG) processes*, 2010.

13 EXPORT.BY In *The world market of ethylene glycol in 2007-2008*, 2009.

14 Research, G. In *Ethylene Dichloride (EDC) Global Supply Dynamics to 2020 - The US Sustains the Leading Position in Global Production*, 2010. pp 141.

15 ICIS In *Ethylbenzene (EB) Uses and Market Data*, 2010.

16 Fan, D.; Dai, D. J.; Wu, H. S. *Materials* **2013**, *6*, 101.

17 ICIS In *Alpha olefins*, 2008.

18 True, W. R. *Oil Gas J.* **2013**, *111*, 90.

19 Zimmermann, H.; Walzl, R. In *Ethylene*; Wiley-VCH Verlag GmbH & Co. KGaA, 2000.

20 Östman, M. In *Information on substances: Acetic Acid*, 2013.

21 Yoneda, N.; Kusano, S.; Yasui, M.; Pujado, P.; Wilcher, S. *Appl. Catal. A-Gen.* **2001**, *221*, 253.

22 Chemical, I. In *Vinyl Acetate*, 2011.

23 Smejkal, Q.; Linke, D.; Baerns, M. *Chem. Eng. Process.* **2005**, *44*, 421.

24 Sunley, G. J.; Watson, D. J. *Catalysis Today* **2000**, *58*, 293.

25 Schultz, R. G.; Montgome.P.D. *Journal of Catalysis* **1969**, *13*, 105.

26 Krzywicki, A.; Marczewski, M. *Journal of Molecular Catalysis* **1979**, *6*, 431.

27 Scurrell, M. S.; Howe, R. F. *Journal of Molecular Catalysis* **1980**, *7*, 535.

28 Takeshi, M.; Kazuhiko, H.; Kenji, S.; Yoshinmi, S. In *Process for preparing organic carboxylic acid*; Chiyoda Corporation, Japan, 1995.

29 Yoneda, N.; Tokyo, Y.; Shiroto, T.; Kazuhiko, H.; Kawasaki, S.; Sachio Asaoka, Y.; Testsuo Maejima, K. In *Process for the production of acetic acid from methanol and carbon monoxide using supported rhodium catalyst*; Chiyoda Corporation, Japan, 1993.

30 Takeshi, M.; Kenji, S.; Kazuhiko, H.; Kawasaki, S.; Yoshimi Shiroto, Y.; Yoneda, N. In *Supported Rhodium catalyst, method for preparing same and process of producing acetic acid by methanol cabonylation using same*; Chiyoda Corporation, Japan, 1993.

31 Karim, K.; Al-Hazmi, M. H.; Mamedov, E. In *Oxidation of ethane to acetic acid and ethylene using molybdenum and vanadium based catalysts*; Saudi Basic Industries Corporation, 2003.

32 Ueda, W.; Chen, N. F.; Oshihara, K. *Chemical Communications* **1999**, 517.

33 Karim, K.; Al-Hazmi, M.; Khan, A. In *Catalysts for the oxidation of ethane to acetic acid, methods of making and using the same* 2000.

34 Karim, K.; Al-Hamzi, M. H.; Mamedov, E. In *Catalysts for the oxidation of ethane to acetic acid, processes of making same and processes of using same*; Saudi Basic Industries Corp, 1999.

35 Okuhara, T. *Chemical Reviews* **2002**, *102*, 3641.

36 Sano, K.; Uchida, H.; Wakabayashi, S. *Catal. Surv. Jpn.* **1999**, *3*, 55.

37 Suzuki, T.; Yoshikawa, H.; Abe, K.; Sano, K. In *Process for producing acetic acid*; Showa Denko, 1994.

38 Abe, K.; Yamada, K.; Oguchi, W.; Uchida, H.; Kaowaki, Y. In *CATALYST FOR PRODUCING ACETIC ACID, METHOD FOR PREPARING THE SAME AND METHOD FOR PRODUCING ACETIC ACID USING THE SAME*; Showa Denko, 1999.

39 Smejkal, Q.; Linke, D.; Baerns, M. *Chemical Engineering and Processing: Process Intensification* **2005**, *44*, 421.

40 Chu, W.; Echizen, T.; Kamiya, Y.; Okuhara, T. *Applied Catalysis A: General* **2004**, *259*, 199.

41 Mussatto, S. I.; Dragone, G.; Guimaraes, P. M. R.; Silva, J. P. A.; Carneiro, L. M.; Roberto, I. C.; Vicente, A.; Domingues, L.; Teixeira, J. A. *Biotechnol. Adv.* **2010**, *28*, 817.

42 Tanabe, K.; Matsuzak.I; Hattori, H.; Ichikawa, I.; Ishiya, C. *Bull. Chem. Soc. Jpn.* **1972**, *45*, 47.

43 Ushikubo, T.; Kurashige, M.; Koyanagi, T.; Ito, H.; Watanabe, Y. *Catal Lett* **2000**, *69*, 83.

44 Muller, J.; Waterman, H. I. *Brennstoff Chem*, *38*, 321.

45 Iwamoto, M.; Tajima, M.; Kagawa, S. *Journal of the Chemical Society, Chemical Communications* **1985**, 228.

46 Ogasawara, K.; Iizuka, T.; Tanabe, K. *Chemistry Letters* **1984**, 645.

47 Isobe, A.; Yabuuchi, Y.; Iwasa, N.; Takezawa, N. *Appl. Catal. A-Gen.* **2000**, *194*, 395.

48 Bai, F. W.; Anderson, W. A.; Moo-Young, M. *Biotechnol. Adv.* **2008**, *26*, 89.

49 Lashinsky, A.; Schwartz, N. D. *Fortune* **2006**, *153*, 74.

50 Licht, F. O. In *Ethanol Industry Outlook 2008-2013*, 2013.

51 Leite, R. C. D.; Leal, M.; Cortez, L. A. B.; Griffin, W. M.; Scandiffio, M. I. G. *Energy* **2009**, *34*, 655.

52 Icoz, E.; Tugrul, K. M.; Saral, A.; Icoz, E. *Biomass Bioenerg.* **2009**, *33*, 1.

53 Persson, T.; Garcia, A. G. Y.; Paz, J.; Jones, J.; Hoogenboom, G. *Agric. Syst.* **2009**, *100*, 11.

54 Nigam, J. N. *J. Biotechnol.* **2001**, *87*, 17.

55 Kopke, M.; Held, C.; Hujer, S.; Liesegang, H.; Wiezer, A.; Wollherr, A.; Ehrenreich, A.; Liebl, W.; Gottschalk, G.; Durre, P. *Proc. Natl. Acad. Sci. U. S. A.* **2010**, *107*, 13087.

56 Kopke, M.; Mihalcea, C.; Bromley, J. C.; Simpson, S. D. *Curr. Opin. Biotechnol.* **2011**, *22*, 320.

57 In *BRI Process Benefits*, 2008.

58 Thorsteinson, E. M.; Wilson, T. P.; Young, F. G.; Kasai, P. H. *Journal of Catalysis* **1978**, *52*, 116.

59 Oyama, S. T.; Somorjai, G. A. *J. Phys. Chem.* **1990**, *94*, 5022.

60 Roy, M.; Gubelmann Bonneau, M.; Ponceblanc, H.; Volta, J. C. *Catal Lett* **1996**, *42*, 93.

61 Roy, M.; Ponceblanc, H.; Volta, J. C. *Top Catal* **2000**, *11*, 101.

62 Linke, D.; Wolf, D.; Baerns, M.; Dingerdissen, U.; Zeyß, S. In *Catalytic partial oxidation of ethane to acetic acid over Mo1V0.25Nb0.12Pd0.0005Ox—Catalyst performance, reaction mechanism, kinetics and reactor operation*; Elsevier, 2001; Vol. Volume 136. pp 477.

63 Rosen, B. In *OXIDATION CATALYST AND ITS PREPARATION* 2004.

64 Brazdil, J. F.; George, R. J.; Rosen, B. In *Catalyst Composition and use thereof in ethane oxidation*, 2005.

65 Galownia, J. M.; Wight, A. P.; Blanc, A.; Labinger, J. A.; Davis, M. E. *Journal of Catalysis* **2005**, *236*, 356.

66 Roussel, M.; Bouchard, M.; Bordes-Richard, E.; Karim, K.; Al-Sayari, S. *Catalysis Today* **2005**, *99*, 77.

67 Li, X.; Iglesia, E. *The Journal of Physical Chemistry C* **2008**, *112*, 15001.

68 Li, X.; Iglesia, E. *Applied Catalysis A: General* **2008**, *334*, 339.

69 Cook, J.; Ellis, B.; Howard, P.; Jones, M. D.; Kitchen, S. J. In *Process for the production of acetic acid*; Nixon & Vanderhye, 2001.

70 McCain, J. H.; Kaiser, S. W.; O'connor, G. L. In *Acetic acid from ethane, ethylene and oxygen.*; Union Carbide Corporation, 1988.

71 Mizuno, N.; Han, W. C.; Kudo, T. *Journal of Catalysis* **1998**, *178*, 391.

72 Moffat, J. B. *Appl. Catal. A-Gen.* **1996**, *146*, 65.

73 Sopa, A.; Waclaw-Held, A.; Grossy, M.; Pijanka, J.; Nowinska, K. *Appl. Catal. A-Gen.* **2005**, *285*, 119.

74 Erdohelyi, A.; Solymosi, F. *Journal of Catalysis* **1991**, *129*, 497.

75 Erdohelyi, A.; Mate, F.; Solymosi, F. *Journal of Catalysis* **1992**, *135*, 563.

76 Bodke, A. S.; Olschki, D. A.; Schmidt, L. D.; Ranzi, E. *Science* **1999**, *285*, 712.

77 Sorokin, A. B.; Kudrik, E. V.; Alvarez, L. X.; Afanasiev, P.; Millet, J. M. M.; Bouchu, D. *Catalysis Today* **2010**, *157*, 149.

78 Sorokin, A. B.; Kudrik, E. V.; Bouchu, D. *Chemical Communications* **2008**, 2562.

79 Osako, T.; Watson, E. J.; Dehestani, A.; Bales, B. C.; Mayer, J. M. *Angewandte Chemie International Edition* **2006**, *45*, 7433.

80 Jones, C. J.; Taube, D.; Ziatdinov, V. R.; Periana, R. A.; Nielsen, R. J.; Oxgaard, J.; Goddard, W. A. *Angew. Chem.-Int. Edit.* **2004**, *43*, 4626.

81 Bar-Nahum, I.; Khenkin, A. M.; Neumann, R. *Journal of the American Chemical Society* **2004**, *126*, 10236.

82 Seki, Y.; Min, J. S.; Misono, M.; Mizuno, N. *The Journal of Physical Chemistry B* **2000**, *104*, 5940.

83 Lunsford, J. H. *Catalysis Today* **2000**, *63*, 165.

84 Wolf, D. *Angewandte Chemie International Edition* **1998**, *37*, 3351.

85 Sen, A. *Accounts of Chemical Research* **1998**, *31*, 550.

86 Periana, R. A.; Taube, D. J.; Gamble, S.; Taube, H.; Satoh, T.; Fujii, H. *Science* **1998**, *280*, 560.

87 V. Nizova, G.; Suss-Fink, G.; B. Shul'pin, G. *Chemical Communications* **1997**, 397.

88 Raja, R.; Ratnasamy, P. *Applied Catalysis A: General* **1997**, *158*, L7.

89 Labinger, J. A. *Fuel Processing Technology* **1995**, *42*, 325.

90 Minren Lin, A. S. *Nature* **1994**, *368*, 613.

91 Periana, R. A.; Taube, D. J.; Evitt, E. R.; Löffler, D. G.; Wentrcek, P. R.; Voss, G.; Masuda, T. *Science* **1993**, *259*, 340.

92 Shilov, A. E.; Shul'pin, G. B. *Russian Chemical Reviews* **1987**, *56*, 442.

93 Suss-Fink, G.; Gonzalez, L.; Shul'pin, G. B. *Appl. Catal. A-Gen.* **2001**, *217*, 111.

94 Shul'pin, G. B.; Süss-Fink, G.; Shul'pina, L. S. *Journal of Molecular Catalysis A: Chemical* **2001**, *170*, 17.

95 Rahman, A. K. M. L.; Indo, R.; Hagiwara, H.; Ishihara, T. *Applied Catalysis A: General* **2013**, *456*, 82.

96 Shul'pin, G. B.; Nizova, G. V.; Kozlov, Y. N.; Gonzalez Cuervo, L.; Süss-Fink, G. *Advanced Synthesis & Catalysis* **2004**, *346*, 317.

97 Ensing, B.; Buda, F.; Blochl, P. E.; Baerends, E. J. *Physical Chemistry Chemical Physics* **2002**, *4*, 3619.

98 Yuan, Q.; Deng, W.; Zhang, Q.; Wang, Y. *Advanced Synthesis & Catalysis* **2007**, *349*, 1199.

99 Colby, J.; Stirling, D. I.; Dalton, H. *Biochem. J.* **1977**, *165*, 395.

100 Tonge, G. M.; Harrison, D. E. F.; Higgins, I. J. *Biochem. J.* **1977**, *161*, 333.

101 Shteinman, A. A. *Russ. Chem. Bull.* **2001**, *50*, 1795.

102 Meinhold, P.; Peters, M. W.; Chen, M. M. Y.; Takahashi, K.; Arnold, F. H. *ChemBioChem* **2005**, *6*, 1765.

103 Xu, F.; Bell, S. G.; Lednik, J.; Insley, A.; Rao, Z.; Wong, L.-L. *Angewandte Chemie International Edition* **2005**, *44*, 4029.

104 Wang, Y.; Otsuka, K. *Journal of Catalysis* **1997**, *171*, 106.

105 Wang, Y.; Otsuka, K. *Journal of Catalysis* **1995**, *155*, 256.

106 Dubkov, K. A.; Sobolev, V. I.; Talsi, E. P.; Rodkin, M. A.; Watkins, N. H.; Shteinman, A. A.; Panov, G. I. *J. Mol. Catal. A-Chem.* **1997**, *123*, 155.

107 Lin, M.; Sen, A. *Journal of the American Chemical Society* **1992**, *114*, 7307.

108 Shul'pin, G. B.; Sooknoi, T.; Romakh, V. B.; Süss-Fink, G.; Shul'pina, L. S. *Tetrahedron Letters* **2006**, *47*, 3071.

109 Hammond, C.; Forde, M. M.; Ab Rahim, M. H.; Thetford, A.; He, Q.; Jenkins, R. L.; Dimitratos, N.; Lopez-Sanchez, J. A.; Dummer, N. F.; Murphy, D. M.; Carley, A. F.; Taylor, S. H.; Willock, D. J.; Stangland, E. E.; Kang, J.; Hagen, H.; Kiely, C. J.; Hutchings, G. J. *Angewandte Chemie International Edition* **2012**, *51*, 5129.

110 Hammond, C.; Jenkins, R. L.; Dimitratos, N.; Lopez-Sanchez, J. A.; ab Rahim, M. H.; Forde, M. M.; Thetford, A.; Murphy, D. M.; Hagen, H.; Stangland, E. E.; Moulijn, J. M.; Taylor, S. H.; Willock, D. J.; Hutchings, G. J. *Chemistry – A European Journal* **2012**, *18*, 15735.

111 Rahman, A. K. M. L.; Kumashiro, M.; Ishihara, T. *Catalysis Communications* **2011**, *12*, 1198.

112 Auerbach, S. M.; Currado, K. A.; Dutta, P. K. *HANDBOOOK OF ZEOLITES SCIENCE AND TECHNOLOGY*; Marcel Dekker Inc, New York, 2003.

113 Smeets, P. J.; Woertink, J. S.; Sels, B. F.; Solomon, E. I.; Schoonheydt, R. A. *Inorganic Chemistry* **2010**, *49*, 3573.

114 Haw, J. F.; Nicholas, J. B.; Xu, T.; Beck, L. W.; Ferguson, D. B. *Accounts of Chemical Research* **1996**, *29*, 259.

115 Cejka, J.; Centi, G.; Perez-Pariente, J.; Roth, W. J. *Catalysis Today* **2012**, *179*, 2.

116 Breck, D. W. *Zeolite Molecular Sieves*; John Wiley and Sons, New York, 1974. pp 771.

117 Vogt, E. T. C.; Kresge, C. T.; Vartuli, J. C. In *Chapter 22 Beyond twelve membered rings*; Elsevier, 2001; Vol. Volume 137. pp 1003.

118 Jacobs, P. A.; Martens, J. A. In *Chapter 12 Introduction to Acid Catalysis with Zeolites in Hydrocarbon Reactions*; Elsevier, 1991; Vol. Volume 58. pp 445.

119 Bellussi, G.; Guisti, A.; Espisito, A.; Buonomo, F. In *Synthetic, crystalline, porous material containing silicon oxide, titanium oxide and aluminium oxide.* ; Enichem Sintesi, 1986.

120 Hammond, C.; Dimitratos, N.; Lopez-Sanchez, J. A.; Jenkins, R. L.; Whiting, G.; Kondratt, S. A.; ab Rahim, M. H.; Forde, M. M.; Thetford, A.; Hagen, H.; Stangland, E. E.; Moulijn, J. M.; Taylor, S. H.; Willock, D. J.; Hutchings, G. J. *Acs Catalysis* **2013**, *3*, 1835.

121 Arguer, R. J.; Landolt, G. R.; Audubon, N. J. In *CRYSTALLINE ZEOLITE ZSM-5 AND METHOD OF PREPARING THE SAME* Mobil Oil Corporation, 1972.

122 Baerlocher, C. H.; McCusker, L. B.; Olson, D. H. *ATLAS OF ZEOLITE FRAMEWORK TYPES*; Elsevier, 2007.

123 Zecchina, A.; Rivallan, M.; Berlier, G.; Lamberti, C.; Ricchiardi, G. *Physical Chemistry Chemical Physics* **2007**, *9*, 3483.

124 Dedecek, J.; Kaucky, D.; Wichterlova, B.; Gonsiorova, O. *Physical Chemistry Chemical Physics* **2002**, *4*, 5406.

125 Lobree, L. J.; Hwang, I. C.; Reimer, J. A.; Bell, A. T. *Journal of Catalysis* **1999**, *186*, 242.

126 Groothaert, M. H.; Pierloot, K.; Delabie, A.; Schoonheydt, R. A. *Physical Chemistry Chemical Physics* **2003**, *5*, 2135.

2

Experimental

2.1 Materials

The materials listed were used in the course of this work. Reagents were used as received unless further purification is implied.

- Ethane (99.999% *BOC gases*)
- Methane (99.999% *BOC gases*)
- Ethane (10 % C_2H_6/Ar, *BOC gases*)
- Methane (10 % C_2H_6/Ar, *BOC gases*)
- Ethene (5% C_2H_4 / N_2, *BOC* gases)
- Helium (99.999% *BOC gases*)
- Oxygen (99.999% *BOC gases*)
- Nitrogen (99.999% *BOC gases*)
- Hydrogen peroxide (50% wt in H_2O, *Sigma Aldrich*)
- ^{13}C Methanol (99%, *Sigma Aldrich*)
- $^{12}CH_3{}^{13}CH_2OH$ (99% ^{13}C, *Sigma Aldrich*)
- $^{13}CH_3{}^{12}COOH$ (99% ^{13}C, *Sigma Aldrich*)
- Aluminium Acetylacetonate, Al $(acac)_3$ (98%, *Sigma Aldrich*)
- Iron Acetylacetonate, Fe $(acac)_3$ (98%, *Sigma Aldrich)*
- Copper Acetylacetonate, Cu $(acac)_2$ (98%, *Sigma Aldrich*)
- Iron (III) nitrate nonahydrate, Fe $(NO_3)_3 . 9H_2O$ (99.99%, *Sigma Aldrich*)
- ZSM-5 (SiO_2 : Al_2O_3 molar ratio= 23,30,50,280, *Zeolyst*)

- Titanium Dioxide, TiO_2 (P25, *Degussa*)
- Silicon Dioxide, SiO_2, (*Degussa*)
- Tetraethylorthosilicate, TEOS (99.999%, *Sigma Aldrich*)
- Tetrapropylammonium hydroxide, TPAOH (1M / H_2O, *Sigma Aldrich*)

2.2 Definitions

2.2.1 Conversion

$$\frac{\text{µmol Carbon in products}}{\text{µmol Carbon in reaction feed/ charge}} \times 100$$

2.2.2 Turnover Frequency (TOF)

Mol (products formed) mol^{-1} (metal) h^{-1}

For ethane work, moles of product formed were weighted to C_2 (carbon weighted).

2.2.3 Catalyst Productivity

Mol (products formed) kg^{-1} (catalyst) h^{-1}

For ethane work, moles of product formed were weighted to C_2 (carbon weighted).

2.3 Catalyst Preparation Techniques

2.3.1 High Temperature Activation

The commercial Zeolites (*Zeolyst*, SiO_2 : Al_2O_3) were activated prior to use via conversion to their acid form. A procedure for activating NH_4-ZSM-5 is as follows;

NH_4- ZSM-5 (SiO_2 : Al_2O_3 molar ratio = 30, 4 g) was transferred to a ceramic calcination boat. This was then placed into a quartz tube, which was placed within a high temperature combustion furnace. The tube was then sealed and a flow of air was passed over it. The

furnace was then heated to 550 ^{o}C (20 ^{o}C min^{-1}) and held at this temperature for the desired time period (typically 3 h). The sample (H-ZSM-5 (30)) was allowed to cool to ambient temperature under the flowing gas.

Supported- metal catalysts were activated prior to use. The procedure for this was typically as follows, unless otherwise stated. The material (typically ~ 2.0 g) was added to a combustion boat, which was placed into a tubeless combustion furnace. The furnace was then heated to the desired temperature (typically 550 ^{o}C) under static air, at the desired heating rate (typically 20 ^{o}C min^{-1}). The furnace was held at this temperature for the desired time period (typically 3 h), after which time the sample was allowed to cool to room temperature before removal for testing.

2.3.2 Chemical Vapour Impregnation (CVI)

Unless otherwise stated, all catalysts featured were prepared by chemical vapour impregnation (CVI) using a Zeolyst H-ZSM-5 with SiO_2 to Al_2O_3 ratio of 23-280. A procedure for preparing 0.4% Fe/ZSM-5 (30) (2.00 g) is as follows.

Prior to addition of Fe, a known mass of H-ZSM-5, typically 3.5 g, was heat treated at 150 ^{o}C for 2 h under continuous vacuum. Subsequently, the desired mass of dried ZSM-5 (30) (1.992g) was added to a Schlenk flask and the desired mass of Fe (III) acetylacetonate ($Fe(acac)_3$) (Sigma Aldrich, 99.9% purity, 0.0506 g, 0.14 mmol) added. Following physical mixing of the metal precursor and zeolite, the dry mixture was heated to sublimation- deposition temperature (150 ^{o}C for Fe containing materials, 140 ^{o}C for Cu-only materials) and heated under continuous vacuum (*ca* 10^{-3} mbar) for the desired time period (typically 2 h for Fe containing catalysts and 1 h for Cu only materials). The sample was then allowed to cool to ambient temperature and then calcined for 3 h at 550 ^{o}C (20 ^{o}C min^{-1}) in static air.

Iron and copper were also supported upon; Silicalite-1, TiO_2 and SiO_2 via the procedure outlined above. For Cu CVI catalysts, $Cu(acac)_2$ was used as the metal precursor.

2.3.3 Liquid Ion Exchange (IE)

2.5% wt Fe/ZSM5 (30) was prepared by ion exchange of ZSM5 (30) with an aqueous solution of Fe $(NO_3)_3$. $9H_2O$. The stepwise procedure was as follows; an aqueous solution of $Fe(NO_3)_3 \cdot 9H_2O$ (0.362 g in 100 ml H_2O) was placed in contact with H-ZSM5 (30) (1.95 g) at 398 K for 24 h. After filtration the solid phase was dried at 80 ^oC prior to calcination at 550 ^oC under static air (3h, 20^oC min^{-1}).

2.3.4 Impregnation (IMP)

2.5% wt Fe/ZSM5 (30) was prepared by impregnation of ZSM5 (30) with an aqueous solution of $Fe(NO_3)_3.9H_2O$. The stepwise procedure was as follows; An aqueous solution of $Fe(NO_3)_3 \cdot 9H_2O$ (0.362 g in 100 ml H_2O) was placed in contact with H-ZSM5 (30) (1.95 g) at 398 K for 24 h. Following this, the water was evaporated and the solid phase was dried at 80 ^oC, prior to calcination at 550 ^oC under static air (3h, 20^oC min^{-1}).

2.3.5 Hydrothermal preparation of Silicalite-1

Silicalite-1 was synthesised following the procedure described by Tarramasso *et al.*[1] The procedure was as follows;

Tetrapropylammonium hydroxide (20 wt % in H_2O, 50.8 g, corresponding to 49.9 mmoles TPAOH) was stirred vigorously (25 ^oC, 1 h). To this solution tetraethylorthosilicate (10.24 g, 49.4 mmoles) was added drop wise. The resulting gel was homogenised (60 ^oC, 5 h) prior to crystallisation in a Teflon lined stainless steel Parr autoclave (175 ^oC, 48 h). The as synthesised material was later recovered by filtration, washed with deionised water (1 L) and dried in air (110 ^oC, 16 h). The dried sample was

then ground in a pestle and mortar, prior to heat treatments (550 ^{o}C, 8 h, 1 ^{o}C min^{-1}) in a flow of N_2 (5 h) followed by (10 h) in flowing air to remove the template.

2.4 Catalyst Testing

2.4.1 Ethane oxidation with H_2O_2 under batch conditions

Catalyst testing for the oxidation of ethane under batch conditions, with H_2O_2 added as oxidant, was carried out in a custom built *Parr* autoclave fitted with either a 50 or 100 ml reaction vessel as shown in Figure 2.1, following the reported procedure.[2, 3] Said autoclaves were fitted with Teflon liners which afforded total internal volumes of 35 and 70 ml respectively. Where a mixed gas phase is indicated, the desired gases were pre-mixed in the mixing burette.

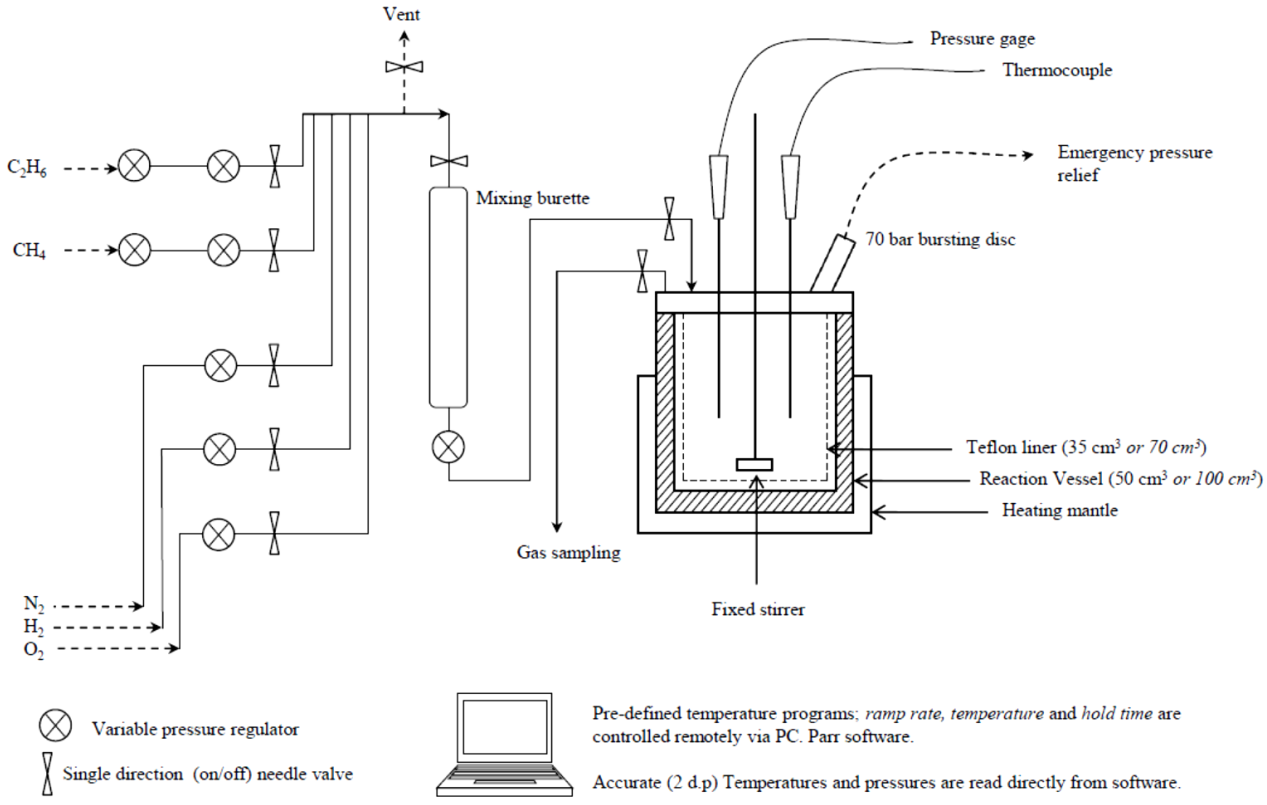

Figure 2.1 Schematic representation of the autoclave batch reactor

A typical batch reaction is outlined below;

To a solution of H_2O_2 (10 ml, 5000 µmol, 0.5 M) in deionised water, the desired catalyst (27 mg) was added. The reactor was sealed, and subsequently purged thrice with C_2H_6 (20 bar) to remove residual air. Following this the reactor was charged with the desired pressure of C_2H_6 (typically 5 or 20 bar), and then heated, under vigorous stirring at 1500 rpm, to the desired reaction temperature (typically 50^{o}C or 70^{o}C), according to a predefined ramping profile. Once the target temperature had been attained, the system was stirred under constant temperature for the desired reaction period (2 min – 24 h). Post- reaction, the stirring was ceased, and system cooled to < 10^{o}C so as to minimise loss of volatile products. Once cooled, system pressure and temperature was accurately recorded for gas quantifications. The gas phase was vented directly into a gas sampling bag, and analysed by GC-FID. The reaction solution was filtered so as to remove the catalyst, and analysed by ^{1}H-NMR and Ce^{4+} titration (described in Section 2.5 of this chapter).

2.4.2 Ethene oxidation with H_2O_2 under batch conditions

For ethene oxidation studies an identical procedure was followed as outlined for ethane oxidation test (Section 2.4.1) with the exception that a gas feed of 5% C_2H_4/ N_2 was used with the reactor charged to a total pressure of 10 bar.

2.4.3 Stability studies $^{12}CH_3{}^{13}CH_2OH$ and $^{13}CH_3{}^{12}COOH$ with added H_2O_2

To a 20 ml solution of H_2O_2 (0.25 M, 5000 µmol) and the desired ^{13}C labelled product (0.166 M) in deionised water, the desired catalyst (27 mg) was added. The reactor was then sealed, and purged 5 times with N_2 (100%) so as to remove residual contaminant gasses. The system was then charged with N_2 (10 bar) and heated to 50^{o}C with vigorous

stirring, and held at the desired temperature for 0.5 h. The post reaction procedure and workup was as in Section 2.4.1

2.4.4 Catalyst reuse studies

To determine the reusability of the CVI catalysts, the following procedure was followed. Four portions of the catalyst (27 mg each) were tested following the procedure outlined previously in Section 2.4.1. Upon completion of the reaction, the solution was filtered and the solid catalyst was dried in air (110 ^{o}C, 16 h). The four portions of spent catalyst were then combined, and reused in three reactions (reuse 1), to allow for loss of material. This reuse process was continued until 4 re-use cycles had been completed.

2.4.5 Hot filtration tests

In order to test the heterogeneity of the Fe and Cu modified ZSM-5 catalysts used throughout this work, hot filtration tests were carried out as follows. A reaction was run following the procedure detailed in Section 2.4.1, with the exception that at the end of the set reaction period (0.5 h), instead of quenching the reaction in ice, the gas phase was purged whilst at reaction temperature, the reactor was opened, solution filtered whilst hot (with a 1 ml aliquot removed for analysis) and reactor cleaned, prior to retuning the filtered solution to the reactor, charging it with ethane once more and running a catalyst-free reaction (0.5 h). The post reaction workup then adhered to the procedure outlined in Section 2.4.1. Evaluation of the heterogeneity of the catalysts was based on a carbon balance of liquid products in the hot-filtered solution and the carbon in the liquid/gas phase of the subsequent catalyst-free reaction system (scaled to account for the 1 ml aliquot removed for ^{1}H-NMR and Ce $(SO_4)_2$ titration).

2.4.6 Ethane oxidation with H_2O_2 under continuous flow conditions

Catalyst testing for the oxidation of ethane under continuous flow conditions, with H_2O_2 added as oxidant was carried out in a custom built trickle bed reactor (Figure 2.2).

A custom built continuous flow fixed bed reactor was assembled for catalytic testing in ethane oxidation, using Swagelock fittings. The stainless steel liner featured in Figure 2.2 had a total length of 13.0 cm and internal diameter of 1.6 cm, bed volume was 3.6 ml. Gas flows of 10% C_2H_6/Ar were controlled using Brooks mass flow controllers (MFCs), and the reactor pressure was maintained using a Swagelock back pressure regulator (BPR). Gas flow rates quoted correspond to the V_{gas} at ambient conditions (298 K, 1 atm). A pressure relief valve was incorporated in the system, pre catalyst bed, in order to address safety concerns. A pressure gauge was placed before the catalyst bed to monitor system pressure. An aqueous solution of H_2O_2 (typically 0.123 M) was pumped into the reactor using an HPLC pump. The liquid product was collected in an 18 ml liquid gas separator (LGS) and removed, periodically, via a sampling reservoir to prevent system depressurisation. The separated effluent gas was fed through a 125 ml Swagelock pressure vessel loaded with molecular sieve 3A, to remove gas phase water, prior to collection in an on/off gas sampling bag.

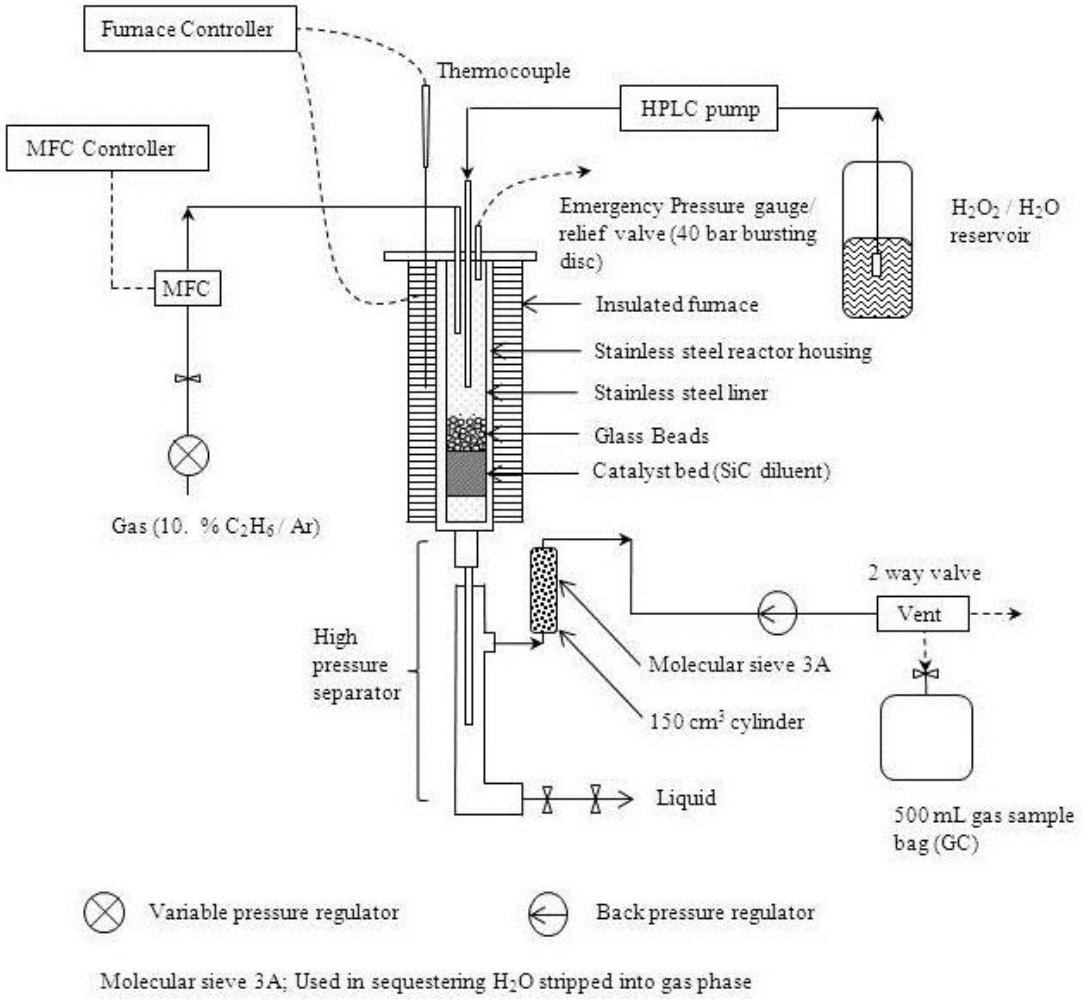

Figure 2.2 Schematic representation of the three phase continuous flow reactor

2.4.6.1 Catalyst bed setup

During initial screening of reaction parameters, the catalyst bed was packed according to the preparation method outlined by M. H. Al-Dahhan *et al.*[4] Prior to use, the desired catalyst was pressed into wafers at a pressure of 20.54 tonnes/ In^2 (0.49 In^2 die). These wafers were subsequently pelleted through sieves (20/40 mesh) to ensure uniform pellet dimensions. The desired mass of pelleted catalyst (typically 2.0 g unless otherwise specified) was then divided into 8 equal parts. SiC (80 grit, 165 µm) followed by a $^1/_8$ portion of the catalyst and then another layer of SiC was added to the stainless steel

reactor tube. This layering process was repeated until 8 layers of catalyst were packed into the bed. Overall SiC accounted for <2% of the catalyst bed volume (excluding glass beads). For lower bed loading tests (< 2.0 g) the catalyst bed volume was maintained using SiC (24 grit, 698 μm), with the bed composed as described above. In order to aid the gas/fluid mixing, 3 cm depth of glass beads were then added.

2.4.6.2 Catalyst testing

The specific reaction parameters set are given in Chapter 4; however a typical reaction procedure is described below.

The desired catalyst bed was assembled as outlined in Section 2.4.8. The stainless steel liner was then sealed within the stainless steel reactor housing, employing Teflon seals to ensure mass flow of gas through the catalyst bed. Prior to testing, the reactor was sealed and purged with substrate feed for *ca* 20 minutes, with the catalyst bed heated to reaction temperature during this period. The reactor system was then pressurised (typically 20 bar) with the substrate feed (10% C_2H_6/Ar). Once the reactor had reached the desired reaction pressure and temperature, the BPR was set to the desired system pressure and the H_2O_2/H_2O flow (typically 0.25 ml min^{-1}) started. The gas and liquid feeds were fed simultaneously through the catalyst bed, from top to bottom. The collected liquid phase was removed at 20 minute intervals, prior to analysis by solvent suppressed ^{1}H-NMR, using D_2O as solvent and a calibrated TMS/$CDCl_3$ insert. The H_2O_2 usage was determined by titration against an acidified $Ce(SO_4)_2$ solution, with ferroin indicator. The gas phase was sampled via gas bags over 60 min periods. Gas phase CO, CO_2, CH_4 and C_2H_4 were determined through GC analysis. Further details of the methods employed in product quantification are given hence.

2.5 Product analysis & quantification

2.5.1 Gas Chromatography

GC analysis was performed using a *Varian 450*-GC fitted with both an FID and TCD, and a CP-Sil 5CB capillary column (50m length, 0.32mm diameter, carrier gas = He)

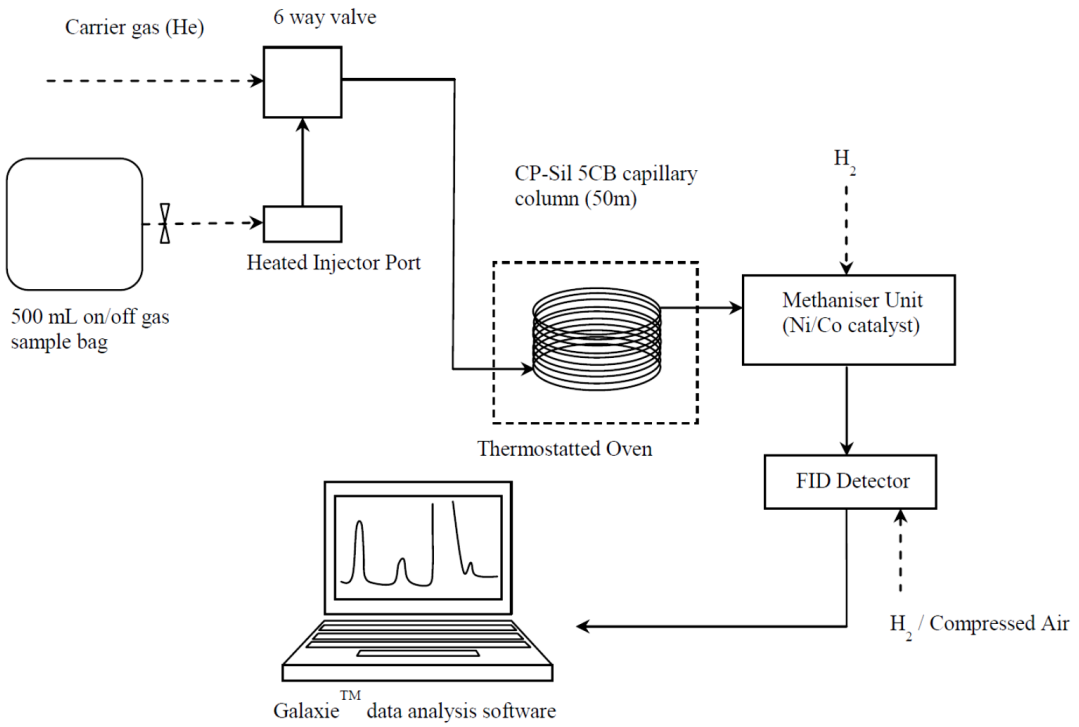

Figure 2.3 Schematic representation of the gas chromatograph

The GC was fitted with a methaniser unit, and CO_2 was quantified against a calibration curve constructed from commercial standards of 10, 100, 500 and 1000 ppm CO_2 /N_2. A schematic of the GC setup is shown in figure 2.3, and an illustrative calibration curve for CO_2, is shown in Figure 2.4. Analogous calibration curves for CH_4, C_2H_4 and C_2H_6 were also constructed. Note; in lieu of commercial standards for CH_4, C_2H_4 and C_2H_6, samples

of varying composition were mixed in the mixing burettes shown in Figure 2.1, prior to injection.

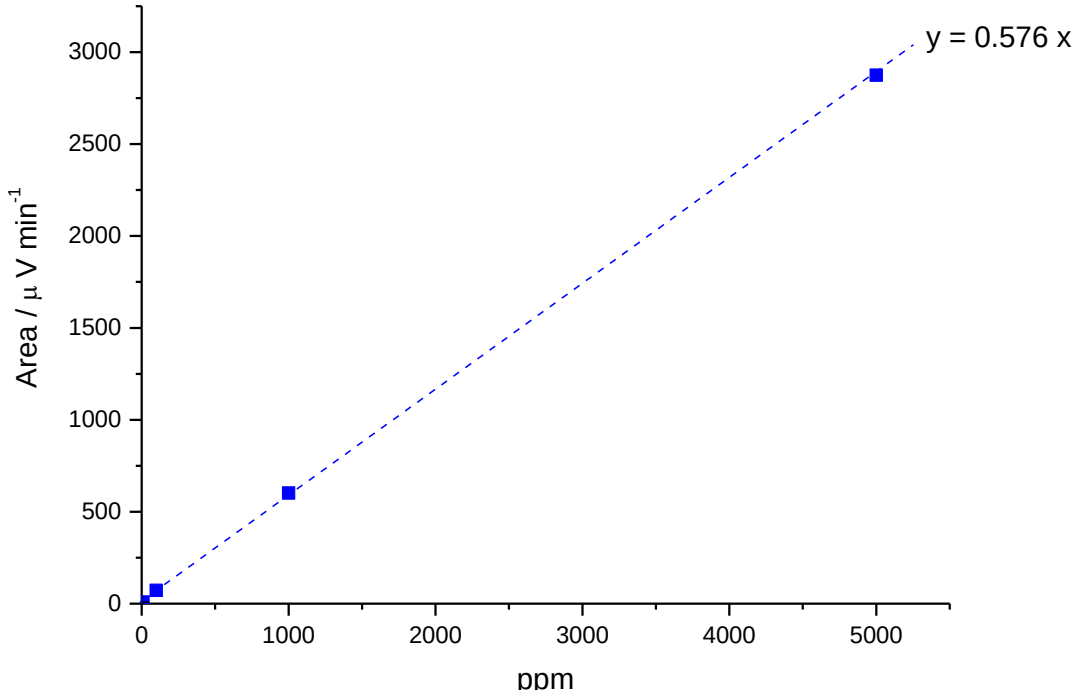

Figure 2.4 Calibration curve for CO_2

The Ideal Gas Equation was employed in order to quantify gaseous products for both batch and flow reactions (Equation 2.1).

$$PV = nRT \text{ which rearranges to } n = PV / RT \qquad \text{(Equation 2.1)}$$

Where; P is the pressure of gas

V is the volume of occupied by gas

R is the gas constant

T is the temperature

n is the moles of gas

For batch reactions, the gaseous products were quantified using the pressure (P) at the end of the reaction (once cooled to < 10^{o}C), the volume of the reactor headspace (V) (either 0.025 or 0.04 dm^{3}) and the temperature (T) post reaction (once cooled to < 10^{o}C). From the GC analysis of a reaction's gas effluent the μmol of a specific gas were calculated using it's calibration factor to calculate ppm of said gas such that;

$$\text{ppm (gas)} = \text{peak area} / \text{calibration factor} \qquad \text{(Equation 2.2)}$$

$$\text{micromoles (gas)} = \text{ppm (gas)} \times n \qquad \text{(Equation 2.3)}$$

Where; *n* is the moles of gas

For flow reactions the quantification of gaseous products followed a similar course. In order to quantify a catalytic system's productivity towards a specific gas, the effluent gas was collected in gas bags over known time periods. By analysing the gas composition at specific intervals (t_a, t_b, t_c, t_d) the productivity towards a gas was calculated such that;

$$\text{Productivity min}^{-1} = (\text{ppm Gas at } t_b \times (\text{volume gas post catalyst bed + volume gas leaving reactor between time } t_a \text{ and } t_b) - (\text{ppm Gas at } t_a \times \text{volume post catalyst bed}) / t_b - t_a \qquad \text{(Equation 2.4)}$$

This method of quantifying gaseous products accounted for the fact that at time t_0 the ppm of a gaseous product in the reactor was 0. As the reaction progressed, an increase in ppm of a gas was observed as the flow out of the reactor was typically 10 ml min^{-1} whilst the post catalyst bed volume equalled 127 ml which at 10 bar equates to 1270 ml gas. In a typical flow reaction 6 different gas bags were collected, over known time periods.

Once more, the Ideal Gas equation was employed in quantifying both the mol gas in the reactor (as in Equation 2.1), and the mol gas leaving the reactor between t_a and t_b such that;

$PV = nRT$ which rearranges to $n = PV / RT$ (Equation 2.5)

Where; P is the BPR outlet pressure (1 bar)

V is the volume gas flow out of the reactor per unit time (dm^3)

R is the gas constant

T is the reactor temperature

n is the moles of gas

2.5.2 Hydrogen peroxide quantification

Hydrogen peroxide was quantified through titration of aliquots of the reaction solution (typically 0.1 ml for batch, 0.5 ml for flow reactions) against an acidified solution of $Ce(SO_4)_2$ (8×10^{-3} mol dm^{-3}) which was standardised versus $(NH_4)_2Fe(SO_4)_2 \cdot 9H_2O$, with a Ferroin indicator.[5]

2.5.3 Liquid phase product quantification via ^{1}H NMR

^{1}H NMR at ambient temperature on a Bruker Ultrashield 500 MHz spectrometer was employed in identifying and quantifying the aqueous products formed throughout this work. Due to the strong solvent peak arising from H_2O, a solvent suppression program was employed.

Typically, 0.70 ml of the filtered reaction sample was added to an NMR tube containing 0.1 ml D_2O and a glass ampule containing Tetramethyl Silane (TMS) in $CDCl_3$. In order to determine the unknown amount of $SiMe_4$ contained within the TMS/$CDCl_3$

standards, Product solutions of varying concentration were made up through a series of dilution steps. Illustrative curves for CH_3OH is shown in Figure 2.5.

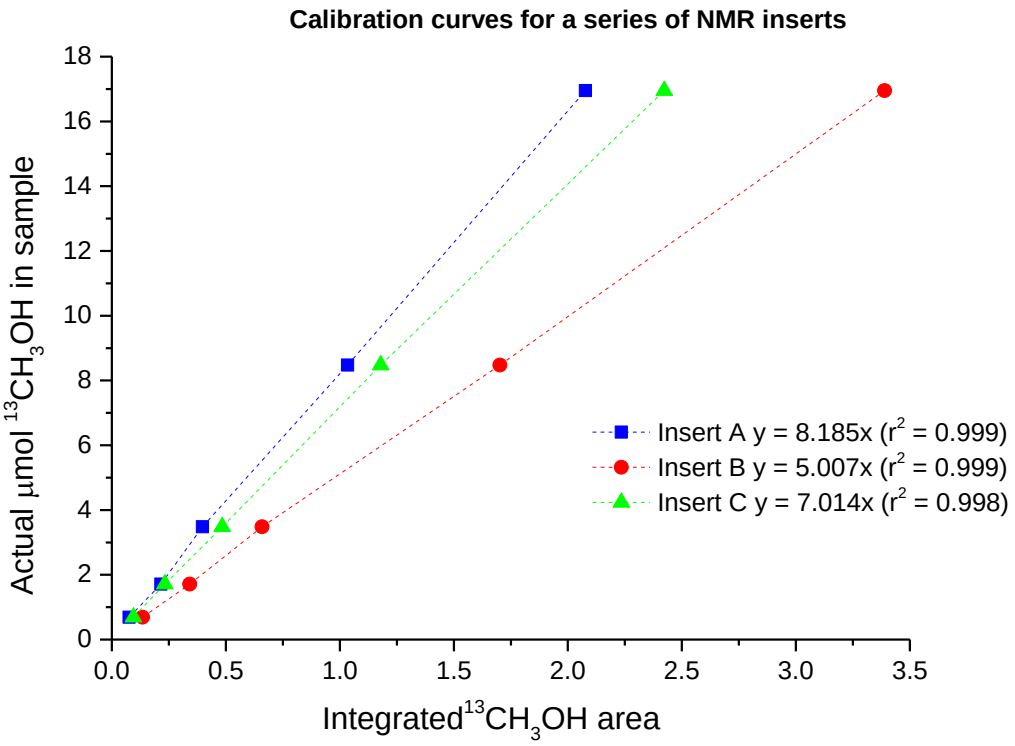

Figure 2.5 A series of ^{1}H-NMR methanol calibration curves

The chemical shifts and splitting for the protons used in quantifying the various C_1 and C_2 products formed are shown in Table 2.1 with a representative ^{1}H-NMR trace shown in Figure 2.6.

Table 2.1 ^{1}H NMR chemical shifts of liquid phase ethane oxidation products

Species	*Formula*	*Chemical Shift/ multiplicity*
Tetramethyl silane (TMS standard)	$Si(CH_3)_4$	δ 0.0 ppm, s
H_2O (in $CDCl_3$)		δ 1.55 ppm, δ 7.25 ppm, s
Ethanol	$C\mathbf{H}_3CH_2OH$	δ 1.2 ppm, t
Acetaldehyde (hydrated)	$C\mathbf{H}_3CHO$	δ 1.3 ppm, d
Acetic Acid	$C\mathbf{H}_3COOH$	δ 2.1 ppm, s
Acetaldehyde	$C\mathbf{H}_3CHO$	δ 2.25 ppm, d
Methanol	$C\mathbf{H}_3OH$	δ 3.35 ppm, s
Methylhydroperoxide	$C\mathbf{H}_3OOH$	δ 3.89 ppm, s
Ethylhydroperoxide	$CH_3C\mathbf{H}_2OH$	δ 4.1 ppm, q
Glycolic Acid	$HOC\mathbf{H}_2COOH$	δ 4.2 ppm, s
Formic Acid	$\mathbf{H}COOH$	δ 8.2 ppm, s

Note; acetaldehyde was observed both in its hydrated and non-hydrated form, dependent upon its concentration. Protons in bold denote those for which chemical shift is shown.

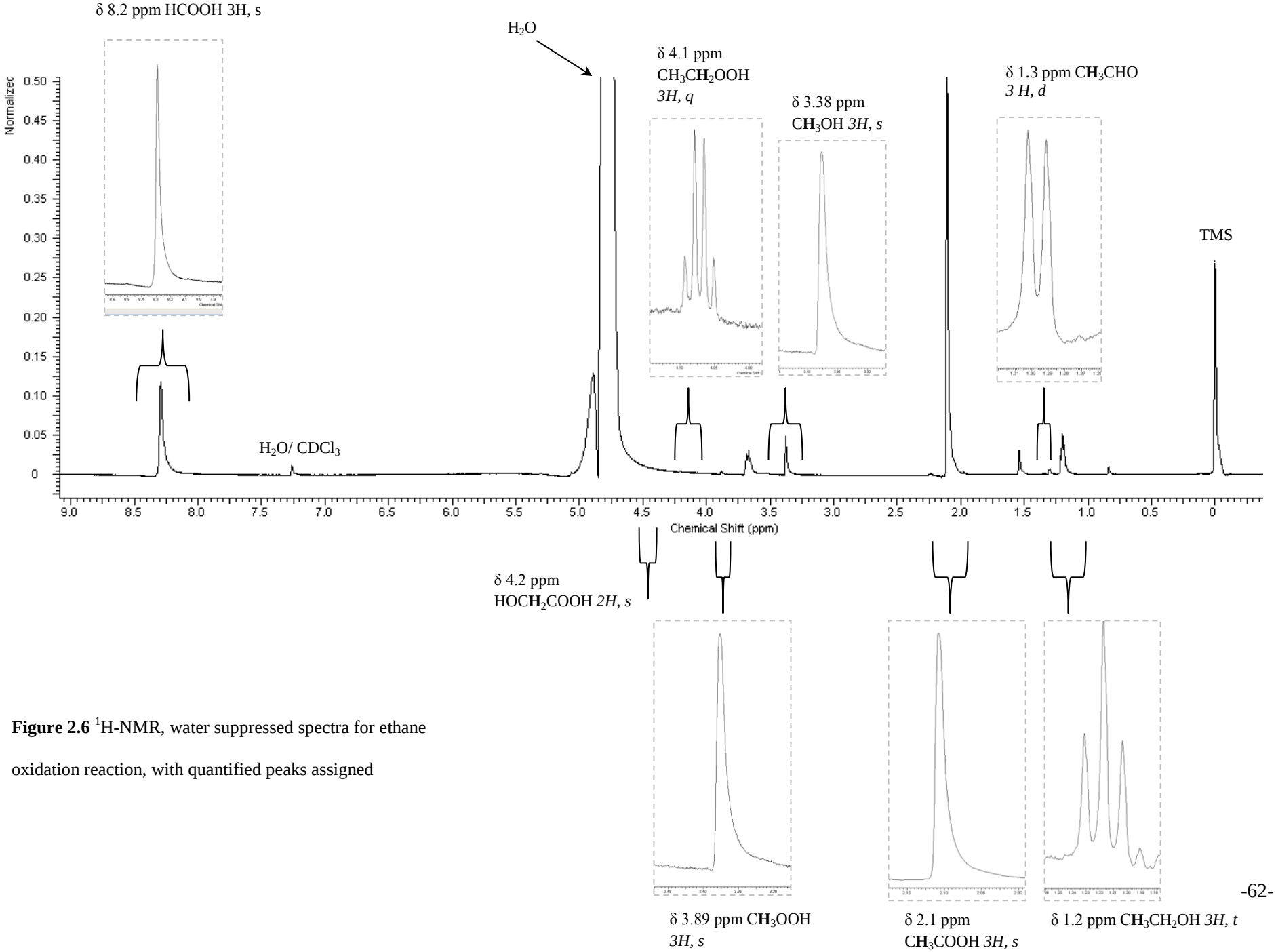

Figure 2.6 [1]H-NMR, water suppressed spectra for ethane oxidation reaction, with quantified peaks assigned

2.6 Catalyst Characterisation Techniques

A variety of characterisation techniques were employed in characterising the catalysts which were prepared and tested over the course of this project. Provided here is an overview of the background theory of these techniques in addition to details of their experimental application.

2.6.1 X-ray powder diffraction (XRD)

XRD allows for the characterisation of the bulk structure of crystalline solids, monitoring of bulk phase transformation kinetics and estimation of crystallite sizes. X-rays are produced by bombarding a metal target (typically copper) with high energy electrons. Said electrons are accelerated towards a target using a voltage, such that electrons within the metal's inner orbitals are excited and expelled. As a result a higher energy valence electron drops down, resulting in the emission of an X-ray of specific wavelength. These X-rays are concentrated into a focused beam, and directed towards the sample. The peaks are derived from X-rays which are scattered by atoms within a particular plane of an ordered lattice as dictated by the Bragg Equation (Equation 2.6)[6]

$$n\lambda = 2\,d \sin\theta;\ \ n = 1,2..... \qquad \text{(Equation 2.6)}$$

Where; n is an integer

λ is the X-ray wavelength

d is the spacing between two lattice planes

θ is is the angle between the incident and normal to the reflecting lattice planes

X-rays have wavelengths of an equal order to molecular bond lengths (10^{-10} m) and are sufficiently energetic to penetrate solids and probe their internal structure. X-ray diffraction patterns are derived from the elastic scattering of X-rays by atoms in the planes of a crystalline lattice. The atomic planes of a crystal cause the incident X-ray to

be refracted at particular angles. Through comparison with a database of XRD patterns, the phases which are present within a sample may be identified and crystallite sizes may be determined from a peak's width via the Scherrer equation, though the latter is limited to species with particle sizes of greater than 5 nm.

The main limitation of XRD stems from its being a bulk technique, meaning that samples require sufficient long range order to observe clear diffraction peaks. Through rotating the powder sample during analysis the fraction of particles which contribute to the diffraction pattern is maximised.

Powder X-ray diffraction was performed using a PANalytical X'PertPRO X-ray diffractometer, with a CuK_{α} radiation source (40 kV and 40 mA) and Ni attenuator. Diffraction patterns were recorded across a range of 5-70 degrees, 0.0167 ^{o} step size (time / step = 150 seconds).

2.6.2 X-ray photoelectron spectroscopy (XPS)

XPS is a characterisation technique which is based upon the photoelectron effect, whereby an atom absorbs a photon of energy ($h\upsilon$), prompting the ejection of a core or valence electron with the binding energy E_b with kinetic energy E_k such that;

$$E_k = h\upsilon - E_b - \varphi \quad \text{(Equation 2.7)}^{6}$$

Where; E_k is the photoelectron's kinetic energy

h is Planck's constant

υ is the frequency of the exciting radiation

E_b is the binding energy of the photoelectron with respect to the Fermi level of the sample

φ is the work function of the spectrometer

A surface specific technique, XPS has a probing depth of between 1.5 and 6 nm, depending on the photoelectron's kinetic energy. As a set of binding energies is characteristic of a specific element, XPS can be employed in analysing the composition of a sample. XPS spectra are typically plotted as the intensity of photoelectrons N_E against the binding energy $E_{b,}$ Binding energies are not solely specific to elements in that they also contain chemical information, as the energy levels of core electrons are somewhat dependent upon the chemical state of the atom.[6] As a general rule an increase in oxidation state is associated with an increase in binding energy, a similar effect on binding energy is observed when electronegative ligands are associated with an atom or fixed oxidation state.[6]

XPS spectra were collected using a Kratos Axis Ultra DLD System using monochromatic Al K_α X-ray source operating at 120 W. Data was collected in the Hybrid mode of operation, using a combination of magnetic and electrostatic lenses, and at pass energies of 40 and 160 eV for high resolution and survey spectra respectively. Magnetically confined charge compensation was used to minimize sample charging and the resulting spectra were calibrated to the Si (2p) line at 103.2 eV.

2.6.3 Brunauer Emmett Teller (BET) surface area analysis

BET analysis proceeds through the adsorption of N_2 onto a sample (at 77K) , to form a monolayer, in order to determine the monolayer capacity (V_m) of a sample, from which the surface area may be computed.[7]

Once a sample surface has been cleaned under vacuum, it is dosed with the adsorbate gas at different pressures. The relationship between gas pressure and the quantity of adsorbate

adsorbed yields an adsorption isotherm. The linearised equation is as follows in Equation 2.8;[8]

$$\frac{P}{V(P_0 - P)} = \frac{1}{V_m \cdot C} + \frac{(C-1)}{V_m \cdot C} \cdot \frac{P}{P_0} \qquad \text{(Equation 2.8)}$$

Where; P is the equilibrium pressure
P_o is t he saturation pressure
V is the volume
V_m is the volume required to cover the surface in a monolayer
C is a constant

The plot of $1/ [V_{STP} (P_o/ P) -1]$ versus P/ P_o should yield a straight line. The intercept for said plot's line of best fit (i) is equal to $(1/ V_m \cdot C)$. The surface area of a sample is therefore calculated from equation 2.9 ;

$$\text{Surface area} = \frac{V_m}{22414} \text{x } (N_A \text{ x } S \text{ x } 10^{-18}) \qquad \text{(Equation 2.9)}$$

Where ; V_m is the volume required to cover the surface in a monolayer
N_A is Avagadro's number (6.022×10^{23})
S is the cross sectional area of N_2 ($0.162\ nm^2$)

80 point BET analysis of materials was conducted on an Autosorb-1 Quantachrome instruments system at 77 K. A Monte Carlo based model was used in determining pore volumes. Points in the range of 0.06 to 0.35 were used in the BET multipoint surface area quantification.

2.6.4 Diffuse Reflectance Infrared Fourier Transform Spectroscopy (DRIFTS)

Fourier Transform Infrared (FTIR) spectroscopy is a vibrational spectroscopy technique which is used to determine qualitative and quantitative features of IR- active species. The energy of most molecular vibrations matches that of the infrared region of the

electromagnetic spectrum, thereby when the energy of the incident IR radiation corresponds to the frequency of a mode of vibration, a molecule will vibrate, thereby undergoing transition to a higher energy vibrational state.[9] The frequency at which a bond vibrates is dependent upon the bond strength and mass of atoms in the bond, and is therefore characteristic of a particular bond. FTIR allows measurement across a range of frequencies (5000 cm^{-1} to 400 cm^{-1}) simultaneously, and is therefore an efficient technique.[9] It is a quick and relatively cheap technique for analysis of crystalline solids, amorphous solids and films. Infrared spectroscopy is most often applied within catalysis as a means of identifying adsorbed species and to study their chemisorptions onto the catalyst surface. It may also be used in identifying phases present within a catalyst material and in studying functional groups on a catalyst surface. DRIFTS was performed during this work in order to investigate the near IR region (4000 – 3000 cm^{-1}) to study the changes in Brønsted acidity of ZSM-5 catalysts upon exchange of cations into acid sites.

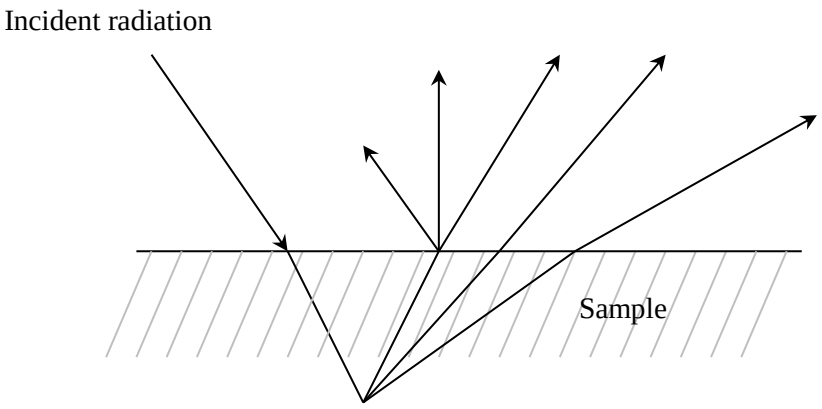

Figure 2.7 An illustration of diffuse reflectance

Of the three physical states, solids are the most challenging when it comes to IR spectroscopy, the key issue being how to maximise interaction between IR radiation and the sample.[6] DRIFTS is used when a light diffusing surface, for example a powder or

roughened surface is to be studied. Through grinding, the particle size of a sample may be reduced (typically to < 10μm, that it doesn't exceed the wavelength of the incident radiation), thereby improving the final spectrum. Equally, a narrow particle size distribution is also favourable. By grinding the sample with a nonabsorbing matrix, for example KBr, spectral distortions which arise from anomalous surface reflections or highly absorbing surfaces may be reduced. With DRIFTS, spectral distortions arise due to constant variation in the effective path length, defined by the beam's depth of penetration into the sample.[10]

IR spectra were collected on a Bruker Tensor 27 spectrometer fitted with a liquid N_2 - cooled Mercury Cadmium Telluride (MCT) detector. Samples were housed within a Praying Mantis high temperature diffuse reflection environmental reaction chamber (HVC-DRP-4) *in situ* cell fitted with zinc selenide windows. Background scans were taken using finely ground KBr. Prior to analysis, samples were mixed with KBr 1:1 by volume, and subsequently ground to a fine powder in an Agate pestle and mortar. For analysis of precalcined catalysts, samples were pretreated prior to acquisition by heating the cell to 200 ^{o}C (10 ^{o}C min^{-1}) under continuous vacuum (10^{-3} mbar) and maintained at this temperature for 2 h to ensure removal of residual water. Scans were collected across the range 4000 cm^{-1} to 1500 cm^{-1}, 4 cm^{-1} frequency, 64 scans.

For *in situ* heat treatments a Harrick ATC heater was used in heating the sample cell according to a predefined heating program which was controlled via Watlow EZ-Zone software. Gas flows were fed down through the sample, with flow rates controlled by a Brooks MFC. Scans were taken at 5 minute intervals (including 2 min scan time, this equalled a 7 min cycle duration) across the range 4000 cm^{-1} to 500 cm^{-1}, 4 cm^{-1} frequency, 64 scans.

2.6.5 UV-Vis spectroscopy

UV- Vis spectroscopy is a well known analytical technique which may be employed in studying of transition metal ions within heterogeneous catalysts. Upon irradiation of a sample with electromagnetic radiation in the UV-Vis region (200 – 800 nm wavelength range) ions or molecules present absorb photons of a specific energy, causing the species to undergo an electronic transition from a lower energy to higher energy ‘’excited’’ state.[11] As the specific energy of an absorbed photon is dependent upon the transition energy between states, the wavelength at which an absorption band is observed provides information as to the ions charge, its local environment and electronic bonding, all of which effect the transition energy.[11]

Spectra obtained in this work present bands which are distinct to specific states of Fe^{3+} thereby allowing for identification of transition metal coordination and agglomeration. It is accepted that iron species in ZSM-5 give rise to distinct UV-Vis bands between; (200-250 nm) isolated framework Fe^{3+}, (250-350 nm) isolated or oligonuclear extraframework Fe species, (350 – 450 nm) Fe_xO_y clusters and (≥450 nm) larger iron oxide species.[12-15]

UV Vis spectra were collected using a Varian 4000 UV-Vis spectrophotometer. Scans were collected across the wavelength range 200-800 nm, at a scan rate of 150 nm min^{-1}, with a UV – visible changeover wavelength of 260nm. Background scans were taken using a high purity PTFE disc. Prior to analysis catalyst samples were ground to a fine powder using an Agate pestle and mortar.

2.6.6 Temperature programmed desorption (TPD)

Also known as thermal desorption spectroscopy (TDS) is a technique which is primarily employed in surface science, to examine desorption of a probe gas from a surface, but may also be used on technical catalysts. TPD may provide; quantitative adsorbate coverage, the adsorption energy and lateral interactions between adsorbates.[6] TPD also provides information regarding the strength of the bond between adsorbate and substrate. It was for this function that NH_3-TPD was employed in this work, in order to probe different zeolite catalysts with ammonia to determine the distribution of weak and strong acid sites (low and high temperature desorption respectively). Quantitative analysis of the desorption signal allowed for quantification of the ammonia adsorption capacity of different materials, and thereby comparison of the materials' acidities.

NH_3 – TPD was carried out using a CHEMBET TPR/TPD chemisorption analyser, Quantachrome Industries fitted with a TCD.

NH_3 – TPD protocol; The samples (50 mg) were pre-treated for 1 h at 130 ^oC (15 ^oC min^{-1}) in a flow of helium (80 ml min^{-1}). Following this, the sample was cooled to ambient temperature and pure ammonia flowed through for 20 min to ensure saturation. The system was then heated 1 h at 100 ^oC (15 ^oC min^{-1}) under a flow of helium (80 ml min^{-1}) to remove physisorbed ammonia. Subsequently, chemisorbed ammonia was desorbed by heating to a T_{max} of 900 ^oC (15 ^oC min^{-1}) in a flow of helium (80 ml min^{-1}) during which period desorbed ammonia was monitored using a TCD, current 180 mV, attenuation 1.

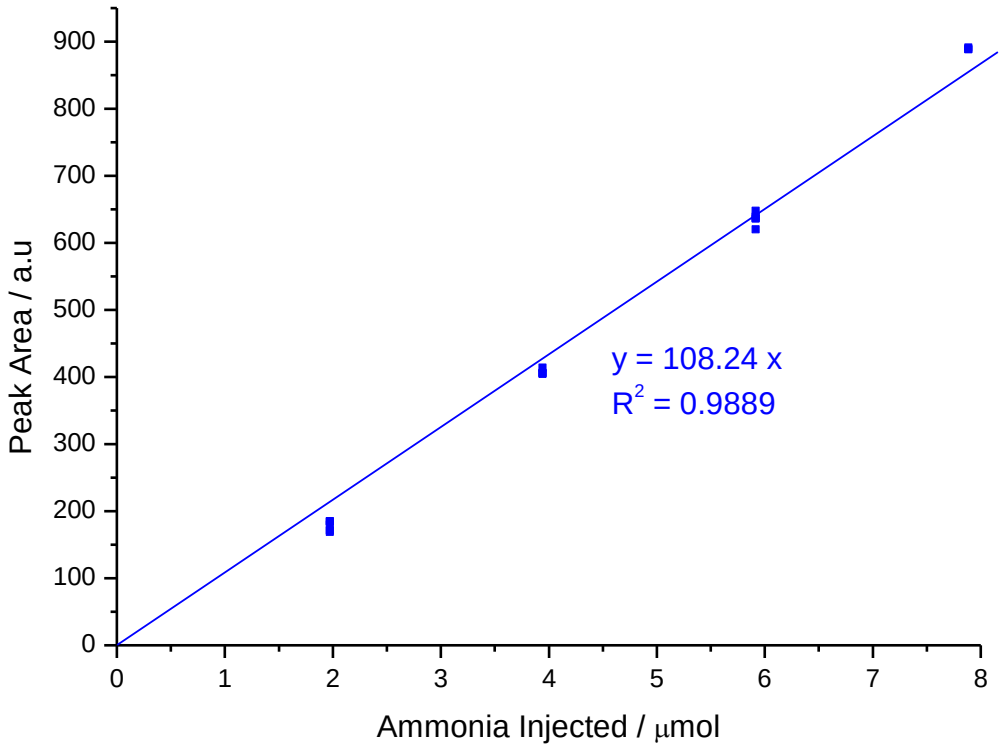

Figure 2.8 Calibration curve for NH_3

NH_3 was calibrated by injecting known volumes of pure NH_3 directly into the TCD sampling loop. By integrating the corresponding TCD signals, a calibration factor for NH_3 was determined (Figure 2.8), with which the desorbed chemisorbed NH_3 of various samples was quantified.

2.6.7 Temperature programmed reduction (TPR)

TPR is a useful technique for determining the reducibility and quantity of reducible species present within a sample. This is achieved by flowing a reducing gas, for example 10% H_2 / Ar over a sample whilst heating the sample according to a programmed, linear temperature ramp.[6] The area under a TPR represents the total hydrogen consumption. The TPR of supported bimetallic catalysts can be used to probe whether the two metals are in

intimate contact or not.[6] Interactions between the support and supported metal may also be inferred by changes in the reduction potential of said metals, evidenced by shifting of reduction temperatures.

Temperature programmed reduction was carried out using a TPDRO 1100 series analyser. Samples (80 mg) were pre-treated for 1 h at 130 ^{o}C (20 ^{o}C min^{-1}) in a flow of Argon (20 ml min^{-1}). Following this the gas flow was changed to 10% H_2 / Argon and the temperature was ramped to 800 ^{o}C (10 ^{o}C min^{-1}) with a 5 min hold at the T_{max}. Hydrogen uptake was monitored using a TCD.

2.6.8 Transmission Electron Microscopy (TEM)

TEM is a useful technique within catalysis, as it allows for determination of attributes of a heterogeneous catalysts including; catalyst particle size, dispersion and chemical composition.[16] This technique works in a similar way to traditional optical microscopes with electromagnetic lenses instead of optical lenses, and electrons as opposed to light. Firstly the primary, high energy/ intensity electron beam is passed through a condenser, thereby forming parallel electron rays, which then impinge on the sample.[6] Given that the electron attenuation is dependent on sample density and thickness, transmitted electrons form a 2D projection of the sample mass distribution, which is magnified via the electron optics to form a bright field image. Supported particles may be distinguished provided there is sufficient contrast between the particles and support material, with contrast dependent on the attenuation of electrons due to variations in density and thickness throughout the sample, coupled with diffraction and interference.[6]

TEM images were collected on a JEOL JEM-2100 transmission electron microscope fitted with a LaB6 filament. Samples were prepared by dispersing powdered catalyst in

high purity ethanol, before adding a drop of the suspension to porous carbon film supported by a meshed copper TEM grid.

2.7 References

1 M. Taramasso, G. P., B. Notari In *Preparation of Porous Crystalline Synthetic Material Comprised of Silicon and Titanium Oxides*, 1982.

2 Hammond, C.; Forde, M. M.; Ab Rahim, M. H.; Thetford, A.; He, Q.; Jenkins, R. L.; Dimitratos, N.; Lopez-Sanchez, J. A.; Dummer, N. F.; Murphy, D. M.; Carley, A. F.; Taylor, S. H.; Willock, D. J.; Stangland, E. E.; Kang, J.; Hagen, H.; Kiely, C. J.; Hutchings, G. J. *Angewandte Chemie International Edition* **2012**, *51*, 5129.

3 Forde, M. M.; Armstrong, R. D.; Hammond, C.; He, Q.; Jenkins, R. L.; Kondrat, S. A.; Dimitratos, N.; Lopez-Sanchez, J. A.; Taylor, S. H.; Willock, D.; Kiely, C. J.; Hutchings, G. J. *Journal of the American Chemical Society* **2013**, *135*, 11087.

4 Al-Dahhan, M. H.; Wu, Y.; Dudukovic, M. P. *Industrial & Engineering Chemistry Research* **1995**, *34*, 741.

5 Lopez-Sanchez, J. A.; Dimitratos, N.; Miedziak, P.; Ntainjua, E.; Edwards, J. K.; Morgan, D.; Carley, A. F.; Tiruvalam, R.; Kiely, C. J.; Hutchings, G. J. *Physical Chemistry Chemical Physics* **2008**, *10*, 1921.

6 Niemantsverdriet, J. W. In *Spectroscopy in Catalysis: An Introduction, Third Edition*; Wiley-VCH Verlag GmbH & Co. KGaA, 2007. pp I.

7 Lowell, S.; Shields, J. E.; Thomas, M. A.; Thommes, M. *Characterization of Porous Solids and Powders: Surface Area, Pore Size and Density*; Springer Netherlands, 2004.

8 Brunauer, S.; Emmett, P. H.; Teller, E. *Journal of the American Chemical Society* **1938**, *60*, 309.

9 Williams, D. H. F., Ian *Spectroscopic methods in organic chemistry* McGraw-Hill, London and New York 1995

10 Coates, J. *A Review Of Sampling Methods For Infrared Spectroscopy*; Academic Press, 1998.

11 Schoonheydt, R. A. *Chemical Society Reviews* **2010**, *39*, 5051.

12 Hensen, E. J. M.; Zhu, Q.; Janssen, R. A. J.; Magusin, P.; Kooyman, P. J.; van Santen, R. A. *Journal of Catalysis* **2005**, *233*, 123.

13 Perez-Ramirez, J.; Groen, J. C.; Bruckner, A.; Kumar, M. S.; Bentrup, U.; Debbagh, M. N.; Villaescusa, L. A. *Journal of Catalysis* **2005**, *232*, 318.

14 Kumar, A. S.; Perez-Ramirez, J.; Debbagh, M. N.; Smarsly, B.; Bentrup, U.; Bruckner, A. *Appl. Catal. B-Environ.* **2006**, *62*, 244.

15 Perez-Ramirez, J.; Kumar, M. S.; Bruckner, A. *Journal of Catalysis* **2004**, *223*, 13.

16 Yang, J. C.; Small, M. W.; Grieshaber, R. V.; Nuzzo, R. G. *Chemical Society Reviews* **2012**, *41*, 8179.

3

Partial oxidation of ethane under batch conditions

3.1 Introduction

As shown in Chapter 1, current synthetic industrial processes for the oxidative upgrading of ethane follow two main routes, specifically; the steam cracking of ethane to ethene and direct oxidation of ethane to acetaldehyde and acetic acid.[1-3] Meanwhile, acetic acid is produced on a global scale via methanol carbonylation (60% global output), a highly ‘’ungreen’’ process which has a huge environmental and economic impact.[4, 5] Whilst academic studies have shown the direct selective oxidation of ethane, these typically require high temperatures, high pressures and acidic media, whilst operating at relatively low conversion. A direct low temperature process for the conversion of ethane to higher value products such as acetic acid, ethanol and ethene would provide a greener, more sustainable route to those traditionally used.

The initial studies of the Dow Methane Challenge built upon the work of Panov *et al* who reported that iron and copper modified ZSM-5 (30) may be activated for the oxidation of methane to a chemisorbed methoxy species, through high temperature pre-treatment in either N_2O or O_2.[6-8] Recent publications from the Hutchings Group, Cardiff have shown Fe- and Cu- containing ZSM-5 (30) catalysts to be active for the partial oxidation of methane to methanol using a green oxidant (H_2O_2) and solvent (H_2O) at low temperatures.[9-11] Key to the activity shown by high temperature-activated H-ZSM-5 (30) and Fe/ZSM-5 (30) was the formation of extraframework diiron μ-oxo active sites which

are capable of activating not only the oxidant but also the C-H bond in methane. Given that ethane is more soluble in water than methane (56 mg $_{gas}$ / L_{water} and 22.7 mg $_{gas}$ / L_{water} respectively, at 20 ^{o}C) coupled with its lower C-H bond strength (423.29 kJ mol^{-1} and 439.57 kJ mol^{-1} respectively) the ZSM-5 (30) based system was tested for ethane oxidation. Initial studies were conducted by M. Forde, who showed that a range of C_2 and C_1 products could be derived from ethane, whilst the process was also optimised to yield 56% conversion with 70% selectivity to acetic acid. In contrast to the methane oxidation system, rather than shut off selectivity to acetic acid and enhance ethanol selectivity, addition of either Cu or Fe/Cu to ZSM-5 led to high selectivity towards ethene of up to 38% (at 1.4% ethane conversion, Productivity $_{Ethene}$ = 8.0 h^{-1}).This work has been published recently,[12] with M. Forde's contributing the process optimisation aspect of the work, whilst R. Armstrong conducted studies as to the elucidation of the reaction scheme as well as catalyst stability and reusability tests. This work forms the latter part of Chapter 3 of this thesis, which also contains novel studies conducted following submission of said article, with all work shown being my own.

3.2 Time on line analysis

Initially, standard reaction conditions were adopted based upon those used in previous methane oxidation studies conducted by C. Hammond *et al*[10] such that a standard reaction volume of 10 ml, temperature of 50 ^{o}C, duration of 0.5 h, hydrogen peroxide concentration of 0.5 M equating to 5,000 μmol, ethane pressure of 20 bar, stirring rate of 1500 rpm and catalyst loading of 27 mg were used.[9] Said conditions were comparable to those used by Yuan *et al* in the $OsCl_3$ catalysed partial oxidation of ethane and methane with H_2O_2, discussed in Chapter 1.[13] For initial studies, ZSM-5 (30) with 2.5 wt% of

deposited Fe, was selected as the catalyst of choice, based upon previous studies which have shown said material to be highly active, showing productivities of 14.0 mol (C_1 oxygenates) kg^{-1} (catalyst) h^{-1} for the partial oxidation of methane with H_2O_2, as discussed in Chapter 1.[9] One alteration was made to the reaction protocol which was reported for ZSM-5 (30) catalysed ethane/ methane – H_2O_2 oxidation systems in that for all batch reaction studies featured in Chapters 3 and 5, the aqueous reaction phase was vigorously stirred whilst ramping to reaction temperature.[9, 12] This was suggested in our recent ethane oxidation article in JACS to have a significant impact upon primary product selectivity through ensuring thermal dissipation during the ramping period. Stirring the system for the 11 minute ramping period dissipated the heat generated due to the self-propagating exothermic nature of H_2O_2 decomposition, thereby avoiding formation of hot-spots on the reactor wall.[12]

To begin with, a time on line analysis of the activity and selectivity of 2.5% Fe/ZSM-5 (30) prepared via CVI, under the standard conditions stated previously (S. 2.4.1) was conducted in order to determine the identity of primary reaction products. Product selectivities and ethane conversion over a 4 h reaction coordinate are shown in Figure 3.1.

It is clear from the time on line in Figure 3.1 that the major aqueous products of 2.5% Fe/ZSM-5 (30) catalysed ethane oxidation are acetic acid and ethanol, whilst acetaldehyde is also observed at appreciable selectivities. A significant degree of C-C scission is evident from the selectivity shown towards formic acid, methanol and methylhydroperoxide. C_1 products are a clear indication of C-C bond cleavage, with proposed cracking products being carbon centred C_1 radicals (·C). Interestingly we detected ethene in the gas effluent, the role of which is explored later. A species which has been identified as ethylhydroperoxide, the C_2 analogue of methylhydroperoxide was

also quantified in the aqueous phase, having a ^{1}H chemical shift of 4.1 ppm. The role of said alkyhydroperoxy species is explored later in this chapter.

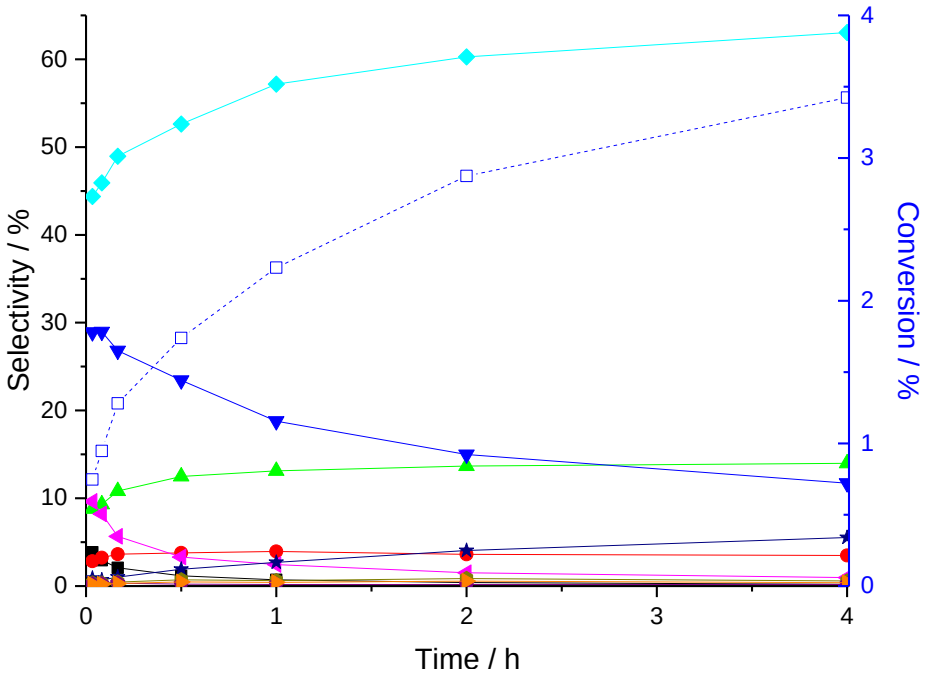

■ Black squares (CH_3OOH), ● Red Circles (CH_3OH), ♦ Aquamarine diamonds (CH_3COOH), ◀ Pink triangles (CH_3CHO), ▼ Blue triangles (C_2H_5OH), ▲ Green triangles (HCOOH, ▶ Orange triangles (CH_3CH_2OOH), ● Beige circles (CH_4), ★Navy Stars (CO_2), ⬟ Purple pentagons (C_2H_4), -□- Blue squares (% Conversion)

Reaction conditions; 27 mg catalyst, [H_2O_2] = 0.5 M (5000 µmol), P (C_2H_6) = 20 bar, Temp = 50°C, Stirring speed 1500 rpm – including ramp period.

Figure 3.1 Time on line profile showing product selectivities for ethane oxidation using 2.5% Fe/ZSM5 (30) CVI.

In order to more accurately present product selectivities at short reaction times (≤ 1h) and thereby determine primary oxidation products and consecutive oxidation pathways, major and minor product selectivities at short reaction durations are shown in Figure 3.2 (a) and (b) respectively, as are ethane conversions.

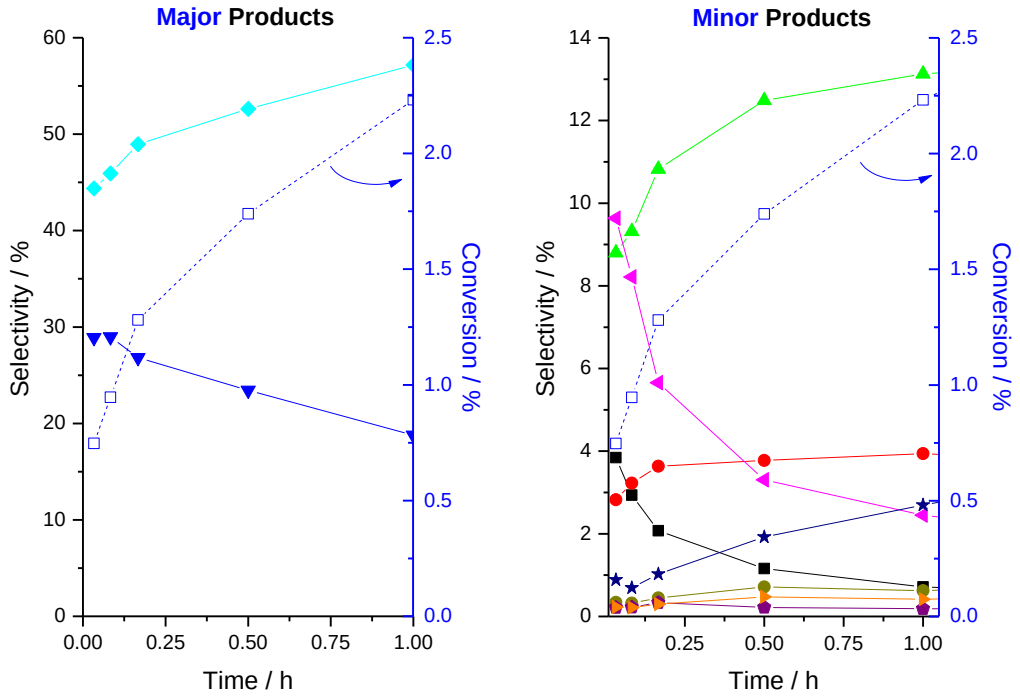

■ Black squares (CH_3OOH), ● Red Circles (CH_3OH), ♦ Aquamarine diamonds (CH_3COOH), ◀ Pink triangles (CH_3CHO), ▼ Blue triangles (C_2H_5OH), ▲ Green triangles (HCOOH, ▶ Orange triangles (CH_3CH_2OOH), ● Beige circles (CH_4), ★Navy Stars (CO_2), ⬟ Purple pentagons (C_2H_4), -□- Blue squares (% Conversion)

Figure 3.2 Time on line profiles showing major (a) and minor (b) product selectivities and ethane conversion at short reaction times (≤ 1h).

Based upon selectivity trends shown in figure 3.2 (a) it is apparent that ethanol is a major primary product of 2.5% Fe/ZSM-5 (30) catalysed ethane oxidation. Given that ethanol selectivity was shown to decrease with time, mirrored by increasing acetic acid selectivity it is suggested that the former undergoes consecutive oxidation to the latter. The decreasing selectivity to acetaldehyde shown in Figure 3.2 (b) suggests that this also undergoes oxidation to acetic acid, which would consistent with previous studies.[14] Acetaldehyde could be formed either through ethanol oxidation, or as an oxidation product of either ethene or ethylhydroperoxide. [15, 16] The decrease in methylhydroperoxide selectivity with time, and increases in methanol and formic acid selectivities is consistent with previous methane oxidation studies, which showed

methylhydroperoxide to be the primary oxidation product, which underwent consecutive oxidation to methanol, formic acid and CO_2 as deep oxidation product. C_1 oxygenates may form either through C-C scission to carbon based radicals (·C) or through oxidation of methane, which is observed as a gaseous reaction product. The presence of methane is itself indicative of C-C scission and the presence of ·C species. EPR radical trapping studies (with 5,5'- dimethylpyrrolidine (DMPO)) have shown the presence of both methyl ($\cdot CH_3$) and hydroxyl (·OH) radicals in the aqueous product.[12] Studies featured later in this chapter (Sections 3.7.1 and 3.7.4) indicate ethylhydroperoxide and ethene as additional primary oxidation products – along with ethanol.

3.3 The role of zeolite acidity

Given that ZSM-5 is a known solid acid catalyst which exhibits both Brønsted and Lewis acidity, and that said properties have been shown to play an important role in hydrocarbon activation,[17] commercial samples of H-ZSM-5 of varying SiO_2: Al_2O_3 molar ratios (Sourced from Zeolyst) were tested for ethane oxidation under standard reaction conditions; 27 mg catalyst, $[H_2O_2]$ = 0.5 M, 10 ml, 50 ^oC, 0.5 h, 1500 rpm, 20 bar. Ethane conversion and H_2O_2 conversion are shown in Figure 3.3.

Higher alumina content is associated with a general decrease in ethane conversion, with H-ZSM-5 (280) being the most active (0.06% conversion) and H-ZSM-5 (23) the least active (0.014% conversion). A similar trend was reflected by the H_2O_2 usage which fell from 31.9% to 14.2% across the range. The product selectivities for tests of H-ZSM-5 of varying acidity are shown in Figure 3.4 (selectivities shown are those observed for reactions represented in Figure 3.3).

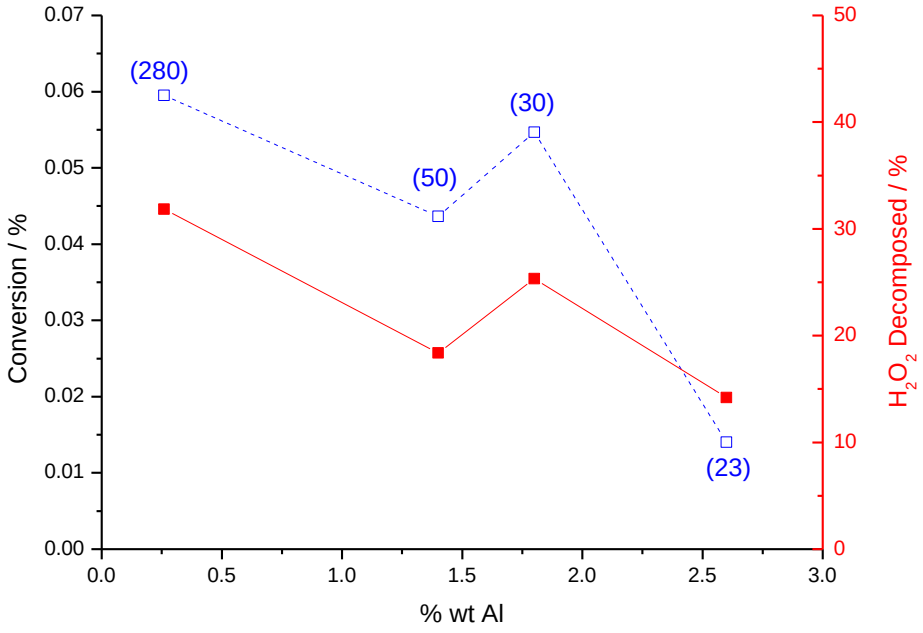

-□- Blue squares (% Conversion, based on Carbon) ■ Red squares (% H_2O_2 used) (SiO_2/Al_2O_3)

Reaction conditions; 27 mg catalyst,10 ml reaction volume, [H_2O_2] = 0.5 M (5000 µmol), P (C_2H_6) = 20 bar, 0.5 h, Temp = 50°C, 1500 rpm .

Figure 3.3 Ethane conversion and H_2O_2 conversion for a range of ZSM-5 materials

Figure 3.4 shows clear trends in ethane oxidation selectivities upon increasing the alumina content of H-ZSM-5. Upon increasing Al content (increasing Brønsted acidity), a corresponding increase in ethanol and ethylhydroperoxide selectivities is observed. This is coupled with a decrease in acetaldehyde and acetic acid selectivities. Later in this chapter it is shown that both ethylhydroperoxide and ethanol oxidise to acetaldehyde and acetic acid under reaction conditions. It therefore appears that Brønsted acid sites may be stabilising both hydrogen peroxide and primary products. The degree of activity shown results from the presence of highly active framework iron species in H-ZSM-5 samples which results from iron contamination (*ca. 100-200 ppm*) which is endemic with zeolites due to contamination during preparation. However, the trends in selectivity were determined not to be proportional to iron content, but rather aluminium content, as shown in Figure 3.4. The stabilisation of ROOH (R= H, CH_3CH_2) hydroperoxide species by Brønsted acids in Fenton's- type systems was found to be consistent with previous studies

by Jung *et al*, suggesting that Al sites may play a stabilising role.[18] It is interesting to note that with increased aluminium content zeolite hydrophilicity also increases, with a major hydrophilic- hydrophobic shift known to occur for ZSM-5 at a SiO_2/Al_2O_3 ratio of 20, meaning that H-ZSM-5 (23) is likely significantly more hydrophilic than H-ZSM-5 (30).[19, 20] As the pores of H-ZSM-5 (23) are predicted to be markedly more hydrophilic than those of the other zeolites tested,[20] it is possible that the enhanced primary product selectivities observed at higher wt% Al results from more efficient removal of primary products from within the zeolite pores, promoted by increased water adsorption. This would reduce contact times and therefore consecutive oxidation steps.

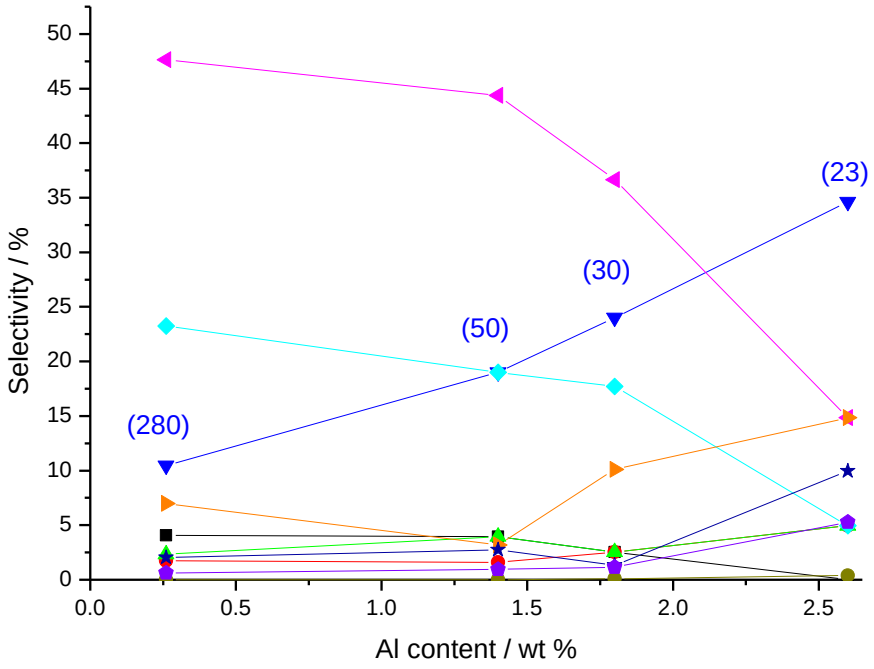

■ Black squares (CH_3OOH), ● Red Circles (CH_3OH), ♦ Aquamarine diamonds (CH_3COOH), ◀ Pink triangles (CH_3CHO), ▼ Blue triangles (C_2H_5OH), ▲ Green triangles ($HCOOH$), ● Beige circles (CH_4), ★Navy Stars (CO_2), ⬟ Purple pentagons (C_2H_4), ▶ Orange triangles (CH_3CH_2OOH), (SiO_2/Al_2O_3)

Figure 3.4 Product selectivities for a range of ZSM-5 materials.

The effect of silica alumina ratio in H-ZSM-5 for aqueous methane oxidation with H_2O_2 was previously reported, with no apparent correlation made between acidity and selectivity.[21] On the other hand SiO_2: Al_2O_3 was shown by Rahman *et al* to influence ethane oxidation product selectivities, with high alumina H-ZSM-5 (23) shown to favour acetic acid and formic acid, coupled with lower CO_2 selectivities than higher silica H-ZSM-5.[22] In said studies, aqueous products were quantified by GC analysis. Given that studies featured later in this chapter have shown ethylhydroperoxide and acetaldehyde to oxidise to acetic acid, it could be suggested that true product distributions were not realised. Due to the relatively high conversion shown by H-ZSM-5 (30) and the intermediate selectivity towards ethanol (24%), H-ZSM-5 (30) was chosen for further investigation and optimisation. Chapter 5 further explores the relationship between Brønsted acidity and product selectivities.

3.4 Choice of Fe/ZSM-5 post synthesis deposition technique

A number of techniques may be used in exchanging cations with the surface protons of zeolites such as H-ZSM-5 (30). Simultaneous deposition of a range of iron oxide species onto the zeolite surface and within micropores also results. To investigate the effect of preparation technique upon catalyst activity 2.5wt% Fe was deposited onto H-ZSM-5 (30) via; impregnation (IMP), ion exchange (IE) and chemical vapour impregnation (CVI).

Physical properties of these catalysts; iron content, surface area and micropore volume, are shown in Table 3.1. It is clear that there is limited variation in the physical properties with deposition technique. BET surface areas are within the 5% instrument error and that the three techniques allow for accurate control of iron loading, with *ca* 2.5% Fe content determined for the three samples.

Table 3.1 Physical characteristics and TOF of 2.5% Fe/ZSM-5 (30) prepared via different techniques

Technique	Fe content (wt %) [a]	S_{BET} (m^2g^{-1})	$V_{Micropore}$ (cm^3g^{-1})
ZSM-5 (30)	0.0132	386.3	0.153
Ion exchange (IE)	2.53	393.3	0.152
Impregnation (IMP)	2.52	405.2	0.163
Chemical vapour infiltration (CVI)	2.50	396.7	0.143

Note: Samples were calcined in static air for 3 h at 550^oC.[a] Determined by ICP-MS

Representative transmission electron microscope images and corresponding size particle distributions (determined using ImageJ software) for 2.5% Fe/ZSM-5 (30) samples prepared via CVI, IMP and IE are shown in Figure 3.5. Upon considering the images and distributions it is clear that CVI affords small iron oxide species of a narrow particle size distribution compared with the other post synthesis deposition techniques, with CVI, IMP and IE showing mean particles diameters of 4.2, 7.1 and 5.9 nm respectively. The CVI sample also showed the lowest standard deviation in size (1.58 nm) of the three samples.

Previous work by Forde *et al* has shown that, whilst Figure 3.5 (a) shows iron nanoparticles of mean 4.2 nm diameter, iron deposited on H-ZSM-5 (30) via CVI actually forms a porous film on the zeolite surface, with the defined nanoparticles observed in TEM images actually being an artefact of the electron beam being on the material.[12] Studies have shown that upon heating under vacuum (in the CVI preparation), the iron precursor Fe $(acac)_3$ sublimes and coats the surface of the zeolite and inside of its micropores, with iron centres isolated due to the steric bulk of the large acetylacetonate ligands.[12] Upon calcination, the ligands decompose and Fe^{3+} migrate to exchange sites, enter the pore structure and aggregate to Fe_xO_y species.

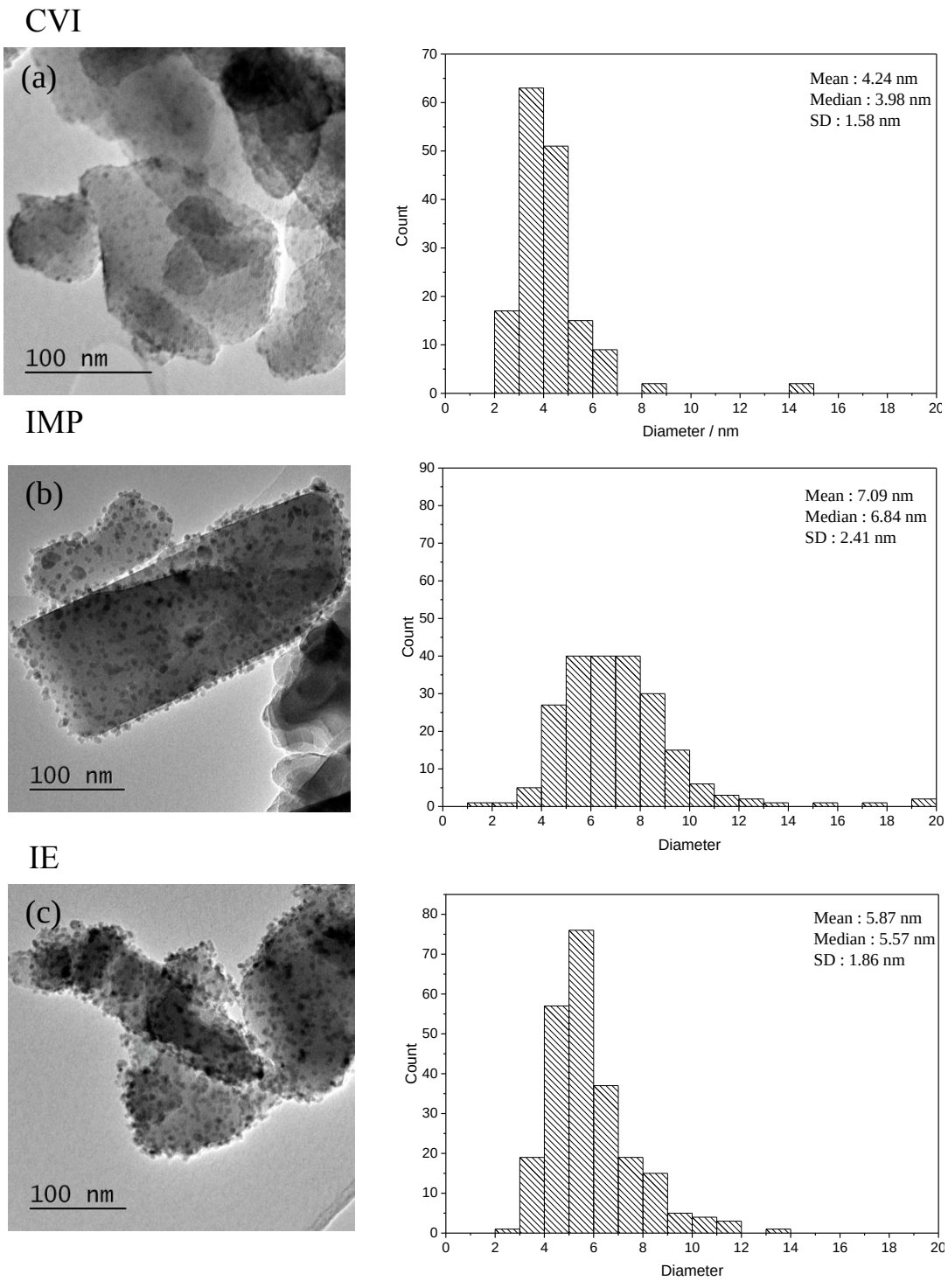

Figure 3.5 Representative low resolution TEM images and particle size distributions for 2.5% Fe/ZSM-5 (30) prepared by (a) chemical vapour impregnation, (b) impregnation and (c) ion exchange.

Comparison of the IR spectra for ZSM-5 (30) and 2.5% Fe/ZSM-5 (30) prepared by different techniques, presented in Figure 3.6, shows that the peak at 3607 cm^{-1}, which is attributed to OH groups which are coordinated to tetrahedral framework Al^{3+} sites decreases following deposition of Fe onto the catalyst.[23, 24] A corresponding increase in the peak at 3660 cm^{-1}, which is attributed to OH groups coordinated to extra-framework T-atom, is also observed.[25, 26] There is also a decrease in the intensity of the peak at 3520 cm^{-1} which corresponds to bridging OH groups with electrostatic character. Coupled with a reduction the in peak associated with terminal silanols/ non acidic surface silanols at 3737 cm^{-1},[27] IR spectra suggest that upon incorporation of Fe we have increased migration of framework Al^{3+} to extra-framework sites and formation of extra-framework of T-atoms (either Fe^{3+} or Al^{3+}).

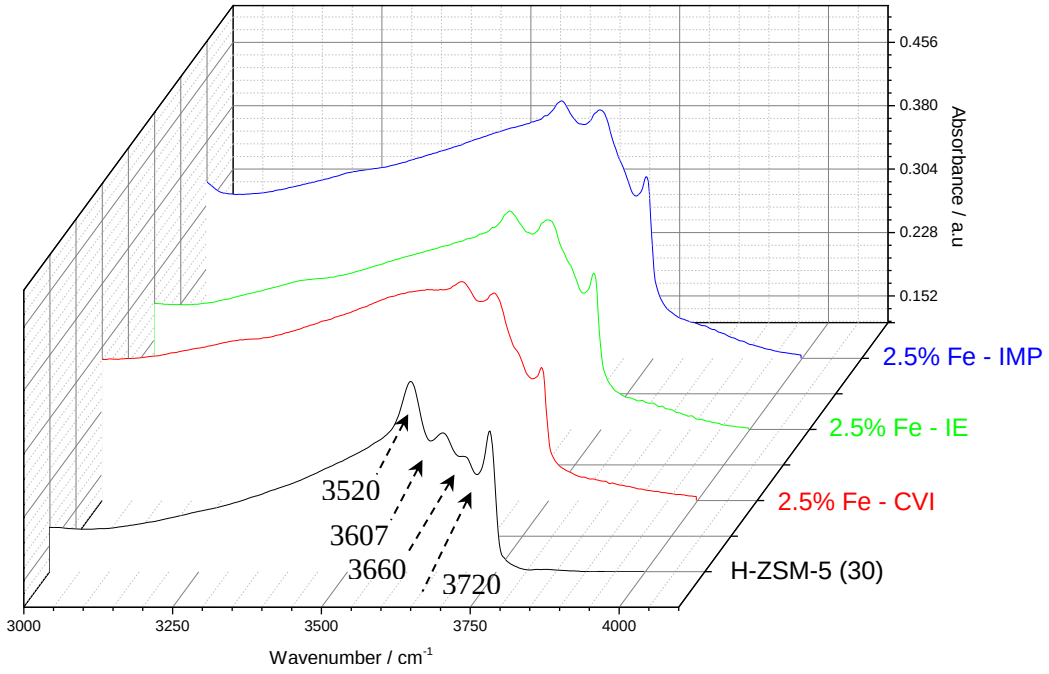

Figure 3.6 DRIFTS- IR spectra in the OH vibrational region for H-ZSM-5 (30) and 2.5% Fe/ZSM-5 (30) prepared via CVI, IMP and IE.

UV-Vis spectra were recorded for H-ZSM-5 (30) and Fe/ZSM-5 (30) loaded with 0.4, 1.25 and 2.5 wt% Fe prepared by CVI. Spectra are shown in Figure 3.7. It is widely accepted that there are four UV-Vis active species in ZSM-5 these are; (a) 200-250 nm (isolated Fe^{3+} in framework sites), (b) 250-350 nm (isolated or oligomeric extra framework Fe species), (c) 350-450 (iron oxide clusters) and (d) > 450 nm (larger iron oxide species on zeolite surface).[28-31] Figure 3.7 suggests that all 4 iron oxide species are present in Fe/ZSM-5 (30) catalysts prepared via CVI. TEM corroborates the presence of iron on the zeolite surface, whilst micropore analysis shows a slight reduction in micropore volume upon incorporation of Fe via CVI (Table 3.1). It appears that there is a significant amount of iron species within the zeolite pores, or exchanged as cationic extra framework species.

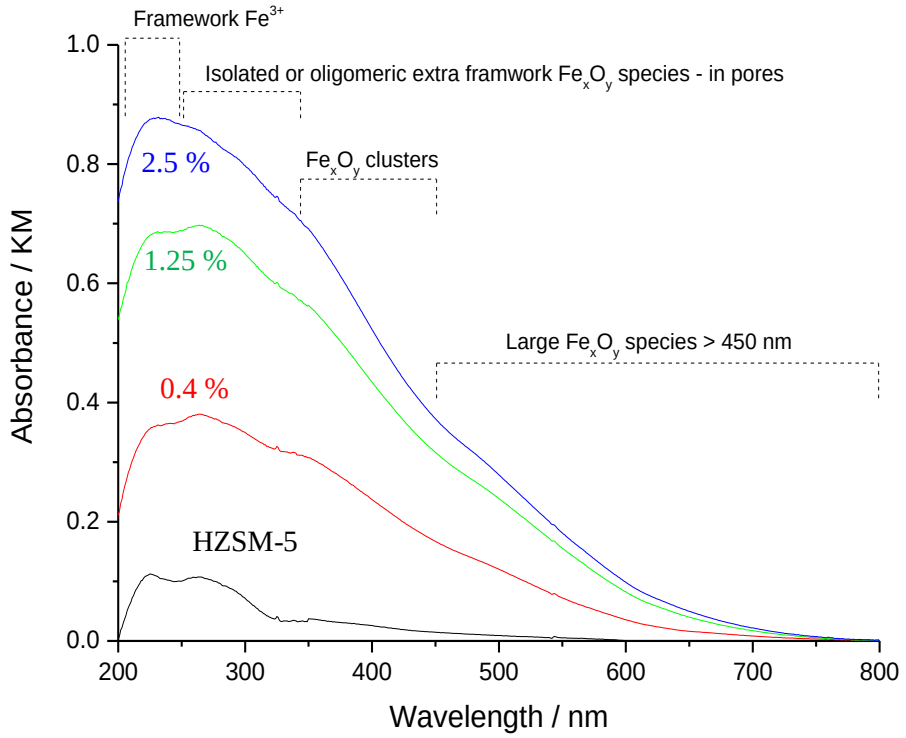

Figure 3.7 UV-Vis Spectra for H-ZSM-5 (30) and varying wt% Fe/ZSM-5 (30) prepared by CVI

Ethane conversion and yield of products formed upon testing of 2.5% Fe/ZSM-5 (30) materials are shown in Figure 3.8. It is clear that the technique used in depositing post synthesis Fe^{3+} impacts greatly upon catalyst activity, with CVI showing the highest ethane conversion (1.73%) followed by IMP (0.50%) and IE (0.45%). The three materials showed comparable C_2 selectivities (80% ± 0.4) however CVI showed the highest selectivity towards ethanol and acetic acid, 23.4% and 52.6% respectively. Iron loadings were quantified by ICP-MS, and shown to equal 2.5 wt% (±0.03). This allowed for calculation of TOF (h^{-1}) based on iron which followed the order of; H-ZSM-5 (30) (354.12 h^{-1}) >> 2.5% Fe/ZSM-5 (30) CVI (60.12 h^{-1}) >> 2.5% Fe/ZSM-5 (30) IMP (16.93 h^{-1}) > 2.5% Fe/ZSM-5 (30) IE (15.15 h^{-1}).

Despite being shown to be physically similar, the three materials differ greater with respect to their catalytic activity which follows the order CVI >> IMP > IE. This suggests that iron species formed for Fe/ZSM-5 catalysts via CVI are more than 4 times as active for the catalytic oxidation of ethane with H_2O_2 as traditional preparation methods.

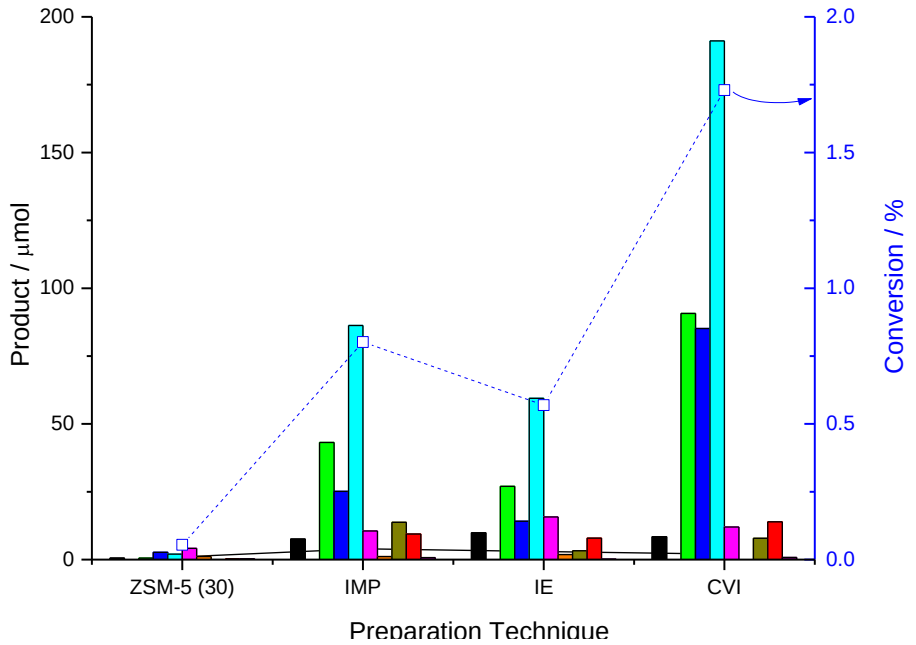

■ Black (CH_3OOH), ■ Navy (CH_3OH), ■ Aquamarine (CH_3COOH), ■ Pink (CH_3CHO), ■ Blue (C_2H_5OH), ■ Green ($HCOOH$), ■ Beige (CH_4), ■ Red (CO_2), ■ Purple (C_2H_4), -□- Blue (% Conversion, based on Carbon)

Test conditions: 27 mg catalyst, 10 ml reaction volume [H_2O_2] = 0.5M, P (C_2H_6) = 20 bar, 50°C, 0.5 h, 1500 rpm

Figure 3.8 Ethane conversion and product distribution for 2.5% Fe/ZSM-5 (30) prepared via various techniques.

It is clear that a number of iron species are present within CVI materials. The activity of said sites has previously been probed by M. Forde, who reported activity for; 2.5% Fe/SiO_2 (CVI), 0.5% Fe-Silicalite-1 (hydrothermal) and 0.4% Fe/ZSM-5 (30) CVI.[12] In 2.5% Fe/SiO_2 prepared by CVI the iron presented exclusively as small surface iron oxide species of *ca* 3 nm. Said material showed a comparable level of ethane conversion to H-ZSM-5 (30), though affording markedly different product selectivities with the silica supported iron sites favouring ethylhydroperoxide and acetaldehyde (*ca* 67% at 0.3% ethane conversion) whereas H-ZSM-5 (30) shows high selectivity towards ethanol (26%) and acetic acid (36%) (at 0.2% ethane conversion). The silica supported catalyst was reported to give significantly higher C_2 selectivity (92 % compared with 70% of H-ZSM-

5 (30)). This work suggested that small iron oxide species contribute to the oxidation of ethane observed for CVI materials, and also that the acid sites in ZSM-5 materials play a major role in the cracking to C_1 products.[12] 0.5% Fe-Silicalite-1 prepared by hydrothermal synthesis (Fe^{3+} incorporated during synthesis), and steamed prior to use has been shown to contain iron at isolated framework positions and also as extra framework iron species.[12] Despite having a similar loading of Fe, 0.4% Fe/ZSM-5 (30) CVI exhibited more than twice the activity of the neutral silicalite material (1.1% and 0.4% conversion respectively), despite decomposing a comparable % of total H_2O_2. (Table 3.2)

Table 3.2 Catalytic activity of 2.5% Fe/SiO_2, 0.5% Fe-Silicalite-1 and 0.4% Fe/ZSM-5 (30) for ethane oxidation. Modified from reference [12]

Catalyst	% Conv	Aqueous phase products **Selectivities[a] / %**					Gas phase products **Selectivities[b]/ %**			H_2O_2 used / products[c]
		CH_3OOH	CH_3OH	$HCOOH$	CH_3COOH	C_2H_5OH	Others[d]	CO_2	C_2H_4	
2.5% Fe/SiO_2 CVI	0.3	0.0	1.2	1.7	13.1	8.5	67.1	4.9	3.5	45
0.5% Fe-Silicalite - 1	0.4	1.3	3.2	6.8	30.4	40.0	14.4	2.4	1.5	20.7
0.4% Fe/ZSM-5 (30) CVI	1.1	1.0	5.0	13.8	49.2	18.9	6.0	2.4	4.7	7.8

[a] Analysed by ^{1}H-NMR [b]Analysed by GC-FID [c]Calculated as µmol H_2O_2 reacted / µmol products formed (C_2) [d] Combined selectivitied for CH_3CHO and CH_3CH_2OOH.

Reaction conditions; 27 mg catalyst, 10 ml reaction volume, [H_2O_2] = 0.5 M (5000 µmol), P (C_2H_6) = 20 bar, 0.5 h, Temp = 50°C, 1500 rpm (non-stirred during heating ramp)

0.4% Fe/ZSM-5 (30) prepared by CVI would have surface iron oxide species as well as extra framework iron at cation exchange sites and also iron oxide species within the zeolite pores as suggested by IR (Figure 3.6) and UV (Figure 3.7) studies. Given that both hydrothermal Fe-Silicalite and Fe/ZSM5 (CVI) materials contained a comparable weighting of iron, and that they both have the MFI structure, it is suggested that catalytic activity is not merely dependent upon total iron content but also the nature of iron species

present, with the multiple iron species present within the iron – modified zeolites being involved in different oxidative pathways. It is supposed that deposition of iron onto ZSM-5 (30) allows for deposition of both highly dispersed surface iron species on the acidic support as well as formation of different iron species within the zeolite pores. This is corroborated by the lower activity, lower C_2 selectivity and broader size distribution / greater mean particle size shown by 2.5% Fe/ZSM-5 (30) materials produced via traditional ion exchange or impregnation techniques (Figures 3.5 and 3.8). This is further explored in Chapter 5.

Given that methane conversion over Fe/ ZSM-5 (30) materials has previously been shown to increase with increasing iron loading, 0.4, 1.25 and 2.5 wt % Fe was deposited onto H-ZSM-5 (30) via CVI.[11] Representative TEM images for 0.4% Fe/ZSM-5 (30) and 2.5% Fe/ZSM-5 (30) are shown in figure 3.9 (a) and (b) respectively, whilst ethane conversion and TOF based on iron content are shown in Figure 3.10.

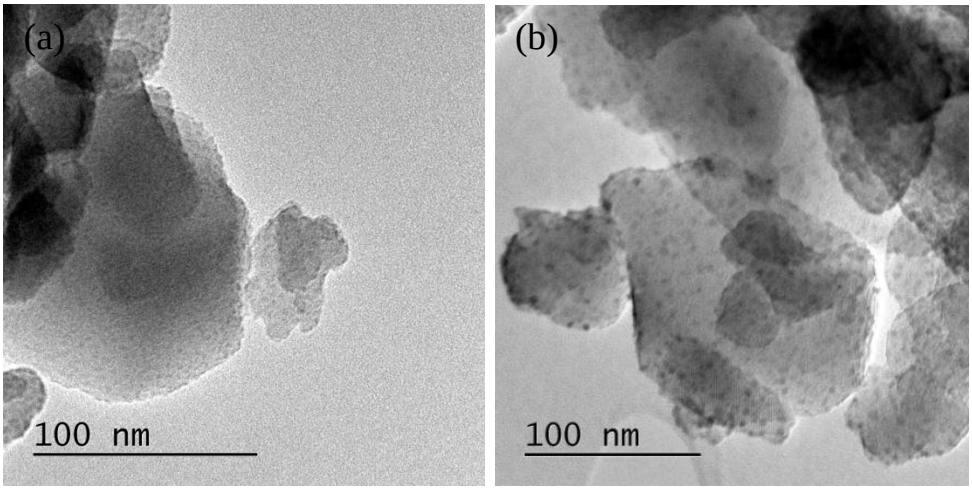

Figure 3.9 Representative low resolution TEM images of (a) 0.4% Fe/ZSM-5 (30) and (b) 2.5% Fe/ZSM-5 (30) prepared by CVI.

TEM images at 0.4 wt% Fe/ ZSM-5 (30) loading (a) show a lack of the large (>5 nm) iron oxide species on the zeolite surface. As such, it was not possible to determine a particle size distribution for deposited Fe_xO_y species at the lowest iron loading.

It is clear that iron species deposited onto ZSM-5 via CVI are active for the partial oxidation of ethane to oxygenates with H_2O_2, with a near linear increase in ethane conversion observed at increasing iron loading in Figure 3.10. Addition of 2.5 wt% Fe to H-ZSM-5 (30) results in increase in conversion from 0.05% to 1.73 %. Though not included, a proportional increase in H_2O_2 decomposition is also observed suggesting that the post synthesis iron species are active not only for the Fentons activation of H_2O_2, but also for the activation of the C-H bond in ethane. However as has been remarked upon previously,[9-12] the iron species present as diiron μ-oxo species in heat treated H-ZSM-5 (30) are significantly more active for alkane oxidation under these conditions than extra framework ion exchanged Fe^{3+} and iron oxide species as formed through deposition techniques such as CVI, IMP and IE. This is reflected in the rapid drop in TOF based on Fe content when 0.4% wt % Fe is deposited on H-ZSM-5 (30) (354.12 h^{-1} for H-ZSM-5 to 69.03 h^{-1} for 0.4% Fe/ZSM-5). The product selectivities for ethane oxidation using Fe/ZSM-5 (30) at various loadings of iron are shown in Figure 3.11.

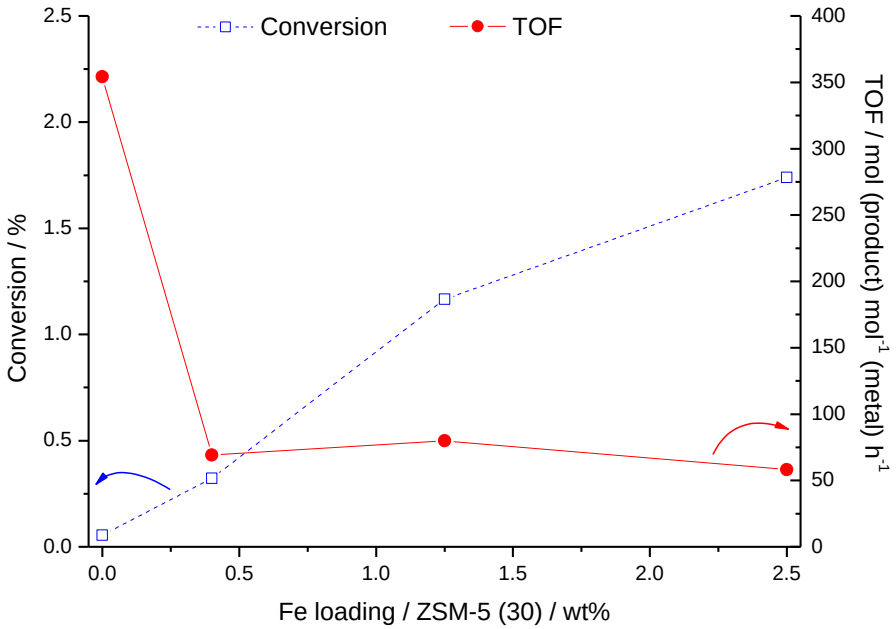

Reaction conditions; 27 mg catalyst, 10 ml reaction volume, [H_2O_2] = 0.5 M (5000 µmol), P (C_2H_6) = 20 bar, 0.5 h, Temp = 50°C, 1500 rpm

Figure 3.10 Ethane conversion and TOF as a function of Fe loading.

Upon addition of 0.4 and subsequently 1.25 wt % Fe onto ZSM-5 (30) via CVI, an increase in ethanol, acetic acid and formic acid selectivities is observed, whilst conversion increases in a linear fashion. Increasing Fe loading is observed to reduce selectivity towards acetaldehyde across the range of Fe loadings investigated. At Fe loadings of greater than 1.25% Fe, a shift in major product selectivity from ethanol to acetic acid is observed, suggesting that at higher loadings catalysts contain a greater proportion of species which play a role in the overoxidation of ethanol and acetaldehyde to acetic acid. Over the range of loadings tested, a decrease in C_2 product selectivity, from 89.6 to 79.6% was observed. Given that UV-Vis spectra suggest an increase in intensity of bands corresponding to large Fe_xO_y species at higher iron loadings, which is supported by the increased iron oxide particle size observed upon TEM analysis of 0.4 and 2.5 wt% Fe/ZSM-5 (30), it is inferred that formation of large iron oxide species becomes more favoured at higher Fe loadings. Given this, and considering the selectivity trends observed with increasing Fe loading, it is suggested that large Fe_xO_y species play a role in

the overoxidation of oxygenated products and in C-C scission to C_1 products, as with the higher conversions observed at 2.5 wt % Fe loading one would expect higher selectivity to ethanol, as the major primary oxidation product.

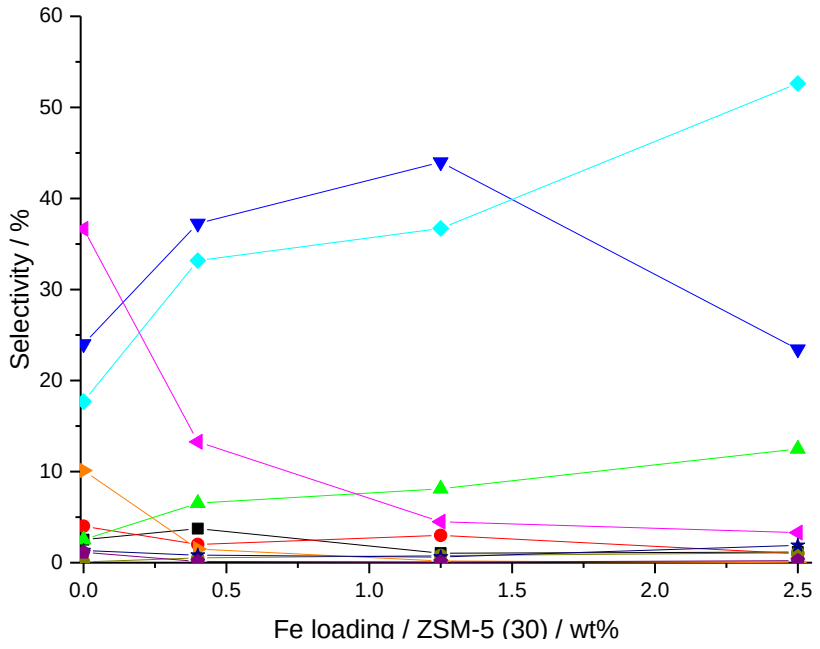

■ Black squares (CH_3OOH), ● Red Circles (CH_3OH), ♦ Aquamarine diamonds (CH_3COOH), ◀ Pink triangles (CH_3CHO), ▼ Blue triangles (C_2H_5OH), ▲ Green triangles (HCOOH, ▶ Orange triangles (CH_3CH_2OOH), ● Beige circles (CH_4), ★Navy Stars (CO_2), ⬟ Purple pentagons (C_2H_4),

Reaction conditions; 27 mg catalyst, 10 ml reaction volume, [H_2O_2] = 0.5 M (5000 µmol), P (C_2H_6) = 20 bar, 0.5 h, Temp = 50°C, 1500 rpm

Figure 3.11 Ethane oxidation product selectivities as a function of Fe loading.

XRD patterns for Fe/ZSM-5(30) CVI catalysts of varying Fe loading are shown in Figure 3.12. Consistent with the low average iron oxide particle diameter of 4.2 nm represented in the TEM image of 2.5% Fe/ZSM-5 (30) (Figure 3.6, a) there was no evidence of either Fe_2O_3 which would present as intense peak lines at 2θ = 33.15° and 35.65° or of Fe_3O_4 which shows intense reflections at 2θ = 30.27 and 35.53.[32, 33] It is accepted that particles of < 5 nm diameter are difficult to observe via XRD. In fact, no major new reflections were observed following deposition of iron.

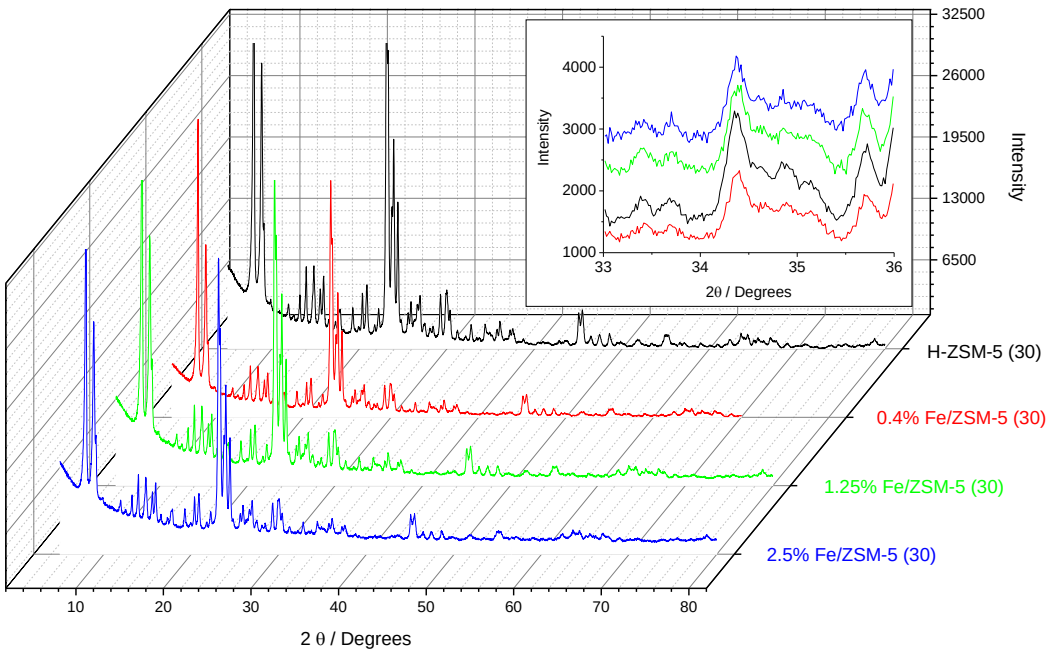

Figure 3.12 XRD patterns for catalyst of varying wt% Fe/ZSM-5 (30), inset graph; enlargement of characteristic Fe_2O_3 region

Diffraction lines were fit and compared with a reference XRD for ZSM-5 (30) (ref no^o 00-044-0003, pattern grade; Star (S)). The unit cell parameters determined for materials presented in Figure 3.12 are shown in Table 3.3. No apparent change in unit cell properties is observed upon deposition of iron ($\alpha,\beta,\gamma = 90\ ^o$, Orthorhombic (P) type Bravais lattice) with unit cell dimensions undergoing no significant change (Table 3.3). This suggests that whilst we are depositing extra framework iron species on the surface and within the micropores, iron is not being incorporated into the zeolite framework.

Table 3.3 Unit cell parameters for Fe/ZSM-5 (30) materials determined from XRD patterns.

Catalyst	a	b	c	Volume ($Å^3$)
[a] Reference	20.10	19.90	13.40	5359.87
H-ZSM-5 (30)	19.88	19.61	13.35	5204.55
0.4% Fe/ZSM-5 (30) CVI	19.94	19.69	13.29	5217.90
1.25% Fe/ZSM-5 (30) CVI	20.10	19.89	13.39	5353.18
2.5% Fe/ZSM-5 (30) CVI	19.92	19.88	13.38	5298.61

[a] Reference pattern no. 00-044-0003

In order to quantify the surface area (via multipoint BET), micropore volume and total pore volume of ZSM-5 (30) following deposition of iron, micropore analyses of these materials was conducted, the results of which are shown in Table 3.4. It is clear that deposition of iron has no significant effect upon surface area, however at higher iron loadings of 1.25 and 2.5 wt% a slight reduction in micropore volume (*ca* 6%) is observed. These results are consistent with previous observations that iron deposited onto ZSM-5 via CVI forms a film of iron species which coats the surface and inside of the zeolite's pore network.

Table 3.4 Physical properties of Fe/ZSM-5 (30) catalysts of varying wt% Fe prepared by CVI.

Catalyst	Fe content (wt %) [a]	S_{BET} (m^2g^{-1})	$V_{Micropore}$ (cm^3g^{-1})	$V_{Pore\ Volume}$ (cm^3g^{-1})
H-ZSM-5 (30)	0.0132	386.3	0.153	0.375
0.4% Fe/ZSM-5 (30)	0.40	395.8	0.152	0.375
1.25% Fe/ZSM-5 (30)	1.25	381.7	0.145	0.346
2.5% Fe/ZSM-5 (30)	2.50	396.7	0.143	0.345

3.5 The Effect of reaction parameters

Given the high catalytic activity and relatively high ethanol selectivity shown for 1.25% Fe/ZSM-5 (30) prepared by CVI, the reaction conditions and kinetic parameters were studied in order to elucidate the possible reaction scheme. A standard set of conditions was selected for this work; 27 mg 1.25% Fe/ZSM-5 (30) CVI, 10 ml reaction volume, $[H_2O_2]$ = 0.5 M (5000 μmol), P (C_2H_6) = 20 bar, 0.5 h, Temp = 50^oC, 1500 rpm

3.5.1 The effect of ethane pressure

The effect of ethane pressure upon conversion, H_2O_2 decomposition, C_2 productivity and C_2 product selectivity (ethanol, ethylhydroperoxide, acetic acid, acetaldehyde and ethene) is presented in Figure 3.13. Upon increasing pressure the conversion is shown to drop rapidly, from 20.1% at 1 bar to 1.2% at 20 bar ethane pressure. Coupled with the relatively stable productivity shown across the range of pressures it is implied that this is non- ethane limited system, as constant productivity suggests that the aqueous system is sufficiently saturated with ethane molecules. Interestingly, a drop in H_2O_2 decomposition and increase in C_2 selectivity is observed upon increasing ethane pressure. Product selectivities for 1.25% Fe/ZSM-5 (30) catalysed ethane oxidation at varying ethane pressure are presented in Figure 3.14.

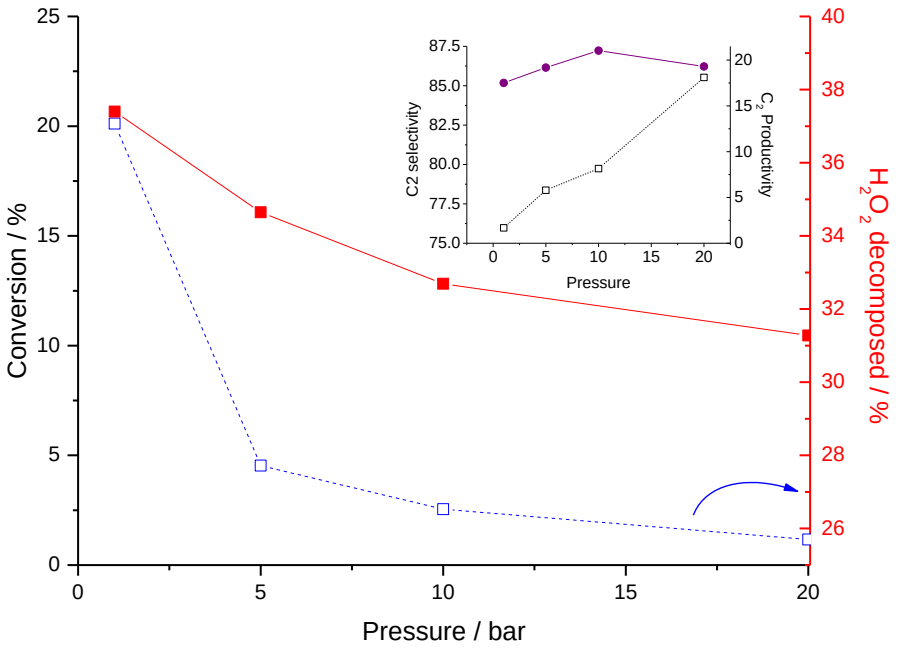

-□- Blue squares (% Conversion, based on Carbon) ■ Red squares (% H_2O_2 used) **Inset Graph -** □- Black squares % C_2 selectivity, ● Purple Circles (catalyst productivity –see experimental)

Reaction conditions; 27 mg 1.25% Fe/ZSM-5 (30) CVI, 10 ml reaction volume, [H_2O_2] = 0.5 M (5000 µmol), 0.5 h, Temp = 50°C, 1500 rpm

Figure 3.13 The effect of ethane pressure on the catalytic activity of 1.25% Fe/ZSM-5 (30).

As the pressure was increased from 1 to 20 bar, formic acid selectivity dropped from 17.8% to 8.11%. A simultaneous decrease in selectivity to acetic acid from 65.1 to 36.7% was also observed, coupled with an increase in ethanol selectivity from 7.8% to 44.0 %. Catalyst productivity across the range of ethane pressures averaged 17.83 h^{-1} ± 1.33 (Figure 3.13, Inset graph) Given that ethanol was suggested to oxidise to acetic acid (Figure 3.2) it appears that at higher pressures of ethane, primary product selectivity increases. Figure 3.13 also shows that C_2 selectivity increases with ethane pressure, coupled with lower hydrogen peroxide use, at higher ethane pressures.

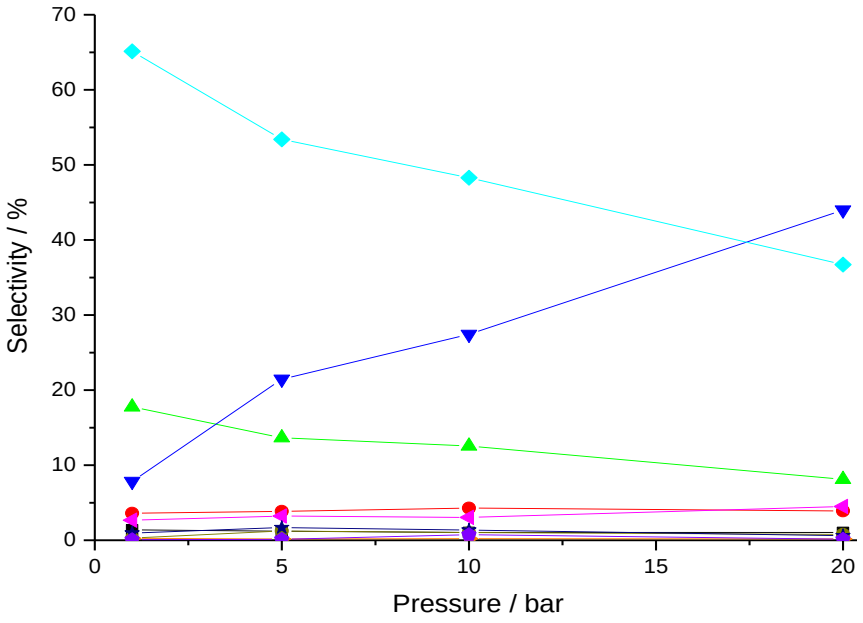

■ Black squares (CH_3OOH), ● Red Circles (CH_3OH), ♦ Aquamarine diamonds (CH_3COOH), ◀ Pink triangles (CH_3CHO), ▼ Blue triangles (C_2H_5OH), ▲ Green triangles ($HCOOH$), ● Beige circles (CH_4), ★Navy Stars (CO_2), ⬟ Purple pentagons (C_2H_4), ▶ Orange triangles (CH_3CH_2OOH)

Reaction conditions; 27 mg 1.25% Fe/ZSM-5 (30) CVI, 10 ml reaction volume, [H_2O_2] = 0.5 M (5000 µmol), 0.5 h, Temp = 50°C, 1500 rpm

Figure 3.14 The effect of ethane pressure on product selectivities for 1.25% Fe/ZSM-5 (30) catalysed ethane oxidation.

These trends are consistent with the previous observations from investigation of reaction conditions and methane oxidation with Fe/ZSM-5 (30) catalysts under batch conditions.[9] In previous studies, it was postulated that at higher pressures resulting in greater gas solubility, the increased ethane concentration had a stabilising effect upon oxygenated products and H_2O_2. This has been attributed to competitive adsorption onto the active site of the catalyst with ethane blocking the re-adsorption of oxygenated species, thereby inhibiting catalytic cracking and secondary oxidation reactions. An alternate or concurrent basis for this could also be that with increased ethane solubility at higher pressures we see a greater ethane to H_2O_2 ratio thereby favouring interaction between

substrate, oxidant and catalyst over desorbed primary product, oxidant and catalyst. This would lead selectivity to favour primary products.

3.5.2 The effect of ethane partial pressure

In order to further investigate the relationship between the partial pressure of ethane and primary product selectivities, a series of reactions were conducted under varying partial pressures of ethane and nitrogen. The effect of varying the reactant gas composition (*i.e.* partial pressures of ethane and nitrogen) at 20 bar total pressure is shown in Figure 3.15.

By varying the reactant gas composition from 10% ethane/ N_2 to 100% ethane composition we observe a significant increase in ethanol selectivity from 8.0% to 44.0% respectively. A corresponding decrease in selectivity towards acetic acid, formic acid and CO_2 is observed across the same range. Catalyst productivity is observed to increase from 15.9 to 17.9 h^{-1} upon increasing the ethane composition from 10% to 100%. The selectivities towards major products shown at 10% ethane content; acetic acid (62.7%), formic acid (16.2%), ethanol (8.0%) and CO_2 (3.5%) are comparable to those achieved at 1 bar ethane pressures as shown in Figure 3.14. Although conversion was shown to increase when moving to lower ethane content, with 1.1% conversion at 100% ethane and 7.9% conversion at 10% ethane/nitrogen content, the decrease in catalyst productivity indicates some competition with nitrogen. At higher partial pressures of nitrogen it is likely that nitrogen will account for a greater proportion of dissolved gas in solution, thereby leading to a similar effect to that seen at lower pressures (Figure 3.14). This is illustrated in Figure 3.15 by the gradual increase in μmol carbon present in products, a measure of productivity, as we move to higher partial pressures of ethane.

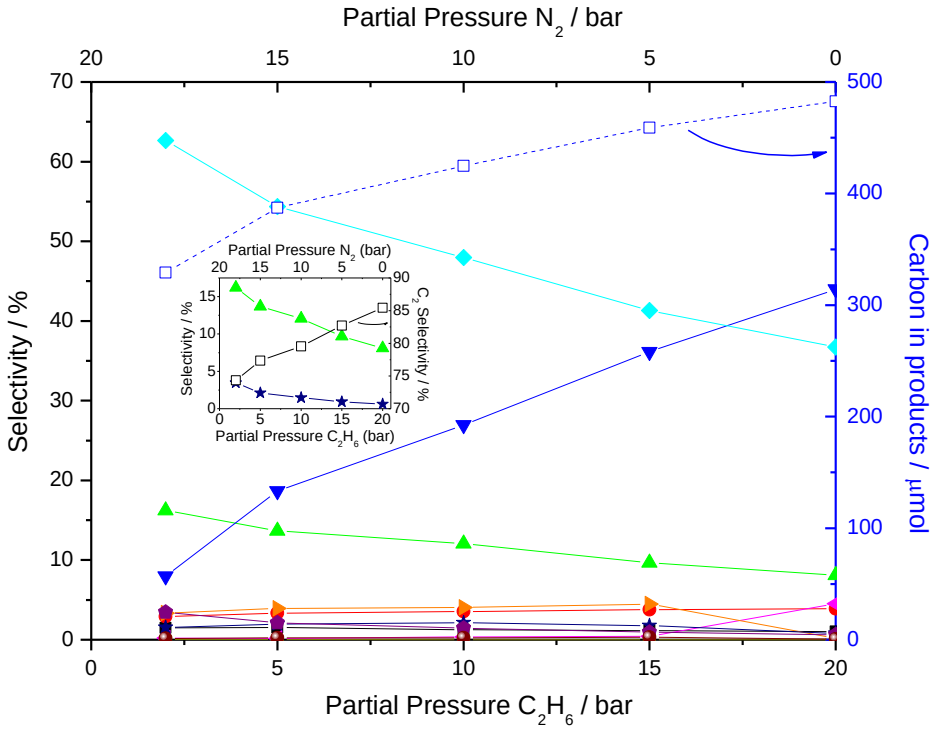

■ Black squares (CH_3OOH), ● Red Circles (CH_3OH), ♦ Aquamarine diamonds (CH_3COOH), ◀ Pink triangles (CH_3CHO), ▼ Blue triangles (C_2H_5OH), ▲ Green triangles ($HCOOH$), ● Beige circles (CH_4), ★Navy Stars (CO_2), ⬟ Purple pentagons (C_2H_4), ▶ Orange triangles (CH_3CH_2OOH), -□- Blue squares (Total Products µmol)

Inset graph; -□- Black squares (C_2 selectivity), ▲ Green triangles ($HCOOH$), ★Navy Stars (CO_2),

Reaction conditions; 27 mg 1.25% Fe/ZM-5 (30) CVI, 10 ml reaction volume, $[H_2O_2]$ = 0.5 M (5000 µmol), P (Total) = 20 bar, 0.5 h, Temp = 50°C, 1500 rpm

Figure 3.15 The effect of partial pressure of ethane upon productivity and selectivity

3.5.3 The effect of reaction temperature

The effect of temperature was then studied across the range of 30 °C to 70 °C with ethane conversion and hydrogen peroxide decomposition shown in Figure 3.16 and product selectivities in Figure 3.17. Higher temperatures were avoided for catalysed reactions due to the fact that auto-oxidation with methane and hydrogen peroxide has previously been observed at temperatures of ≥ 90 °C.

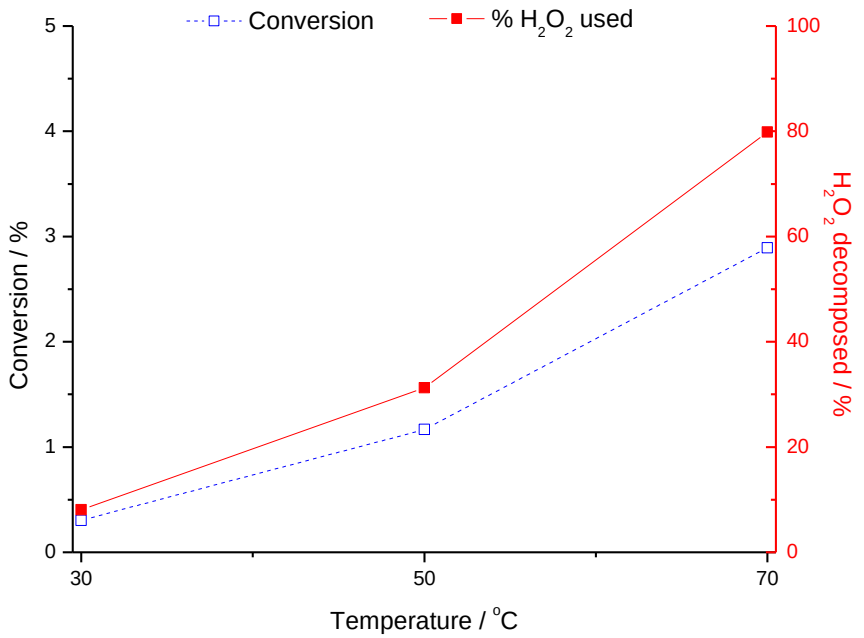

-□- Blue squares (% Conversion, based on Carbon) ■ Red squares (% H_2O_2 used)

Reaction conditions; 27 mg 1.25% Fe/ZSM-5 (30) CVI, 10 ml reaction volume, [H_2O_2] = 0.5 M (5000 µmol), P(C_2H_6) = 20 bar , 1500 rpm

Figure 3.16 The effect of reaction temperature on the catalytic activity of 1.25% Fe/ZSM-5 (30).

Ethane conversion is shown to increase with temperature, from 0.30% at 30 °C to 2.89% at 70 °C. A proportional increase in H_2O_2 decomposition, from 8.1% to 79.9% was also observed over the same temperature range. Product selectivities across the temperature range are presented in Figure 3.17. The key selectivity changes upon increasing reaction temperature are a reduction in ethanol selectivity, and increase in acetic acid and formic acid selectivities. At the lowest temperature studied (30 °C) ethanol selectivity equalled 61.7% which fell linearly to 18.1% at 70 °C. A corresponding increase in acetic acid (21.7 to 54.6%) and formic acid (3.8 to 15.8%) selectivities was also shown over the same range suggesting that ethanol is undergoing both overoxidation to acetic acid and C-C scission (Figured 3.17). A gradual decrease in C_2 selectivity is observed upon increasing

reaction temperature from 30 to 70 °C (91.3% and 74.3% respectively) suggesting that C-C scission becomes more favourable at elevated temperatures.

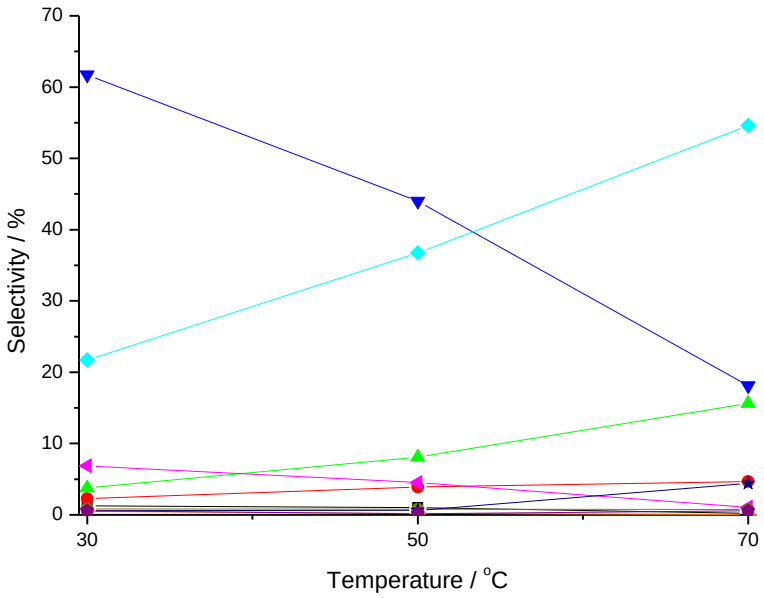

■ Black squares (CH_3OOH), ● Red Circles (CH_3OH), ♦ Aquamarine diamonds (CH_3COOH), ◀ Pink triangles (CH_3CHO), ▼ Blue triangles (C_2H_5OH), ▲ Green triangles (HCOOH, ▶ Orange triangles (CH_3CH_2OOH), ● Beige circles (CH_4), ★Navy Stars (CO_2), ⬟ Purple pentagons (C_2H_4)

Reaction conditions; 27 mg 1.25% Fe/ZM-5 (30) CVI, 10 ml reaction volume, [H_2O_2] = 0.5 M (5000 µmol), P (C_2H_6) = 20 bar, 0.5 h, 1500 rpm

Figure 3.17 The effect of reaction temperature upon product selectivities

It is clear from these studies that the consecutive oxidation of ethanol to acetic acid becomes more facile at higher temperatures. The drop in C_2 selectivity observed upon increasing temperature, resulting from increased deep oxidation to formic acid, implies that the increase in the concentration of hydroxyl radicals at higher temperatures enhances the potential for C-C scission of C_2 products.

3.5.4 The effect of hydrogen peroxide concentration

The effect of oxidant concentration was also studied over the range of 0.031 to 1 M, with ethane conversion, catalyst TOF and % H_2O_2 usage shown in Figure 3.18. At lower concentrations (0.031 M to 0.5M) a first order relationship between hydrogen peroxide concentration and activity is observed for the reaction when the first four points are fit to 0,0 origin. At the highest hydrogen peroxide concentration tested (1 M) some mass transfer limitation is apparent, given that conversion does not fit the linear trend. Interestingly, the percentage of peroxide which is decomposed appears to be independent of concentration.

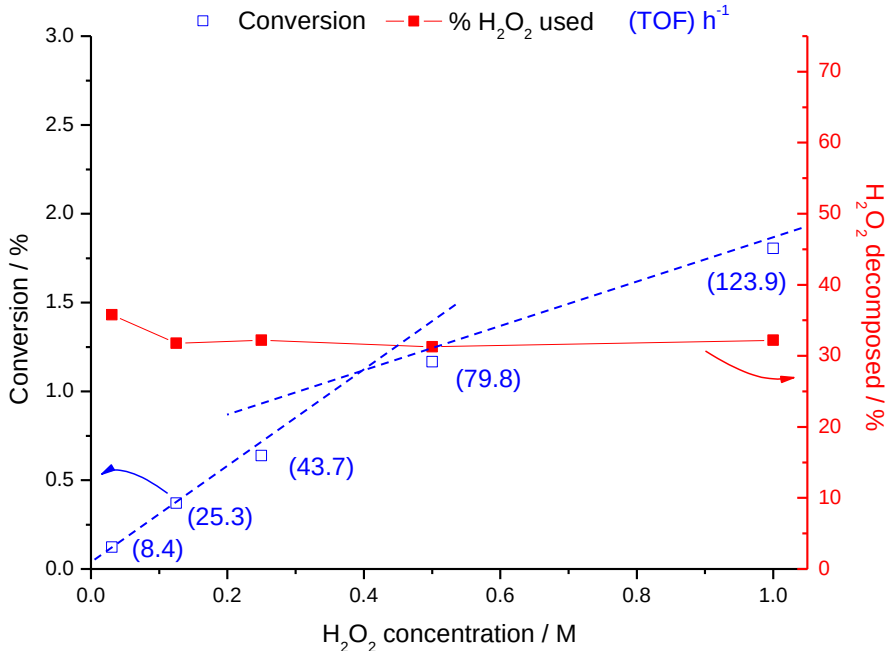

Reaction conditions; 27 mg 1.25% Fe/ZM-5 (30) CVI, 10 ml reaction volume, 50 ^{o}C, P (C_2H_6) = 20 bar, 0.5 h, 1500 rpm

Figure 3.18 The effect of H_2O_2 concentration on catalytic activity of 1.25% Fe/ZSM-5 (30)

Given that the reaction volume was maintained as constant, whilst the µmol H_2O_2 decomposed increases linearly with increased hydrogen peroxide concentration (as % decomposed remained constant), comparison of product selectivities (Figure 3.19) will provide important information regarding the role of hydroxyl (·OH) and hydroperoxy (·OOH) radicals in solution.

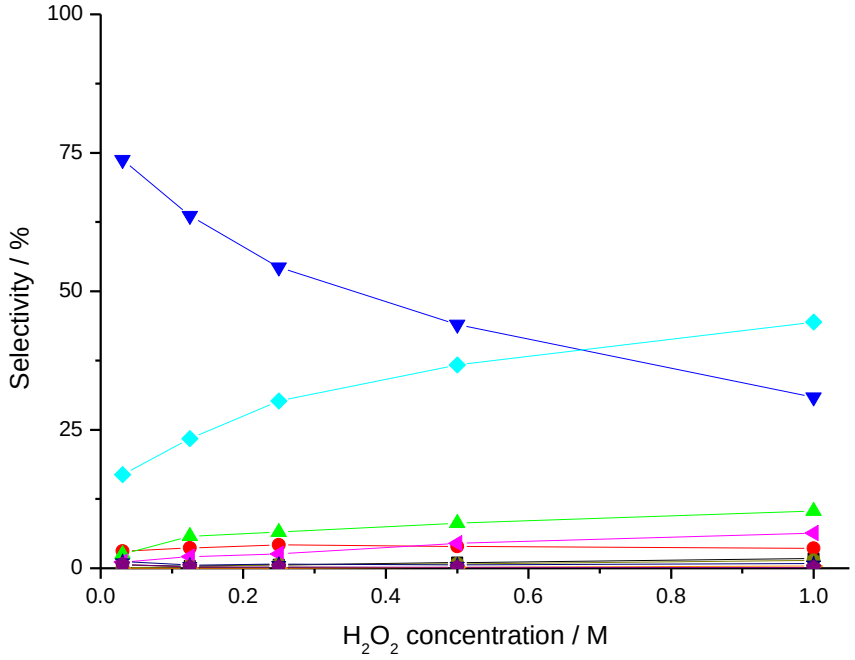

■ Black squares (CH_3OOH), ● Red Circles (CH_3OH), ♦ Aquamarine diamonds (CH_3COOH), ◀ Pink triangles (CH_3CHO), ▼ Blue triangles (C_2H_5OH), ▲ Green triangles (HCOOH, ▶ Orange triangles (CH_3CH_2OOH), ● Beige circles (CH_4), ★Navy Stars (CO_2), ⬟ Purple pentagons (C_2H_4),

Reaction conditions; 27 mg 1.25% Fe/ZM-5 (30) CVI, 50 °C, 10 ml reaction volume, P (C_2H_6) = 20 bar, 0.5 h, 1500 rpm

Figure 3.19 The effect hydrogen peroxide concentration upon product selectivities

As was shown for reactions under increasing conditions, an increase in the availability of oxidising radicals led to a gradual decrease in ethanol selectivity (74.9% to 30.9%), and corresponding increase in acetic acid (16.9% to 44.4%) and formic acid (2.5% to 10.3%) selectivities moving from 0.031 M to 1 M. This observation further suggests that ethanol

is being oxidised to acetic acid, which is then undergoing C-C cleavage to yield formic acid. Said oxidative pathway is shown to be in operation in Section 3.7.2.

3.5.5 The effect of catalyst mass

The final set of conditions studied was the effect of catalyst mass. Figure 3.20 demonstrates that under standard conditions, 1.25% Fe/ZSM-5 (30) is operating within the kinetic regime up to and including 54 mg loading. However, some diffusion limitation is implied at 108 mg.

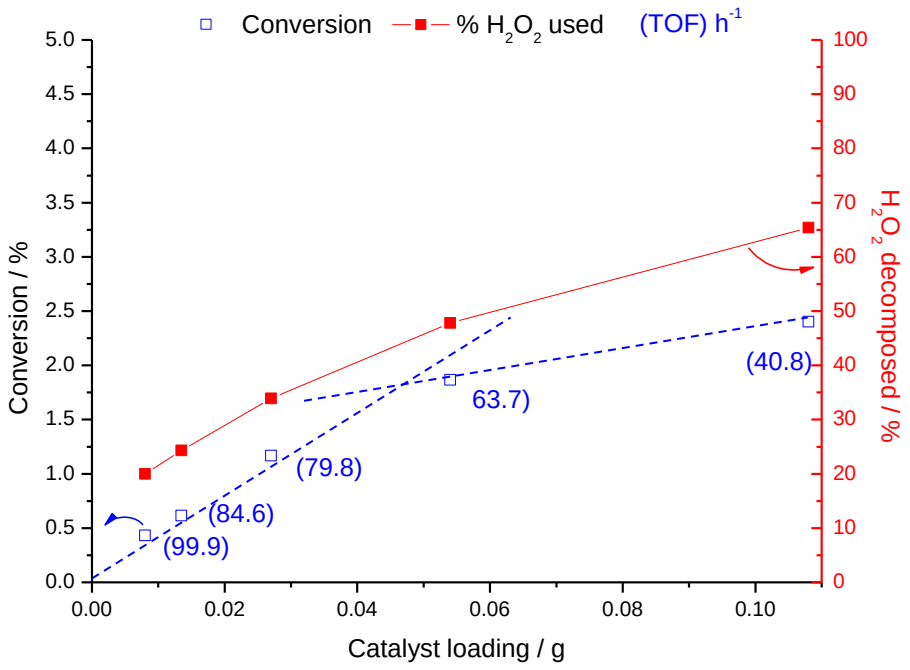

Reaction conditions; 1.25% Fe/ZM-5 (30) CVI, 10 ml reaction volume, [H_2O_2] = 0.5 M (5000 µmol), 50 ^oC, P (C_2H_6) = 20 bar, 0.5 h, 1500 rpm

Figure 3.20 The effect of catalyst loading on ethane conversion and hydrogen peroxide use

Upon increasing catalyst mass from 6.75 mg to 108 mg, ethane conversion is shown to increase, from 0.43 to 2.40% respectively, whilst hydrogen peroxide decomposition also

increased (from 20.0 to 65.4%). Whilst catalyst-free blank reactions conducted under the reaction conditions stated in Figure 3.20 showed no ethane activation, 13.1% hydrogen peroxide decomposition was observed. With the blank decomposition taken into account, peroxide decomposition is shown to not be directly proportional to catalyst mass, as the catalyst productivity for H_2O_2 decomposition decreases from 101.6 mol (H_2O_2) kg^{-1} (catalyst) h^{-1} at 6.75 mg loading to 48.4 (same units) at 108 mg loading. That ethane conversion increases with catalyst mass, as seen with increasing hydrogen peroxide concentrations at constant catalyst mass (Figure 3.18), implies that we have sufficient substrate in solution with mass transport of oxidant to active site limiting conversion. This is further supported by the decreasing catalyst productivity with respect to hydrogen peroxide decomposition at increasing catalyst loadings.

A similar trend in product selectivities is observed upon increasing catalyst loading as was seen with increasing oxidant concentration in that upon increasing catalyst mass, from 6.75 to 108 mg, an increase in acetic acid (27.3% to 52.7%), formic acid (6.1% to 14.3%) and CO_2 (0.6 to 2.2 %) selectivities was also observed. This was coupled with a decrease in ethanol selectivity (49.8% to 22.9%) and a consistent decrease in C_2 selectivity from 87.1% at 6.75 mg to 77.3% at 108 mg loading (Figure 3.21).

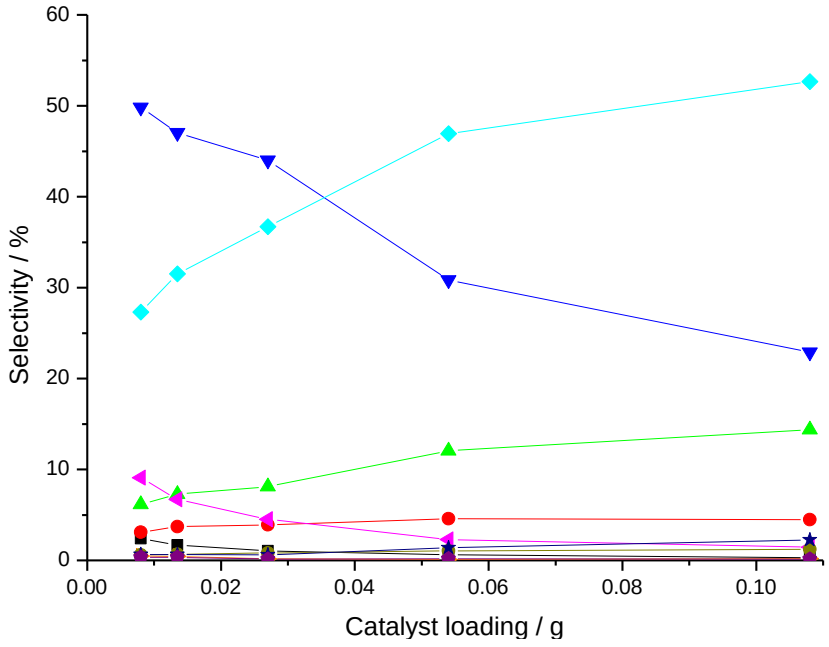

■ Black squares (CH_3OOH), ● Red Circles (CH_3OH), ♦ Aquamarine diamonds (CH_3COOH), ◀ Pink triangles (CH_3CHO), ▼ Blue triangles (C_2H_5OH), ▲ Green triangles (HCOOH, ▶ Orange triangles (CH_3CH_2OOH), ● Beige circles (CH_4), ★Navy Stars (CO_2), ⬟ Purple pentagons (C_2H_4),

Reaction conditions; 1.25% Fe/ZM-5 (30) CVI, 10 ml reaction volume, [H_2O_2] = 0.5 M (5000 µmol), 50 ^oC, P (C_2H_6) = 20 bar, 0.5 h, 1500 rpm

Figure 3.21 The effect of catalyst loading on product selectivities

From the data in this section (**3.5**), it appears that selectivity is dependent upon the starting C: O molar ratio, with low C_2H_6 to H_2O_2 ratio reactions showing increasing selectivity towards secondary products. This might be neatly illustrated by plotting product selectivities, observed in; ethane pressure, partial pressure and [H_2O_2] studies (from figures 3.14, 3.15 and 3.19) versus the reactions' C_2H_6:H_2O_2 molar ratios, as shown in Figure 3.22.

It appears that selectivity to secondary products increases with decreasing C_2H_6: H_2O_2 ratio, tending towards acetic acid and formic acid in particular.

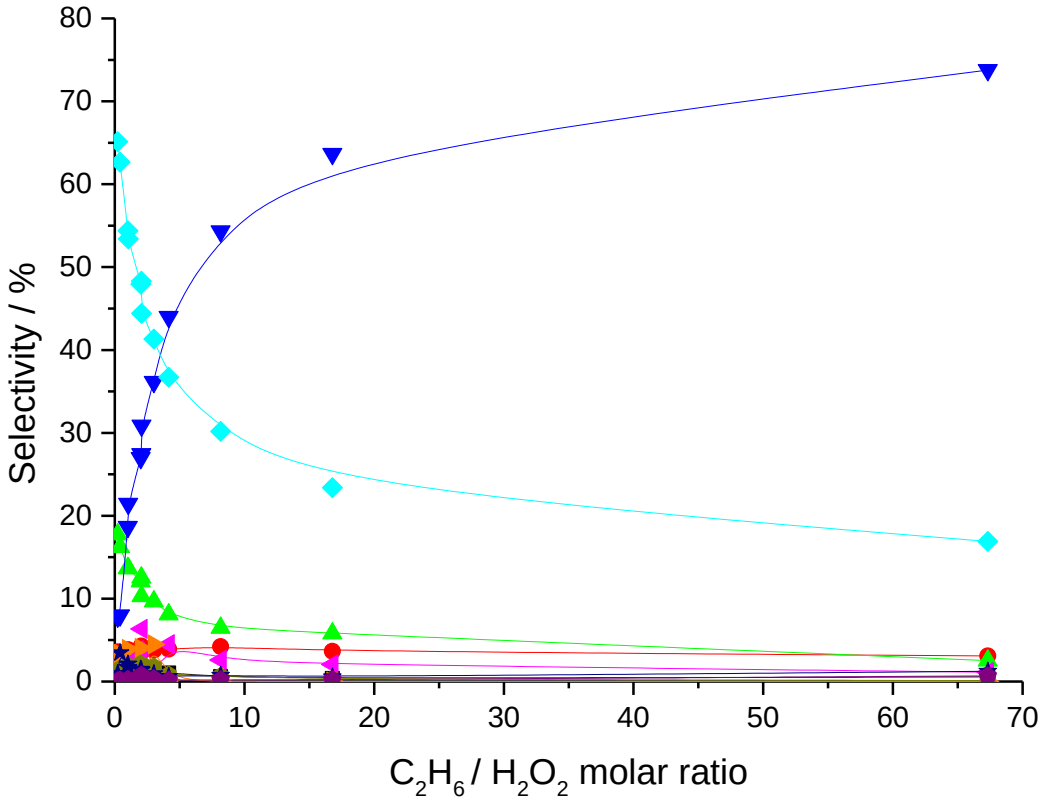

■ Black squares (CH_3OOH), ● Red Circles (CH_3OH), ♦ Aquamarine diamonds (CH_3COOH), ◀ Pink triangles (CH_3CHO), ▼ Blue triangles (C_2H_5OH), ▲ Green triangles (HCOOH, ▶ Orange triangles (CH_3CH_2OOH), ● Beige circles (CH_4), ★Navy Stars (CO_2), ⬟ Purple pentagons (C_2H_4),

Figure 3.22 The effect of C_2H_6: H_2O_2 ratio upon product selectivities

3.6 High Ethene selectivity through incorporation of copper

Since addition of Cu^{2+}, either as ion exchanged species or homogeneous copper, has been shown to suppress the overoxidation of methanol to formic acid under ZSM-5 and Fe/ZSM-5 catalysed methane oxidation systems with H_2O_2,[9] varying wt% of Cu^{2+} were deposited onto ZSM-5, along with 1.25 wt% Fe to ascertain whether high selectivity to ethanol may be achieved in the same way, ethane conversion and product selectivities are shown in Figure 3.23.

Aside from a slight decrease in conversion upon addition of an increase wt% Cu loading (CVI), the key and rather surprising effect of the addition of copper is the high selectivity towards ethene which is observed. Addition of copper leads to lower ethanol and acetic acid selectivity, with formic acid no longer observed as a reaction product at Cu: Fe ratios of greater than 1: 1 (by wt). At 1: 1 wt ratio Fe: Cu (1.25% wt of each metal), conversion of 1.15% to methanol (6.0%), ethanol (26.6%), acetic acid (19.9%), acetaldehyde (1.3%), CO_2 (0.41%) and ethene (45.5%) are observed. Given that Hammond *et al* reported that in the methane oxidation system, Cu^{2+} was scavenging ·OH radicals and thereby preventing oxidation of methanol to formic acid,[9] it is plausible that it is playing a similar role with respect to the oxidation of ethene. This would imply that ethene is a primary product of the reaction, which is then rapidly oxidised to ethanol and acetic acid in the absence of copper. This is further explored later in this chapter.

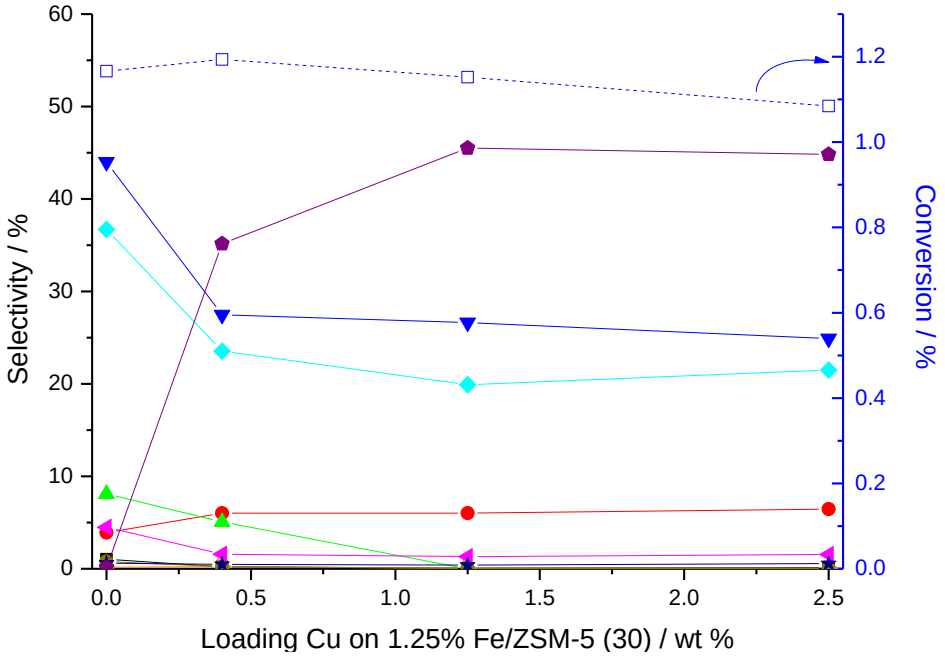

■ Black squares (CH_3OOH), ● Red Circles (CH_3OH), ♦ Aquamarine diamonds (CH_3COOH), ◀ Pink triangles (CH_3CHO), ▼ Blue triangles (C_2H_5OH), ▲ Green triangles (HCOOH, ▶ Orange triangles (CH_3CH_2OOH), ● Beige circles (CH_4), ★Navy Stars (CO_2), ⬟ Purple pentagons (C_2H_4), -□- Blue squares (% Conversion based on carbon)

Reaction conditions; 27 mg catalyst, CVI, 10 ml reaction volume, [H_2O_2] = 0.5 M (5000 µmol), 50 ^oC, P (C_2H_6) = 20 bar, 0.5 h, 1500 rpm

Figure 3.23 The effect of addition of varying wt% Cu to 1.25% Fe//ZSM-5 (30)

The IR spectrum for 1.25% Fe 1.25% Cu/ZSM-5 (30) is shown in Figure 3.24, with that of H-ZSM-5 (30) and 2.5% Fe/ZSM-5 (30) for comparison. For bimetallic Fe-Cu/ZSM-5 (30) the OH vibrational region is comparable to that of H-ZSM-5 (30) barring a shift in wavenumber of the peak attributed to T-atom coordinated OH groups (3650 cm^{-1} as opposed to 3662 cm^{-1}).

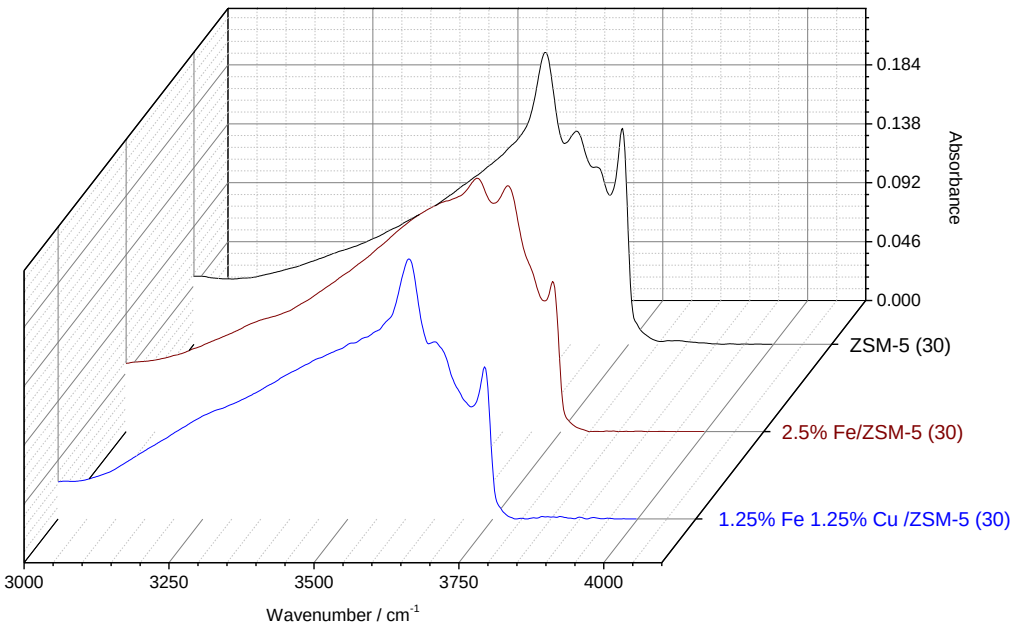

Figure 3.24 Drifts- IR spectra in the OH vibrational region for ZSM-5 (30), 2.5% Fe/ZSM-5 (30) CVI and 1.25% Fe 1.25% Cu/ZSM-5 (30)

Based upon these studies, a number of important insights may be gleaned with regards to the mechanism of ethane oxidation with Fe/ZSM-5 and H_2O_2.Firstly, it is clear that the oxidation of ethane is a catalytic process at 50 ^oC, given that no apparent conversion was observed in the absence of catalyst, at 50 ^oC (not included). Secondly, it is clear that ethanol is formed as a major primary product of ethane oxidation, and that it then undergoes catalytic oxidation to acetaldehyde and acetic acid. It is interesting to note the high selectivity towards ethylhydroperoxide (CH_3CH_2OOH) exhibited by Fe/SiO_2 (Table 3.2). Given that the C_1 analogue of this species (CH_2OOH) has previously been shown to be the sole intermediate in ZSM-5 catalysed methane oxidation with H_2O_2, it remains possible that ethylhydroperoxide, which is observed throughout this work at low concentrations, is a possible intermediate in the ethane oxidation pathway. C_2 oxygenated products then appear to undergo C-C scission, leading to the formation of C_1 products. It is also possible that ethane is itself undergoing C-C scission, with methyl radicals then

undergoing oxidation to C_1 oxygenates. The presence of methane in gas phase products further suggests that carbon based radicals may have a role in the mechanism. Electron paramagnetic resonance (EPR) radical trapping studies conducted by M. Forde with 5,5'-dimethylpyrrolidine (DMPO) have confirmed the presence of methyl ($\cdot CH_3$) and hydroxyl ($\cdot OH$) radicals in the aqueous product, however the presence of other species of either low concentration (such as $\cdot OOH$) of short lifetime cannot be discounted.[12]

In order to better understand the reaction pathway operating under ZSM-5 catalysed ethane oxidation conditions, a series of mechanistic studies were conducted.

3.7 Mechanistic Studies

3.7.1 CH_3CH_2OOH stability studies

It could be assumed that the *in situ* decomposition of the C_2 alkyl hydroperoxide, (CH_3CH_2OOH), progresses via a similar pathway to that of the C_1 intermediate CH_3OOH, such that the hydroperoxide decomposes to yield the alcohol as primary product, and the aldehyde and carboxylic acids as subsequent products.

To determine the role played by ethylhydroperoxide, stability studies were conducted in the presence of a range of heterogeneous, ZSM-5 catalysts. A solution containing an excess of ethylhydroperoxide (with respect to other products) was prepared under the following conditions;

''1.25% Fe/TiO_2 (85 mg), 30,000 µmol H_2O_2 (1M), total aqueous volume 30 ml $P(C_2H_6)$ = 20 bar, reaction duration = 20 h, temperature = 30^oC, solvent = D_2O.''

Samples of the filtered reaction mixture (0.7 ml) were added to NMR tubes along with (a) No catalyst, (b) ZSM-5 (30) – 1.8 mg, (c) 2.5% Cu/ZSM-5 (30) – 1.8 mg and (d) 2.5% Fe 2.5% Cu/ZSM-5 (30) – 1.8 mg. Multiple ^{1}H NMR were run at 15 min intervals so as to monitor the decomposition of the intermediate *in situ* at ambient temperature in the presence of ZSM-5 catalysts, results are shown in Figure 3.25. In all instances the metal: aqueous phase ratio reflected that encountered under standard batch reaction conditions.

Ethylhydroperoxide appears to be relatively stable under ambient conditions (Figure 3.25 a). In the absence of a catalytic surface, little decomposition is observed over a 12 h period. When brought into contact with H-ZSM-5 (30), ethylhydroperoxide is seen to decompose to acetaldehyde, which then undergoes further oxidation to acetic acid. Acetaldehyde and acetic acid then appear to undergo C-C scission, yielding formaldehyde and formic acid (b).

Introduction of 2.5% wt extra framework Cu^{2+} to the H-ZSM-5(30) leads to slight difference in the C_2 pathway (c), with ethylhydroperoxide yielding acetaldehyde primarily which rapidly oxidises to acetic acid. The key distinction seen is in the C_1 cracking products, whereby methylhydroperoxide, methanol and formaldehyde are seen in comparable amounts. The lack of formic acid is consistent with studies of FeCu/ZSM-5 (30) (Figure 3.23). When 2.5% wt of Fe is added (d), the rate with which the hydroperoxy species decomposes increases dramatically, yet follows a similar pathway with rapid oxidation of ethylhydroperoxide to acetaldehyde and then acetic acid. C_1 cracking products methanol and formic acid are observed, yet formaldehyde (CH_2O) is no longer formed. All products decompose to deep oxidation products (CO_2) within 8 h in the

presence of the extra-framework iron species present in 2.5% Fe 2.5% Cu/ZSM-5 (30). CO_2 / gas evolution is indicated by a pressure buildup within the NMR tube.

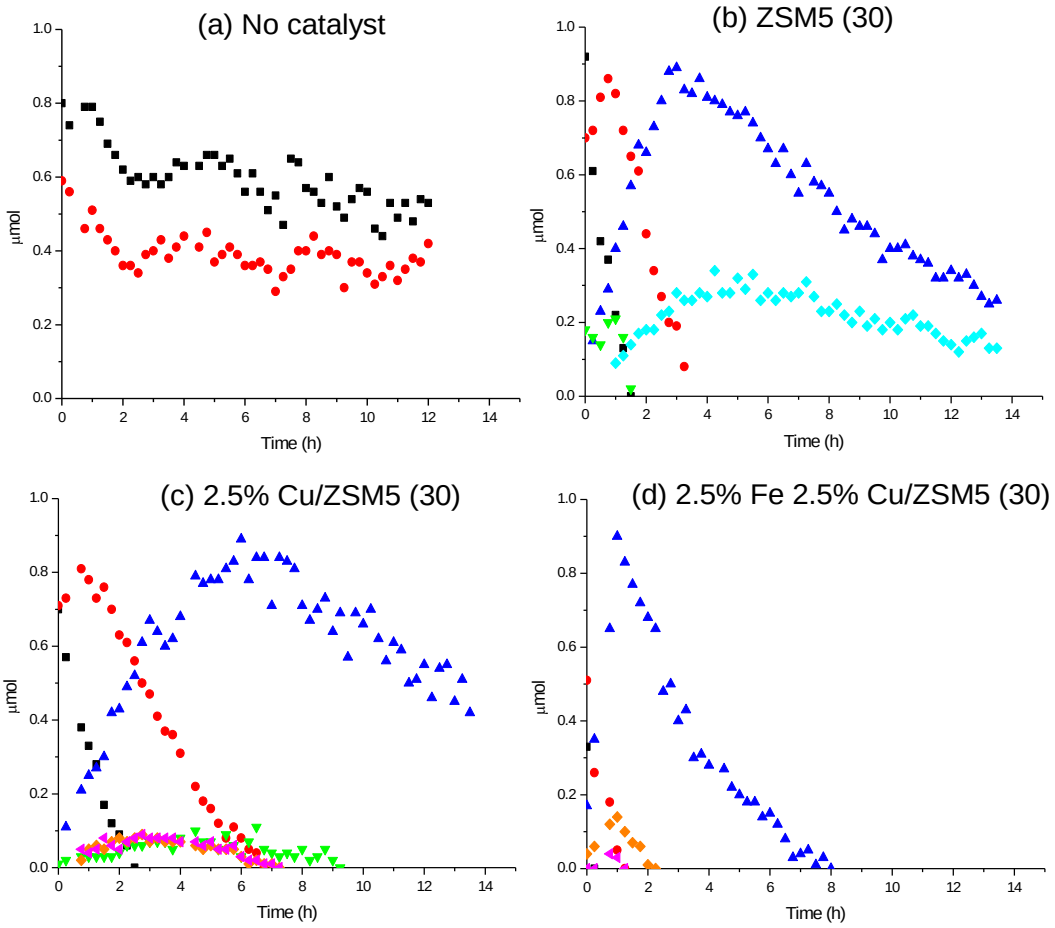

■ Black squares (CH_3CH_2OOH), ● Red Circles (CH_3CHO), ▲ Blue triangles (CH_3COOH), ♦ Aquamarine diamonds (HCOOH), ◄ Pink triangles (CH_3OOH), ♦ Orange diamonds (CH_3OH), ▼ Green triangles (CH_2O)

Figure 3.25 Ethylhydroperoxide decomposition in the presence of various catalysts. Plots represent µmol of products against time (h). ICP-MS shows residual Fe content in H-ZSM-5 (30) to equal 0.0132% wt.

Interestingly ethylhydroperoxide decomposition studies suggest that it plays no discernible role in the formation of the ethanol which is seen consistently *in situ* within the C_2H_6 system, however it does appear to contribute to acetaldehyde, acetic acid and C_1 cracking products observed. The instability of the ethylhydroperoxide in the presence of ZSM5-supported Fe (Figure 3.25 d) and observation in H-ZSM-5 catalysed ethane oxidation (Figure 3.4) means that it cannot be discounted as a reactive intermediate. The direct transformation of ethylhydroperoxide to acetaldehyde, with consecutive oxidation to acetic acid is in agreement with previous studies,[15, 16] yet contrasts the conclusions

drawn from homogeneous catalytic ethane oxidation systems, whereby it was concluded that the ethylhydroperoxide observed led to formation of other oxygenated products including; ethanol, acetaldehyde and acetic acid.[34, 35]

3.7.2 $^{12}CH_3{}^{13}CH_2OH$ stability studies

To study the reaction of ethanol in contact with hydrogen peroxide and Fe- and Cu-containing ZSM-5 catalysts, the oxidation of ^{13}C labelled ethanol ($^{12}CH_3{}^{13}CH_2OH$) was performed under modified reaction conditions whereby a larger reaction volume was used to promote product desorption and reduce oxidant concentration. Results are shown in Table 3.5. (*Note*; for C_1 products, the carbon isotope is indicated by the ^nC outside of the brackets).

It is clear from Table 3.5 that in the presence of ZSM-5 catalysts and hydrogen peroxide, ethanol is rapidly oxidised to acetaldehyde and acetic acid. Cracking of C_2 products is then observed, with formic acid a major C_1 product in the absence of copper, and methanol when copper is present. Once more a distinction between silica and ZSM-5 supported Fe species is made, with 2.5% Fe/SiO_2 favouring oxidation of ethanol to acetaldehyde, whereas 2.5% Fe/ZSM-5 catalyses the consecutive oxidation of ethanol to acetic acid (through acetaldehyde). Gas phase analysis shows formation of both methane and ethane, which supports the theory that C-C scission of C_2 oxygenates leads to production of methyl radicals. Significant increases in ^{12}C (^{12}C) ethanol for 2.5% Fe/ZSM-5 (30) and 2.5% Fe 2.5% Cu/ZSM-5 (30) goes on to suggest that ethanol is undergoing C-C cleavage to form methyl radicals, which recombine to form ^{12}C (^{12}C) ethane, which is then oxidised to non isotopically labelled ethanol. Ethanol conversion follows the order 2.5% Cu/SiO_2< H-ZSM-5< 2.5% Fe/SiO_2< 2.5% Cu/ZSM-5< 2.5% Fe 2.5% Cu/ZSM-5< 2.5% Fe/ZSM-5.

Table 3.5 A table showing the products formed when ^{13}C labelled ethanol was exposed to typical reaction conditions (under N_2), in the presence of a range of catalysts

		C Isotope arrangement (L to R)	Aqueous phase products **µmol**[a]								Gas products **µmol**[b]			Total C/µmol
			CH_3COOH	CH_3CHO	CH_3OH	$HCOOH$	CH_3OOH	CH_3CH_2OOH	CH_3CH_2OH	CH_2O	CO_2	CH_4	C_2H_6	
ZSM-5 (30)	Initial	^{13}C (^{12}C)	-	-	-	-	-	-	1984.87	-	-	-	-	3977
		^{12}C (^{12}C)	-	-	-	-	-	-	3.64	-	-	-	-	
	Final	^{13}C (^{12}C)	37.43	43.14	0	8.29	0	0	1764.44	7.43	1	3.6	3.73	3736.8
		^{12}C (^{12}C)	0	0	3.14	1.14	0.57	1.14	8.57	3.13				
2.5% Cu/ ZSM-5 (30) CVI	Initial	^{13}C (^{12}C)	-	-	-	-	-	-	1979.1	-	-	-	-	3985.4
		^{12}C (^{12}C)	-	-	-	-	-	-	3.6	-	-	-	-	
	Final	^{13}C (^{12}C)	19.43	74.57	0	3.43	0	0	1827.18	17.7	1.4	0.2	2.94	3893.4
		^{12}C (^{12}C)	0	0	6.86	0.57	0.57	1.71	7.29	0				
2.5% Fe/ ZSM-5 (30) CVI	Initial	^{13}C (^{12}C)	-	-	-	-	-	-	1974.74	-	-	-	-	3956.7
		^{12}C (^{12}C)	-	-	-	-	-	-	3.62	-	-	-	-	
	Final	^{13}C (^{12}C)	344.13	22.29	0	98	0	0	1176.86	12.9	11	30	2.73	3537.2
		^{12}C (^{12}C)	3.14	0	66.57	45.43	0.57	0.86	84.86	2.1				
2.5% Fe 2.5% Cu / ZSM-5 (30) CVI	Initial	^{13}C (^{12}C)	-	-	-	-	-	-	1977.7	-	-	-	-	3965.4
		^{12}C (^{12}C)	-	-	-	-	-	-	3.6	-	-	-	-	
	Final	^{13}C (^{12}C)	318.23	36.57	0	0	0	0	1332.15	6	9.2	2.8	2.87	3634.8
		^{12}C (^{12}C)	4.57	0	109.14	0	0	0	57.44	4				
2.5% Cu/SiO_2 (CVI)	Initial	^{13}C (^{12}C)	-	-	-	-	-	-	1983.88	-	-	-	-	3975
		^{12}C (^{12}C)	-	-	-	-	-	-	3.63	-	-	-	-	
	Final	^{13}C (^{12}C)	0	18.1	0	0	0	0	1857.01	1.71	1	0	4.26	3772.3
		^{12}C (^{12}C)	0	0	1.13	0	0.29	0.86	3.63	0				
2.5% Fe/SiO_2 (CVI)	Initial	^{13}C (^{12}C)	-	-	-	-	-	-	1972.95	-	-	-	-	3953.1
		^{12}C (^{12}C)	-	-	-	-	-	-	3.61	-	-	-	-	
	Final	^{13}C (^{12}C)	6.86	74.57	0	0	0	0	1757.15	21.14	1.2	0.1	8.51	3737.4
		^{12}C (^{12}C)	0	0	1.14	0	1.71	2.57	6.44	0				

Test Conditions; $[H_2O_2]$ = 0.25 M (5,000 µmol), 20ml reaction volume, P (N_2) = 10 bar, 26.8 mg catalyst, 0.5h, 50°C, 1500 rpm. (inc ramp) Liquid phase comprised of 10 ml H_2O and 10 ml of 0.22 M $^{12}CH_3{}^{13}CH_2OH$ solution. [a]Analysed by ^{1}H-NMR [b]Analysed by GC-FID. For C_1 products, carbon isotope is indicated outside of the bracket. **H** signifies ^{1}H used in product quantification.

3.7.3 $^{13}CH_3{}^{12}COOH$ stability studies

To further study the reaction mechanism, the oxidation of $^{13}CH_3{}^{12}COOH$ with H_2O_2 and the range of catalysts tested in Table 3.5, was investigated. Results are shown in Tables 3.6 and 3.7.

Table 3.6 A table showing the products formed when ^{13}C labelled acetic acid was exposed to typical reaction conditions (under N_2), in the presence of a range of ZSM-5 (30) catalysts

		C Isotope arrangement (L to R)	Aqueous phase products **μmol**[a]					Gas phase products **μmol**[b]			
			C**H**$_3$COOH	C**H**$_3$OH	H**C**OOH	C**H**$_3$OOH	CH_2O	CO	CO_2	CH_4	C_2H_6
ZSM-5	Initial	^{13}C (^{12}C)	1643.2	-	-	-	-	-	-	-	-
		^{12}C (^{12}C)	0	-	-	-	-	-	-	-	-
	Final	^{13}C (^{12}C)	1422.57	0.57	0.57	3.14	0.86	1.36	7.63	1.36	13.72
		^{12}C (^{12}C)	7.14	0	0	0	0				
2.5% Cu/ZSM-5	Initial	^{13}C (^{12}C)	1642.31	-	-	-	-	-	-	-	-
		^{12}C (^{12}C)	0	-	-	-	-	-	-	-	-
	Final	^{13}C (^{12}C)	1554.29	3.14	0	0	1.71	0.16	9.88	0.1	29.3
		^{12}C (^{12}C)	7.71	0	0	0	0				
2.5% Fe/ZSM-5	Initial	^{13}C (^{12}C)	1619.25	-	-	-	-	-	-	-	-
		^{12}C (^{12}C)	0	-	-	-	-	-	-	-	-
	Final	^{13}C (^{12}C)	1387.14	5.14	48.86	5.14	6.01	1.52	11.36	4.07	8.7
		^{12}C (^{12}C)	9.14	0	1.71	0	0				
2.5% Fe 2.5% Cu /ZSM-5	Initial	^{13}C (^{12}C)	1623.2	-	-	-	-	-	-	-	-
		^{12}C (^{12}C)	0	-	-	-	-	-	-	-	-
	Final	^{13}C (^{12}C)	1481.43	34.29	0	0.57	2.57	0.46	50.51	0.29	8.81
		^{12}C (^{12}C)	6.86	0	0	0	0				

Conditions; [H_2O_2] = 0.25 M (5,000 μmol), 20ml reaction volume, P (N_2) = 10 bar, 26.8 mg catalyst, 0.5h, 50^{o}C, 1500 rpm. (inc ramp) Liquid phase comprised of 10 ml H_2O and 10 ml of 10 ml of 0.166 M $^{13}CH_3COOH$ solution. [a] Analysed by ^{1}H-NMR

[b]Analysed by GC-FID. For C_1 products, carbon isotope is indicated outside of the bracket. **H** signifies ^{1}H used in product quantification.

Table 3.7 A table showing the products formed when ^{13}C labelled acetic acid was exposed to typical reaction conditions (under N_2), in the presence of 2.5% Cu/SiO_2 and 2.5% Fe/SiO_2 (both prepared via CVI).

		C Isotope arrangement (L to R)	Aqueous phase products **µmol**[a]					Gas phase products **µmol**[b]			
			$C\mathbf{H}_3COOH$	$C\mathbf{H}_3OH$	$H\mathbf{C}OOH$	$C\mathbf{H}_3OOH$	CH_2O	CO	CO_2	CH_4	C_2H_6
2.5% Cu/SiO_2	Initial	^{13}C (^{12}C)	1791.41	-	-	-	-	-	-	-	-
		^{12}C (^{12}C)	0	-	-	-	-	-	-	-	-
	Final	^{13}C (^{12}C)	1715.71	0	0	0	0	0.05	1.56	0.03	7.16
		^{12}C (^{12}C)	7.43	0	0	0	0				
2.5% Fe/SiO_2	Initial	^{13}C (^{12}C)	1782.1	-	-	-	-	-	-	-	-
		^{12}C (^{12}C)	0	-	-	-	-	-	-	-	-
	Final	^{13}C (^{12}C)	1702.86	0	5.23	1.43	4.86	0.21	29.25	0.04	4.91
		^{12}C (^{12}C)	12.1	0	0	0	0				

Conditions; $[H_2O_2]$ = 0.25 M (5,000 µmol), 20ml reaction volume, P (N_2) = 10 bar, 26.8 mg catalyst, 0.5h, 50°C, 1500 rpm. (inc ramp) Liquid phase comprised of 10 ml H_2O and 10 ml of 10 ml of 0.166 M $^{13}CH_3COOH$ solution.

[a] Analysed by ^{1}H-NMR [b]Analysed by GC-FID. For C_1 products, carbon isotope is indicated outside of the bracket.

It is clear from Tables 3.6 and 3.7 that acetic acid undergoes rapid C-C scission in the presence of ZSM-5 catalysts, particularly when framework and extraframework Al species are present as with 2.5% Fe/ZSM-5 (30) and 2.5% Fe 2.5% Cu/ZSM-5 (30). The major products of acetic acid oxidation are; formic acid (in absence of copper), methanol (in presence of copper) and CO_2 (for all catalysts). In accordance with ethanol stability studies, both methane and ethane were observed within the gas phase of all tests. Given the lower C-C bond enthalpy in ethane compared with its C-H bonds (377.23 kJ mol^{-1} and 423.29 kJ mol^{-1} respectively) it is also plausible that under standard ethane reaction conditions, methyl radicals may be derived directly through C-C cleavage of ethane.[36]

3.7.4 Ethene oxidation using ZSM-5 catalysts

Given that data from Figure 3.23 implies a potential role for ethene as a product in the ethane oxidation system being studied, a range of ZSM-5 (30) catalysts were screened for ethene oxidation across a range of temperatures. Results are presented in Figure 3.26.

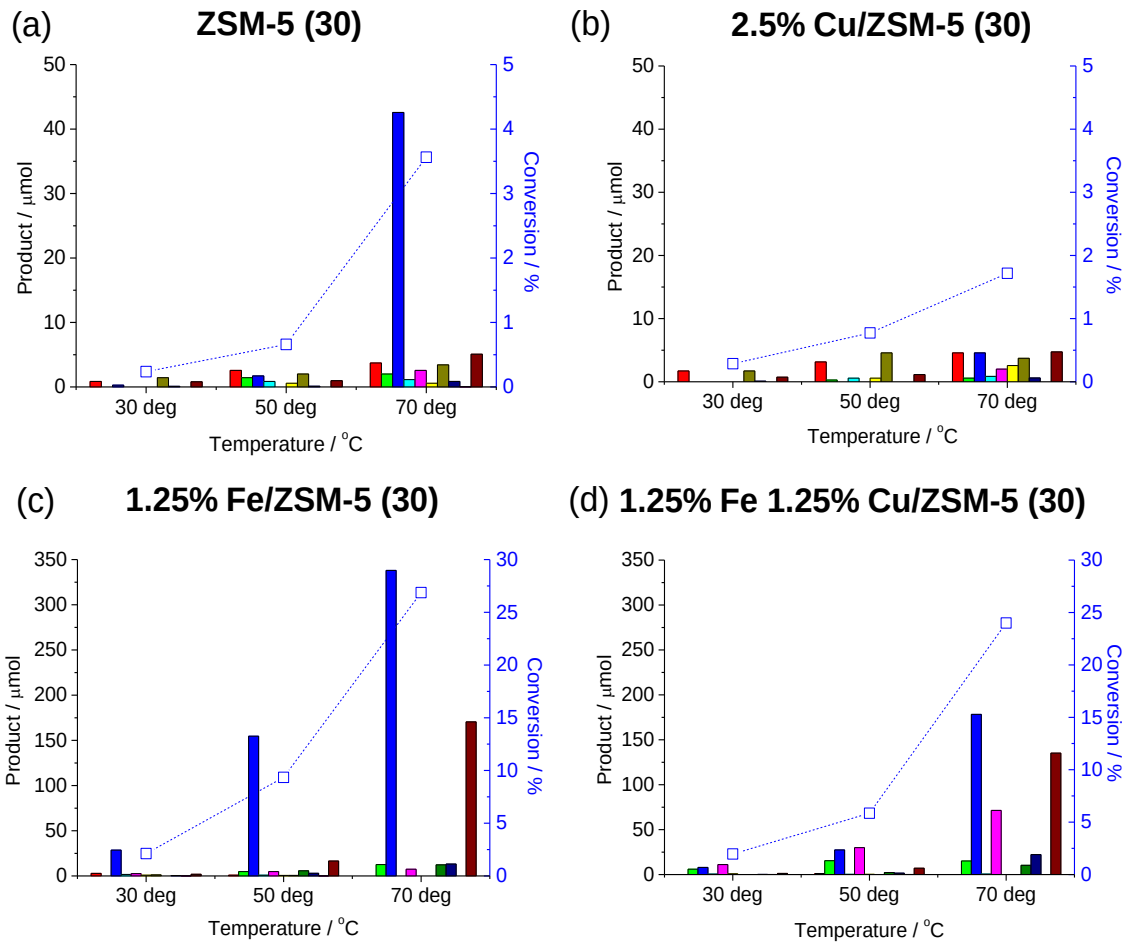

■ Red (CH_3OOH), ■ Green (CH_3OH), ■ Pink (CH_3COOH), ■ Yellow (CH_3CHO), ■ Aquamarine (C_2H_5OH), ■ Blue ($HCOOH$), ■ Beige (CH_3CH_2OOH), ■ Navy (CO), ■ Wine (CO_2), ■ Purple (CH_4), -□- Blue (% Conversion, based on Carbon)

Test conditions: **(a)** ZSM5 (30), **(b)** 2.5% CuZSM5 (30) CVI, **(c)** 1.25% Fe/ZSM5 (30) CVI and **(d)** 1.25% Fe 1.25% Cu/ZSM5 (30), 56 mg catalyst, reaction volume = 20 ml, $[H_2O_2]$ = 0.25 M, Gas phase volume = 40 ml, P(5% C_2H_4/ N_2)= 10 bar

Figure 3.26 Ethene oxidation at various temperatures using ZSM-5 catalysts.

The data in Figure 3.26 provides some crucial insights into the role of ethene in the ethane oxidation scheme. Firstly, upon comparison of ZSM-5 (30) and 2.5% Cu/ZSM-5 (30) at 70 ^{o}C it is clear that copper is inhibiting the oxidation of ethene, as ethene conversion is shown to decrease from 3.3% to 1.6%. Central to this is the significant reduction in formic acid productivity, with H-ZSM-5 (30) yielding 42.6 μmol compared with only 4.6 μmol for 2.5% Cu/ZSM-5. Addition of 2.5 wt% extra framework iron (c) leads to a significant increase in ethene conversion across the range of temperatures, with formic acid and CO_2 the major products at 50 ^{o}C and 70 ^{o}C. Interestingly, upon addition of copper, acetic acid becomes a major product accounting for 27.7% selectivity (compared with 34.6% and 26.2% for formic acid and CO_2). These studies lend further credence that ethene is a reactive intermediate, and provide information as to the reactive pathway of ethene.

A time on line analysis of 1.25% Fe/ZSM-5 (30) catalysed ethene oxidation is shown in Figure 3.27. In the absence of copper, acetic acid is consistently observed at low selectivities (3-6% selectivity) implying that it is being turned over, most probably to formic acid and CO_2, based upon acetic acid stability studies. Interestingly, another product was observed in the ^{1}H NMR with a chemical shift of δ 4.2 ppm. This has been identified as glycolic acid[12] via HSQC-NMR (through correlation with a ^{13}C shift of δ 59.35 ppm) in D_2O.

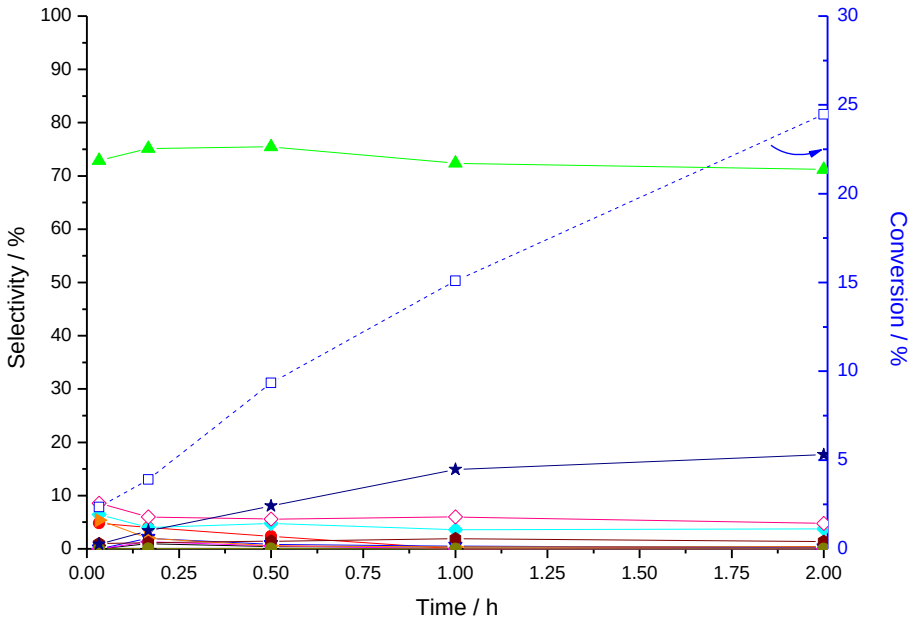

■ Black squares (CH_3OOH), ● Red Circles (CH_3OH), ♦ Aquamarine diamonds (CH_3COOH), ◄ Pink triangles (CH_3CHO), ▼ Blue triangles (C_2H_5OH), ▲ Green triangles (HCOOH, ► Orange triangles (CH_3CH_2OOH), ● Beige circles (CH_4), ★Navy Stars (CO_2),, ● Beige circles (CO), ◊ Pink hollow diamonds ($HOCH_2COOH$) , -□- Blue squares (% Conversion based on carbon)

Test conditions: 1.25% Fe/ZSM5 (CVI) 56 mg, reaction volume = 20 ml, [H_2O_2] = 0.25 M, Gas phase volume = 40 ml, P(5% C_2H_4/ N_2)= 10 bar

Figure 3.27 Time on line ethene oxidation catalysed by 1.25% Fe/ZSM-5 (30)

Based upon ethylhydroperoxide, ethanol, acetic acid and ethene stability studies a reaction scheme for ZSM-5 (and Fe- and Cu- ZSM-5) catalysed ethane oxidation with H_2O_2 may be proposed (Scheme 3.1).

It is apparent that ethane is being activated according to three reaction pathways; oxidation to ethylhydroperoxide, direct oxidation to ethanol and H- abstraction or oxidative dehydrogenation of ethane to ethene. Through stability studies it has been shown that both the alkyl hydroperoxide and ethanol undergo sequential steps through acetaldehyde to acetic acid. Ethene is also shown to undergo oxidation directly to acetic acid. Catalytic cracking of C_2 oxygenated products leads to formation of the C_1

oxygenated products which are observed in ^{1}H NMR; methylhydroperoxide, methanol, formaldehyde and formic acid in addition to carbon centred (methyl) radicals as determined by EPR studies. The presence of methyl radicals is evidenced experimentally by the formation of both methane and ethane during the cracking of C_2 oxygenates. These products of radical recombination then re-enter the catalytic cycle. Deep oxidation to CO_x is observed for all reaction products. Copper has been shown to suppress the oxidation of ethene at 50 ^{o}C (Figure 3.26 (a) and (b)) and deep oxidation of methanol to formic acid.

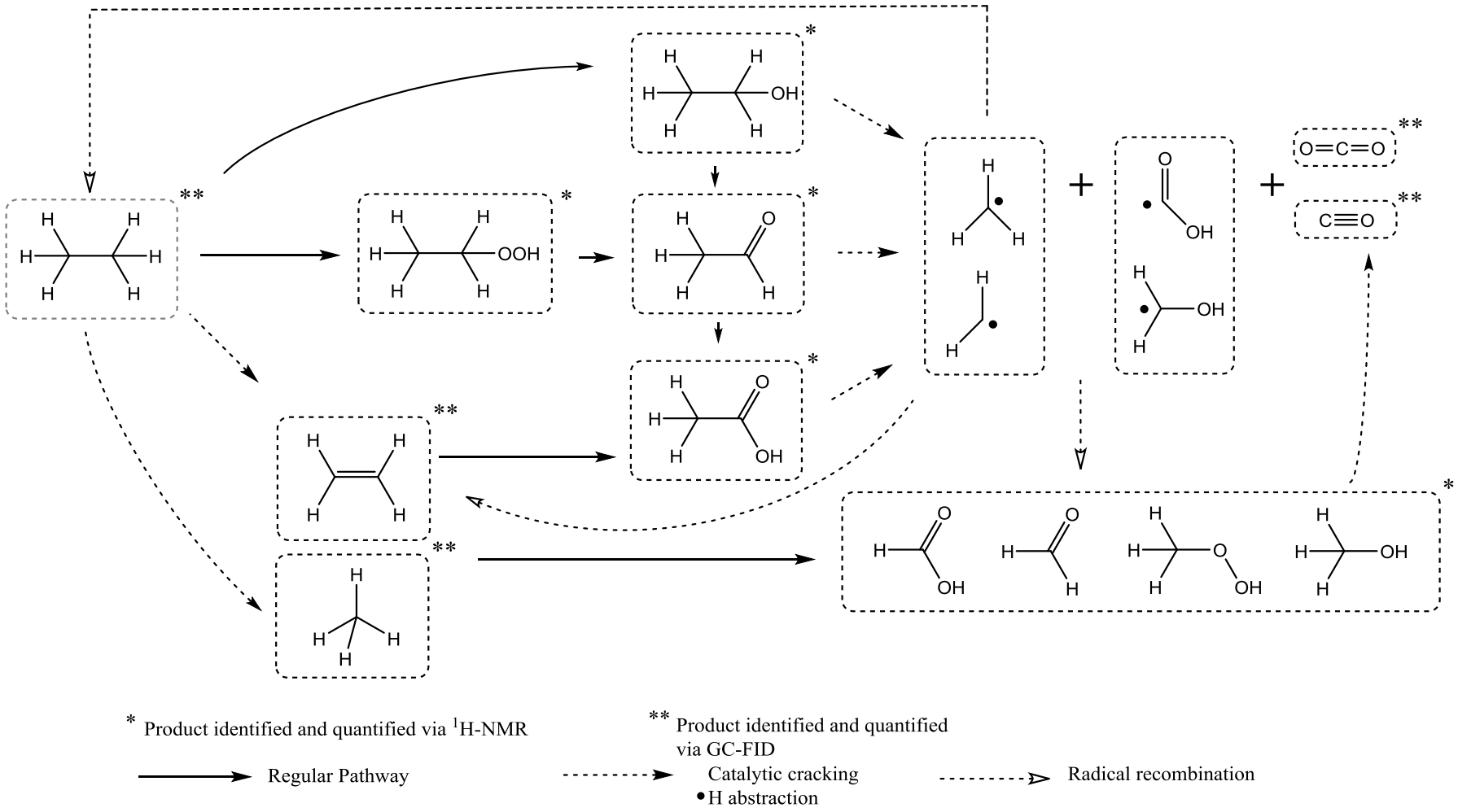

Scheme 3.1 Proposed reaction scheme for ethane using H_2O_2 over ZSM-5 catalysts, based on batch reactions and stability studies

3.8 Catalyst reusability and hot filtration studies

Finally, the reusability and heterogeneity of Fe- and Cu- containing ZSM-5 catalysts was investigated. Reusability of a 1.25% wt Fe/ZSM-5 (30) CVI catalyst was tested according to the procedure outlined in Experimental 2.4.4. Ethane conversion and product selectivities across 5 use cycles are shown in Figure 3.28.

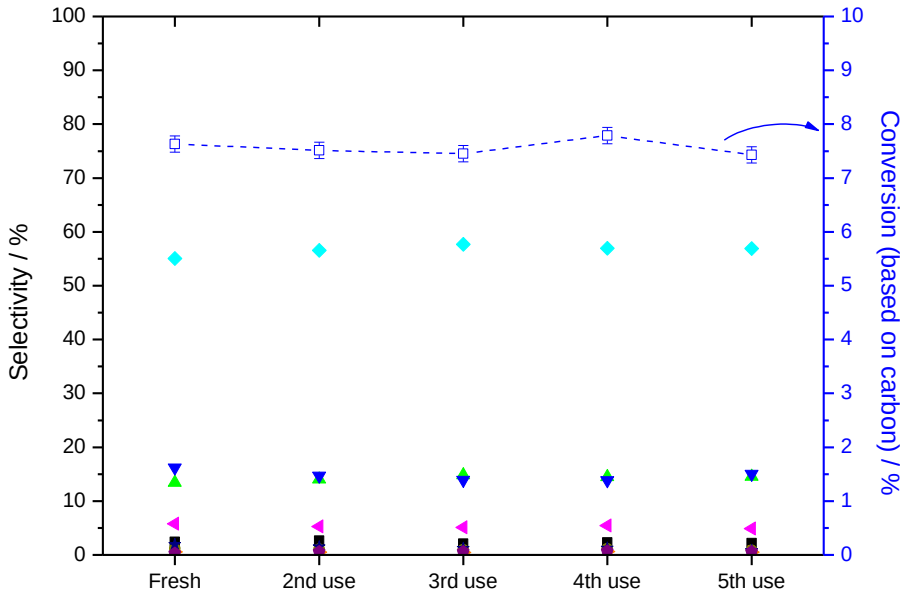

■ Black squares (CH_3OOH), ● Red Circles (CH_3OH), ♦ Aquamarine diamonds (CH_3COOH), ◀ Pink triangles (CH_3CHO), ▼ Blue triangles (C_2H_5OH), ▲ Green triangles (HCOOH, ▶ Orange triangles (CH_3CH_2OOH), ● Beige circles (CH_4), ★Navy Stars (CO_2), ⬟ Purple pentagons (C_2H_4), -□- Blue squares (% Conversion, based on Carbon)

Reaction Conditions; Catalyst 1.25% Fe/ZSM5(30) CVI (56 mg), 30 ml reaction volume, 40 ml headspace, [H_2O_2]= 0.66 M (20,000 µmol), P(C_2H_6) = 5 bar, 0.5 h, 50°C, 1500 rpm

Figure 3.28 Catalyst reusability studies for 1.25% Fe/ZSM-5 (30)

It is clear from Figure 3.28 that 1.25% Fe/ZSM-5 (30) CVI is a highly reusable catalyst for low temperature ethane oxidation as catalytic activity was maintained across 5 use cycles, with no significant change in product selectivities observed. To further probe the stability of this material, and of Cu- containing catalysts, hot filtration tests were conducted on 2.5% Fe/ZSM-5 (30) and 1.25% Fe 1.25% Cu-ZSM-5 (30) (Table 3.8).

Table 3.8 A table showing the hot filtration products for 2.5% Fe/ZSM-5 (30) (A1 / A2) and 1.25% Fe 1.25% Cu/ZSM-5 (30) (B1/ B2)

Entry	Aqueous phase products' **µmol**						Gas Phase product µmol				Carbon in Products (µmol)	µmol H_2O_2 remaining
	CH_3OOH	CH_3OH	HCOOH	C_2H_5OH	CH_3COOH	CH_3CH_2OOH	CH_3CHO	CO	CH_4	CO_2	C_2H_4	
A1	23.57	73.72	392.20	111.02	674.67	4.50	21.00	-	-	-	-	2111.87	12822.98
A2	20.15	64.72	370.34	100.73	646.81	5.14	24.86	0.018	9.12	5.49	0.050	2025.02	12434.40
B1	3.86	109.30	0.00	85.72	220.75	3.87	12.86	-	-	-	-	759.56	15543.00
B2	3.00	106.16	0.00	70.72	213.17	1.93	13.29	0.021	1.31	2.81	1.46	714.44	15413.48

A1 = Catalysed reaction 2.5% Fe/ZSM5 (30). A2 = Filtered solution from A1 run under reaction conditions

B1 = Catalysed reaction 1.25% Fe 1.25% Cu/ZSM5 (30). B2 = Filtered solution from B1 run under reaction conditions

Test Conditions; Catalyst CVI (56 mg), [H_2O_2] = 0.66 M (20,000 µmol), 30ml reaction volume, 40 ml gas phase, P (C_2H_6) = 5 bar, 50^oC, 0.5h , 1500 rpm

Given the propensity for Fe to leach into solution[37] it is important to determine that supported metals are not leaching into the reaction medium. This is an important step in the development of heterogeneous catalysts and may be achieved through hot filtration studies.[38] The procedure is described in 2.4.5 and consists of two stages; a standard reaction with catalyst (followed by opening the reactor whilst at reaction temperature, removing catalyst via filtration and analysis of aqueous products), after which the liquid phase is put back into the reactor and catalyst-free reaction run as per the standard reaction protocol.

It is clear from Table 3.8 that no activity is exhibited by the reaction solution, suggesting that no homogeneous reaction is in operation. The presence of gaseous products may be put down to the fact that the solution was not degassed prior to the filtered reactions (A2/ B2). Fe-ZSM-5 and FeCu-ZSM-5 CVI catalysts therefore appear to be stable heterogeneous catalysts.

3.9 Conclusions

Post deposition supported iron zeolite catalysts of MFI structure (ZSM-5) have been prepared, characterised and tested for ethane oxidation with hydrogen peroxide. It has been shown that deposition of iron as oxides and exchanged ions via chemical vapour impregnation (CVI) yields highly active catalysts relative to traditional deposition techniques (IMP and IE). It was determined that, although catalyst productivity may be enhanced through deposition of increasing wt% iron, this leads to heightened formation of large Fe_xO_y species which have been implicated in C-C cleavage of products and deep oxidation to CO_2.

The activity exhibited by the liquid phase heterogeneous system studied is unprecedented within the literature, with catalyst productivities of up to 44.3 h^{-1} (2.89 % conversion) observed at 70 ^{o}C for ZSM-5 (30) onto which 1.25 wt% Fe had been deposited via CVI. Oxygenate selectivity for monometallic Fe/ZSM-5 (30) catalysts is high, typically > 95%. The catalysts serve to activate not only the oxidant (hydrogen peroxide) but also ethane itself, to yield a range of C_2 and C_1 oxygenated products and have been shown to be both heterogeneous and reusable for this reaction.

From time online studies, coupled with mechanistic investigations, it has been concluded that the reaction proceeds via three primary products which are; ethylhydroperoxide (CH_3CH_2OOH), ethanol and ethene. The two aqueous primary products were shown to react under test conditions to yield acetaldehyde and acetic acid through consecutive oxidation steps, whilst ethene was shown to react to yield acetic acid. Through ^{13}C labelling studies it was determined that C_2 oxygenates undergo C-C scission to yield carbon based radicals (the presence of which has been confirmed through EPR studies) which yield methane, ethane and, dependent on the catalyst used; methylhydroperoxide, methanol, formic acid and formaldehyde. Deep oxidation to CO_2 is observed though typically at selectivities of < 5%.

The effect of reaction conditions and kinetic parameters including temperature, ethane pressure, ethane partial pressure, hydrogen peroxide concentration and catalyst mass were investigated. At low ethane pressures, or low ethane partial pressures product selectivity was shown to favour acetic acid, which is a secondary oxidation product and also formic acid and CO_2 at comparable catalyst productivity. An increase in either of these parameters has been shown to lead to increased C_2 selectivity overall, with ethanol

coming to be favoured as major product. It has been concluded that the adsorption of the non-polar substrate onto the catalyst surface might be suppressing overoxidation and cracking processes.

Addition of Cu simultaneously to Fe via CVI has been shown to lead to ethene being the major reaction product at 45.5% selectivity, at near isoconversion compared with a comparable monometallic Fe/ZSM-5 (30) catalyst of equal iron content. At the low temperature of 50 ^{o}C ethene productivities of 4.0 h^{-1} (1.0% ethane conversion) were observed for 1.25% Fe 1.25% Cu/ZSM-5 (30) prepared by CVI. The selective conversion of ethane to ethene over a heterogeneous catalyst, within an aqueous phase system at such low temperatures is believed to have been unprecedented prior to this catalytic system.

Much of the work in this chapter was contributed to Reference (12).

3.10 References

1 Rahimi, N.; Karimzadeh, R. *Applied Catalysis A: General* **2011**, *398*, 1.

2 Yoneda, N.; Kusano, S.; Yasui, M.; Pujado, P.; Wilcher, S. *Appl. Catal. A-Gen.* **2001**, *221*, 253.

3 Uragami, Y.; Otsuka, K. *Journal of the Chemical Society, Faraday Transactions* **1992**, *88*, 3605.

4 Jones, J. H. *Platinum Metals Rev* **2000**, *44*, 94.

5 Sunley, G. J.; Watson, D. J. *Catalysis Today* **2000**, *58*, 293.

6 Dubkov, K. A.; Sobolev, V. I.; Talsi, E. P.; Rodkin, M. A.; Watkins, N. H.; Shteinman, A. A.; Panov, G. I. *J. Mol. Catal. A-Chem.* **1997**, *123*, 155.

7 Panov, G. I.; Uriarte, A. K.; Rodkin, M. A.; Sobolev, V. I. *Catalysis Today* **1998**, *41*, 365.

8 Groothaert, M. H.; Smeets, P. J.; Sels, B. F.; Jacobs, P. A.; Schoonheydt, R. A. *Journal of the American Chemical Society* **2005**, *127*, 1394.

9 Hammond, C.; Forde, M. M.; Ab Rahim, M. H.; Thetford, A.; He, Q.; Jenkins, R. L.; Dimitratos, N.; Lopez-Sanchez, J. A.; Dummer, N. F.; Murphy, D. M.; Carley, A. F.; Taylor, S. H.; Willock, D. J.; Stangland, E. E.; Kang, J.; Hagen, H.; Kiely, C. J.; Hutchings, G. J. *Angewandte Chemie International Edition* **2012**, *51*, 5129.

10 Hammond, C.; Jenkins, R. L.; Dimitratos, N.; Lopez-Sanchez, J. A.; ab Rahim, M. H.; Forde, M. M.; Thetford, A.; Murphy, D. M.; Hagen, H.; Stangland, E. E.; Moulijn, J. M.; Taylor, S. H.; Willock, D. J.; Hutchings, G. J. *Chemistry – A European Journal* **2012**, *18*, 15735.

11 Hammond, C.; Dimitratos, N.; Lopez-Sanchez, J. A.; Jenkins, R. L.; Whiting, G.; Kondratt, S. A.; ab Rahim, M. H.; Forde, M. M.; Thetford, A.; Hagen, H.; Stangland, E. E.; Moulijn, J. M.; Taylor, S. H.; Willock, D. J.; Hutchings, G. J. *Acs Catalysis* **2013**, *3*, 1835.

12 Forde, M. M.; Armstrong, R. D.; Hammond, C.; He, Q.; Jenkins, R. L.; Kondrat, S. A.; Dimitratos, N.; Lopez-Sanchez, J. A.; Taylor, S. H.; Willock, D.; Kiely, C. J.; Hutchings, G. J. *Journal of the American Chemical Society* **2013**, *135*, 11087.

13 Yuan, Q.; Deng, W.; Zhang, Q.; Wang, Y. *Advanced Synthesis & Catalysis* **2007**, *349*, 1199.

14 Bartolomeu, R.; Henriques, C.; da Costa, P.; Ribeiro, F. *Catalysis Today* **2011**, *176*, 81.

15 Hou, H.; Li, J.; Song, X.; Wang, B. *The Journal of Physical Chemistry A* **2005**, *109*, 11206.

16 Chen, D.; Jin, H.; Wang, Z.; Zhang, L.; Qi, F. *The Journal of Physical Chemistry A* **2011**, *115*, 602.

17 Ivanova, II; Kolyagin, Y. G. *Chemical Society Reviews* **2010**, *39*, 5018.

18 Jung, Y.; Park, J. Y.; Ko, S. O.; Kim, Y. H. *Chemosphere* **2013**, *90*, 812.

19 Kawai, T.; Tsutsumi, K. *Colloid Polym. Sci.* **1992**, *270*, 711.

20 Auerbach, S. M.; Currado, K. A.; Dutta, P. K. *HANDBOOOK OF ZEOLITES SCIENCE AND TECHNOLOGY*; Marcel Dekker Inc, New York, 2003.

21 Rahman, A. K. M. L.; Kumashiro, M.; Ishihara, T. *Catalysis Communications* **2011**, *12*, 1198.

22 Rahman, A. K. M. L.; Indo, R.; Hagiwara, H.; Ishihara, T. *Applied Catalysis A: General* **2013**, *456*, 82.

23 Qin, G. L.; Zheng, L.; Xie, Y. M.; Wu, C. C. *Journal of Catalysis* **1985**, *95*, 609.

24 Schuetze, F. W.; Roessner, F.; Meusinger, J.; Papp, H. In *Hydrogen/deuterium exchange on dealuminated H-ZSM-5 zeolites studied by time resolved FTIR spectroscopy*; Elsevier Science Publ B V, Amsterdam, 1997; Vol. 112. pp 127.

25 Bordiga, S.; Platero, E. E.; Arean, C. O.; Lamberti, C.; Zecchina, A. *Journal of Catalysis* **1992**, *137*, 179.

26 Kustov, L. M.; Kazansky, V. B.; Beran, S.; Kubelkova, L.; Jiru, P. *J. Phys. Chem.* **1987**, *91*, 5247.

27 Jacobs, P. A.; Vonballmoos, R. *J. Phys. Chem.* **1982**, *86*, 3050.

28 Hensen, E. J. M.; Zhu, Q.; Janssen, R. A. J.; Magusin, P.; Kooyman, P. J.; van Santen, R. A. *Journal of Catalysis* **2005**, *233*, 123.

29 Perez-Ramirez, J.; Groen, J. C.; Bruckner, A.; Kumar, M. S.; Bentrup, U.; Debbagh, M. N.; Villaescusa, L. A. *Journal of Catalysis* **2005**, *232*, 318.

30 Kumar, A. S.; Perez-Ramirez, J.; Debbagh, M. N.; Smarsly, B.; Bentrup, U.; Bruckner, A. *Appl. Catal. B-Environ.* **2006**, *62*, 244.

31 Perez-Ramirez, J.; Kumar, M. S.; Bruckner, A. *Journal of Catalysis* **2004**, *223*, 13.

32 Urquieta-González, E. A.; Martins, L.; Peguin, R. P. S.; Batista, M. S. *Materials Research* **2002**, *5*, 321.

33 Safari, J.; Zarnegar, Z.; Heydarian, M. *Bull. Chem. Soc. Jpn.* **2012**, *85*, 1332.

34 Suss-Fink, G.; Gonzalez, L.; Shul'pin, G. B. *Appl. Catal. A-Gen.* **2001**, *217*, 111.

35 Shul'pin, G. B.; Süss-Fink, G.; Shul'pina, L. S. *Journal of Molecular Catalysis A: Chemical* **2001**, *170*, 17.

36 Blanksby, S. J.; Ellison, G. B. *Accounts of Chemical Research* **2003**, *36*, 255.

37 Melian-Cabrera, I.; Kapteijn, F.; Moulijn, J. A. *Catalysis Today* **2005**, *110*, 255.

38 Sheldon, R. A.; Wallau, M.; Arends, I.; Schuchardt, U. *Accounts of Chemical Research* **1998**, *31*, 485.

4

Partial oxidation of Ethane to oxygenates with Fe- and Cu- ZSM-5 in a continuous flow reactor

4.1 Introduction

The partial oxidation of ethane to oxygenated products at low temperatures represents an attractive alternative to current commercial technologies for the activation of lower alkanes, which typically require highly energy intensive, non-green processes. In the current state of the art, acetic acid is typically produced on an industrial scale via methanol carbonylation, for example by the BP Cativa Process,[1] whilst ethene is produced through energy intensive steam cracking of mixed hydrocarbon feeds.[2]

In Chapter 3 it has been shown that iron and copper modified ZSM-5 (30) catalysts are effective for the partial oxidation of ethane to oxygenated products with H_2O_2. Through extensive mechanistic studies it was determined that a complex reaction scheme is in operation which results in a range of C_2 products, which can undergo C-C scission to yield a range of C_1 products (Scheme 3.1). It was concluded that ethanol could be formed directly from ethane, whilst ethylhydroperoxide was observed as an additional primary oxygenated product. Through time resolved ^{1}H-NMR studies ethylhydroperoxide and ethanol were then shown to undergo consecutive oxidation steps through acetaldehyde to acetic acid. C-C scission reactions yielded methylhydroperoxide, methanol, formic acid and CO_x. The direct transformation of ethylhydroperoxide to acetaldehyde, bypassing ethanol, was found to be consistent with previous studies.[3, 4] Ethene was also observed as a primary product, which was oxidised within the system to yield glycolic acid, acetic acid and C_1 oxygenates, with product distributions dependent upon the metal composition

of the catalyst. High ethene selectivity of 45.5% was observed in Fe- Cu- modified ZSM-5 (30) catalysts. Ethene was shown to be relatively stable with respect to oxidation under reaction conditions with 2.5% Cu/ZSM-5 (30), when compared with H-ZSM-5 (30) and 2.5% Fe/ZSM-5 (30) across a range of temperatures.

With applications in biochemical, petrochemical, waste treatment and chemical industries trickle bed reactors (TBRs) are scalable, efficient three phase continuous reaction systems.[5, 6] In fact, of the three phase gas- liquid- solid reaction setups used within industry, TBRs are the most commonly used.[7] TBR systems consist of a fixed bed composed of pelleted solid catalyst particles through which liquid and gas feeds are fed, usually in a co-current downwards direction.[6] Plug flow is assumed due to the particulate nature of the fixed bed, implying that there is no backwards mixing, which is an important feature of TBRs when product stability within the catalyst bed is a concern. Given that the partial oxidation products of ethane are inherently more reactive than ethane itself, with C_2 products having been shown in Chapter 3 to undergo oxidation and C-C scission, deep oxidation becomes a limiting factor in the viability of catalytic systems. Reduction of these non-selective oxidation processes requires short residence times of products within the catalyst bed. It is plausible that this may be achieved through use of an optimised plug-flow system, which represents an intriguing prospect for a detailed study into selective ethane oxidation.

This Chapter aims to show that the reaction system investigated in Chapter 3 may be applied in a three phase continuous flow reactor. A reactor schematic is show in Chapter 2 (Figure 2.2) whilst the procedures for setting up the catalyst bed and for testing are described in Chapter 2, Sections 2.4.6.1 and 2.4.6.2 respectively. A detailed investigation of reaction conditions is shown and the effect of ZSM-5 (30) supported metals studied.

4.2 Catalyst Characterisation

In screening the effect of reactor parameters upon ethane conversion based on previous work[8] and product selectivities, 0.4% wt Fe/ZSM-5 (30) CVI was selected as a suitable catalyst candidate. Through use of a low iron loading which is known to limit the formation of large iron oxide clusters which have been implicated as having a role in product cracking and deep oxidation. This material was characterised using transmission electron microscopy and BET micropore analysis in order to determine the distribution of iron across the surface of ZSM-5, and quantify the microporosity of materials used.

4.2.1 Transmission electron microscopy (TEM)

TEM images of 0.4% Fe/ZSM-5 (30) at varying magnifications are shown in Figure 4.1.

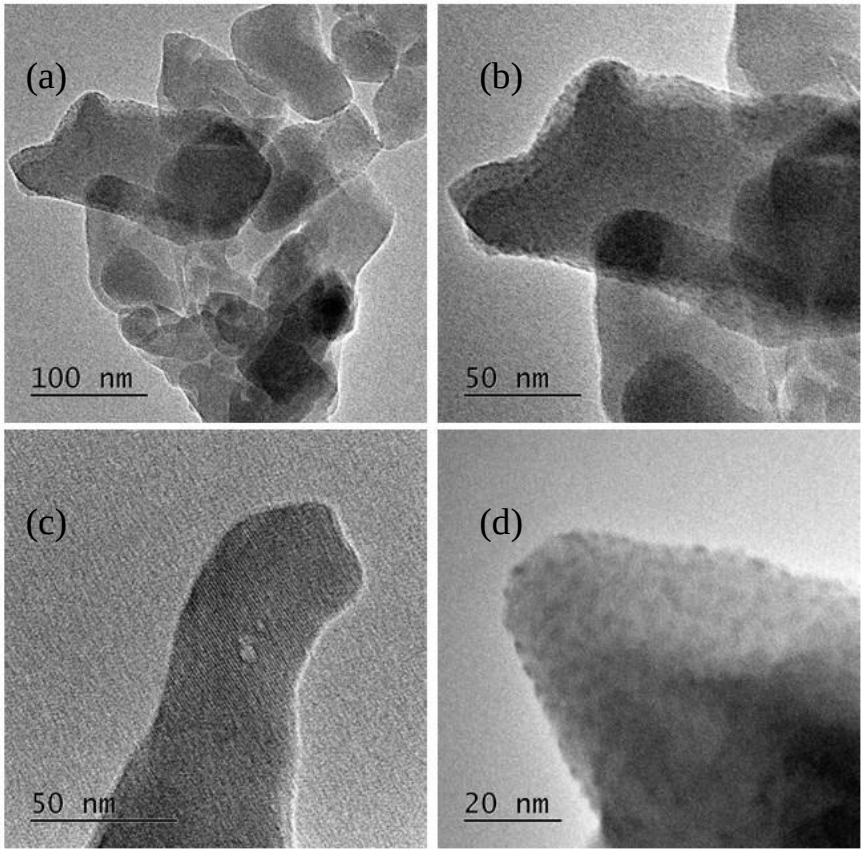

Figure 4.1 Representative low resolution TEM images of 0.4% Fe/ZSM-5 (30) at varying magnifications

As previously seen with 2.5% Fe/ZSM-5 (30) CVI catalysts in Chapter 3, 0.4% Fe/ZSM-5 (30) shows an even distribution of iron across the zeolite surface. STEM-HAADF images of the same material have been reported to show that the iron species form a porous film on the zeolite surface,[8] with the nanoparticle-like supported species observed in TEM images actually being an artefact of the image processing process.[8] This is clearly represented in Figure 4.1 (c).

4.2.2 BET micropore analysis

Catalyst pelleting is required to prevent backwards fluid/ gas pressure build-up as it ensures flow through the bed by increasing permeability.[9, 10] The result is a trade-off between activity and system stability, as pelleting reduces the liquid-solid mixing efficiency, thereby reducing productivity per unit mass. Addition of a layer of glass beads prior to the catalyst bed maximises liquid-gas mixing and aids in the dispersion of the liquid phase across the top of the catalyst bed.

To ensure that the process of pelleting has no detrimental effect upon reactive surface area, micropore analysis with multipoint BET was performed on both powder and pelleted H-ZSM-5 (30).

Figure 4.2 clearly shows that no change in total micropore volume per gram is observed upon pelleting H-ZSM-5 (30). Changes in meso and macroporous regions, particularly the latter, are likely the result of N_2 condensation between pellets. Added to this, no significant difference in surface area is observed upon pelleting, with powdered and pelleted H-ZSM-5 (30) showing surface areas of 386.3 $m^2 g^{-1}$ (± 38.6) and 401.0 $m^2 g^{-1}$ (± 40.1) respectively.

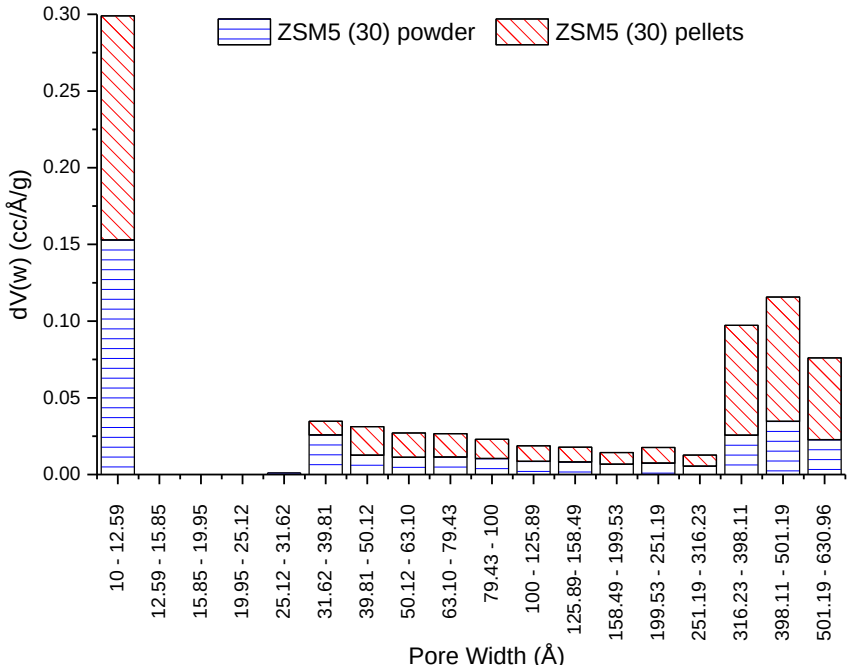

Figure 4.2 Pore volume distribution according to pore width (Å)

4.3 Investigation of reaction parameters

Within the initial half of this chapter concerning screening of conditions, results are presented in two forms; (i) ethane conversion plots and (ii) selectivity versus conversion plots. For the former format (for example Figure 4.3) each data point represents the averaged steady state conversion of ethane (over 4 h), determined from carbon balance based on carbon in products, under the condition implied by the x-axis. For the latter, an average of the steady state selectivity shown to the four major products; ethanol, acetic acid, formic acid and CO_2 are shown (for example Figure 4.4).

In this section the effect of continuous flow reaction parameters are investigated, with the aim of allowing for enhancement of conversion and product selectivities; specifically towards acetic acid.

4.3.1 The effect of gas flow rate

The effect of the gas flow rate was studied using 0.4% Fe/ZSM-5 (30), with all other reaction parameters held as constant (*Test conditions*: 2.0 g 0.4% Fe/ZSM-5 pelleted + SiC diluent, liquid flow rate 0.25 ml min^{-1} H_2O_2/H_2O (0.123 M, 30.6 µmol min^{-1} H_2O_2), 10 bar of 10% C_2H_6/Ar, Temp = 50 ^oC), in order to determine the optimum flow rate to use for subsequent reactions. The ethane conversion achieved and selectivity versus conversion plots for major products at increasing gas flow rates are shown in Figures 4.3 and 4.4.

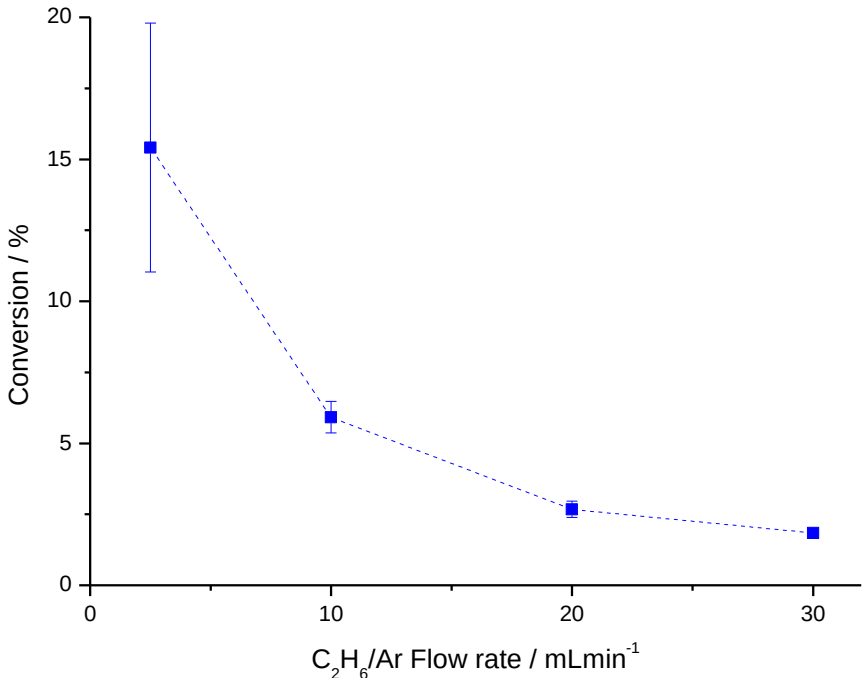

Test conditions: 2.0 g 0.4% Fe/ZSM-5 pelleted + SiC diluent, liquid flow rate 0.25 ml min^{-1} H_2O_2/H_2O (0.123 M, 30.6 µmol min^{-1} H_2O_2), 10 bar of 10% C_2H_6/Ar, Temp = 50 ^oC

Figure 4.3 The effect of ethane/argon flow rate upon conversion.

Although high ethane conversion (*ca.* 20%) was initially observed at a gas flow rate of 2.5 ml min^{-1}, this gradually decreased as the reaction progressed. The high error in conversion shown in Figure 4.3 at a gas flow rate of 2.5 ml min^{-1} is due to fluid build-up

before the catalyst bed, which led to a rapid drop in activity once the bed had been fully saturated. This was clear as upon opening the reactor, the aqueous phase had built up to fill the reaction tube. The deactivation of the system occurred as the H_2O_2 was not being carried effectively through the catalyst bed, leading to an oxidant limited system and non selective use of H_2O_2 through decomposition. It was concluded from this study that a gas flow rate of $\geq$ 10 ml min^{-1} were required in order to reach a steady continuous flow of the aqueous H_2O_2 through the catalyst bed. A gas flow rate of 10 ml min^{-1} was therefore used as standard for the remainder of the study.

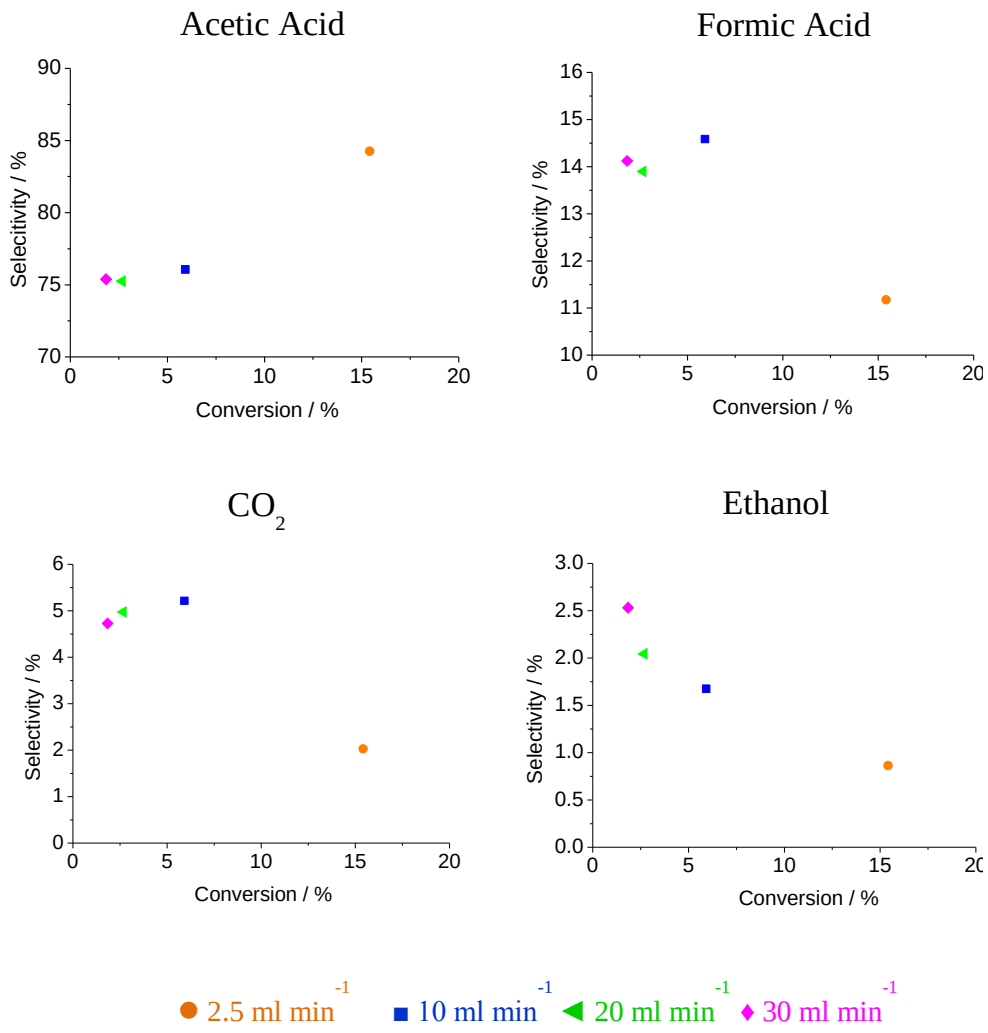

Test conditions: 2.0 g 0.4% Fe/ZSM-5 pelleted + SiC diluent, liquid flow rate 0.25 ml min^{-1} H_2O_2/H_2O (0.123 M, 30.6 µmol min^{-1} H_2O_2), 10 bar of 10% C_2H_6/Ar, Temp = 50 ^{o}C

Figure 4.4 Effect of ethane/argon flow rate upon ethane conversion and major product selectivities.

As shown in Figure 4.4, negligible variation in selectivity towards major product was observed at the higher flow rates within the region of 10 – 30 ml min^{-1}. As the gas flow rate was increased the residence time of ethane over the catalyst bed decreases, thereby leading to the lower conversion seen at higher flow rates.

4.3.2 Catalyst Stability

It was shown in Chapter 3 that Fe- and Cu-ZSM-5 (30) CVI catalysts are strictly heterogeneous catalysts through hot filtration tests and catalyst re-use testing under batch conditions. In order to determine whether 0.4% Fe/ZSM-5 (30) shows stability at steady state operation under continuous flow conditions, said catalyst was monitored over a 10 h period. Ethane conversion and product selectivities are shown in Figure 4.5.

Under the conditions represented in Figure 4.5, average selectivity to acetic acid of 76%, with formic acid and CO_2 selectivities of 15% and 6% respectively were observed. There was no apparent deactivation of the catalyst once steady state operation was reacted (4 h). It is interesting to note the low ethanol selectivity (*ca.* 2%). This is consistent with trends observed under batch reaction conditions, at varying pressures of ethane (Chapter 3 Figure 3.14) and ethane/N_2 partial pressures (Chapter 3 Figure 3.15) whereby it was determined that at either lower pressures of 100% ethane, or low partial pressures of ethane, comparable to the 10% C_2H_6/Ar feed used in this study, significantly higher selectivities to secondary oxidation products; acetic acid, formic acid and CO_2 were observed, coupled with a decrease in ethanol selectivity.

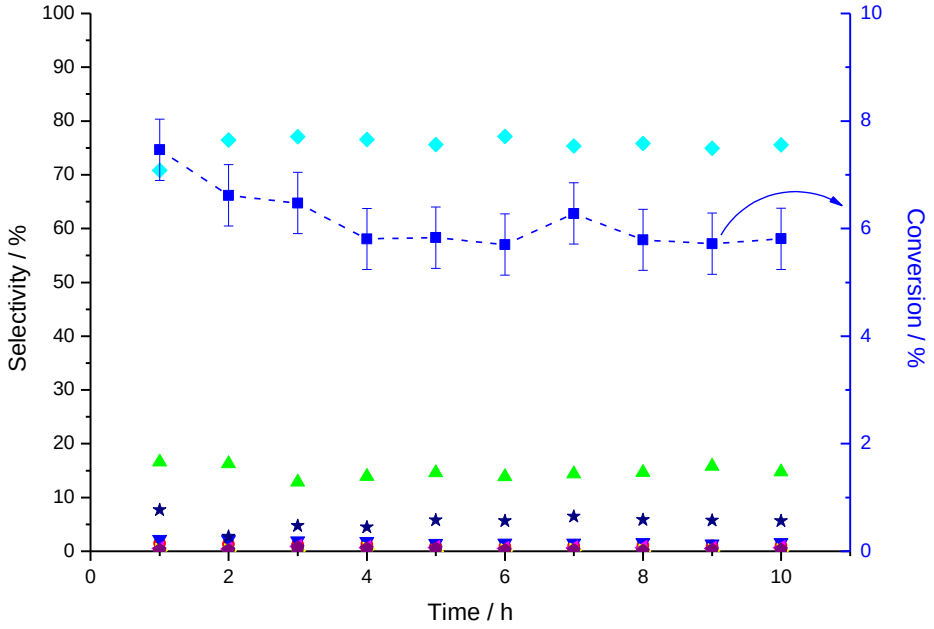

■ Black squares (CH_3OOH), ● Red Circles (CH_3OH), ♦ Aquamarine diamonds (CH_3COOH), ◀ Pink triangles (CH_3CHO), ▼ Blue triangles (C_2H_5OH), ▲ Green triangles ($HCOOH$), ● Beige circles (CH_4), ★Navy Stars (CO_2), ⬟ Purple pentagons (C_2H_4), -■- Blue squares /dashes (% Conversion, based on Carbon)

Test conditions: 2.0 g 0.4% Fe/ZSM-5 pelleted + SiC diluent, liquid flow rate 0.25 ml min^{-1} H_2O_2/H_2O (30.6 µmol min^{-1} H_2O_2), 10 ml min^{-1} of 10% C_2H_6/Ar (37 µmol min^{-1} C_2H_6), P(C_2H_6/Ar) = 10 bar, Temp = 50 ^{o}C

Figure 4.5 Conversion and product selectivities as observed over a 10 h reaction period.

4.3.3 The effect of total pressure

The effect of gas pressure (10% C_2H_6/Ar) in the flow system was investigated, whilst maintaining standard conditions (2.0 g 0.4% Fe/ZSM-5 (30) pelleted + SiC diluent, liquid flow rate 0.25 ml min^{-1} H_2O_2/H_2O (0.123 M, 30.6 µmol min-1 H_2O_2), 10 ml min^{-1} of 10% C_2H_6/Ar, Temp = 50 ^{o}C), using a 0.4% Fe/ZSM-5 catalyst (30). Based upon results observed at varying gas flow rates, a standard flow of 10 ml min^{-1} was selected to maximise conversion, yet allow sufficient gas flow to establish steady state operation. The results are shown in Figures 4.6 and 4.7.

Upon increasing the gas pressure, an increase in ethane conversion was observed, most likely due to increased ethane solubility. The non-linear nature of the pressure/conversion relationship indicates that mass transfer limitations are inhibiting a proportional increase of conversion at pressures of greater than 5 bar.

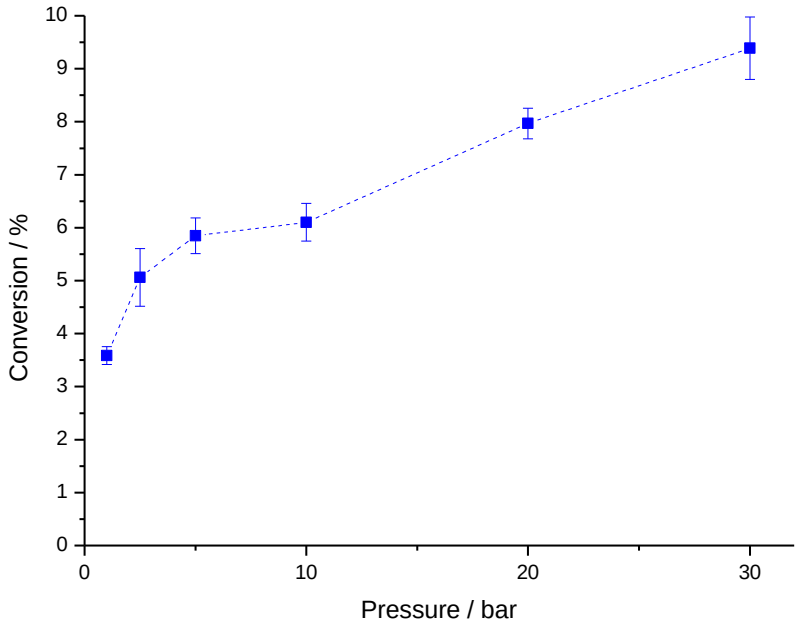

Test conditions: 2.0 g 0.4% Fe/ZSM-5 pelleted + SiC diluent, liquid flow rate 0.25 ml min^{-1} H_2O_2/H_2O (0.123 M, 30.6 µmol min^{-1} H_2O_2), 10 ml min^{-1} of 10% C_2H_6/Ar (37 µmol min^{-1} C_2H_6) , Temp = 50 ^{o}C

Figure 4.6 The effect of reactor pressure upon ethane conversion.

As the pressure was increased from 1 to 30 bar, oxygenate selectivity increased from 45.7% to 97.7%, and this was accompanied by a decrease in CO_2 selectivity from 49.7 to 2.2 % (Figure 4.7). As the pressure increased, acetic acid, formic acid and ethanol selectivities also increased, with the selectivity to C_1 and C_2 acids stabilising at pressures in excess of 10 bar. These trends are consistent with those observed under batch reaction

conditions at varying pressures of ethane and partial pressures of ethene/nitrogen, presented in Chapter 3 Figures 3.14 and 3.15.

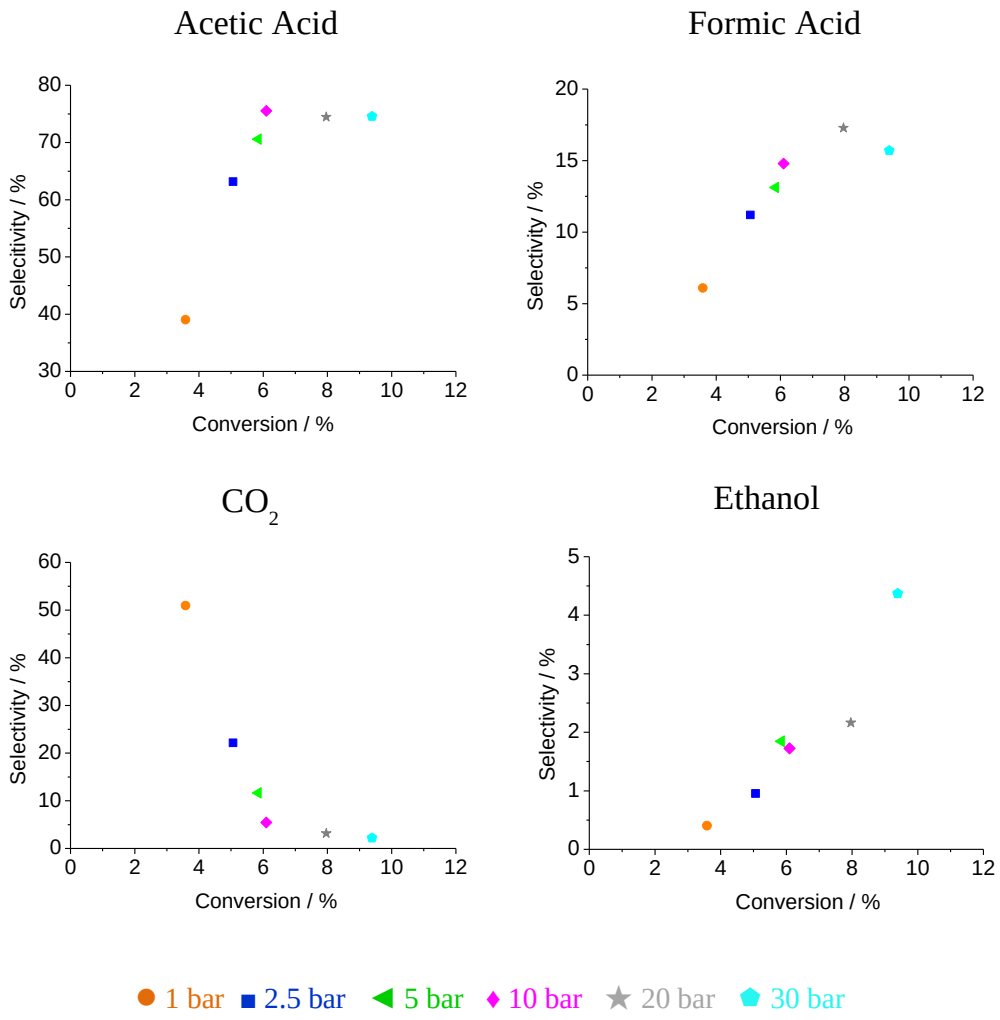

Test conditions: 2.0 g 0.4% Fe/ZSM-5 pelleted + SiC diluent, liquid flow rate 0.25 ml min^{-1} H_2O_2/H_2O (0.123 M, 30.6 µmol min^{-1} H_2O_2), 10 ml min^{-1} of 10% C_2H_6/Ar (37 µmol min^{-1} C_2H_6) , Temp = 50 ^{o}C

Figure 4.7 The effect of total gas pressure upon ethane conversion and major product selectivities.

In concordance with previous methane oxidation studies,[11] heightened selectivity towards primary oxygenated products was attributed to competitive adsorption of ethane onto the catalyst's active site's blocking of the re-adsorption of oxygenated species, thereby

inhibiting catalytic cracking and secondary oxidation reactions. Alternately or concurrently this could also be due to the fact that due to increased ethane solubility at higher pressures, we see a greater ethane to H_2O_2 ratio in solution thereby favouring interaction between substrate, oxidant and catalyst over desorbed primary product, oxidant and catalyst. This would lead selectivity to favour primary products. Within the flow system, the high CO_2 selectivity observed at the lowest pressures of 1 bar and 2.5 bar could also be the result of poor heat distribution within the catalyst bed due to lower gas density and therefore thermal conduction. Were isolated high temperature regions to form, specifically in close proximity to the reactor walls, such regions would exhibit higher rates of H_2O_2 onsumption and lead to increased deep oxidation of products to CO_2. Given the low CO_2 selectivity (3.1%) observed at 20 bar, this pressure was selected as standard for further catalyst evaluation.

4.3.4 The effect of reaction temperature

The effect of temperature upon ethane conversion and product selectivities was then investigated with the results presented in Figures 4.8 and 4.9. At the lowest reaction temperature tested (30 ^oC), the lowest conversion (4.4%) and highest CO_2 selectivity (5.0 %) were observed. When the reaction temperature was increased from 30 ^oC to 50 ^oC, ethane conversion was shown to increase from 4.4 % to 8.0 % across the same range, whilst a further increase in reaction temperature to 60 ^oC led to a slight reduction in ethane conversion to 6.8 %. The detrimental effect at temperatures in excess of 50 ^oC is inconsistent with studies performed in a batch process (as in Chapter 3 Figure 3.16), in which a linear increase of conversion was achieved through increasing the reaction temperature from 30 to 70 ^oC.

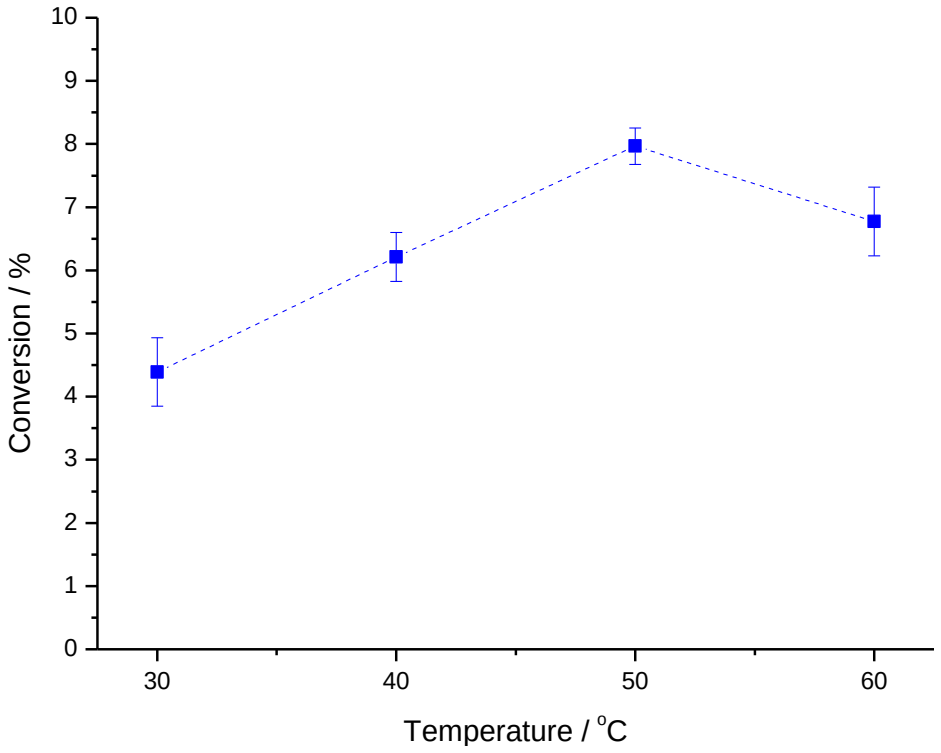

Test conditions: 2.0 g 0.4% Fe/ZSM-5 pelleted + SiC diluent, liquid flow rate 0.25 ml min^{-1} H_2O_2/H_2O (0.123 M, 30.6 µmol min^{-1} H_2O_2), 10 ml min^{-1} of 10% C_2H_6/Ar (37 µmol min^{-1} C_2H_6) , P(C_2H_6/Ar) = 20 bar

Figure 4.8 The effect of reactor temperature on ethane conversion.

As the temperature was increased from 40 °C to 60 °C, selectivity to ethanol and formic acid were shown to decrease from 4.3 to 1.3 % and 19.1 to 15.6 % respectively. Across the same temperature range an increase in acetic acid selectivity from 69.8 to 78.1 % was observed. This is considered to be an important result as it suggests that whilst the ethanol is undergoing sequential oxidation to acetic acid, probably through acetaldehyde (based on previous studies in Chapter 3), a simultaneous increase in acetic acid cracking was not observed. These trends contrast those observed under batch reaction conditions (Figure 3.17) whereby an increase in temperature from 30 to 70 °C led to a linear decrease in ethanol selectivity coupled with a corresponding increase in acetic acid, formic acid and CO_2 selectivities. This implies reduced C-C scission (and thereby higher C_2 selectivity)

under the flow regime than in the batch reaction system, which may be attributed to more facile removal of products from the catalyst bed leading to shorter residence time, and is also consistent with plug flow together with relatively high gas flow rate facilitating forward transport of the C_2 products down through the catalyst bed and into the liquid-gas separator. Within the batch reaction system, solid catalyst and aqueous oxidant/product phase are in constant intimate contact for the duration of the reaction, which leads to longer contact times and therefore increased cracking.

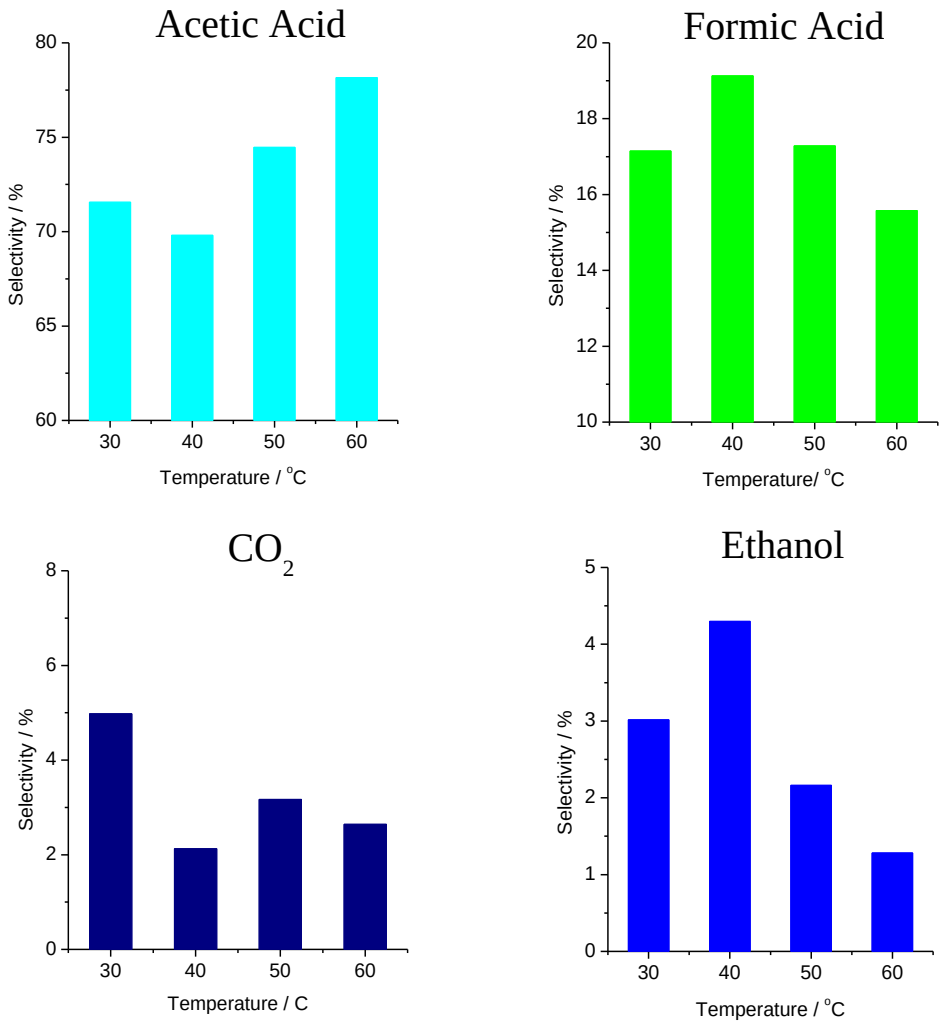

Test conditions: 2.0 g 0.4% Fe/ZSM-5 pelleted + SiC diluent, liquid flow rate 0.25 ml min^{-1} H_2O_2/H_2O (0.123 M, 30.6 µmol min^{-1} H_2O_2), 10 ml min^{-1} of 10% C_2H_6/Ar (37 µmol min^{-1} C_2H_6) , P(C_2H_6/Ar) = 20 bar.

Figure 4.9 The effect of reactor temperature on major product selectivities.

4.3.5 The effect of liquid flow rate

The effect of the liquid feed rate (HPLC output flow) upon the 0.4% Fe/ZSM-5 (30) catalysed system was then investigated, with all other reaction parameters held as constant. Figure 4.10 represents the ethane conversion rates achieved, and percentage of the feed H_2O_2 which was decomposed per unit time. Upon increasing the liquid feed rate from 0.125 ml min^{-1} to 1.0 ml min^{-1}, at a constant hydrogen peroxide concentration (0.123 M), ethane conversion increased from 3.7 % to 13.4 %. Upon increasing flow rates from 0.125 ml min^{-1} to 0.25 ml min^{-1} an increase in conversion was observed, suggesting that the catalyst is capable of higher productivities given a sufficient feed of oxidant and substrate. A degree of limitation is observed at flow rates in excess of 0.25 ml min^{-1}. Upon increasing the liquid flow rate a decrease in the percentage of hydrogen peroxide decomposed was observed, suggesting that reduced contact times impair its activation.

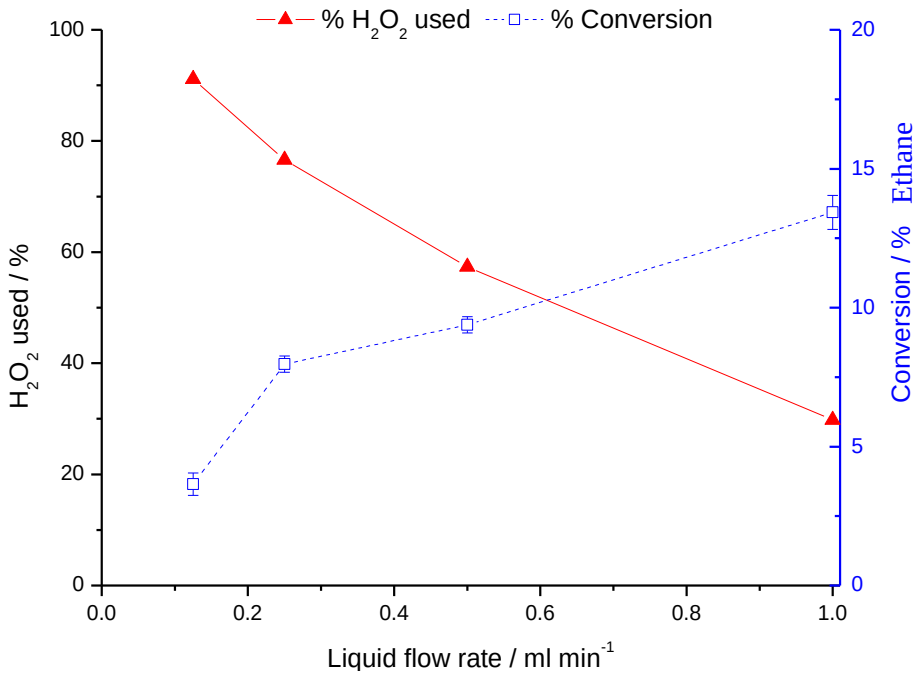

Test conditions: 2.0 g 0.4% Fe/ZSM-5 pelleted + SiC diluent, H_2O_2/H_2O flow (0.123 M H_2O_2), 10 ml min^{-1} of 10% C_2H_6/Ar (37 µmol min^{-1} C_2H_6) , P(C_2H_6/Ar) = 20 bar, Temp = 50 ^{o}C

Figure 4.10 The effect of liquid feed (H_2O_2/H_2O) flow rate on ethane conversion /oxidant usage.

The major product selectivities which were observed at the different flow rates are presented in Figure 4.11. When the liquid flow rate was increased, formic acid and CO_2 selectivities also increased, whilst a gradual decrease in selectivity towards acetic acid and ethanol was observed. At higher liquid flow rates we see a decreased ethane: H_2O_2 ratio, which results in increased conversion of intermediates and selectivity to deeper oxidation products, in particular CO_2. Favouring of secondary C_1 oxidation products is consistent with previous observations, as greater ethane solubility, at higher C_2H_6/Ar pressure, led to reduced C-C scission and thereby higher C_2 selectivity (Figure 4.7).

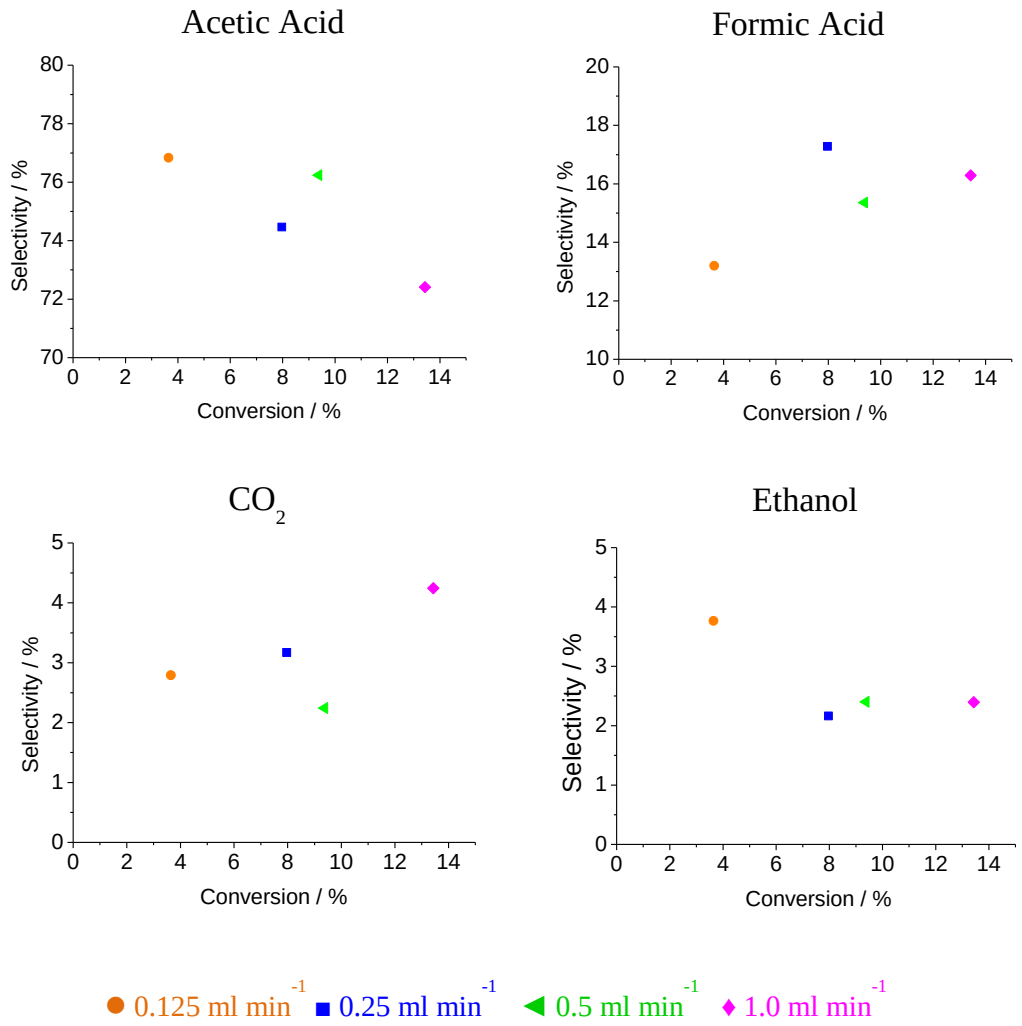

Test conditions: 2.0 g 0.4% Fe/ZSM-5 pelleted + SiC diluent, H_2O_2/H_2O flow (0.123 M H_2O_2), 10 ml min^{-1} of 10% C_2H_6/Ar (37 µmol min^{-1} C_2H_6) , P(C_2H_6/Ar) = 20 bar, Temp = 50 ^{o}C

Figure 4.11 The effect of liquid feed (H_2O_2 / H_2O) flow rate on major product selectivities.

4.3.6 The effect of hydrogen peroxide concentration

The effect of hydrogen peroxide concentration upon ethane conversion and product selectivities was then investigated, whilst maintaining all other reaction parameters constant. Analogous studies conducted under batch reaction conditions showed a 1st order increase in conversion with [H_2O_2], with a degree of mass transfer limitation shown at concentrations of greater than 0.5 M (Chapter 3 Figure 3.18). Under flow conditions an increase in conversion is also observed with increased hydrogen peroxide concentration as shown in Figure 4.12, with the initial two points suggesting a 1st order relationship. That the relationship between hydrogen peroxide concentration and conversion is not as well defined as was observed under batch conditions reflects the greater complexity inherent in TBRs when compared with batch reactor systems.

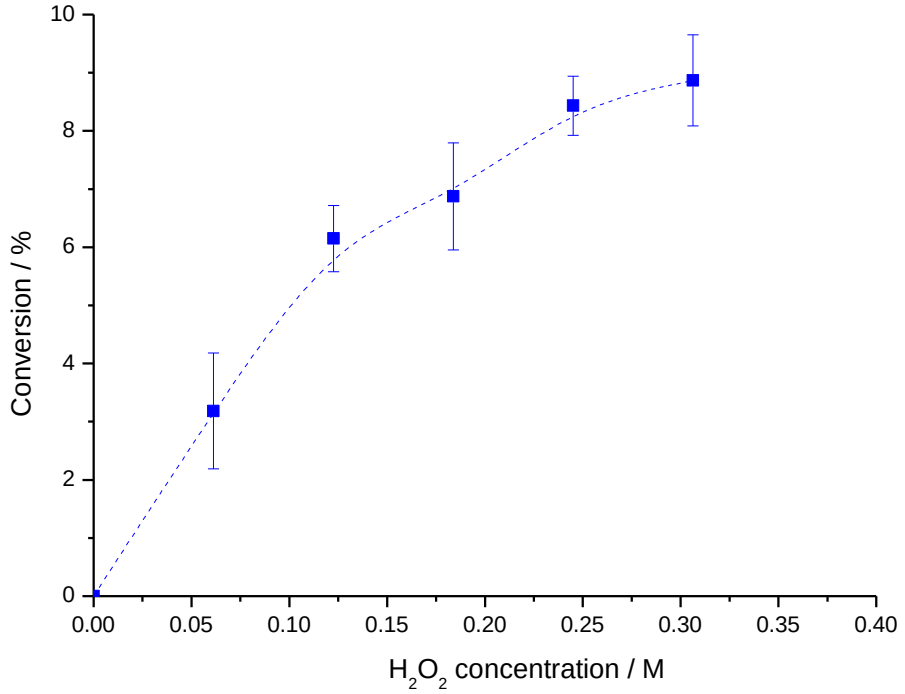

Test conditions: 2.0 g 0.4% Fe/ZSM-5 pelleted + SiC diluent, liquid flow rate 0.25 ml min^{-1} H_2O_2/H_2O, 10 ml min^{-1} of 10% C_2H_6/Ar (37 µmol min^{-1} C_2H_6) , P(C_2H_6/Ar) = 10 bar, Temp = 50 ^oC

Figure 4.12 Effect of H_2O_2 concentration on ethane conversion.

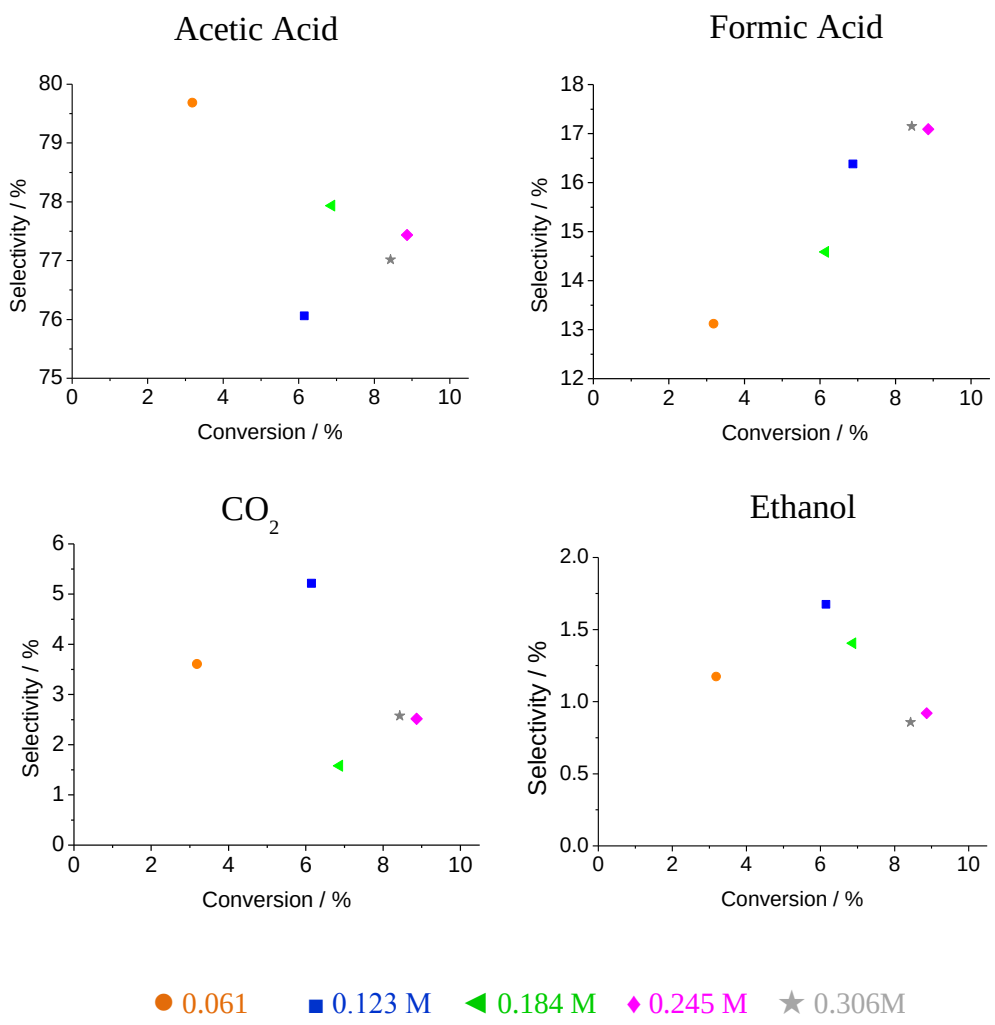

Test conditions: 2.0 g 0.4% Fe/ZSM-5 pelleted + SiC diluent, liquid flow rate 0.25 ml min^{-1} H_2O_2/H_2O flow, 10 ml min^{-1} 10% C_2H_6/Ar (37 µmol min^{-1} C_2H_6), P(C_2H_6/Ar) = 20 bar, Temp = 50 ^oC

Figure 4.13 Effect of H_2O_2 concentration on ethane conversion and major product selectivities.

An increase in hydrogen peroxide concentration from 0.061 M to 0.306 M, led to increased ethane conversion (3.2 % to 8.9 % respectively). The effect of hydrogen peroxide concentration upon product selectivities is illustrated in Figure 4.13. An increase in hydrogen peroxide concentration from 0.061 M to 0.306 M led to a reduction in acetic acid selectivity (79.7% to 77.4%), coupled with increased formic acid selectivity (13.1% and 17.1% respectively). To some extent this is consistent with batch reaction results, where the key selectivity change observed upon increasing hydrogen peroxide concentration was that of the major product, with acetic acid favoured over ethanol at

increasing concentrations. Given that formic acid is derived from acetic acid under reaction conditions (Chapter 3), and that acetic acid has consistently been shown to be the major product for Fe/ZSM-5 catalysed ethane oxidation under this flow regime, with ethanol a minor product, batch and flow systems may be considered to be comparable

4.3.7 Optimised 0.4% Fe/ZSM-5 (30) catalysed reaction

With the aim of determining the extent to which ethane may be converted to oxygenated products within the flow system (within the limitations of the reactor), reaction conditions were chosen to reflect the optimal conditions identified in the experimental results presented thus far. Through use of 2.00 g 0.4% Fe/ZSM-5 , total pressure of 20 bar, 10 ml min^{-1} gas feed (10% C_2H_6/Ar, 37 µmol min^{-1} C_2H_6), 1.00 ml min^{-1} liquid feed (0.306 M H_2O_2/H_2O, 306.4 µmol min^{-1}) at 50 ^oC; 23.4 % ethane conversion was achieved with major products; acetic acid (73.1 % selectivity) and formic acid (18.8% selectivity). Low selectivity to CO_2 was observed (1.3%). The steady state conversion and product selectivities observed are presented in Figure 4.14.

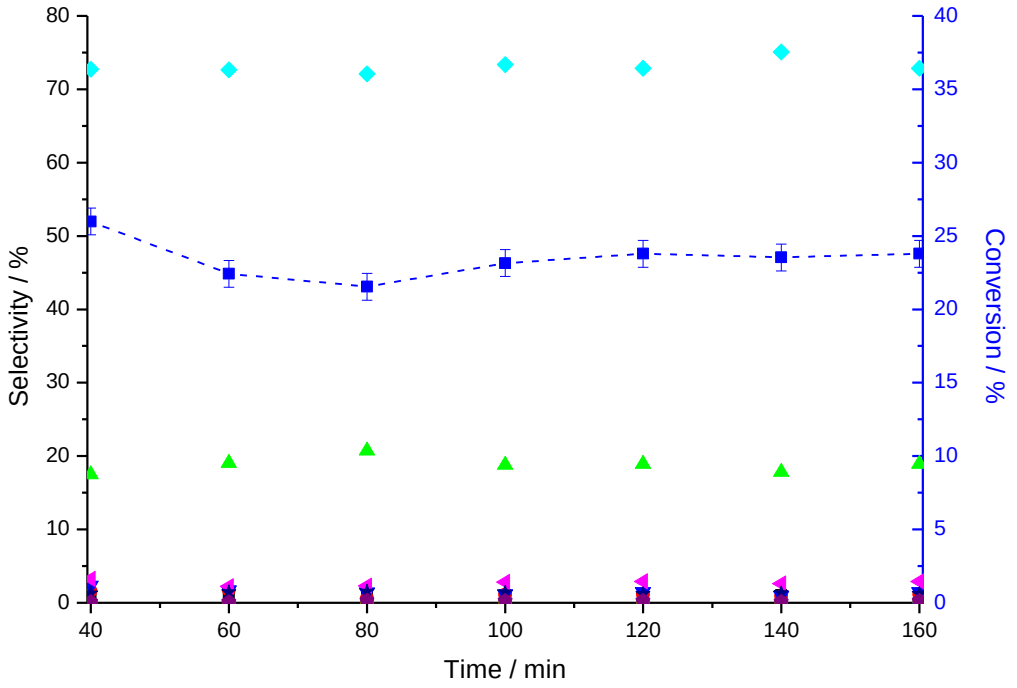

■ Black squares (CH_3OOH), ● Red Circles (CH_3OH), ♦ Aquamarine diamonds (CH_3COOH), ◀ Pink triangles (CH_3CHO), ▼ Blue triangles (C_2H_5OH), ▲ Green triangles ($HCOOH$), ● Beige circles (CH_4), ★Navy Stars (CO_2), ⬟ Purple pentagons (C_2H_4), -■- Blue squares /dashes (% Conversion, based on Carbon)

Test conditions: 2.0 g 0.4% Fe/ZSM-5 pelleted + SiC diluent, liquid flow rate 1.00 ml min^{-1} H_2O_2/H_2O (0.306 M, 306 µmol min^{-1} H_2O_2), 10 ml min^{-1} of 10% C_2H_6/Ar (37 µmol min^{-1} C_2H_6), $P(C_2H_6/Ar)$ = **20** bar, Temp = 50 ^{o}C

Fig 4.14 Conversion and product selectivities as observed under optimised conditions.

4.4 The effect of catalyst composition

One striking aspect of batch ethane oxidation studies was the high selectivity towards ethene achieved through post synthesis doping of Cu and Fe/Cu to ZSM-5 (30) by CVI. In a recent publication,[8] we have shown that under batch testing conditions used in the publication,[8] 0.2 % ethane conversion to ethene (30.2 %) could be achieved within 0.5 h at 50 ^{o}C using 2.5% Cu/ZSM-5 (30) and that 1.6 % ethane conversion with higher ethene selectivity (34.2 %) can be attained using 1.25% Fe-1.25% Cu/ZSM-5.[8] Furthermore it

was shown in Chapter 3 of this thesis that by stirring the batch-testing system during the ramping period, enhanced ethene selectivity (45.5%) may be achieved, at the expense of lower ethane conversion (1.15%).

To determine whether the high degree of ethene selectivity attained under batch reactor conditions could be effectively applied in a continuous flow TBR system, 8 h tests of 2.5% Cu/ZSM-5 (30) and 0.4% Fe 0.4% Cu/ZSM-5 (30) were performed. A full breakdown of product selectivities and conversion for 2.5% Cu/ZSM-5 (30) are shown in Figure 4.15. An average steady state ethene selectivity of 49.8 % at an average conversion of 1.6 % was observed for the Cu only catalyst, with average selectivities to ethanol and acetaldehyde of 13.8 % and 18.0 % respectively. This is consistent with the previously proposed reaction scheme (Chapter 3 Scheme 3.1), in which we observed facile oxidation of ethanol to acetaldehyde in the presence of ZSM-5 catalysts. The presence of methanol, and absence of formic acid is in accordance with previously reported Cu/ZSM-5 catalysed C_1 and C_2 oxidation data.[8] The absence of acetic acid in the product stream is an interesting result, as it suggests that of the C_2 primary products which have been shown to undergo oxidation under batch conditions to acetic acid; ethene, ethanol and ethylhydroperoxide, none are undergoing overoxidation to acetic acid in this catalyst system, whereas C-C scission is occurring. This is consistent with Cu mopping up ·OH radicals, as proposed for the Cu/ZSM-5 (30) catalysed methane oxidation system.[11]

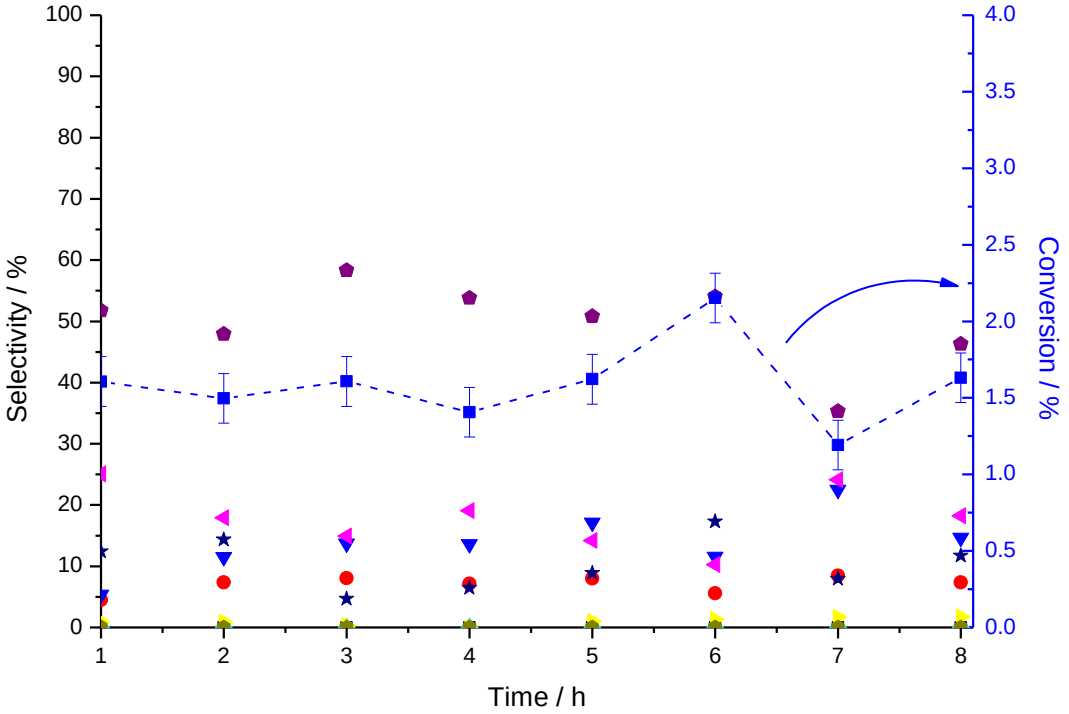

■ Black squares (CH_3OOH), ● Red Circles (CH_3OH), ♦ Aquamarine diamonds (CH_3COOH), ◀ Pink triangles (CH_3CHO), ▼ Blue triangles (C_2H_5OH), ▲ Green triangles ($HCOOH$), ● Beige circles (CH_4), ★Navy Stars (CO_2), ⬟ Purple pentagons (C_2H_4), -■- Blue squares /dashes (% Conversion, based on Carbon)

Test conditions: 2.0 g 2.5% Cu/ZSM-5 pelleted + SiC diluent, liquid flow rate 0.25 ml min^{-1} H_2O_2/H_2O (0.123 M, 30.6 µmol min^{-1} H_2O_2), 10 ml min^{-1} of 10% C_2H_6/Ar (37 µmol min^{-1} C_2H_6), P(C_2H_6/Ar) = 20 bar, Temp = 50 ^{o}C

Fig 4.15 Conversion and product selectivities as observed over an 8 h evaluation of 2.5% Cu/ZSM-5 (30) CVI.

It was previously shown that a combination of Fe and Cu on ZSM-5 (30) via CVI, exhibit enhanced levels of ethane conversion when compared Cu only ZSM-5 catalyst, whilst maintaining high ethene selectivity observed with 2.5% Cu/ZSM-5 (30).[8] Upon evaluating 0.4% Fe-0.4% Cu/ZSM-5 (30), a steady state conversion of 8.2 % ethane to acetic acid (43.0%), formic acid (13.6%) and ethene (31.2 %) as major products was achieved as shown in Figure 4.16. The high acetic acid and formic acid selectivities observed are consistent with ethene being oxidised and cracked to the C_2 and C_1 acids, as shown in the ethene stability studies in Chapter 3. As proposed in Chapter 3 it is probable

that acetic acid is formed not only through oxidation of ethene, but also from ethanol which is formed directly from ethane. This is supported by the consistently low ethanol selectivity encountered under flow conditions, when compared with analogous catalytic systems under batch conditions (for example 0.4% Fe/ZSM-5 (30) shown in Chapter 3 Figure 3.10).

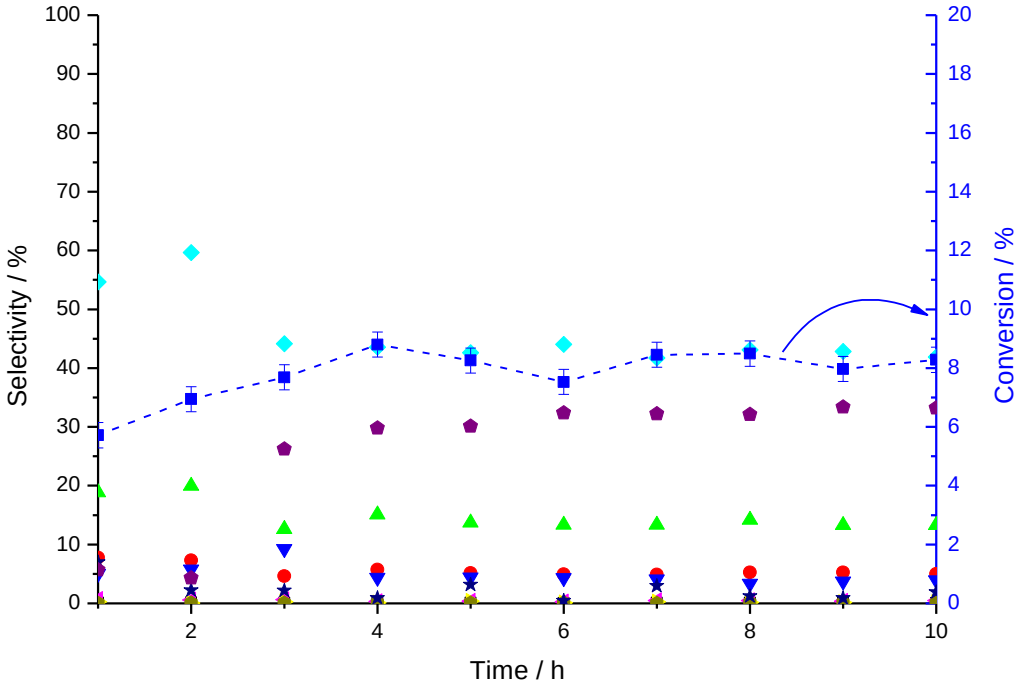

■ Black squares (CH_3OOH), ● Red Circles (CH_3OH), ♦ Aquamarine diamonds (CH_3COOH), ◀ Pink triangles (CH_3CHO), ▼ Blue triangles (C_2H_5OH), ▲ Green triangles ($HCOOH$), ● Beige circles (CH_4), ★Navy Stars (CO_2), ⬟ Purple pentagons (C_2H_4), -■- Blue squares /dashes (% Conversion, based on Carbon)

Test conditions: 2.0 g 0.4% Fe 0.4% Cu/ZSM-5 pelleted + SiC diluent, liquid flow rate 0.25 ml min^{-1} H_2O_2/H_2O (0.123 M, 30.6 µmol min^{-1} H_2O_2), 10 ml min^{-1} of 10% C_2H_6/Ar (37 µmol min^{-1} C_2H_6), P(C_2H_6/Ar) = 20 bar, Temp = 50 ^{o}C

Figure 4.16 Conversion and product selectivities as observed over a 10 h investigation of 0.4% Fe 0.4% Cu/ZSM-5 (30) CVI.

Given that the oxidative conversion of C_1 and C_2 alkane has been shown to be dependent upon Fe loading,[11] with increased loading associated with increased conversion (increased catalyst productivity) as shown in Figure 3.10, Fe/ZSM-5 (30) catalysts with 0,

1.25 and 2.5 wt% loading of Fe were tested (ICP-MS showed H-ZSM-5 (30) to contain 0.013 wt% Fe as an impurity). The effect of wt% Fe loading upon conversion is presented in Figure 4.17.

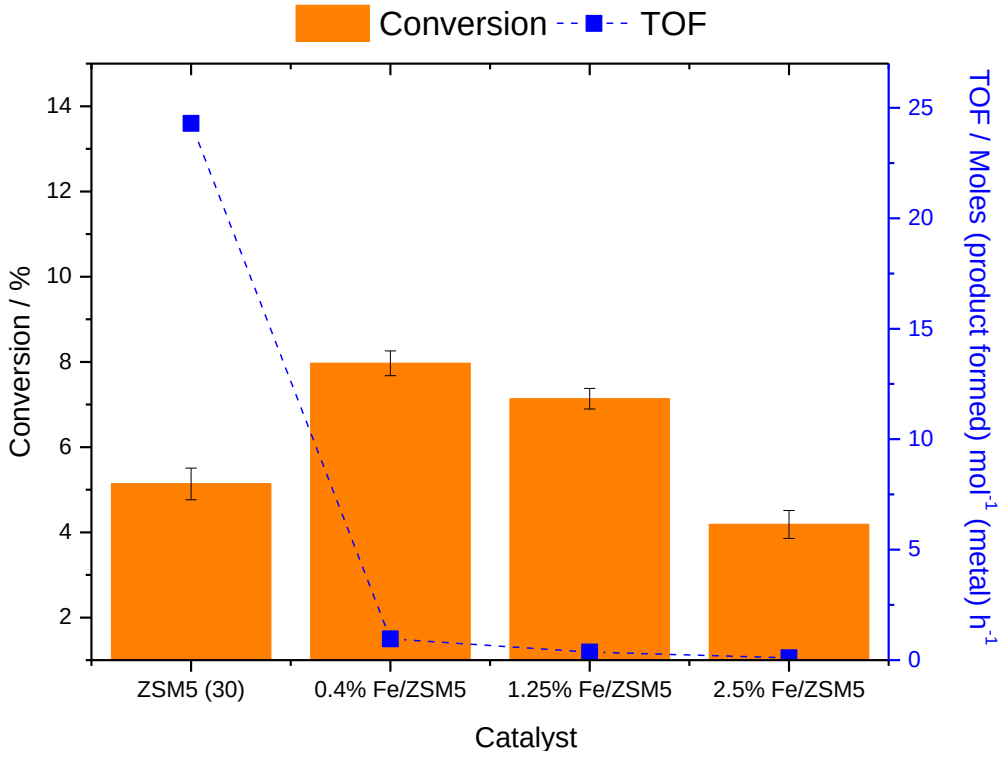

Test Conditions: 2.0 g % catalyst prepared by CVI, pelleted + SiC diluent, liquid flow rate 0.25 ml min^{-1} H_2O_2/H_2O (0.123 M, 30.6 µmol min^{-1} H_2O_2), 10 ml min^{-1} of 10% C_2H_6/Ar (37 µmol min^{-1} C_2H_6), P(C_2H_6/Ar) = 20 bar, Temp = 50 ^{o}C

Figure 4.17 Effect of Fe loading on ethane conversion and catalyst turnover frequency (mol (product) mol $(Fe)^{-1}$ h^{-1}).

When 0.4 wt% Fe was loaded onto H-ZSM-5 (30) ethane conversion increased, from 5.2 to 7.9 %. When additional Fe was added, leading to loadings of 1.2 and 2.5 wt%, a decrease in conversion to 7.1 and 4.2 % was observed respectively. This inhibitory effect of extraframework Fe has been attributed to an increase in non-selective H_2O_2 decomposition to diatomic oxygen, which was observed within the effluent gas feed at higher loadings. A gas chromatogram showing the presence of oxygen in the effluent gas

is shown in Figure 4.18. Additionally, an oxygen balance (%), calculated as (mol O_2 in products)/ (mol O_2 in decomposed H_2O_2 x 100), clearly shows a linear decrease in the efficiency with which the oxygen from H_2O_2 is incorporated into oxygenated products upon increasing the wt % Fe/ZSM-5 loading for CVI catalysts up to a point, then decreases because of unselective decomposition. This is shown in Figure 4.19.

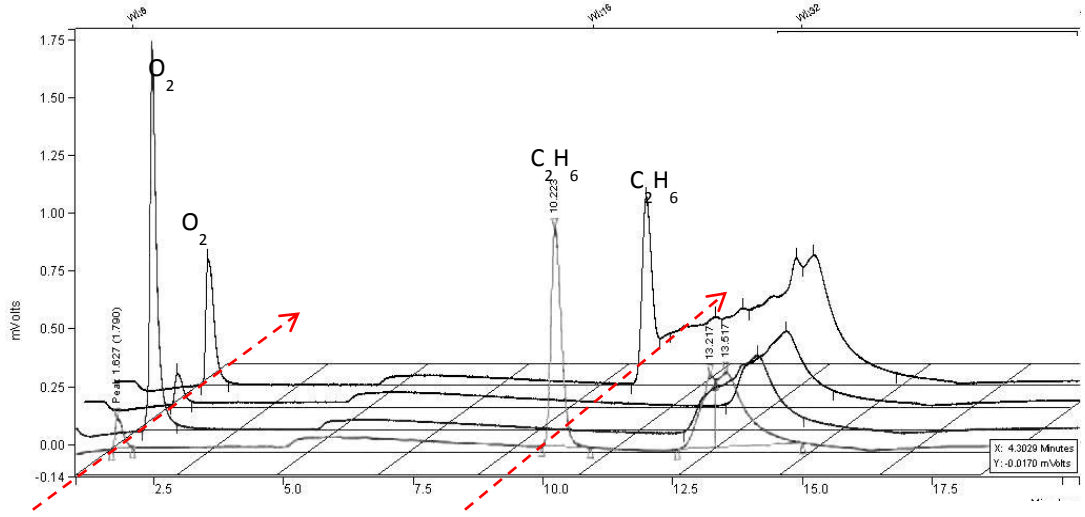

O_2 (1.89 minutes) C_2H_6 (9.30 minutes)

Figure 4.18 A gas chromatogram showing O_2 in the effluent gas of Fe/ZSM-5 (30) catalysed ethane oxidation under flow conditions

It is likely that given the relatively high mass of catalyst within the bed (2.00 g), and comparatively low hydrogen peroxide concentration (0.123 M), active site availability is in excess, with the mass transfer of substrate and oxidant to the active site being rate limiting.

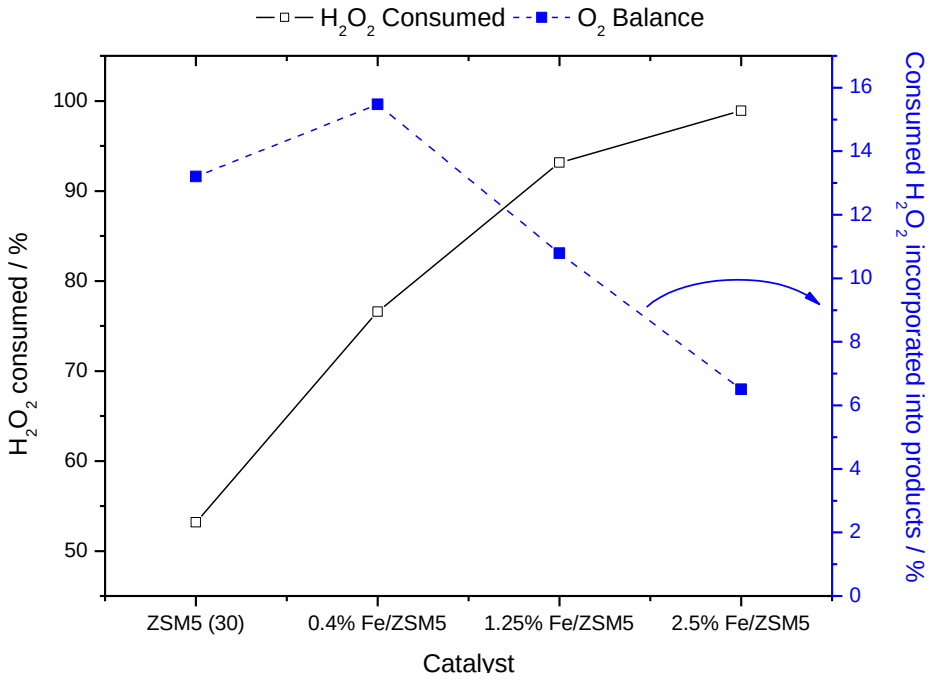

Figure 4.19 The effect of Fe loading on the percentage H_2O_2 consumed and O balance.

In order to test this hypothesis, the hydrogen peroxide concentration was scaled relative to Fe content such that a constant molar ration H_2O_2 min^{-1}: mol (iron) in bed was maintained. The results for these experiments are shown in Figure 4.20.

When the rate at which the oxidant was fed over the catalyst bed was increased (increased concentration, constant flow rate) proportionally with increased wt% Fe/ZSM-5 (30) a linear increase in ethane conversion was observed, from 0.86% for H-ZSM-5 (30) to 12.0% for 1.25% Fe/ZSM-5 (30). Though a drop in TOF h^{-1} from 4.2 to 0.58 is observed moving from H-ZSM-5 (30) to 1.25% Fe/SM-5 (30), this data suggests that catalyst bed productivity may be increased by increased iron loading provided sufficient oxidant is present (Figure 4.20). It is interesting to note that no significant variation in the product distribution was observed at increasing loadings of Fe/ZSM-5 (30) with both 0.4 and 1.25 wt% Fe catalysts showing *ca* 75% acetic acid, 2% ethanol, 17% formic acid and 3% CO_2 selectivity. An O_2 balance as in Figure 4.19 showed that, once again, an increase in Fe

loading from 0.0132% to 0.4 wt% and 1.25 wt% led to a decrease in retention of O_2 in the products with the percentage retained falling from 43.4% to 14.4% and 5.15% respectively, as shown in Figure 4.21.

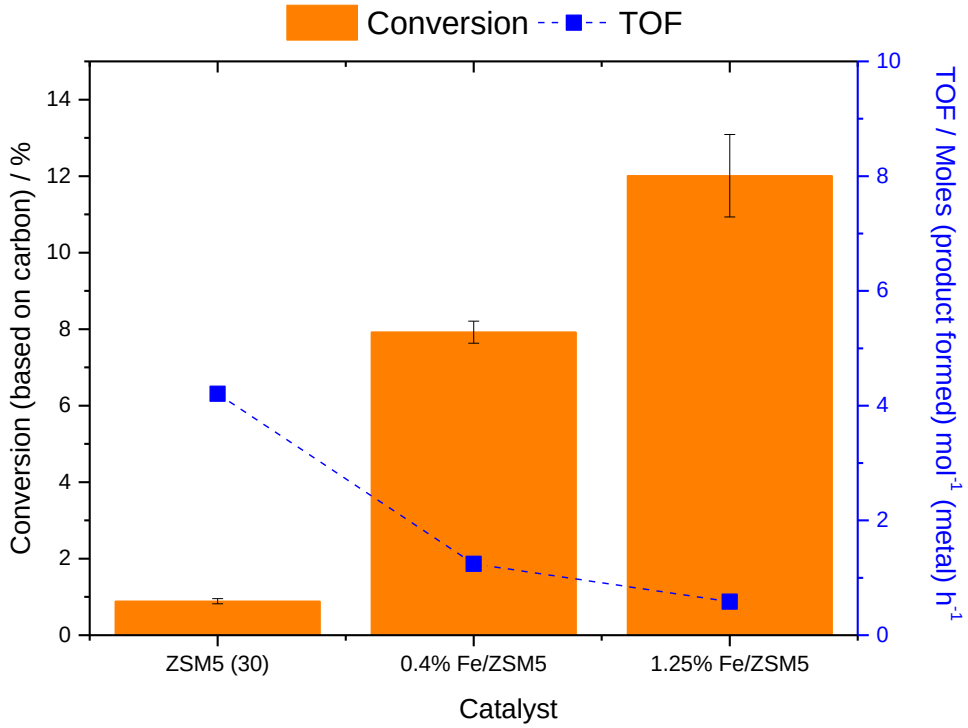

Test Conditions; 2.0 g Catalyst pelleted + SiC diluent, 0.25 mLmin^{-1} H_2O_2/H_2O flow, 10 mLmin^{-1} of 10% C_2H_6/Ar (37 µmolmin^{-1} C_2H_6), P(C_2H_6) = **20** bar, Temp = 50 ^{o}C
ZSM5 (1.07 µmolmin^{-1} H_2O_2) **0.4% Fe/ZSM5** (30.63µmolmin^{-1} H_2O_2) **1.25% Fe/ZSM5** (95.74 µmolmin^{-1} H_2O_2)

Figure 4.20 The Effect of Fe loading on ethane conversion and catalyst turnover frequency (TOF) with constant molar ratio H_2O_2 min^{-1} : Fe mol/bed.

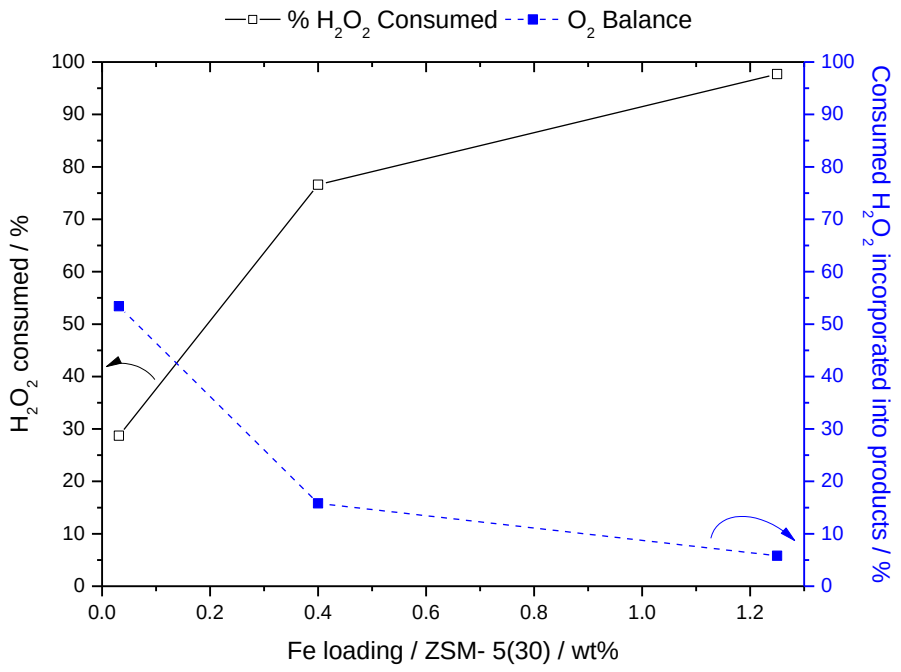

Test Conditions; *2*.0 g Catalyst pelleted + SiC diluent, 0.25 mLmin^{-1} H_2O_2/H_2O flow, 10 mLmin^{-1} of 10% C_2H_6/Ar (37 µmolmin^{-1} C_2H_6), P(C_2H_6) = **20** bar, Temp = 50^{o}C

Figure 4.21 The Effect of Fe loading on H_2O_2 consumption and product retention constant molar ratio H_2O_2 min^{-1}: Fe mol/bed.

4.5 The effect of catalyst bed mass

To allow for quantitative comparison of the activity of different supported- metal catalysts in the current flow regime an active site – limited system was required as, when using a 2.00 g catalyst bed, activity is shown to be limited by oxidant availability at Fe/ZSM-5 (30) loadings of greater than 0.4 wt %. To identify such a system, the effect of catalyst mass was investigated in the flow system. A range of different catalyst beds were therefore tested, with the bed made up to constant volume (3.6 ml) with SiC. Ethane conversion and TOF (based on Fe) for reactions using varying catalyst loadings (0.125 – 2.00 g) of 1.25% Fe/ZSM-5 (30) are shown in Figure 4.22. Two additional points

representing TOFs observed under comparable reaction parameters under batch reaction conditions are included for comparison of the two reactor regimes.

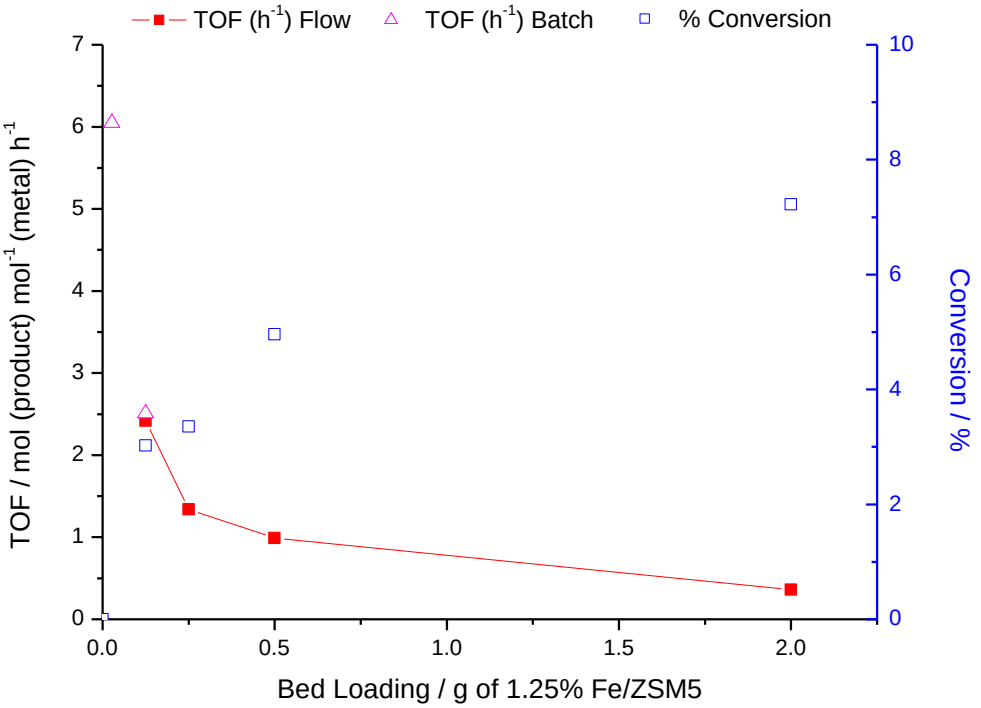

Flow conditions; 1.25% Fe/ZSM-5 pelleted + SiC diluent (24 grit), liquid flow rate 0.25 ml min^{-1} H_2O_2/H_2O (0.123 M, 30.6 µmol min^{-1} H_2O_2), 10 ml min^{-1} of 10% C_2H_6/Ar (37 µmolmin^{-1} C_2H_6), P(C_2H_6/Ar) = 20 bar, Temp = 50 ^{o}C**. Batch Conditions**; [H_2O_2] = 0.123 M, 10 ml reaction volume, P (C_2H_6) = 20 bar, 125 mg pelleted catalyst, 0.5 h, 50 ^{o}C, 1500 rpm

Figure 4.22 Effect of bed-catalyst loading upon ethane conversion and catalyst turnover frequency.

As shown in Figure 4.22 ethane conversion increased with increased catalyst mass loading. The fact that a nonlinear increase in ethane conversion, and by implication a reduction in TOF, was observed at increasing catalyst- bed loadings suggests reduced catalyst productivity (per unit mass) at higher catalyst loadings, which is likely of kinetic origin. The TOF observed with 1.25% Fe/ZSM-5 at 0.125 g loading (2.42 h^{-1}) under continuous flow conditions, is of an equal order of magnitude to an analogous batch

reaction (2.51 h^{-1}) as shown in Figure 4.22. This suggests that a significant degree of mass transfer limitation (with regards to oxidant and substrate) is not in operation under these test conditions and implies that comparable catalyst productivities to those achieved under batch conditions might be attainable under continuous flow conditions were a pure ethane feed and concentrated H_2O_2 feed used.

4.6 The effect of supported metals

Given that mass transfer limitation may be circumvented through use of lower catalyst-bed loadings, the effect of Fe loading on ZSM-5 (30) was investigated once more in the flow system, this time using a lower catalyst loading (0.25 g) within the bed. Steady state ethane conversion values and the percentage of hydrogen peroxide decomposed under steady state operation are shown in Figure 4.23.

Unlike trends seen at higher catalyst loadings (2.00g, Figure 4.16), at increasing loadings of Fe on ZSM-5 (30), a linear increase in the percentage of ethane converted and percentage of H_2O_2 decomposed is observed in Figure 4.23. Product distributions for Fe/ZSM-5 (30) catalysts are shown in Figure 4.24. As the Fe loading was increased, selectivity towards ethanol, ethene, acetaldehyde, methyl hydroperoxide, methanol and CO_2 decreased, whilst acetic acid and formic acid selectivities were determined to increase (Figure 4.23). The fact that an increase in C_2 selectivity was observed at increased iron loadings, with 73.1% and 79.6% selectivity for H-ZSM-5 (30) and 2.5% Fe/ZSM-5 (30) respectively, indicates that C-C cracking is not proportional to Fe loading within this system.

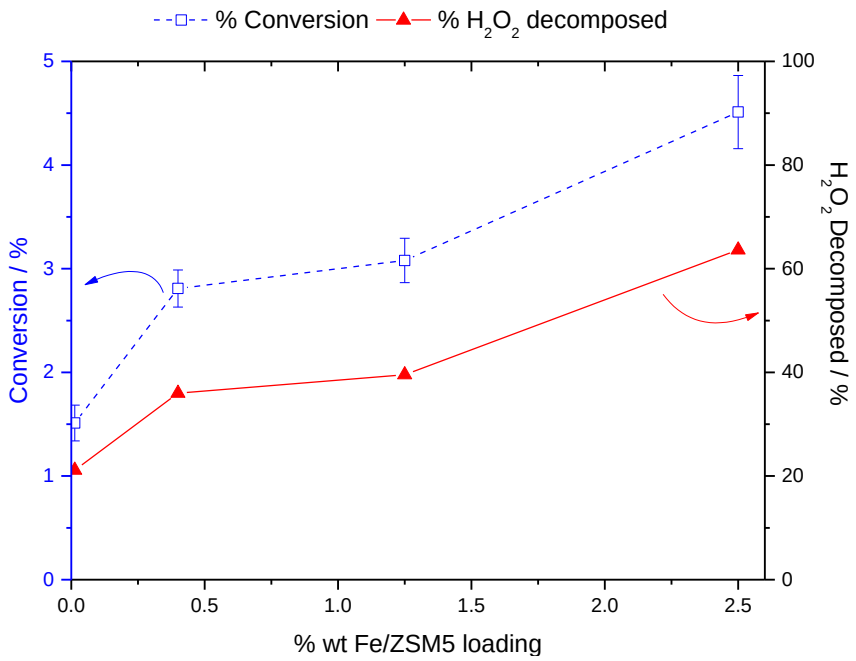

Test conditions: 0.25g catalyst CVI pelleted + SiC diluent (24 grit), liquid flow rate 0.25 ml min^{-1} H_2O_2/H_2O (0.123 M, 30.6 µmol min^{-1} H_2O_2), 10 ml min^{-1} of 10% C_2H_6/Ar (37 µmol min^{-1} C_2H_6), P(C_2H_6/Ar) = 20 bar, Temp = 50 ^oC

Figure 4.23 The effect of Fe loading on ZSM-5 upon ethane conversion and H_2O_2 usage

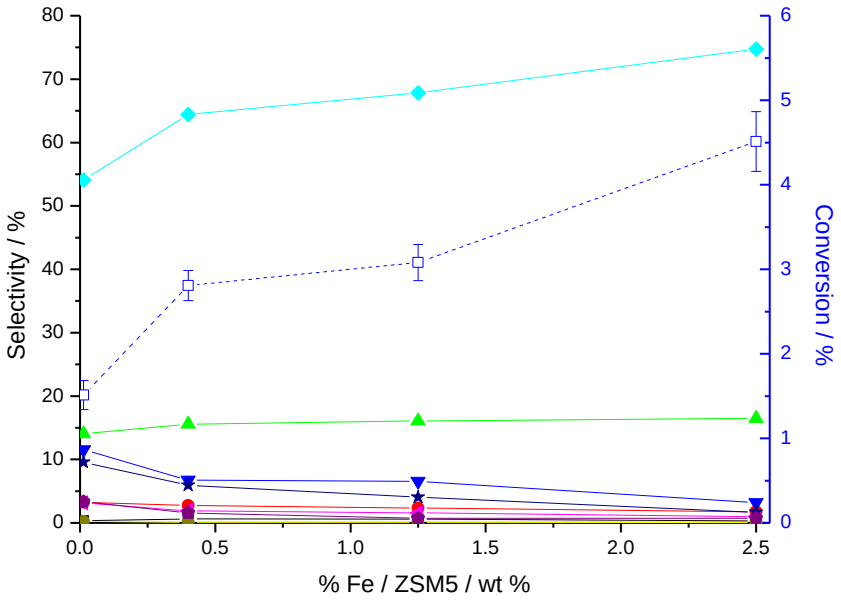

■ Black squares (CH_3OOH), ● Red Circles (CH_3OH), ♦ Aquamarine diamonds (CH_3COOH), ◄ Pink triangles (CH_3CHO), ▼ Blue triangles (C_2H_5OH), ▲ Green triangles ($HCOOH$), ● Beige circles (CH_4), ★Navy Stars (CO_2), ⬟ Purple pentagons (C_2H_4), -□- Blue squares (% Conversion, based on Carbon

Figure 4.24 The effect of Fe loading on ZSM-5 upon product selectivities

It was shown in Chapter 3 (Figure 3.23) that addition of varying wt% Cu to 1.25% Fe/ZSM-5 (30) led to an increased ethene selectivity up to and including 1:1 Fe: Cu wt ratio, with 1.25% Fe 1.25% Cu/ZSM-5 (30) showing 1.15% ethane conversion to methanol (6.0%), ethanol (26.6%), acetic acid (19.9%), acetaldehyde (1.3%), CO_2 (0.41%) and ethene (45.5%). This study was replicated under continuous flow conditions in order to determine the extent to which ethene selectivity may be elicited (0.25 g bed loading). Conversion and product selectivities observed are presented in Figure 4.25. Consistent with trends observed under batch reaction conditions (Figure 3.20), addition of Cu to 1.25% Fe/ZSM-5 (30) had no beneficial impact upon ethane conversion.

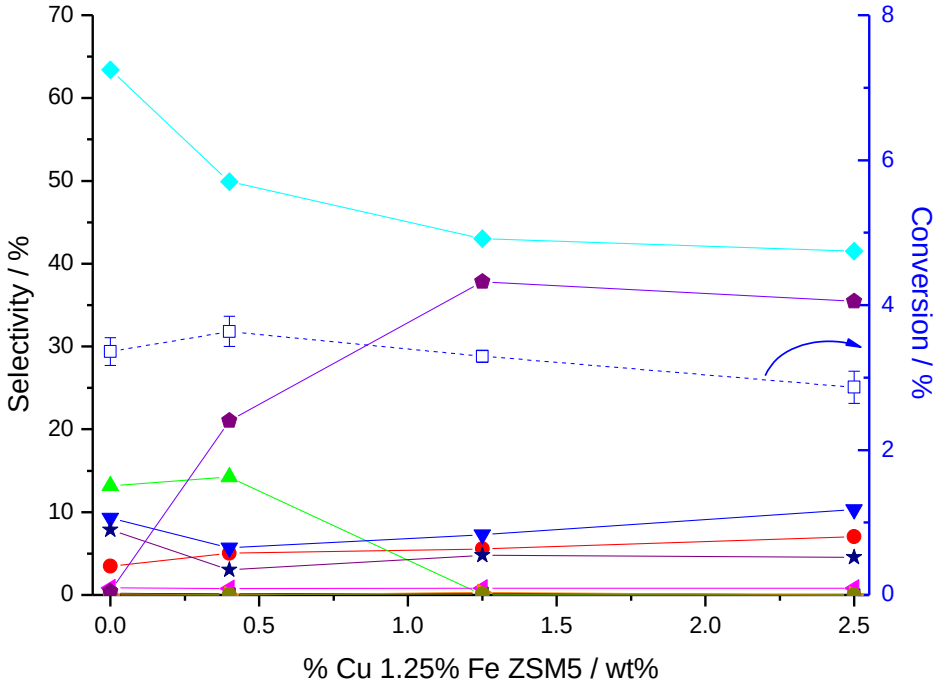

■ Black squares (CH_3OOH), ● Red Circles (CH_3OH), ♦ Aquamarine diamonds (CH_3COOH), ◀ Pink triangles (CH_3CHO), ▼ Blue triangles (C_2H_5OH), ▲ Green triangles ($HCOOH$), ● Beige circles (CH_4), ★Navy Stars (CO_2), ⬟ Purple pentagons (C_2H_4), -□- Blue squares (% Conversion, based on Carbon)

Test conditions: 0.25g catalyst CVI pelleted + SiC diluent (24 grit), liquid flow rate 0.25 ml min^{-1} H_2O_2/H_2O (0.123 M, 30.6 µmol min^{-1} H_2O_2), 10 ml min^{-1} of 10% C_2H_6/Ar (37 µmol min^{-1} C_2H_6), P(C_2H_6/Ar) = 20 bar, Temp = 50 ^oC

Figure 4.25 The effect of %wt Cu loading on 1.25% Fe/ ZSM-5 upon conversion and product selectivities.

At increasing Cu loadings a gradual decrease in acetic acid selectivity was observed, with a simultaneous increase in ethene selectivity shown. As was observed under batch conditions, ethene and acetic acid selectivities levelled off at Cu:Fe ratios in excess of 1:1 wt%, at 37.8 % and 43.0 % respectively. Once more formic acid was not observed at Cu:Fe wt ratios of greater than 1:1. Interestingly, whilst the trends in ethanol and acetic acid selectivity at increasing Cu loading mirror those observed in the corresponding batch reaction study, whereas under batch conditions the major aqueous product was ethanol, with acetic acid a close second, under flow conditions the only major aqueous product is acetic acid. Given that the substrate feed under investigation comprises a low partial pressure ethane (10%) in argon (90%), which has been implicated in the relatively high selectivity shown by Fe/ZSM-5 (30) catalysts to acetic acid under flow conditions, it is perhaps not surprising that ethanol selectivity for FeCu/ZSM-5 (30) materials is markedly lower under flow conditions than in the comparable batch studies.

Interestingly a similar effect upon the distribution of ethene and its oxidation products (acetic acid, C_1 oxygenates and CO_2) is not observed under dilute ethane feeds for 1.25% Fe 1.25% Cu/ZSM-5 (30). This implies that either (i) the oxidation of oxygenated products is more facile than that of ethene or (ii) desorption of ethene from the active site is more efficient than that of oxygenated products. Ethene stability studies in Chapter 3 (Figure 3.26) showed low ethene conversion at 50 ^{o}C to acetic acid, formic acid, methanol and CO_2 in a 10% Ethene/N_2 atmosphere. Future studies should be conducted using a pure ethane feed, to determine whether higher ethene and ethanol selectivities may be attained under flow conditions, through preferentially saturating the liquid phase with ethane, to inhibit the re-dissolving/ oxidation of ethene.

4.7 Conclusions

The selective partial oxidation of ethane may be conducted under continuous flow conditions in a laboratory scale TBR, with appreciable single pass ethane conversion (23%) to acetic acid (73% selectivity) observed. The effect of reaction parameters was investigated by varying; gas flow rate, pressure, temperature, liquid feed flow rate, oxidant concentration and Fe loading. Of the conditions tested, ethane pressure was shown to have the most significant influence upon product selectivities, with higher pressures reducing the propensity for C-C scission and deep oxidation to CO_2. Unfortunately the reactor setup was limited to a maximum operating pressure of 30 bar, however trends suggest that greater oxygenate selectivity may be achieved through use of higher total gas pressures. Given that batch studies have shown the partial pressure of ethane in a diluent gas to have a significant effect upon the C_2 product distribution it is highly likely that were a pure feed of ethane to be used, the flow system would favour ethanol as the major product for Fe/ZSM-5 (30) (Fe < 2.5 wt% loading), and allow access to higher ethane conversion. Unfortunately this was not currently possible due to safety considerations.

It has also been shown that ethane conversion may be enhanced in a linear manner through increasing the rate at which the oxidant, hydrogen peroxide, is delivered through the catalyst bed. This may be done either through increasing oxidant concentration in the liquid feed or by increasing the rate at which said feed is pumped through the catalyst bed, though an increase in either was observed to lead to slight increase in C_1 selectivity.

Through use of an active site- limited system, achieved by reducing the catalyst bed loading, ethane conversion (and therefore catalyst productivity) was shown to increase with increased loading of Fe onto ZSM-5 (30). Additionally, conversion of ethane to ethene may be achieved under continuous flow conditions at low temperatures of 50 ^{o}C

with Cu/ZSM-5 (30) and FeCu/ZSM-5 (30) catalysts. The relatively high conversion of ethane (8.2%) to acetic acid (43% selectivity) and ethene (31% selectivity) at 50 ^{o}C under continuous conditions is considered to be a significant result. When compared with the SABIC process outlined in Chapter 1, Section 1.2.2, which showed 53% ethane conversion to acetic acid (49.9%) and ethene (10.5) at a far higher temperature of 260 ^{o}C one could conclude that the higher cost of hydrogen peroxide used in our system when compared to the SABIC oxidant (air) may potentially be offset by the lower operating costs resulting from low reaction temperatures.[12] Furthermore when compared with the highly energy intensive industrialised steam cracking processes which are conducted at temperatures of 500-800 ^{o}C and account for a significant portion of total global ethene production (*ca.* 143 Mt/annum),[13] as well as 40% of the petrochemical industry's energy requirement, the low temperature process explored here becomes more attractive.[14] This is especially so when one considers that, of the estimated energy requirements of said process (*ca*¸ 15,000-27,000 kJ/ kg $_{ethylene}$), the majority is required in firing the cracking furnaces to these high temperatures and in cooling the effluent gas to avoid deep oxidation of products.[14] It is possible that the low temperatures required for selective conversion of ethane to ethene and oxygenated products with Cu- and Fe-Cu- ZSM-5 (30) under flow conditions increase the viability of this catalytic system in spite of the expense of hydrogen peroxide.

Results suggest that with reactor engineering/ scaling, and use of a pure ethane feed, higher conversion of ethane to acetic acid, ethanol and ethene may be achieved at low temperatures using modified zeolite catalysts and H_2O_2 under continuous flow conditions. The potential ability to switch the selectivity of Fe/ZSM-5 (30) catalysed ethane oxidation from ethanol to acetic acid by varying the C_2H_6: Ar would be an interesting system to explore.

4.8 References

1 Jones, J. H. *Platinum Metals Rev* **2000**, *44*, 94.

2 Rahimi, N.; Karimzadeh, R. *Applied Catalysis A: General* **2011**, *398*, 1.

3 Hou, H.; Li, J.; Song, X.; Wang, B. *The Journal of Physical Chemistry A* **2005**, *109*, 11206.

4 Chen, X.; Li, W.; Schwank, J. W. *Catalysis Today* **2011**, *175*, 2.

5 Ramachandran, P. A.; Dudukovic, M. P.; Mills, P. L. *Sadhana-Acad. Proc. Eng. Sci.* **1987**, *10*, 269.

6 Mederos, F. S.; Ancheyta, J.; Chen, J. W. *Appl. Catal. A-Gen.* **2009**, *355*, 1.

7 Al-Dahhan, M. H.; Larachi, F.; Dudukovic, M. P.; Laurent, A. *Industrial & Engineering Chemistry Research* **1997**, *36*, 3292.

8 Forde, M. M.; Armstrong, R. D.; Hammond, C.; He, Q.; Jenkins, R. L.; Kondrat, S. A.; Dimitratos, N.; Lopez-Sanchez, J. A.; Taylor, S. H.; Willock, D.; Kiely, C. J.; Hutchings, G. J. *Journal of the American Chemical Society* **2013**, *135*, 11087.

9 Wakao, N.; Smith, J. M. *Chemical Engineering Science* **1962**, *17*, 825.

10 Novak, M.; Schneider, P. *Applied Catalysis* **1990**, *66*, 209.

11 Hammond, C.; Forde, M. M.; Ab Rahim, M. H.; Thetford, A.; He, Q.; Jenkins, R. L.; Dimitratos, N.; Lopez-Sanchez, J. A.; Dummer, N. F.; Murphy, D. M.; Carley, A. F.; Taylor, S. H.; Willock, D. J.; Stangland, E. E.; Kang, J.; Hagen, H.; Kiely, C. J.; Hutchings, G. J. *Angewandte Chemie International Edition* **2012**, *51*, 5129.

12 Karim, K.; Al-Hamzi, M. H.; Mamedov, E. In *Catalysts for the oxidation of ethane to acetic acid, processes of making same and processes of using same*; Saudi Basic Industries Corp, 1999.

13 Fan, D.; Dai, D. J.; Wu, H. S. *Materials* **2013**, *6*, 101.

14 Zimmermann, H.; Walzl, R. In *Ethylene*; Wiley-VCH Verlag GmbH & Co. KGaA, 2000.

5

Identifying the role of Al in Cu- modified ZSM-5 catalysts

5.1 Introduction

Investigations into the reaction pathway for Fe- and Cu- ZSM-5 (30) catalysed ethane oxidation with H_2O_2 have been discussed in Chapter 3. From said studies it was concluded that there are three primary reaction products; ethanol, ethylhydroperoxide and ethene. The two oxygenated products were shown to undergo consecutive oxidations to acetaldehyde and acetic acid, whilst ethene oxidised under reaction conditions to yield acetic acid. Additionally, C_2 oxygenates were involved in C-C scission reactions to yield an array of C_1 oxygenates and the deep oxidation product CO_2. It was also shown that upon increasing Fe loading on ZSM-5 (30) a significant shift in product distribution was observed at loadings of greater than 1.25 wt% Fe. Whilst conversion increased linearly with Fe content, previous studies have shown the catalytic activity of 2.5% Fe/ZSM-5 (30) to be an order of magnitude higher than that of 2.5% Fe/SiO_2 despite said materials having the same loading of iron, deposited via CVI in both instances.[1] This may be attributed to both the confinement effect of the ZSM-5 pore sizes, which has been shown to play an integral role in the activity of ZSM-5 (30) in the partial oxidation of methane with H_2O_2 and the ion exchange capacity of zeolite supports.[2]

As described in Chapter 1, the substitution of trivalent heteroatoms such as Al into the framework structure of MFI type zeolites forms a charge defect which leads to the formation of a cation exchange site as shown in Figure 5.1. When the exchanged cation is a proton, as in Figure 5.1, this induces Brønsted acidity.[3] It also known that whilst the

overall acidity of zeolites increases with framework Al (Td^{III} atom) content,[4] the acid strength of specific Brønsted sites in high aluminium content materials is dependent upon the total number of Al atoms in the next neighbour position (NNN) where a heteroatom may be located.[5] This leads to heterogeneity with regards to the acid strength of acid sites in high Al zeolites, whereby a completely isolated Al tetrahedron will support the most acidic Brønsted acid framework site. Furthermore, by varying the Si/Al ratio, the number and electronic density of bridging hydroxyl groups shown in Figure 5.1 may be varied, thus changing the strength of a Brønsted acid site.[6] As such, high Si/Al ratio zeolites show isolated strong acid sites, yet have lower acidity overall.[3]

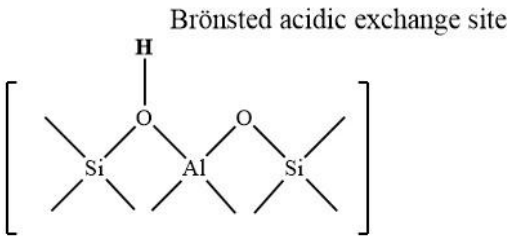

Figure 5.1 Structural representation of Al- site induced Brønsted acidity

It is also well known that upon high temperature heat treatment, heteroatoms may migrate from framework to extraframework sites, thereby inducing the Lewis acidic nature of zeolite materials.[7]

In order to assess the role played by Al in the M/ZSM-5 (30) catalysed system, the catalytic activities of 2.5wt % Fe, 2.5 wt% Cu and 1.25wt % Fe 1.25 wt% Cu on ZSM-5 (30) and an isostructural, Al free zeolite of MFI structure, Silicalite-1 were compared. The results are shown in Table 5.1. Note all catalysts were prepared via CVI.

Table 5.1 Catalytic activity of 2.5% Fe, 2.5% Cu and 1.25% Fe 1.25% Cu on ZSM-5 (30) and Silicalite-1 prepared by CVI

Catalyst	% Conversion	Aqueous phase products Selectivities[a]							Gas phase product Selectivities[b]			C_2 Selectivity (%)	% H_2O_2 used
		CH_3OOH	CH_3OH	HCOOH	CH_3COOH	C_2H_5OH	CH_3CHO	CH_3CH_2OOH	CO_2	CH_4	C_2H_4		
2.5% Fe/ZSM-5 (30)	1.74	1.16	3.77	12.48	52.61	23.43	3.30	0	1.91	1.08	0.22	79.56	43.00
2.5% Fe/Silicalite-1	0.061	1.15	2.86	0.57	9.16	24.06	45.82	12.60	2.42	0	1.13	92.77	7.57
2.5% Cu/ZSM-5 (30)	0.068	1.56	6.22	0	11.41	31.11	18.67	1.04	2.39	0	27.07	89.30	33.89
2.5% Cu/Silicalite-1	0.094	1.49	1.49	1.12	16.42	23.88	35.82	5.22	1.45	0	12.84	94.18	47.07
1.25% Fe 1.25% Cu/ZSM-5 (30)	1.19	0.21	6.02	5.08	23.54	27.47	1.58	0.23	0.47	0.23	35.16	87.98	34.94
1.25% Fe 1.25% Cu /Silicalite-1	0.072	0.48	1.44	0.96	7.68	31.67	33.59	16.31	1.55	0	6.11	95.6	19.85

[a] Analysed by 1H-NMR [b]Analysed by GC-FID

Reaction conditions; 27 mg catalyst, 10 ml reaction volume, [H_2O_2] = 0.5 M (5000 µmol), P (C_2H_6) = 20 bar, 0.5 h, Temp = 50^{o}C, 1500 rpm

A number of conclusions may be drawn from the data in Table 5.1. Firstly, it is clear that the presence of Al within the MFI structure is integral for the high catalytic activity of Fe and bimetallic FeCu catalyst systems given that the ZSM-5 (30) supported catalysts show significantly higher ethane conversion than analogous Silicalite-1 materials. This may be attributed to either; the exchange capacity imbued by the presence of framework Al^{3+} and nature of the resulting ion exchanged cationic transition metal species or the presence of extra framework Lewis acidic Al centres. It is also interesting to note the activity of 2.5% Cu/Silicalite-1 and selectivity shown by said material towards ethene. Whilst not as highly selective to ethene as 2.5% Cu/ZSM-5 (30) this result suggests that deposited copper oxide species may play a similar role to that shown in Chapter 3 Ethene studies, whereby Cu^{2+} was shown to arrest the cracking/ oxidation of ethene to formic acid. The high rate of H_2O_2 decomposition with copper only catalysts is consistent with previous studies which have shown that copper species may promote Fenton's type chemistry, generating ·OH radicals via the decomposition of H_2O_2.[8-10] Perez-Benito *et al* proposed that, at low concentrations of Cu as in the reactions in Table 5.1, this proceeds via the pathway shown in Scheme 5.1.[10]

$$Cu\ (II) + H_2O_2 \rightleftharpoons CuOOH^+ + H^+$$

$$CuOOH^+ \rightarrow Cu\ (I) + O_2^- + H^+\ (slow)$$

$$Cu\ (I) + H_2O_2 \rightarrow Cu\ (II) + OH^- + \cdot OH$$

$$\cdot OH + H_2O_2 \rightarrow H_2O + O_2^- + H^+$$

$$O_2^{=} + H_2O_2 \rightarrow O_2 + OH^- + \cdot OH$$

$$O_2^- \rightarrow \text{reactor wall (termination)}$$

Scheme 5.1 Cu (II) activated decomposition of H_2O_2

In this chapter, the roles of Brønsted and Lewis acid sites upon the activity and selectivity of M/ZSM-5 catalysts are considered. Commercial ZSM-5 materials of varying

aluminium content, coupled with catalyst characterisation techniques are used to elucidate this, and allow for enhancing product selectivities; specifically towards high ethene selectivity.

5.2 The role of ZSM-5 Aluminium content

It was previously shown in Chapter 3 that decreasing SiO_2/Al_2O_3 ratio in H-ZSM-5 (increasing initial Brønsted acidity), led to a corresponding increase in ethanol, ethylhydroperoxide and ethene selectivities when the materials were employed in the oxidation of ethane. This was coupled with a decrease in acetaldehyde and acetic acid selectivities. Figure 3.4 is reproduced below to illustrate this effect.

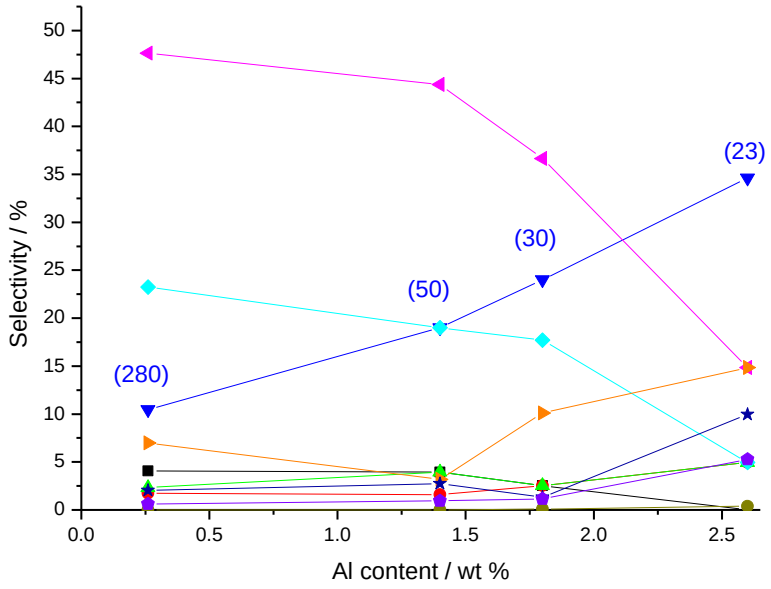

■ Black squares (CH_3OOH), ● Red Circles (CH_3OH), ♦ Aquamarine diamonds (CH_3COOH), ◀ Pink triangles (CH_3CHO), ▼ Blue triangles (C_2H_5OH), ▲ Green triangles ($HCOOH$), ● Beige circles (CH_4), ★Navy Stars (CO_2), ⬟ Purple pentagons (C_2H_4), ▶ Orange triangles (CH_3CH_2OOH), (SiO_2/Al_2O_3) ratio

Reaction conditions; 27 mg catalyst, [H_2O_2] = 0.5 M (5000 µmol), P (C_2H_6) = 20 bar, 0.5 h, Temp = 50°C, 1500 rpm .

Figure 3.4 Product selectivities for a range of ZSM-5 materials.

Added to the trends represented in Figure 3.4, a general decrease in both hydrogen peroxide decomposition and ethane conversion was observed as the Al content of the zeolite was increased. The degree of activity shown results from the presence of highly active extraframework cationic iron species, the result of iron contamination (*ca. 100-200 ppm*) which is endemic to zeolites due to contamination during preparation. However, the trends in selectivity were not directly related to iron content, but rather aluminium content, as shown in Figure 3.4. The stabilisation of ROOH (R= H, CH_3CH_2) species by Brønsted acids in Fenton's- type systems was found to be consistent with previous studies by Jung *et al*, suggesting that Al sites may play a stabilising role.[11]

Given that ethene selectivity was shown to increase with increasing aluminium content, ethene oxidation reactions were conducted using H-ZSM-5 of SiO_2/Al_2O_3 = 23, 30, 50 and 280 in order to determine whether the enhanced ethene selectivity observed in ethane oxidation tests was due to (i) increased conversion to ethene promoted by Brønsted acid sites or (ii) enhanced ethene stability with increasingly Brønsted acidic character of the zeolite. The results for these tests are shown in Figure 5.1.

It is clear from Figure 5.1 that barring a gradual increase in formic acid selectivity and corresponding decrease in selectivity to methylhydroperoxide and ethylhydroperoxide moving from least acidic H-ZSM-5 (280) to H-ZSM-5 (30), there is little change in ethene stability, with conversion shown to be consistent for these catalysts. Moving from H-ZSM-5 (30) to H-ZSM-5 (23) however, a significant reduction in ethene conversion is observed, with a marked decrease in formic acid selectivity and increase in selectivity towards ethylhydroperoxide and methylhydroperoxide, both of which have been shown in Chapter 3 to yield formic acid as oxidation products. It is interesting to note that whilst an increase in Al content leads to heightened zeolite hydrophilicity, a major hydrophilic-hydrophobic shift is known to occur for ZSM-5 at a SiO_2/Al_2O_3 ratio of 20, meaning that

H-ZSM-5 (23) is likely significantly more hydrophilic than H-ZSM-5 (30).[7, 12] Studies have shown that through tailoring of the hydrophobicity of zeolite voids, water sensitive active sites located in the pores of zeolites may be protected in aqueous reactions through partition of reactants/ products/ solvents, thereby enabling catalytic turnover.[13] This was neatly illustrated by Khouw *et al* who compared the catalytic activity of TS-1 (hydrophobic) and amorphous TiO_2-SiO_2 (hydrophilic) for the epoxidation of 1-hexene and oxidation of *n*-octane in methanol and water as solvent, the latter being known to coordinate strongly to Ti, thereby inhibiting catalytic turnover.[14] For TS-1, near identical conversion was observed under aqueous conditions as when methanol was used as solvent, whereas the conversions shown by hydrophilic TiO_2-SiO_2 were an order of magnitude lower under aqueous conditions suggesting that water was partitioned from accessing the active site.[13, 14] Given that the pores of H-ZSM-5 (23) are predicted to be significantly more hydrophilic than those of the other zeolites tested,[7] it is plausible that the enhanced primary product selectivities observed at higher aluminium content is due to more efficient removal of ethanol, ethylhydroperoxide and ethene from within the void space of the zeolite pores, facilitated by increased water adsorption. Extraction of primary products from the zeolite pore and back into the bulk aqueous phase would mitigate secondary oxidation steps to acetaldehyde and acetic acid respectively by reducing contact times.

Parallel to the trend in ethene conversion at increasing Al content was a corresponding decrease in hydrogen peroxide decomposition as shown in Table 5.2. Additionally, elemental analysis of the commercial ZSM-5 samples shows that of the constituent metals; Al, Fe, Na and Ti, the only key trend is between aluminium content and ethene/hydrogen peroxide conversion.

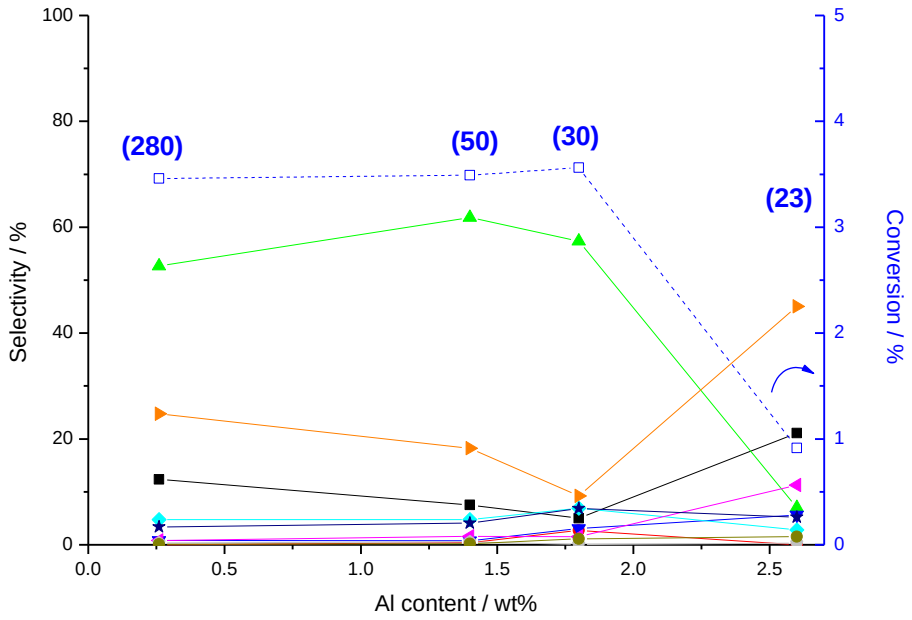

Reaction conditions; 27 mg catalyst, [H_2O_2] = 0.5 M (5000 µmol), P (5% C_2H_4/ N_2) = 10 bar, 0.5 h, Temp = 50°C, 1500 rpm.

■ Black squares (CH_3OOH), ● Red Circles (CH_3OH), ♦ Aquamarine diamonds (CH_3COOH), ◀ Pink triangles (CH_3CHO), ▼ Blue triangles (C_2H_5OH), ▲ Green triangles (HCOOH, ▶ Orange triangles (CH_3CH_2OOH), ● Beige circles (CH_4), ★Navy Stars (CO_2), ⬟ Grey pentagons (CO), - □- Blue squares (% Conversion), (Si/Al) ratio

Figure 5.1 Ethene oxidation conversions and product selectivities for a range of ZSM-5 materials.

Table 5.2 Elemental composition of ZSM-5 catalysts (determined by ICP-MS) and their corresponding ethene and H_2O_2 conversions

Catalyst	Trace metal content ppm[a]				% Ethene Conversion	% H_2O_2 used
	Al	Fe	Na	Ti		
ZSM-5 (23)	26000	120	550	32	0.98	4.35
ZSM5 (30)	18000	140	320	35	3.35	16.35
ZSM5 (50)	14000	210	58	47	3.49	15.48
ZSM5 (280)	2600	160	190	60	3.46	19.71

This work shows that through variation of the aluminium content of H-ZSM-5, H_2O_2 and primary product stability may be controlled. In light of this, and with the aim of designing a catalyst which may display high ethene selectivity, catalysts of 2.5 wt% Cu deposited onto ZSM-5 (SiO_2/Al_2O_3 = 23, 30, 50 and 280) were prepared via CVI and tested for ethane oxidation with H_2O_2. The ethane conversions and % H_2O_2 decomposed upon testing of said catalysts are shown in Figure 5.2.

It is clear that by decreasing SiO_2/Al_2O_3 a decrease in hydrogen peroxide decomposition results. Additionally, an increase in ethane conversion is observed, with 0.11% for 2.5% Cu/ZSM-5 (23) and 0.048% for 2.5% Cu/ZSM-5 (280), though conversion is consistently low for these Cu- only catalysts.

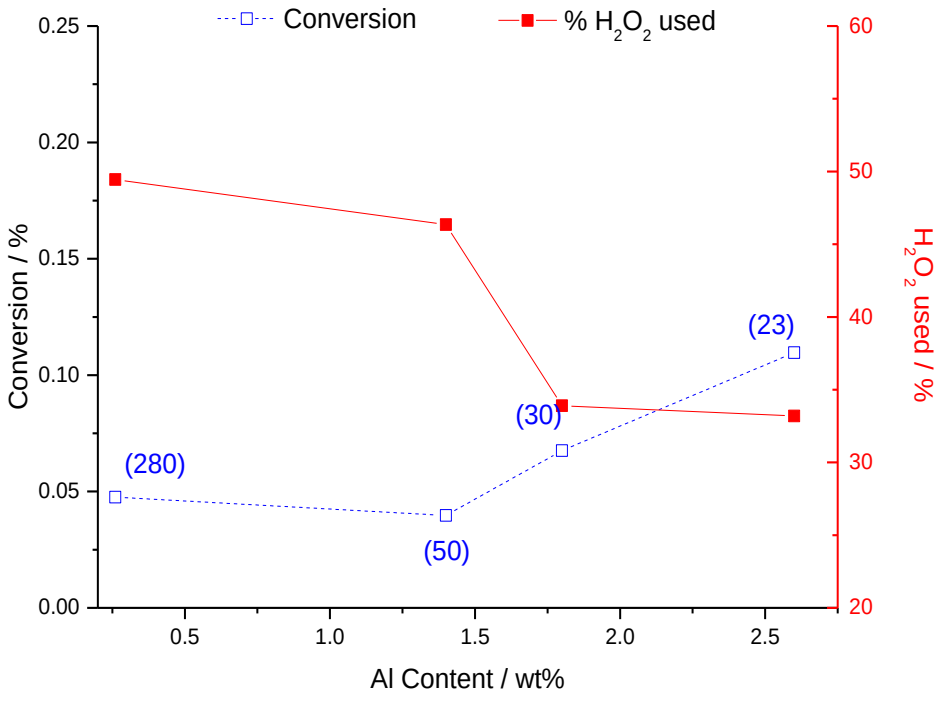

Test conditions: 27 mg catalyst, 10 ml reaction volume [H_2O_2] = 0.5M, P(C_2H_6) = 20 bar, 50°C, 0.5 h, 1500 rpm

Figure 5.2 Ethane conversion and H_2O_2 decomposition for 2.5% Cu/ZSM-5 catalysts of varying aluminium content

Given that H-ZSM-5 (23) exhibited the lowest activity of H-ZSM-5 materials tested in the oxidation of ethane (0.014%, 14.18% H_2O_2 decomposition) yet 2.5% Cu/ZSM-5 (23) exhibits the highest catalytic activity (0.11% conversion, 33.2% H_2O_2 decomposition), it is implied that there is a different amount of catalytically active Cu species in the latter than are formed on ZSM-5 materials of a lower Al content. This is further suggested by the reduction in ethane conversion observed upon deposition of 2.5 wt% of Cu onto H-ZSM-5 (280) (from 0.06% to 0.05%) despite increasing H_2O_2 decomposition (49.5% compared with 31.9%). The product selectivities for 2.5% Cu/ZSM-5 catalysts are shown in Figure 5.3.

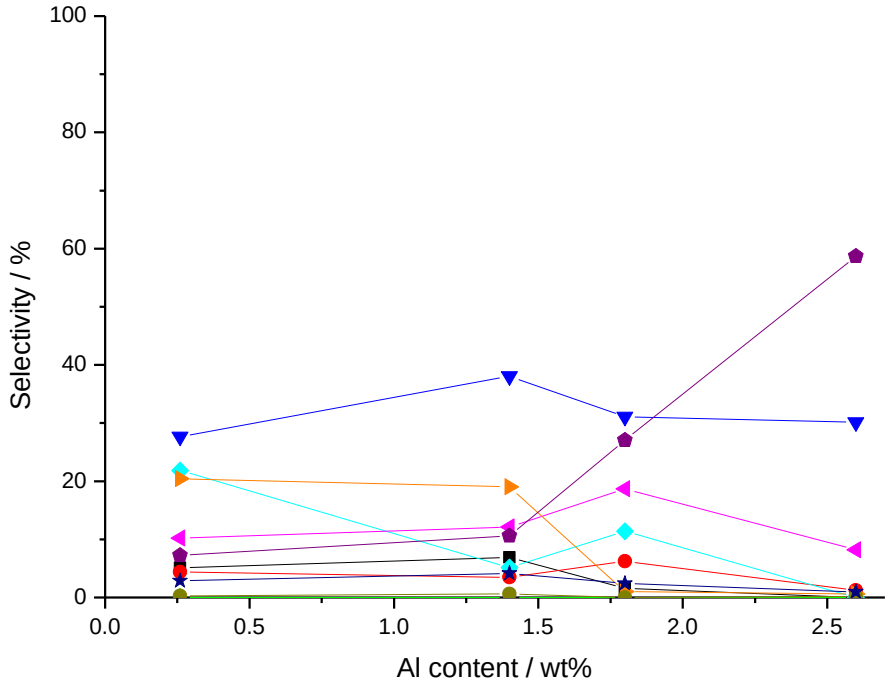

■ Black squares (CH_3OOH), ● Red Circles (CH_3OH), ♦ Aquamarine diamonds (CH_3COOH), ◀ Pink triangles (CH_3CHO), ▼ Blue triangles (C_2H_5OH), ▲ Green triangles ($HCOOH$), ● Beige circles (CH_4), ★Navy Stars (CO_2), ⬟ Purple pentagons (C_2H_4), ► Orange triangles (CH_3CH_2OOH), -□- Blue squares (% Conversion)

Figure 5.3 Ethane oxidation product selectivities for 2.5% Cu/ZSM-5 (*n*)

At increasing Al contents, a startling shift in product selectivities is observed for 2.5% Cu/ZSM-5 catalysts, in particular the selectivity to ethene. 2.5% Cu/ZSM-5 280, 50, 30 and 23 show ethene selectivities of 7.3, 10.6, 27.1 and 58.7 % respectively (Figure 5.3). The unprecedented ethene selectivity exhibited by 2.5% Cu/ZSM-5 (23) might be attributed to a number of factors. Firstly it may be that due to the increased hydrophilicity of its pore, with respect to lower Al content zeolites, leading to more efficient extraction of hydrated gaseous products from the micropores due to lesser solvent- pore partitioning. Similarly the heightened conversion observed with 2.5% Cu/ZSM-5 (23) may be due to increased access of the aqueous oxidant to active sites situated within the pore structure. However, this cannot be the sole contributing factor, as in the absence of supported Cu species higher ethane conversion was exhibited by more siliceous zeolites. This therefore leads to the second possibility specifically that the higher aluminium/ ion exchange capacity of ZSM-5 (23) leads to the formation of a greater population of Cu species which are active for the formation of ethene.

In order to probe the nature of Cu species present in this catalyst, H_2-TPR studies were conducted on the 2.5% Cu/ZSM-5 catalysts. The H_2 uptake traces are shown in Figure 5.4, along with that of 2.5% Cu/Silicalite-1 to allow for comparison with an exchanged-ion free material. All profiles, including 2.5% Cu/ Silicalite-1 exhibit a reduction peak at between 182 ^{o}C and 213 ^{o}C, with temperature increasing with increased Al content. This peak is an amalgamation of two separate reduction peaks and may be associated with the reduction of isolated Cu^{2+} ions and Cu^{2+} oxocations to Cu^{+} and also the reduction of Cu^{2+} in CuO to Cu^{O}, the latter being the sole reduction in 2.5% Cu/Silicalite -1.[15-17] A second, high temperature peak presented by Cu/ZSM-5 catalysts, but not 2.5% Cu/Silicalite-1, is generally attributed to the reduction of Cu^{+} ions to Cu^{0}.[15, 18]

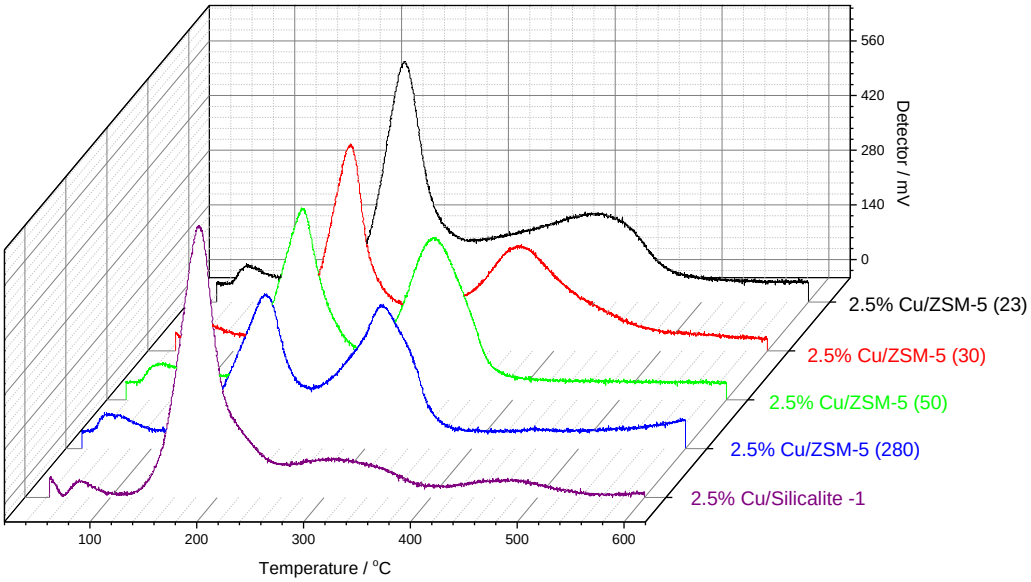

Figure 5.4 H_2-TPR profiles for 2.5% Cu/ zeolite CVI catalysts

It is clearly seen in Figure 5.4 that the high temperature reduction peak representing the reduction of Cu^+ to Cu^0 undergoes a significant shift towards lower temperatures with increasing Si/Al of the zeolites tested (increasing Cu/Al), suggesting that the Cu^+ ions are more readily reduced as the catalyst Si/Al increases. This has been attributed to stronger bonding of Cu ions to framework oxygens in more highly negatively charged zeolite frameworks (higher AlO_4^- content).[19] This is consistent with previous studies of Cu/ZSM-5 materials.[16, 18, 19] The increasing breadth of the high temperature peak observed for Cu/ZSM-5 catalysts suggests the presence of oligomeric Cu species of varying nuclearity.[20] Reduction peak T_{max} temperatures and relative areas are shown in Table 5.3.

Table 5.3 Temperatures related to the reduction profiles in Figure 5.4

Catalyst	1st Peak T_{max} (°C)	2nd Peak T_{max} (°C)	Area 1st Peak/ 2nd Peak
2.5% Cu/ZSM-5 (280)	205	316	0.86
2.5% Cu/ZSM-5 (50)	208	324	0.96
2.5% Cu/ZSM-5 (30)	213	366	0.97
2.5% Cu/ZSM-5 (23)	220	415	1.05

Though not clear in Figure 5.4, a similar shift towards higher temperatures is also observed for the low temperature reduction peak at increasing Al contents. This is shown in Table 5.3, and is found to be consistent with previous studies which showed that the reduction of both Cu^{+} ($Cu^{+} \rightarrow Cu^{0}$) at high temperatures and Cu^{2+} ($Cu^{2+} \rightarrow Cu^{+}$) at low temperatures occurs more easily when exchanged into the matrix of a low aluminium-content zeolite.[19] Additionally the greater shift observed in the high temperature peak upon increasing Al content was found to be consistent with the literature.[19] Upon comparing integrated areas of the two reduction peaks, we observed a general increase in the area of the low temperature peak, relative to the high temperature reduction, at increasing aluminium content (Table 5.3). This suggests that there is a slightly higher proportion of CuO species in Al rich zeolites.[18, 21]

It is interesting to note that for both 2.5% Cu/Silicalite-1 and 2.5% Cu/ZSM-5 catalysts a catalyst colour change is observed post reaction with the degree of colour change following the order; 2.5% Cu/Silicalite-1 ~ ZSM-5 (280) > ZSM-5 (50)>> ZSM-5 (30)> ZSM-5 (23). Photographs of the 2.5% Cu/ZSM-5 catalysts post reaction are shown in Figure 5.5.

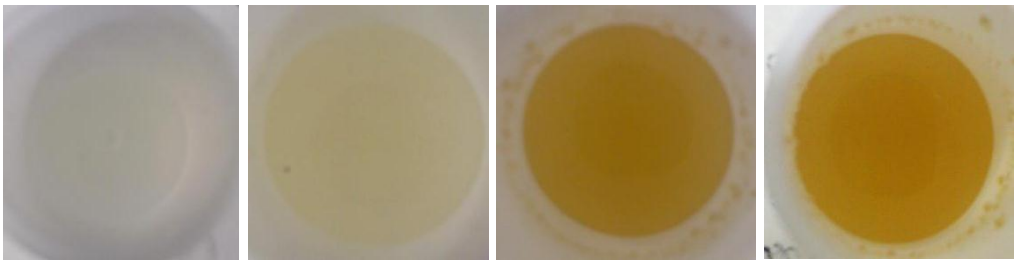

2.5% Cu/ZSM-5 **(23)** | 2.5% Cu/ZSM-5 **(30)** | 2.5% Cu/ZSM-5 **(50)** | 2.5% Cu/ZSM-5 **(280)**

Figure 5.5 Photographs of used Cu/ZSM-5 catalysts

This colour change could be attributed to the formation of Cu-OOH, in a similar way as TS-1 has been reported to undergo a white to yellow colour change due to formation of Ti-OOH, an active oxygen species, upon interaction with H_2O_2.[22] However colour changes in transition metals are also often attributed to changes in oxidation state and/or geometry. XPS spectra for fresh and used 2.5% Cu/ZSM-5 of SiO_2/Al_2O_3= 23,30 and 280 catalysts were collected. The Cu (2p) regions for spectra of used catalysts are shown in Figure 5.6 (*note*; the Cu (2p) region for used 2.5% Cu/ZSM-5 (280) has been deconvoluted).

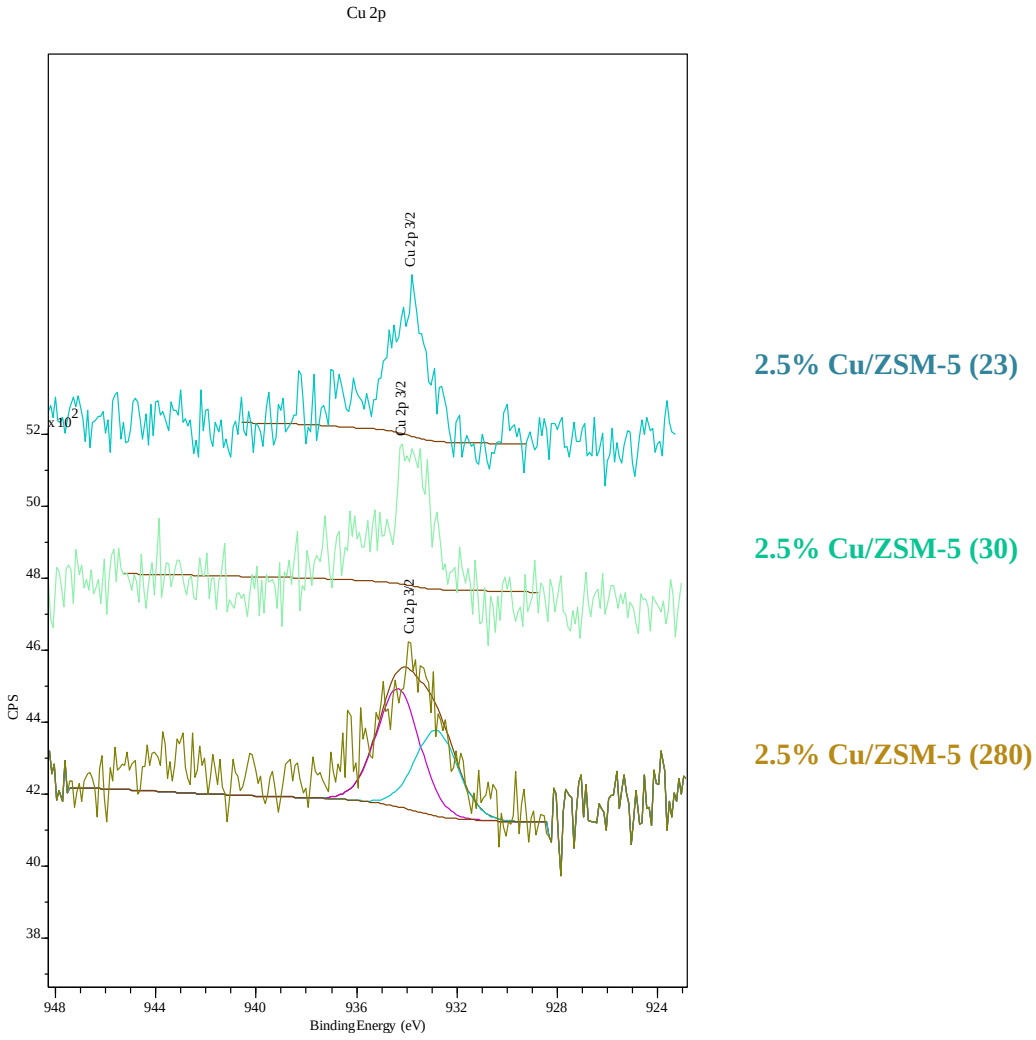

Figure 5.6 XPS spectra showing the Cu (2p) region of used 2.5% Cu/ZSM-5 catalysts spectra were calibrated to the Si (2p) line at 103.2 eV.

XPS analysis of fresh catalysts show Cu^{2+} solely, independent of ZSM-5 used, whereas XPS spectra of 2.5% Cu/ZSM-5 (280), the material which exhibited the most significant degree of colour change following testing, shows reduced (Cu^0/Cu^+) character as shown in Figure 5.6. Furthermore, though the catalysts were observed to gradually re-oxidise back to its original state (and, in the process, become blue once more), this required > 24 h at room temperature in air at ambient conditions to reach completion suggesting that the reduced species formed is relatively stable.

Given that Scheme 5.1 showed the two Cu catalysed H_2O_2 decomposition steps shown in Equations 5.1 and 5.3, it is possible that if the copper species present in high Si/Al Cu/ZSM-5 catalysts are more readily reduced to a lower oxidation state Cu (I) as in Equation 5.2, then the Fenton's type decomposition of H_2O_2 shown in Equation 5.3 would be more facile. Given that previous EPR studies have shown Cu^{2+} in ZSM-5 (30) to scavenge ·OH,[2] and that addition of Cu^{2+} leads to increased ethene selectivity, more facile reduction would increase the ·OH formation, which would likely to result in lower ethene selectivity. Additionally monocopper species, including $CuOOH^+$ are currently under investigation as highly active oxidative intermediates in the enzymes Amine Oxidase and Dopamine β- monooxygenase.[23]

$$Cu\ (II) + H_2O_2 \rightleftharpoons CuOOH^+ + H^+ \qquad \text{(Equation 5.1)}$$

$$CuOOH^+ \rightarrow Cu\ (I) + O_2^- + H^+\ \text{(slow)} \qquad \text{(Equation 5.2)}$$

$$Cu\ (I) + H_2O_2 \rightarrow Cu\ (II) + OH^- + \cdot OH \qquad \text{(Equation 5.3)}$$

Studies have shown that the redox potentials of Cu cations in zeolites are controlled by the local Si/ Al ratio, with Cu cations in low Si/Al zeolites showing a higher interaction with the zeolite structure, thereby stabilising Cu^+ cations. Furthermore the work of

Lobree *et al* suggested that upon exchange of copper and iron ions onto ZSM-5, γ exchange sites are filled preferentially, with β and the least energetically favourable α sites also filled as the M/Al ratio is increased.[24, 25] M^{n+1} exchanged at α sites were shown to reduce (to M^{+}) more readily than those at β or γ sites.[24, 26] As ZSM-5 (280) has a significantly lower Al content than ZSM-5(23 and 30), at constant Cu loading 2.5% Cu/ZSM-5 (280) is likely to have a greater degree of α site population, thereby making it more susceptible to deactivation through reduction to Cu^{+} or a long lived species such as $CuOOH^{+}$.

In order to compare the stability of 2.5% Cu/ZSM-5 catalysts, time on line studies of 2.5% Cu/ZSM-5 (23), 2.5% Cu/ZSM-5 (30) and 2.5% Cu/ZSM-5 (280) catalysed ethane oxidation were conducted. Overlaid conversion plots are shown in Figure 5.7, with major product selectivity breakdowns shown in Figure 5.8.

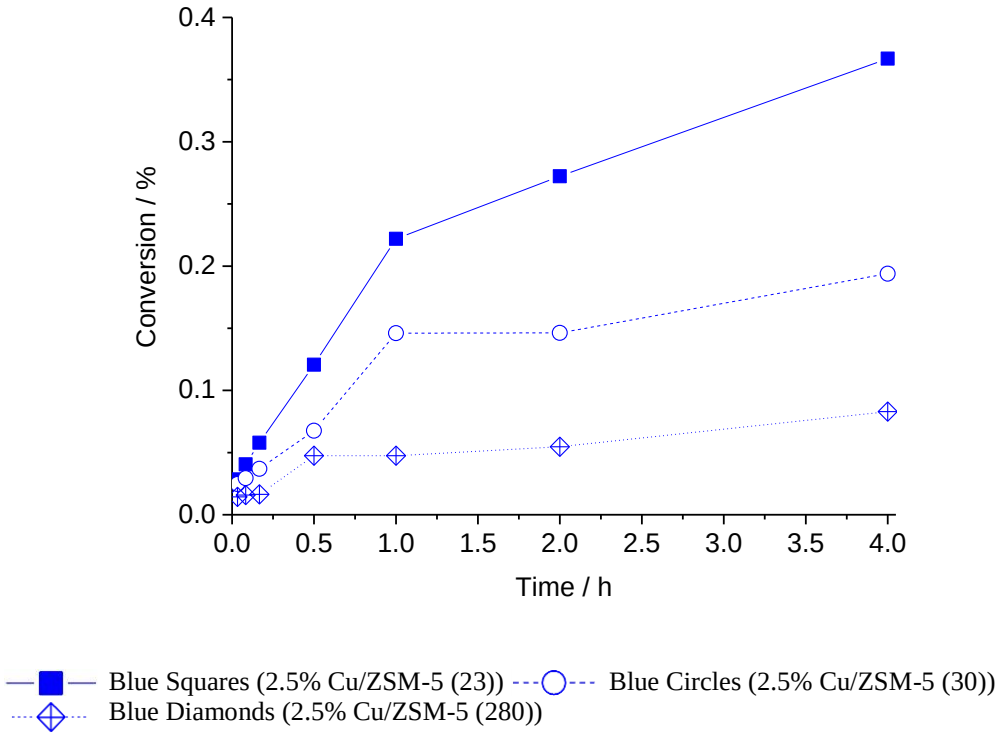

Figure 5.7 Time on line conversion plots for 2.5% Cu/ZSM-5 catalysed ethane oxidation

It is clear that SiO_2/Al_2O_3 has a significant, consistent effect upon ethane conversion over 4 hour testing periods. It is shown in Figure 5.7 that 2.5% CuZSM-5 (23) was observed to be the most active across the reaction duration. A gradual decrease in catalyst productivity is observed for all catalysts with time though, for example productivity for 2.5% Cu/ZSM-5 (23, 30 and 280) fell from 1.81, 1.01 and 0.71 h^{-1} at 0.5 h reaction coordinate to 0.68, 0.36 and 0.16 h^{-1} at 4 h respectively. This amounts to a 62% drop in productivity for 2.5% Cu/ZSM-5 (23), 64% drop in productivity for 2.5% Cu/ZSM-5(30) and 78% decline in productivity for 2.5% Cu/ZSM-5 (280) over said time period. The relatively high activity exhibited by 2.5% Cu/ZSM-5 (23) may be attributed either to; the higher hydrophilicity of ZSM-5 (23) allowing for ·OH to access active sites within the micropores or, a greater population of active Cu species. Given that ZSM-5(23) has more γ, β and α exchange sites overall, at constant Cu mass it is likely that a greater number of γ and β sites would be occupied by Cu species. The occupation of these sites in Cu/ZSM-5 CVI catalysts has not yet been corroborated by spectroscopic data.

Figure 5.8 shows that the selectivity trends observed in Figure 5.3 remain constant at 4 h reaction times in that with decreasing SiO_2/Al_2O_3 there is a marked increase in ethene selectivity. This is coupled with a decrease in acetic acid, acetaldehyde and CO_2 selectivity. In fact as Figure 5.8 (f) shows, oxygenate selectivity falls significantly with increased Al content of ZSM-5 catalysts. The significant difference between SiO_2/Al_2O_3 of 23 and 30 suggests that pore hydrophilicity may be the key property affecting the difference in conversion and selectivity as, as previously stated, a hydrophobic/hydrophilic shift is observed at SiO_2/Al_2O_3 of around 20.[7] Whilst the exchange capacity of ZSM-5 (23) is greater than that of ZSM-5(30), with 1.44 times the Al content, the difference in activity between ZSM-5(30) and ZSM-5 (280) is not proportional to their Al content ratio (6.92:1).

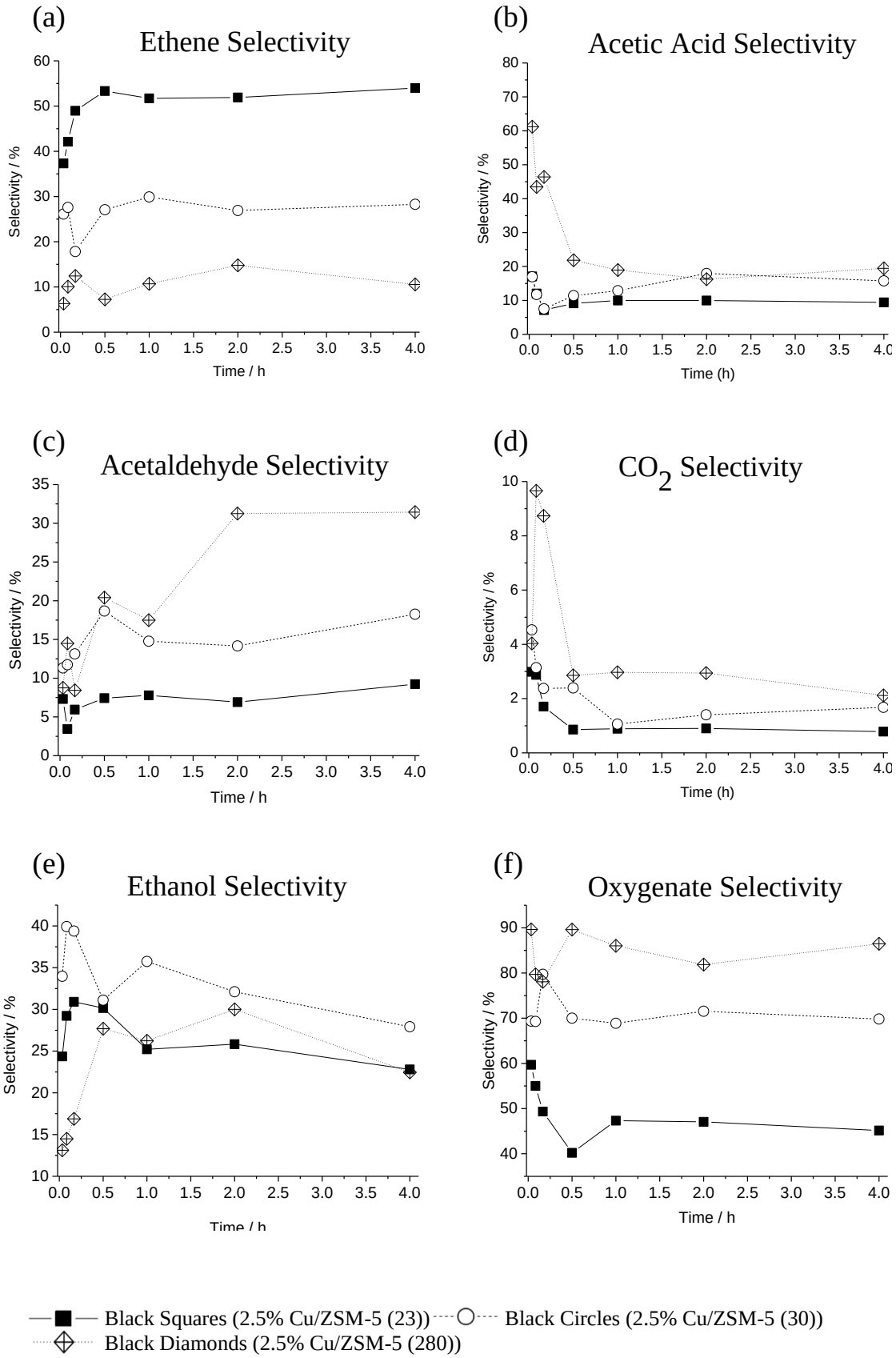

Figure 5.8 Major product selectivity time on lines for 2.5% Cu/ZSM-5 catalysts.

TPR analysis has shown that Cu species in 2.5% Cu/ZSM-5 materials differ chemically, with lower SiO_2/Al_2O_3 associated with a broadening of the high temperature reduction peak. This broadening was tentatively attributed to the presence of Cu^+ species of varying nuclearity.[20] In order to determine and compare the physical state of the Cu species present in 2.5% Cu/ZSM-5 (23), 2.5% Cu/ZSM-5 (30) and 2.5% Cu/ZSM-5 (280), TEM analysis of said materials was performed. Representative images at varying magnifications and corresponding particle size distributions are shown in Figure 5.9.

It is interesting to note that with increasing zeolite aluminium content, a corresponding increase in the average particle size of copper oxide observed on the zeolite surface in TEM images in Figure 5.9 is also seen. The average particle size increases from 2.00 nm when ZSM-5 (280) is the support, to 7.18 nm for ZSM-5 (30) and 9.06 nm for ZSM-5 (23). The size distribution also broadens across the same range, with a standard deviation in particle size of 0.44 nm, 2.03 nm and 4.20 nm for ZSM-5 280, 30 and 23. This is consistent with the broadening of the Cu^+ to Cu^o high temperature reduction peak with increasing Al content which was shown in Figure 5.4.

TEM investigations of 2.5% Cu/ZSM-5 catalysts shows a clear metal support interaction which might be due to an increased interaction between the copper precursor $Cu(acac)_2$ and the zeolite surface upon CVI deposition. As previously described in Chapter 3, under CVI preparation conditions the hydrophobic metal precursor is heated to sublimation temperature under vacuum, leading to its being deposited across the zeolite surface. This leads to formation of isolated Cu species, separated by the steric bulk of the acetylacetonate ligands. Upon high temperature heat treatment the ligands decompose leading to the formation of copper oxide species and, based on previous UV studies, copper ions.[1] TEM images and particle size distributions shown in Figure 5.9 suggest that a metal support interaction is in operation, as evidenced by the increasing breadth of the

size distribution, and increased average particle size with increased aluminium content. This interaction might be attributed to the differing hydrophobicity of the zeolite materials, such that ZSM-5 (280) is the most hydrophobic support represented. As such the small average particle size and narrow size distribution for 2.5% Cu/ZSM-5 (280) might be due to the hydrophobic nature of the support leading to a stronger interaction with the hydrophobic $Cu(acac)_2$ precursor. Further TEM studies of non heat treated variants of the materials represented in Figure 5.9 would determine whether (i) the interaction governs the efficiency with which the precursor is distributed across the zeolite surface during deposition via CVI or (ii) the interaction stabilises the precursor and copper oxide species formed upon initial decomposition of $Cu(acac)_2$ during high temperature heart treatment, which might prevent copper agglomeration.

The decrease in copper oxide particle size with increasing SiO_2/Al_2O_3 raises the possibility that it is these species which are undergoing reduction *in situ*, given that smaller copper oxide particles have a higher surface area: bulk volume ratio. Therefore there is a higher probability of there being surface Cu ions compared to bulk oxide Cu. These surface ions may form Cu-OOH, a species which is relatively long lived and not directly active for ethane oxidation. This could lead to the trends represented in Figure 5.5 and 5.6 and also to the drop in catalyst productivities with time, as shown in Figure 5.8. Additionally, the decrease in H_2O_2 decomposition with increasing Al content of 2.5% Cu/ZSM-5 shown in Figure 5.2 may result from reduced presence of Cu (I) on the zeolite surface, which Equation 5.3 shows to play a role in the decomposition of H_2O_2. The heightened activity of 2.5% Cu/ZSM-5 (23) and trend of increasing ethane conversion with increasing Al content would imply therefore that aside from the copper oxide clusters observed in TEM investigations, there are catalytically active species within the micropore network or at cation exchange sites.

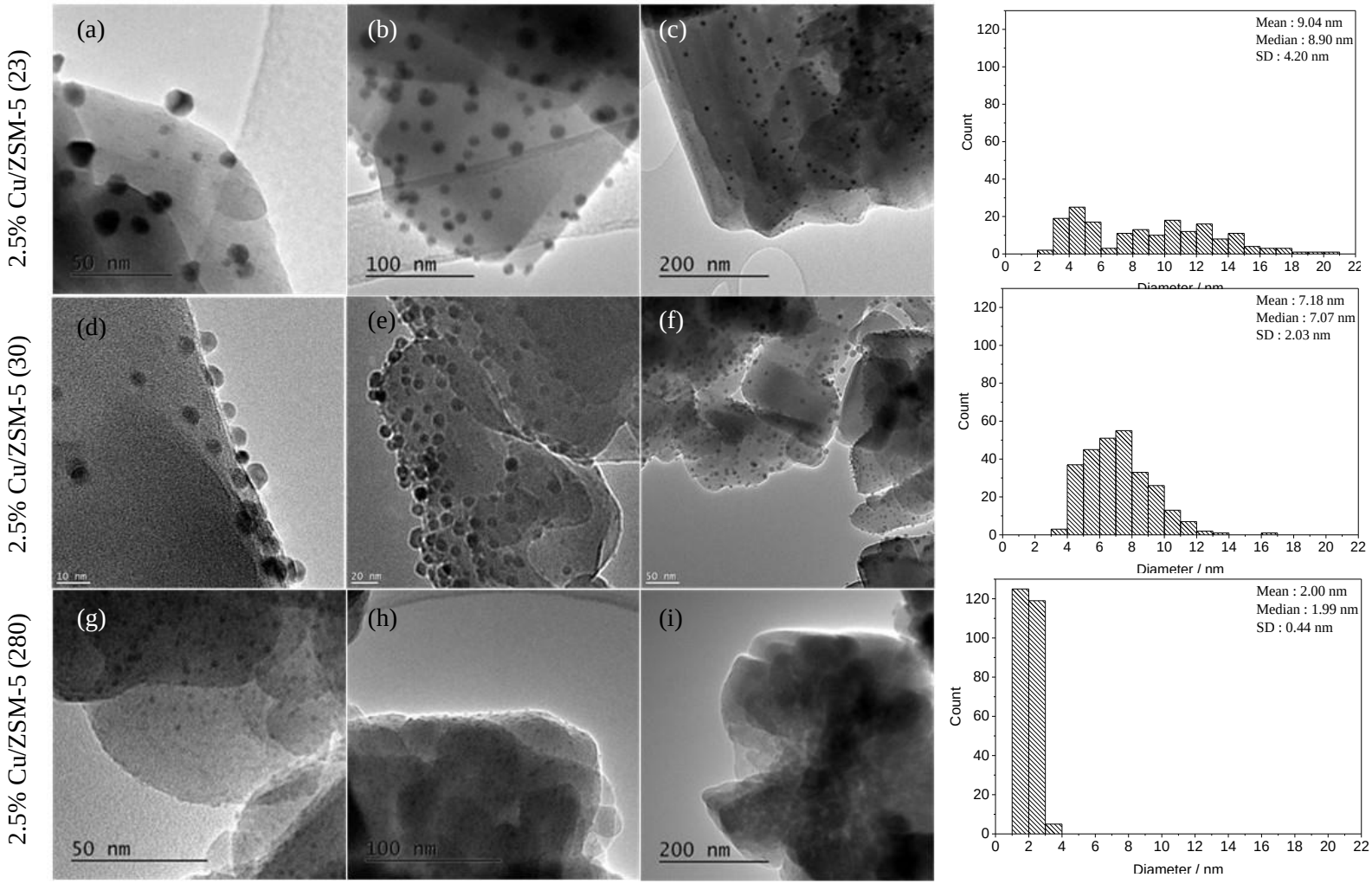

Figure 5.9 Representative low resolution TEM images and particle size distributions for 2.5% Cu on ZSM-5 (23) (a,b,c), ZSM-5 (30) (d,e,f) and ZSM-5 (280) (g,h,i)

Another interpretation of this data may be based on the works of Bulanek, Wichterlova, Dedecek and co-workers who showed that upon exchange of Cu ions into MFI zeolites, Cu ions of four spectroscopically distinct coordinations are formed.[19, 26-28] Said species, denoted as Cu-I, Cu-II, Cu-III and Cu-IV were shown to have differing structural properties, with Cu-I and Cu-II showing a square bipyramidal Cu^{2+} geometry and favouring formation in exchange sites with adjacent Al pairs, and Cu-IV showing square planar Cu^{2+} coordination, and favouring formation in isolated Al sites.[26, 27]

It was shown that exchange as Cu-IV ions balanced by a single AlO_4^- became more favourable with an increasing Cu/Al ratio, with Cu-IV ions dominating at Cu/Al of greater than 0.5,[27] whilst low Cu concentrations and high Al content favoured formation of Cu-II species.[19] The Cu ions balanced by a single AlO_4^- (Cu-IV) were shown to be most easily reduced due to the low negative charge resulting from lack of adjacent AlO_4^- sites.[27] Additionally, such sites predominate in high Si/Al zeolites, where formation of single Al framework arrangements is favoured.[27] Furthermore, a number of studies have shown the Cu ions which are adjacent to single framework Al atoms, found in high Cu/Si/Al catalysts to be more active for the catalytic decomposition of NO, a process which requires monovalent Cu^+. This led to the conclusion that Cu ions in Cu-IV sites are more reducible than those occupying sites adjacent to Al pairs, thereby leading to the heightened NO decomposition observed for high Cu/Al catalysts..[26, 27] This was supported by the heightened NO decomposition at Cu/Al > 0.5.[26]

For comparison with the literature, Cu/Al ratios for 2.5% Cu/ZSM-5 catalysts of varying Si/Al are shown in Table 5.4.

Table 5.4 Cu/Al ratios for 2.5% Cu/ZSM-5 catalysts

Entry	Catalyst	Wt% Al	Moles Al/g	Moles Cu/g	Cu/Al
1	2.5% Cu/ZSM-5 (23)	2.6	0.000964	0.000393	0.408
2	2.5% Cu/ZSM-5 (30)	1.8	0.000667	0.000393	0.589
3	2.5% Cu/ZSM-5 (50)	1.4	0.000519	0.000393	0.758
4	2.5% Cu/ZSM-5 (280)	0.26	0.0000964	0.000393	4.082

It is clear from Table 5.4 that not only does moving from ZSM-5 (30) to ZSM-5 (23) cross a hydrophobic- hydrophilic pore-transition but, at 2.5% loading of Cu, also crosses the Cu/Al ratio of 0.5. The latter implies that of Cu species present in 2.5% Cu/ZSM-5 catalysts for $SiO_2/Al_2O_3 \geq 30$, a greater proportion are likely to be bonded to isolated Al sites as Cu-IV species, which are more reducible. Given the loss of productivity observed over time for all catalysts in Figure 5.8, which was more significant at increasing SiO_2/Al_2O_3, and the lower activity shown by catalysts of $SiO_2/Al_2O_3 > 23$, this would imply that Cu-II type exchanged species are not only more active for the oxidation of ethane (to ethene), but are also more stable with respect to reductive deactivation than Cu-IV species, which are likely to become more predominant moving down Table 5.4, Entries 2, 3 and 4. One possible interpretation is that upon interaction with H_2O_2, Cu-IV forms an oxidising species which is not active for the oxidation of ethane, such as $CuOOH^+$ which is long lived and would therefore lead to reduced catalyst productivity.

In order to draw a direct comparison between the Brønsted acidity of 2.5% Cu/ZSM-5 catalysts and catalytic activity, quantitative NH_3-TPD studies were conducted following the procedure described in Chapter 2, Section 2.6.6. The temperature programmed ammonia desorptions, shown in Figure 5.10, illustrate a clear trend of increased NH_3 chemisorption capacity at decreasing SiO_2/Al_2O_3, such that following deposition of 2.5

wt% Cu, ZSM-5 with a SiO_2/Al_2O_3 ratio of 23 retains a greater number of Brønsted acidic Al- coordinated protons. Given the relatively low Cu/Al ratio shown in Table 5.4 for this catalyst, this should not be surprising as only one Cu^{2+} may be associated with a particular framework aluminium exchange site. Two key desorptions are observed, at *ca.* 270 and 450 ^{o}C, the lower being attributed to weakly adsorbed NH_3 (at either Brønsted or extraframework Al sites)[29, 30] and the higher temperature being assigned to NH_3 strongly adsorbed to Brønsted acid sites. [24, 31, 32] Given that the high temperature peak may be unambiguously attributed to NH_3 strongly adsorbed at Brønsted acid sites, it may be used to quantify changes in the concentration of Brønsted acid sites. To quantify the loss of Brønsted acidity at increasing SiO_2/Al_2O_3, the high temperature desorptions featured in Figure 5.10 were integrated, and treated according to the NH_3 calibration featured in Chapter 2, Figure 2.7.

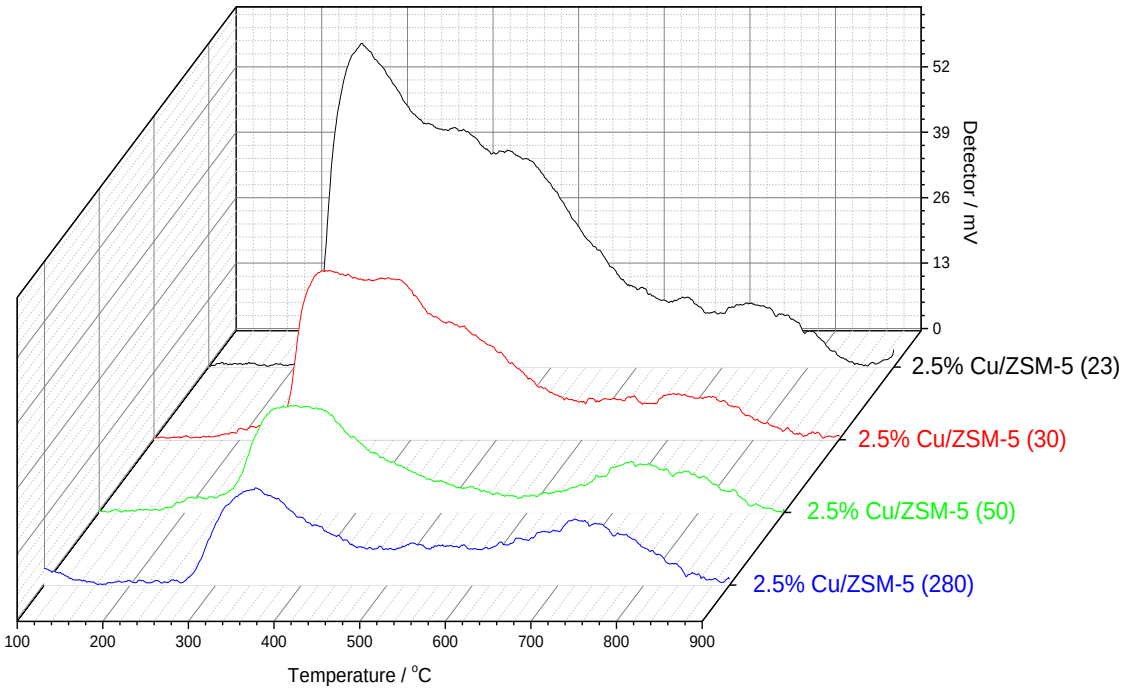

Figure 5.10 Temperature programmed desorption plots for 2.5% Cu/ZSM-5 catalysts of varying SiO_2/Al_2O_3

A plot of ethene and total oxygenate selectivities, versus µmol NH_3 associated with Brønsted / gram of catalyst for 2.5% Cu/ZSM-5 catalysts is shown in Figure 5.11. This shows a clear relationship between NH_3 adsorbed (which is proportional to Brønsted acidity) and ethene and oxygenates selectivities. For the former, ethene selectivity is directly proportional to ammonia uptake, whilst for the latter a reduction in oxygenate selectivity is observed at increasing acidity. It is therefore possible that Brønsted sites located at the surface of ZSM-5 may be stabilising ethene and hydrogen peroxide.

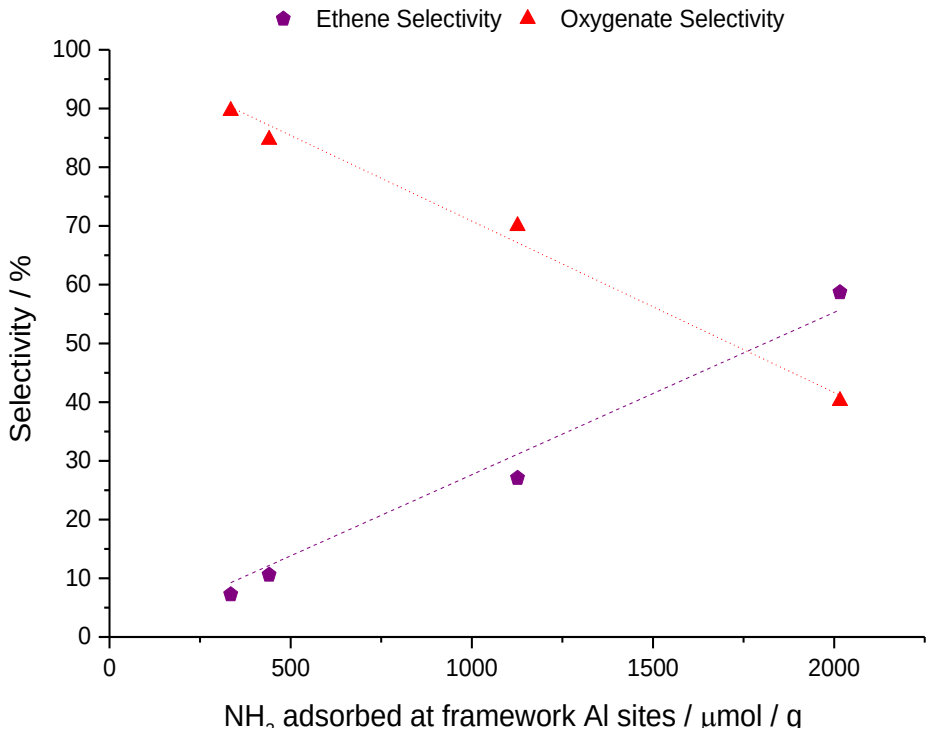

Figure 5.11 A plot of µmol/g NH_3 adsorbed to Brønsted acidic framework Al sites versus ethene and total oxygenate selectivities

In order to decouple the two variables of hydrophilicity and Cu/Al ratio, varying loadings of Cu were deposited onto ZSM-5(23) and ZSM-5(30) supports. The resulting materials were tested for activity in ethane oxidation tests. The corresponding conversion, H_2O_2 decomposition and selectivity plots are shown in Figure 5.12, whilst Table 5.5 shows Cu/Al ratios and ethane conversion for the catalysts tested.

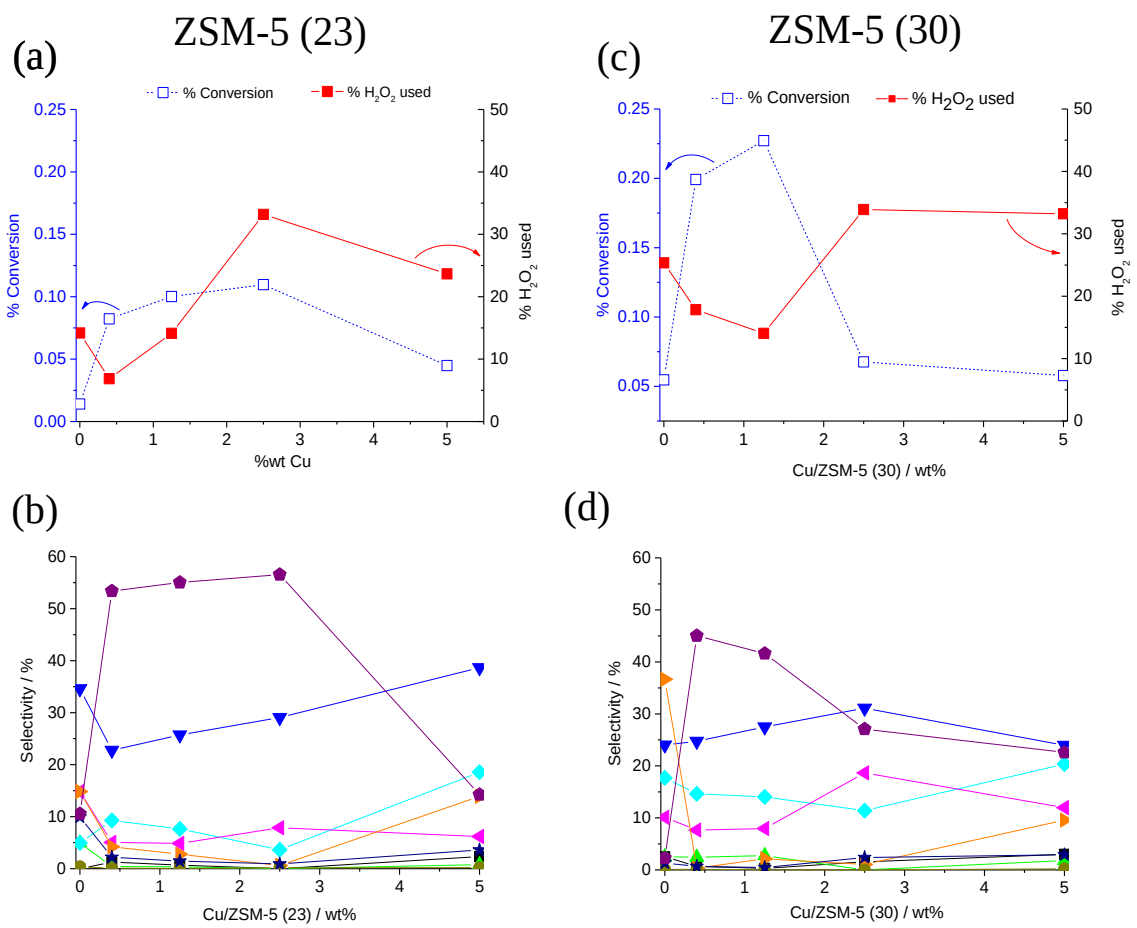

-□- Blue Squares (% Conversion), ■ Red squares (% H_2O_2 decomposed)

■ Black squares (CH_3OOH), ● Red Circles (CH_3OH), ♦ Aquamarine diamonds (CH_3COOH), ◀ Pink triangles (CH_3CHO), ▼ Blue triangles (C_2H_5OH), ▲ Green triangles ($HCOOH$), ● Beige circles (CH_4), ★Navy Stars (CO_2), ⬟ Purple pentagons (C_2H_4), ▶ Orange triangles (CH_3CH_2OOH)

Test conditions; 27 mg catalyst, reaction volume 10 ml, 0.5 h, [H_2O_2]= 0.5M, 50°C, P(C_2H_6) = 20 bar, 1500 rpm

Figure 5.12 Ethane conversion and hydrogen peroxide decomposition, and product selectivity plots for varying wt% Cu on ZSM-5 (23) (a & b) and ZSM-5 (30) (c & d)

Table 5.5 Cu/Al ratios and ethane conversion for catalysts of varying wt% Cu/ZSM-5 (23 & 30)

Loading Cu/ wt%	Cu/Al/ ZSM-5 (23)	% Ethane Conversion	Cu/Al/ ZSM-5 (30)	% Ethane Conversion
0.4	0.065315	0.083	0.094344	0.20
1.25	0.204109	0.100	0.294825	0.23
2.5	0.408219	0.11	**0.589649**	**0.068**
5	**0.816438**	**0.045**	1.179299	0.058

The data in Figure 5.12, (a) and (c), coupled with that in Table 5.5 clearly shows the effect of overexchanging ZSM-5 with Cu such that Cu/Al ≥ 0.5. It is clear that for ZSM-5 (23) an increase in conversion is observed with increased Cu loading to 2.5 wt%, for which the Cu/Al = 0.41, with a drop in conversion shown to 5% Cu loading (Cu/Al = 0.82). ZSM-5 (30) follows a similar trend, actually showing higher conversion at low Cu loadings than ZSM-5 (23), but with conversion falling between 1.25% Cu and 2.5% wt Cu loadings (Cu/Al of 0.29 and 0.59 respectively). Meanwhile Figure 5.12 (b) and (d) show product selectivities for Cu/ZSM-5 catalysts of increasing Cu loading.

Cu loading also impacts greatly upon product selectivities, with a general increase in ethene selectivity observed up to the point at which conversion was shown to decrease (corresponding to Cu/Al ≥ 0.5). At higher loadings, ethene selectivity is seen to decrease, with increased ethanol and acetic acid selectivity observed. Consistent with previous tests, Cu/ZSM-5 (23) catalysts show higher ethene selectivity than do Cu/ZSM-5 (30) materials with comparable Cu loadings, the exception being 5% wt loading.

From this data it is clear that pore hydrophilicity is not the key rate determining factor for Cu/ZSM-5 catalysed ethane oxidation. This data may be interpreted such that the Cu-II type species shown in previous studies to be predominant at Cu/Al < 0.5 are more catalytically active than Cu-IV species which come to dominate at higher Cu loadings (Cu/Al ≥ 0.5). If so it would appear that the presence of a significant concentration of the latter species effectively deactivates the catalyst system, in spite of the fact that higher Cu loadings of 2.5 and 5% show a greater degree of H_2O_2 decomposition. This would imply that the two proposed Cu species interact in a different manner with H_2O_2 and its decomposition products and further supports that catalytic activity/ selectivity is dependent upon Cu^{2+}.

Given that Cu/ZSM-5 monometallic catalysts show low activity for ethane oxidation with H_2O_2, with the highest conversion shown being 0.37% to ethene (54.0%) over 2.5% Cu/ZSM-5 (23) after 4 h on stream, bimetallic FeCu/ZSM-5 catalysts were prepared via CVI using commercial ZSM-5 of SiO_2/Al_2O_3 = 280, 50, 30 and 23.

Ethane conversion and H_2O_2 decomposition observed for 1.25% Fe 1.25% Cu/ZSM-5 for zeolites of varying Si/Al are shown in Figure 5.13. Consistent with previous batch and flow studies, co-deposition of Fe, in addition to Cu, onto ZSM-5 leads to a significant increase in conversion compared with monometallic Cu catalysts, as shown in Figure 5.13.

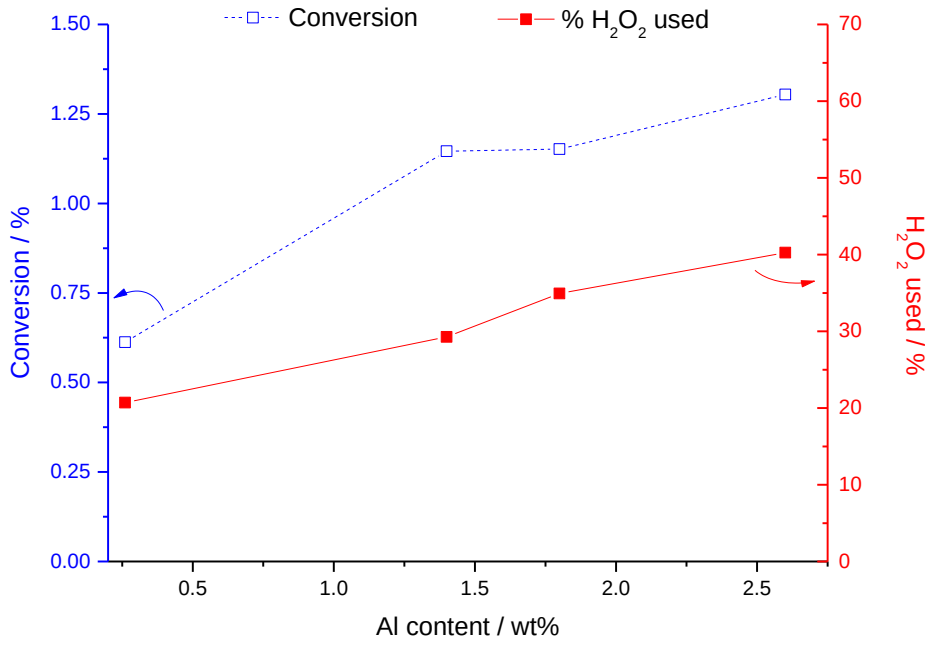

Test conditions; 27 mg catalyst reaction volume 10 ml, 0.5 h, $[H_2O_2]$= 0.5M, 50°C, $P(C_2H_6)$ = 20 bar, 1500 rpm

Figure 5.13 Ethane conversion and hydrogen peroxide decomposition for 1.25% Fe 1.25% Cu/ ZSM-5 of varying Al content

A linear increase in ethane conversion is observed upon increasing the Al content of the ZSM-5 (decreasing the SiO_2/Al_2O_3 ratio of the zeolite support) used. A corresponding increase in H_2O_2 decomposition was also observed over the range tested. Unlike with monometallic Cu/ZSM-5 catalysts, the increase in conversion is gradual and consistent between ZSM-5 (280) and ZSM-5 (23), as is the increase in hydrogen peroxide decomposition, which shows an opposing trend to that observed for 2.5% Cu/ZSM-5 at increasing Al content in Figure 5.2. The increase in conversion observed across this range of catalyst amounts to an increase in catalyst productivity from 9.3 h^{-1} to 20.1 h^{-1}. Product selectivities for ethane oxidation catalysed by 1.25% Fe 1.25% Cu/ZSM-5 catalysts are shown in Figure 5.14.

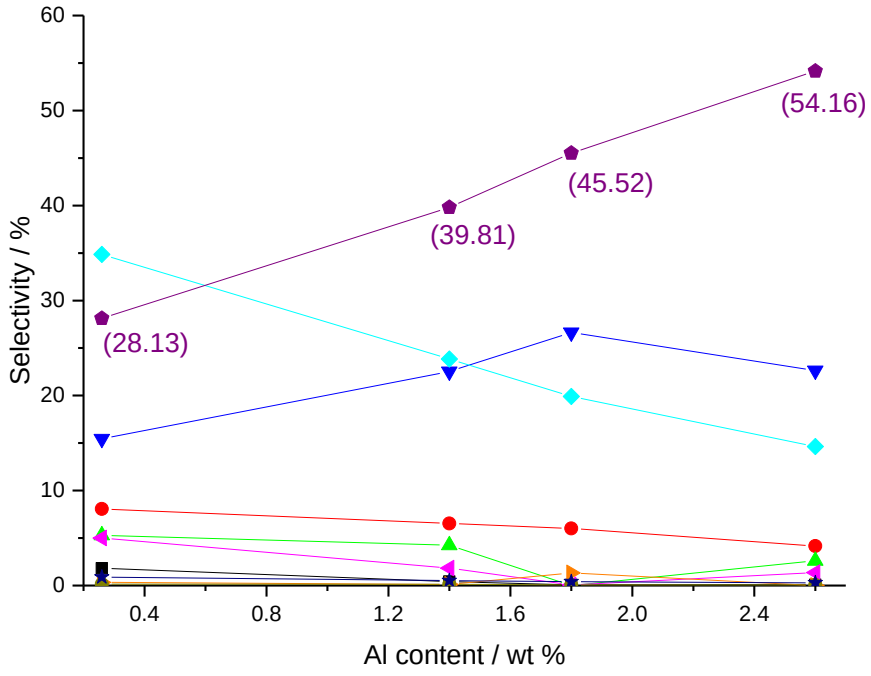

■ Black squares (CH_3OOH), ● Red Circles (CH_3OH), ♦ Aquamarine diamonds (CH_3COOH), ◀ Pink triangles (CH_3CHO), ▼ Blue triangles (C_2H_5OH), ▲ Green triangles ($HCOOH$), ● Beige circles (CH_4), ★Navy Stars (CO_2), ⬟ Purple pentagons (C_2H_4), ▶ Orange triangles (CH_3CH_2OOH), (Ethene Selectivity)

Test conditions; 27 mg catalyst reaction volume 10 ml, 0.5 h, $[H_2O_2]$= 0.5M, 50°C, $P(C_2H_6)$ = 20 bar, 1500 rpm

Figure 5.14 Ethane oxidation product selectivities for 1.25% Fe 1.25% Cu/ ZSM-5 of varying Al

Figure 5.14 shows that upon increasing the Al content, and thereby decreasing the Cu/Al and Fe/Al ratio, a linear increase in ethene selectivity from 28.1 to 54.2% may be achieved. Across the same range a corresponding decrease in acetic acid selectivity, from 34.9% for 1.25% Fe 1.25% Cu/ZSM-5 (280) to 14.6% for 1.25% Fe 1.25% Cu/ZSM-5 (23) was also observed. Given that ethene was shown in Chapter 3 to undergo oxidation to acetic acid under reaction conditions, it would appear that this transformation becomes less favourable with increased Al content, thereby leading to the high ethene selectivity observed. An overall increase in C_2 selectivity was observed with increased Al content, from 83.8% to 92.8% (ZSM-5 280 and 23 respectively), thereby showing that C-C cracking becomes less favourable with increasing Brønsted acidity/ increasing hydrophilicity/ increased exchange capacity/ decreased Fe:Al & Cu: Al.

Upon consideration of the productivities shown by this group of catalysts towards specific reaction products, as shown in Figure 5.15, trends shown in Figures 5.13 and 5.14 may be put into context and the source of enhanced activity supposed upon. From Figure 5.15 it is clear that with increasing zeolite aluminium content a linear increase in ethene productivity is observed. Additionally, a general decrease in acetic acid productivity is also seen, coupled with increased ethanol productivity across the same range. A linear increase in ethene productivity with increasing Al content is consistent with Cu/ZSM-5 studies, suggesting that the Al-dependence of Cu ion distributions (Cu-II and Cu-IV) may be leading to the enhanced conversion and ethene productivity. Due to the inclusion of Fe^{3+}, in addition to Cu^{2+}, activation of both H_2O_2 and ethane are heightened relative to the monometallic Cu catalyst. The high acetic acid selectivity when compared with analogous Cu/ZSM-5 catalyst is also the result of consecutive oxidation of ethanol to acetaldehyde and acetic acid over iron sites, based on studies in Chapter 3.

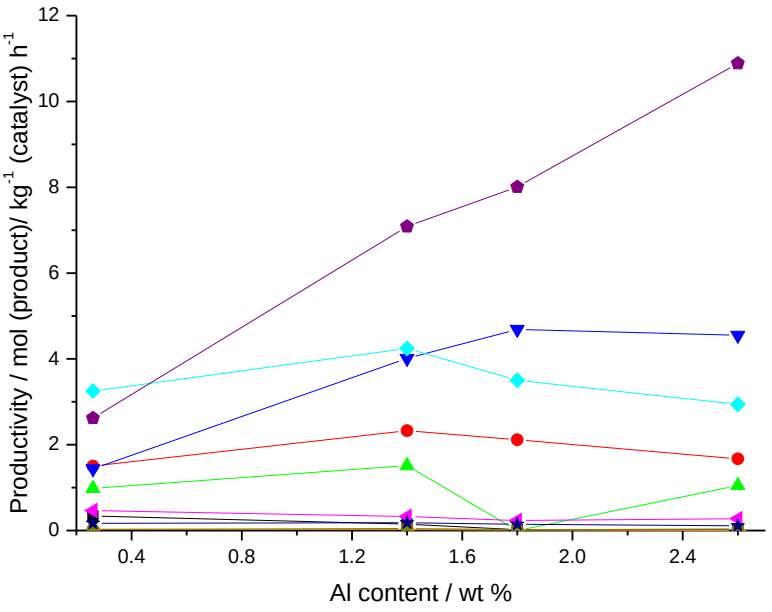

■ Black squares (CH_3OOH), ● Red Circles (CH_3OH), ♦ Aquamarine diamonds (CH_3COOH), ◀ Pink triangles (CH_3CHO), ▼ Blue triangles (C_2H_5OH), ▲ Green triangles ($HCOOH$), ● Beige circles (CH_4), ★Navy Stars (CO_2), ⬟ Purple pentagons (C_2H_4), ► Orange triangles (CH_3CH_2OOH),
Test conditions; 27 mg catalyst reaction volume 10 ml, 0.5 h, [H_2O_2]= 0.5M, 50^oC, P(C_2H_6) = 20 bar, 1500 rpm
Figure 5.15 Ethane oxidation product selectivities for 1.25% Fe 1.25% Cu/ ZSM-5 of varying Al

In order to determine whether the trends in ethene productivity observed in Figure 5.15 result from enhanced stability of ethene, as a primary product, in the presence of less siliceous FeCu/ ZSM-5 catalysts, ethene stability studies akin to those conducted in Chapter 3 were run in order to determine the relative conversion of ethene over 1.25% Fe 1.25% Cu/ZSM-5 catalysts, at a 30, 50 and 70 ^oC. Product selectivity plots and ethene conversion over said catalysts, at varying reaction temperatures, are shown in Figure 5.16 (a,b,c) and (d) respectively. Whilst a general decrease in ethene conversion is observed upon increasing the Al content at 50 and 70 ^oC reaction temperatures (Figure 5.16 d) this trend applies only to catalysts of $SiO_2/Al_2O_3 \geq 50$. As such, whilst ethene does appear to be more stable at higher Al/FeCu ratios, this trend does not appear to be as clearly defined as in Figure 5.14. Interestingly selectivity to ethylhydroperoxide, the primary ethene oxidation product is observed to decrease with increasing Al content, as are formic acid

and CO_2 selectivities, whilst a general increase in acetaldehyde, acetic acid and methanol selectivity is observed with increasing Al content across a range of reaction temperatures. It therefore appears that the data in Figures 5.13 and 5.14, namely the increase in ethane conversion and ethene selectivity with increasing framework Al content, may be indicative of an increasing population of catalytically active Cu sites as was suggested for monometallic Cu/ZSM-5 catalysts.

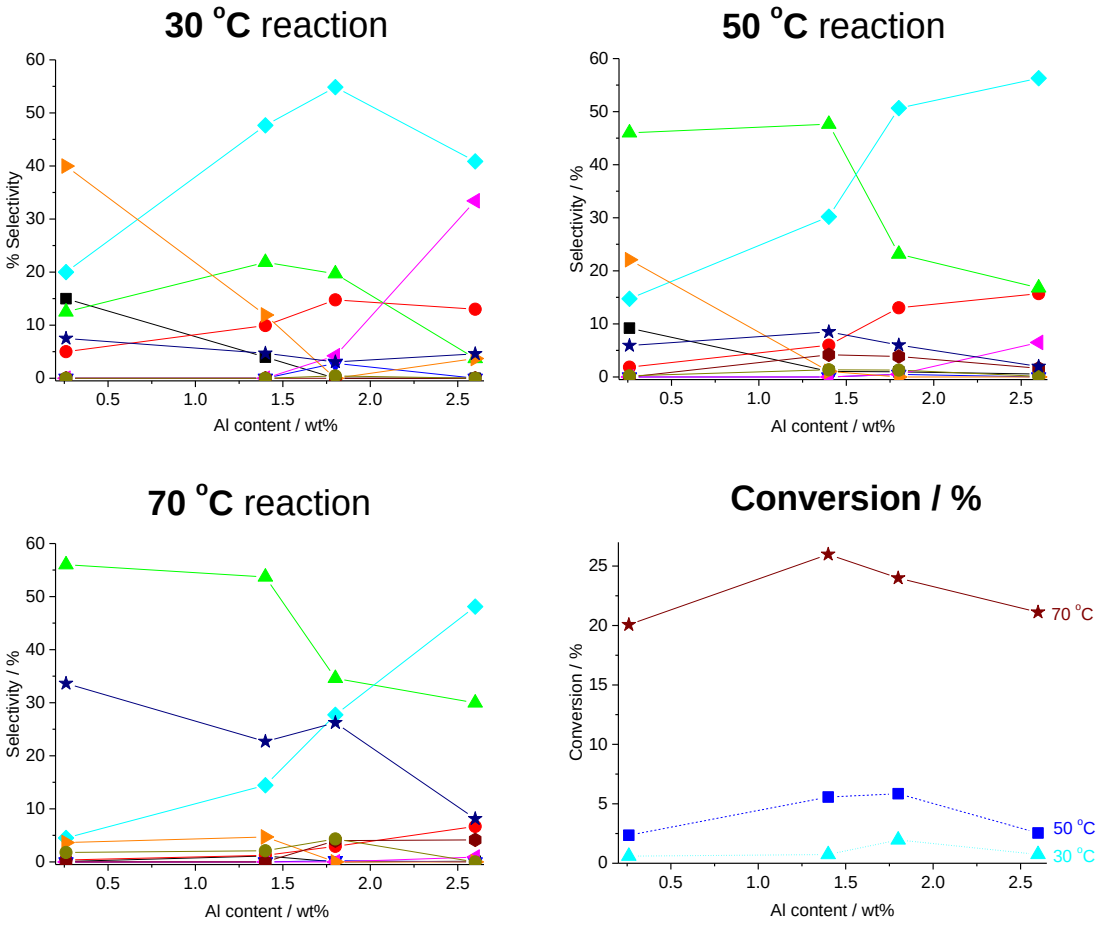

■ Black squares (CH_3OOH), ● Red Circles (CH_3OH), ♦ Aquamarine diamonds (CH_3COOH), ◀ Pink triangles (CH_3CHO), ▼ Blue triangles (C_2H_5OH), ▲ Green triangles ($HCOOH$), ● Beige circles (CH_4), ★Navy Stars (CO_2), ⬟ Purple pentagons (C_2H_4), ▶ Orange triangles (CH_3CH_2OOH)

Test conditions: 56 mg catalyst, reaction volume = 20 ml, [H_2O_2] = 0.25 M, Gas phase volume = 40 ml, P(5% C_2H_4/ N_2)= 10 bar

Figure 5.16 Ethene oxidation product selectivities (a,b,c) and conversion (d) for 1.25% Fe 1.25% Cu/ ZSM-5 of varying Al content at different reaction temperatures

Given that ethane conversion over 1.25% Fe/ZSM-5 (30) was shown in Chapter 3 to increase linearly upon increasing the reaction temperature from 30 to 70 ^{o}C, the effect of temperature upon the productivity and selectivity of 1.25% Fe 1.25% Cu/ZSM-5 (23) was investigated in order to determine the extent to which ethene productivity may be enhanced. Results for the temperature range of 30 ^{o}C to 70 ^{o}C (at 10 ^{o}C intervals) are represented in Figure 5.17 (a) and (b). It is clear that conversion may be increased through increasing the reaction temperature, with a linear increase in both H_2O_2 decomposition and ethane conversion being observed over the range of temperatures tested. The catalyst productivity increased from 2.75 h^{-1} at 30 ^{o}C to 51.11 h^{-1} at 70 ^{o}C. It is interesting to note that an increase in ethene selectivity is observed up to and including 60 ^{o}C, with a slight decline to the highest temperature investigated (70 ^{o}C). That said, at 70 ^{o}C ethene selectivity still equalled 49.9% which equated to an ethene productivity of 25.5 mol (ethene) kg^{-1} (1.25% Fe 1.25% Cu/ZSM-5 (23)) h^{-1}, which is considered to be a major development of the previously published system, which showed ethene productivity of 8.19 h^{-1} at 50 ^{o}C (for comparison, an ethene productivity of 11.3 h^{-1} was shown at 50 ^{o}C in Figure 5.15). Given that three primary products were implied from work in Chapter 3, one of which being ethene, it is possible that at higher temperatures the ethene producing pathway may be promoted. Alternately, increasing temperatures may promote the relatively slow decomposition of $CuOOH^{+}$ shown in Equation 5.2 to give an active oxygen species, thereby increasing catalyst productivity.

Given that it was shown in Chapter 3 that with increasing Fe loading onto ZSM-5 (30) (increased Fe/Si/Al) formation of large Fe_xO_y species became more favourable, and that such species might play a role in secondary oxidations and C-C scission, it is plausible that a different distribution of Fe_xO_y species are formed upon deposition onto low SiO_2/Al_2O_3 zeolites, and that these affect the trends in selectivity shown in Figure 5.14.

(a)

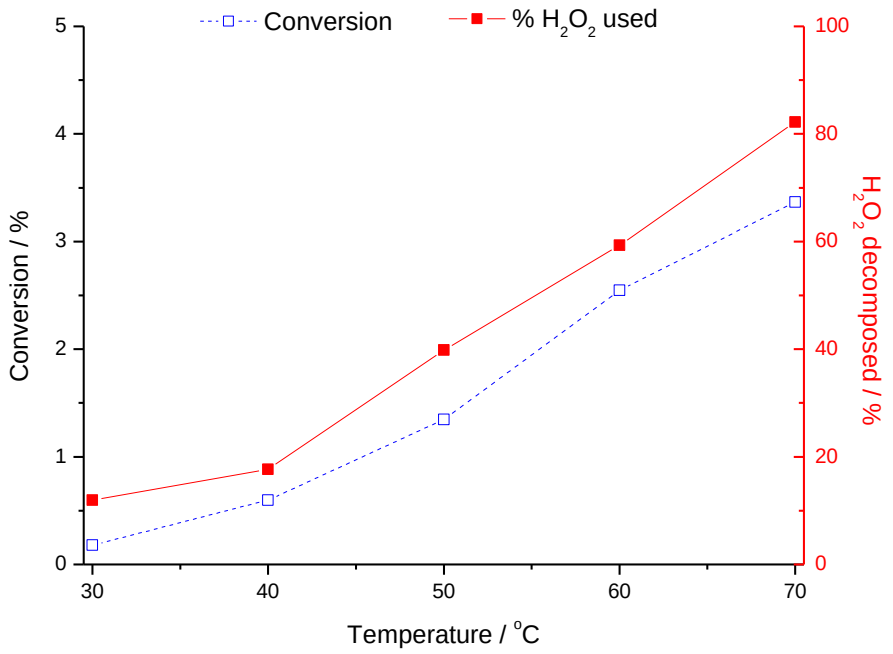

(b)

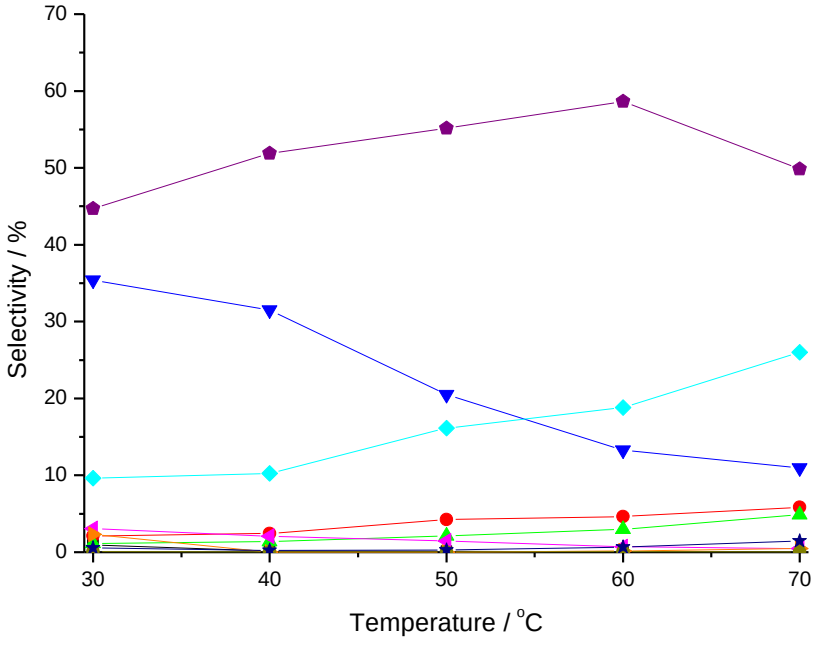

■ Black squares (CH_3OOH), ● Red Circles (CH_3OH), ♦ Aquamarine diamonds (CH_3COOH), ◀ Pink triangles (CH_3CHO), ▼ Blue triangles (C_2H_5OH), ▲ Green triangles ($HCOOH$), ● Beige circles (CH_4), ★Navy Stars (CO_2), ⬟ Purple pentagons (C_2H_4), ► Orange triangles (CH_3CH_2OOH)

Test conditions: 27 mg 1.25% Fe 1.25% Cu/ZSM5 (23), 10 ml reaction volume [H_2O_2] = 0.5M, P(C_2H_6) = **20** bar, 0.5 h, 1500 rpm

Figure 5.17 Ethane conversion and H_2O_2 decomposition (a) and product selectivities for 1.25% Fe 1.25% Cu/ZSM-5 (23) at a range of reaction temperatures

5.3 The role of Lewis Acid Sites

As described in Chapter 1, in addition to their Brønsted acidity, zeolites may also exhibit Lewis acidic character through framework dealumination.[7] Upon high temperature heat treatment, Si-O-Al bond cleavage occurs, leading to the formation of extra framework aluminium species. Above pre-treatment temperatures of 550 ^{o}C there is a sharp increase in Lewis acidity. This results in a proportional decrease in Brønsted acidity as the dealumination of the zeolite framework reduces its charge and thereby leads to a reduction in the concentration of charge compensating cations associated with framework Al^{3+} sites.[7] Such extraframework species in zeolites have been identified as being active in the activation of short chain alkanes via hydride abstraction at Lewis acid sites.[33]

Two approaches were taken in order to determine the role of extraframework, Lewis acidic aluminium sites upon the activity of ZSM-5 catalysts in ethane oxidation; firstly samples of 1.25% Fe 1.25% Cu/ZSM-5 (23) were calcined at temperatures of between 350 and 750 ^{o}C (100 ^{o}C intervals), the aim being to assess the effect of forced dealumination of the zeolite lattice. This also allowed investigation of the effect of reducing the Al content of a given zeolite catalyst, at constant Fe- and Cu- loading, upon its catalytic activity. Secondly, varying wt% of extraframework Al were deposited onto 1.25% Fe 1.25% Cu/ZSM-5 (23) via CVI using $Al(acac)_3$ in order to directly study the effect of an increased concentration of extraframework Al species.

As Lewis acidity may be induced through high temperature activation via forced migration of framework Al^{3+} into extraframework sites, samples of 1.25% Fe 1.25% Cu/ZSM-5 (23) were calcined at increasing temperatures under static air. Dealumination was monitored and quantified by NH_3-TPD, which allows for measurement and quantification of the ammonia- chemisorptions capacity of a given catalyst's Brønsted acid sites. TPD traces for said catalysts are shown in Figure 5.18.

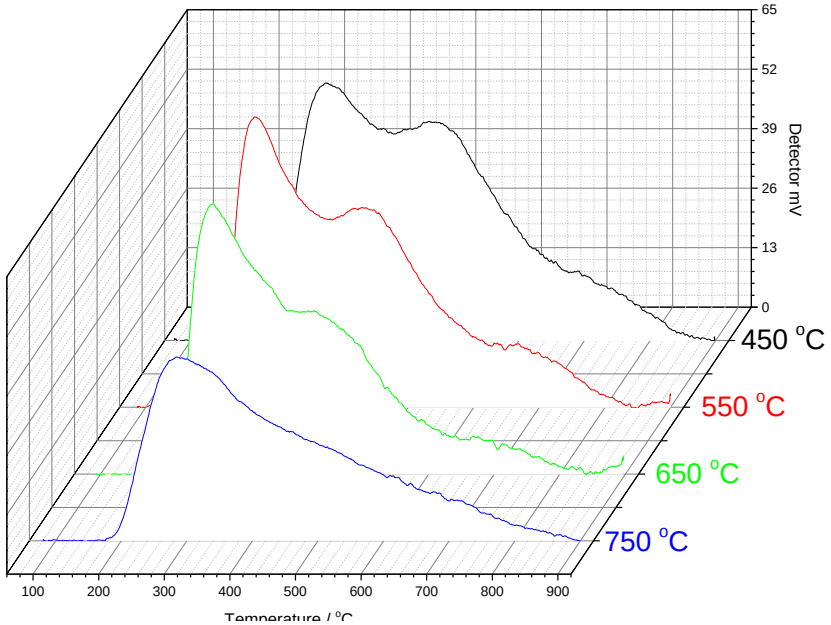

Figure 5.18 NH_3-TPD traces for 1.25% Fe 1.25% Cu/ZSM-5 (23) catalyst calcined at increasing temperatures

NH_3-TPD traces in figure 5.18 show a clear trend of reduced NH_3 chemisorption capacity at increasing calcination temperatures, suggesting increasing loss of Brønsted acidic Al sites as would be expected. As in Figure 5.10 two main desorptions are observed, at *ca.* 270 and 450 °C, associated with weakly adsorbed NH_3 (at either Brønsted or extraframework Al sites)[29, 30] and NH_3 strongly adsorbed to Brønsted acid sites respectively. [24, 31, 32] To quantify the loss of Brønsted acidity at increasing calcination temperatures, the high temperature desorptions featured in Figure 5.18 were integrated, and treated according to the NH_3 calibration featured in Chapter 2, Figure 2.7. A plot of ammonia adsorption (μmol g^{-1}) at strong acid sites versus calcination temperature for these samples is shown in Figure 5.19.

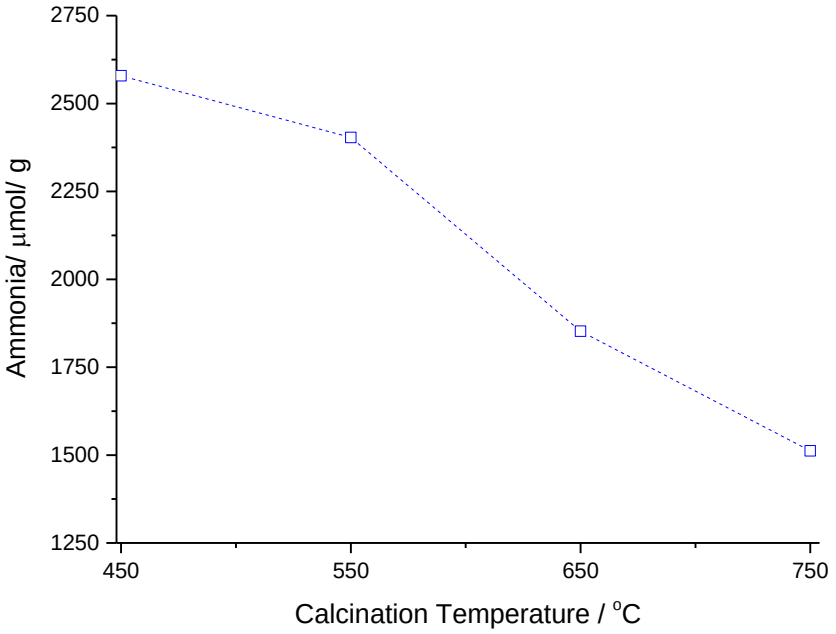

Figure 5.19 Ammonia adsorption capacities of 1.25% Fe 1.25% Cu/ZSM-5 (23) calcined at various temperatures

The trend shown in Figure 5.19 is indicative of greater dealumination of the zeolite framework at increasing heat treatment temperatures. This is consistent with previous studies.[7] In order to determine the effect of losing these exchange sites upon catalytic activity, samples were tested for ethane oxidation with H_2O_2. Given that a key structural difference in 1.25% Fe 1.25% Cu/ZSM-5 catalysts represented in Figure 5.14 was the concentration of framework aluminium sites, one would expect conversion and selectivity trends at increasing calcination temperatures to reflect those observed at 1.25% Fe 1.5% Cu/ZS-5 of increasing SiO_2/Al_2O_3 (decreasing Al content).

Ethane conversion/ hydrogen peroxide decomposition and product selectivities for these materials are represented in Figure 5.20 (a and b respectively)

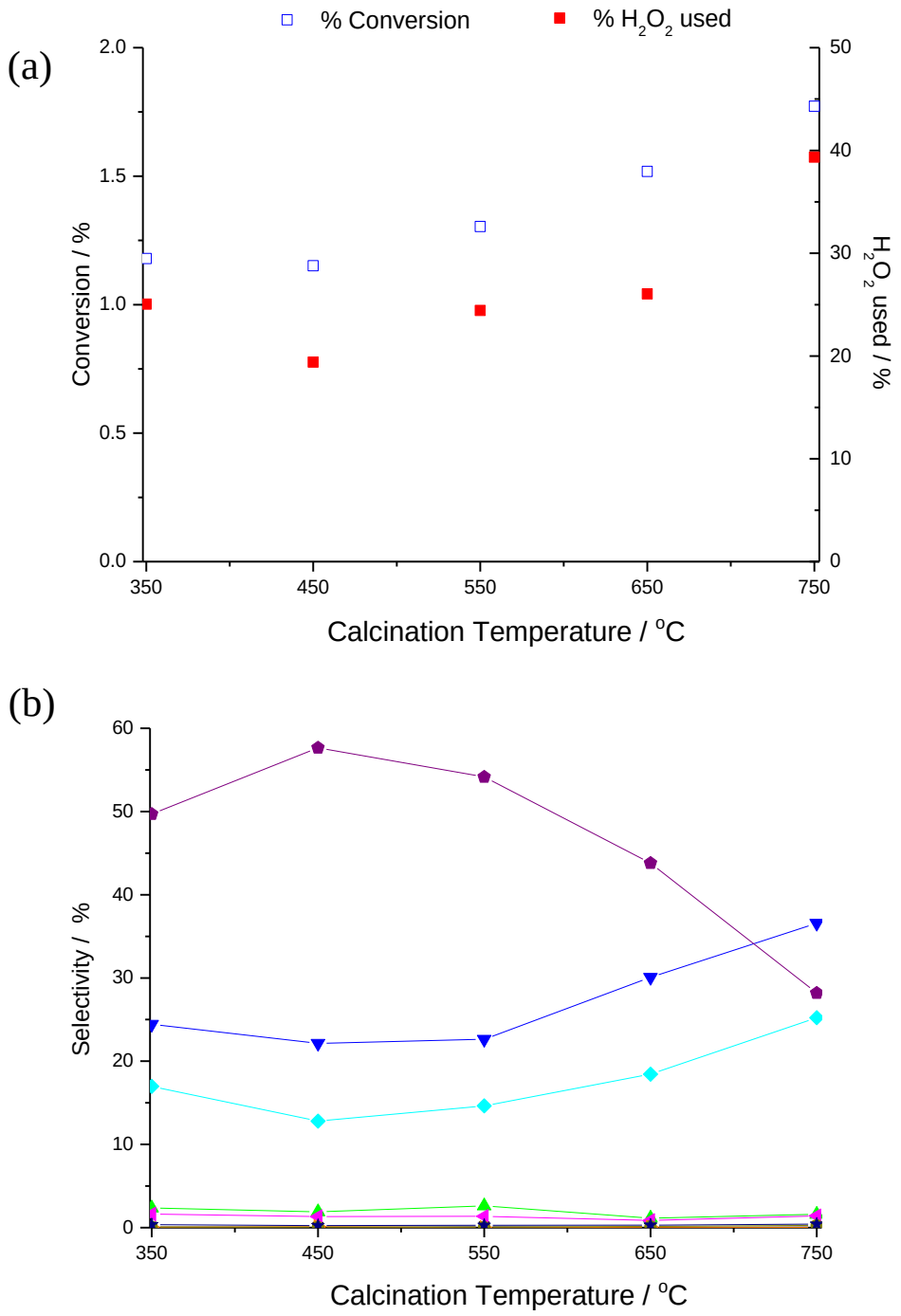

■ Black squares (CH_3OOH), ● Red Circles (CH_3OH), ♦ Aquamarine diamonds (CH_3COOH), ◀ Pink triangles (CH_3CHO), ▼ Blue triangles (C_2H_5OH), ▲ Green triangles ($HCOOH$), ● Beige circles (CH_4), ★Navy Stars (CO_2), ⬟ Purple pentagons (C_2H_4),
Test conditions; 27 mg catalyst reaction volume 10 ml, 0.5 h, [H_2O_2]= 0.5M, 50°C, P(C_2H_6) = 20 bar, 1500 rpm

Figure 5.20 Ethane oxidation conversion and H_2O_2 decomposition (a) and product selectivities (b) over 1.25% Fe 1.25% Cu/ZSM-5 (23) catalysts calcined at varying temperatures.

From Figures 5.20 (a) and (b) it is clear that the presence of high concentrations of framework Al is integral to ethene selectivity, whether through Brønsted acid stabilisation of ethene, as a primary product, through promoting formation of catalytically active sites (Cu-II) or by favouring formation of smaller Fe_xO_y species through lowering the Fe/Si/Al. Contrary to trends shown in Figure 5.13 a lower concentration of framework Al, achieved through calcination at high temperatures, is associated with increased hydrogen peroxide decomposition and ethane conversion (calcined at temperatures > 350 ^oC). The increase in activation of the oxidant and substrate with decreasing framework Al content may tentatively be attributed to an increasing population of Fe_xO_y clusters at non framework positions, as such species appear to play a role in the ethanol- acetic acid oxidation step, based on studies in Chapter 3.[1] Heightened Al extraction at temperatures of 450 ^oC to 750 ^oC also leads to a steady decrease in ethene selectivity (57.7% to 28.2%), and corresponding increase in selectivity towards ethanol (24.4% to 36.6%) and acetic acid (17.0% to 25.2%). To correlate the decreasing framework Al content (Brønsted acidity) shown at calcination temperatures of > 450 ^oC as determined by NH_3-TPD (Figure5.19), major product selectivities for 1.25% Fe 1.25% Cu/ZSM-5 (23) catalysed reactions, being ethene, ethanol and acetic acid were plotted versus ammonia uptake (μmol/ g based on the high temperature desorption).

The effect of increasing calcination temperature, and thereby loss of framework Al exchange sites upon major product selectivities and ethane conversion is illustrated in Figure 5.21. It is clear from Figure 5.21 that, as shown in Figure 5.11 for 2.5% Cu/ZSM-5 catalysts, a linear increase in ethene selectivity and linear decrease in both ethanol and acetic acid selectivities is observed with increasing ammonia uptake at strongly acidic framework Al sites, with the highest uptake being seen at a calcination temperature of 450 ^oC. The increased activation of both H_2O_2 and ethane observed at higher calcination

temperatures may be due to an increased population of large Fe_xO_y species, resulting from loss of Al framework sites at high calcination temperatures.

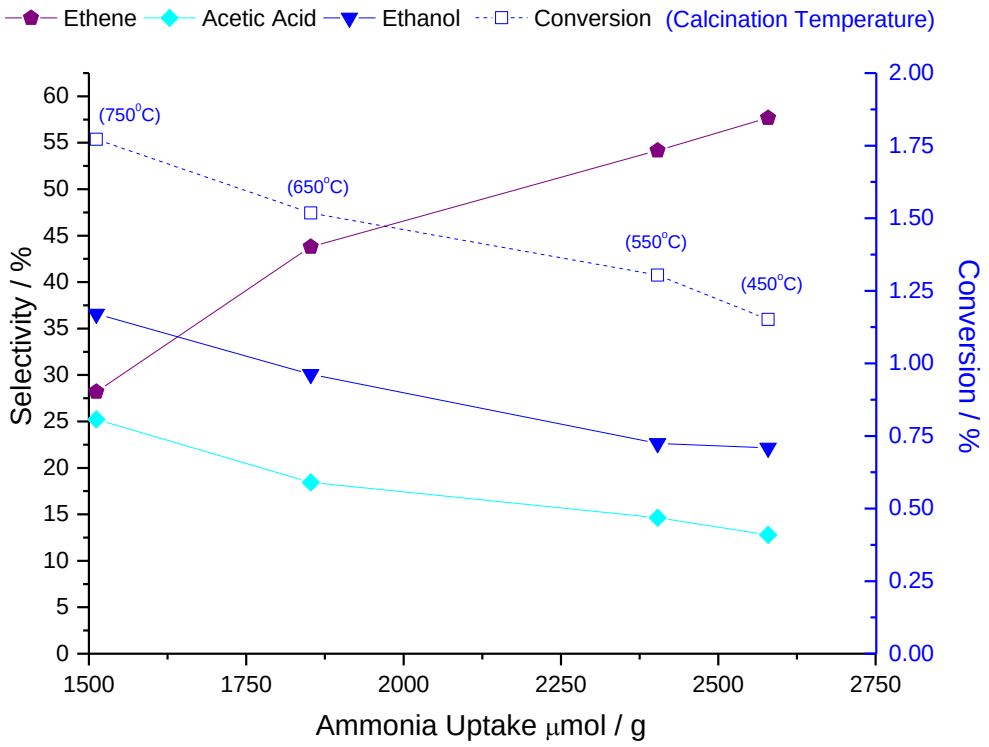

Figure 5.21 Major product selectivities as a function of catalyst ammonia uptake, as determined by NH_3-TPD.

In order to determine the role, if any, which extraframework Al species may play in Fe- and Cu- ZSM-5 catalysed ethane oxidation with H_2O_2, varying wt% of Al (ranging from 0.1 to 0.7 wt %) were deposited onto 1.25% Fe 1.2% Cu/ZSM-5 (23) via CVI. The percentages of ethane converted and of H_2O_2 decomposed are shown in Figure 5.22 (a), whilst product selectivities are presented in Figure 5.22 (b).

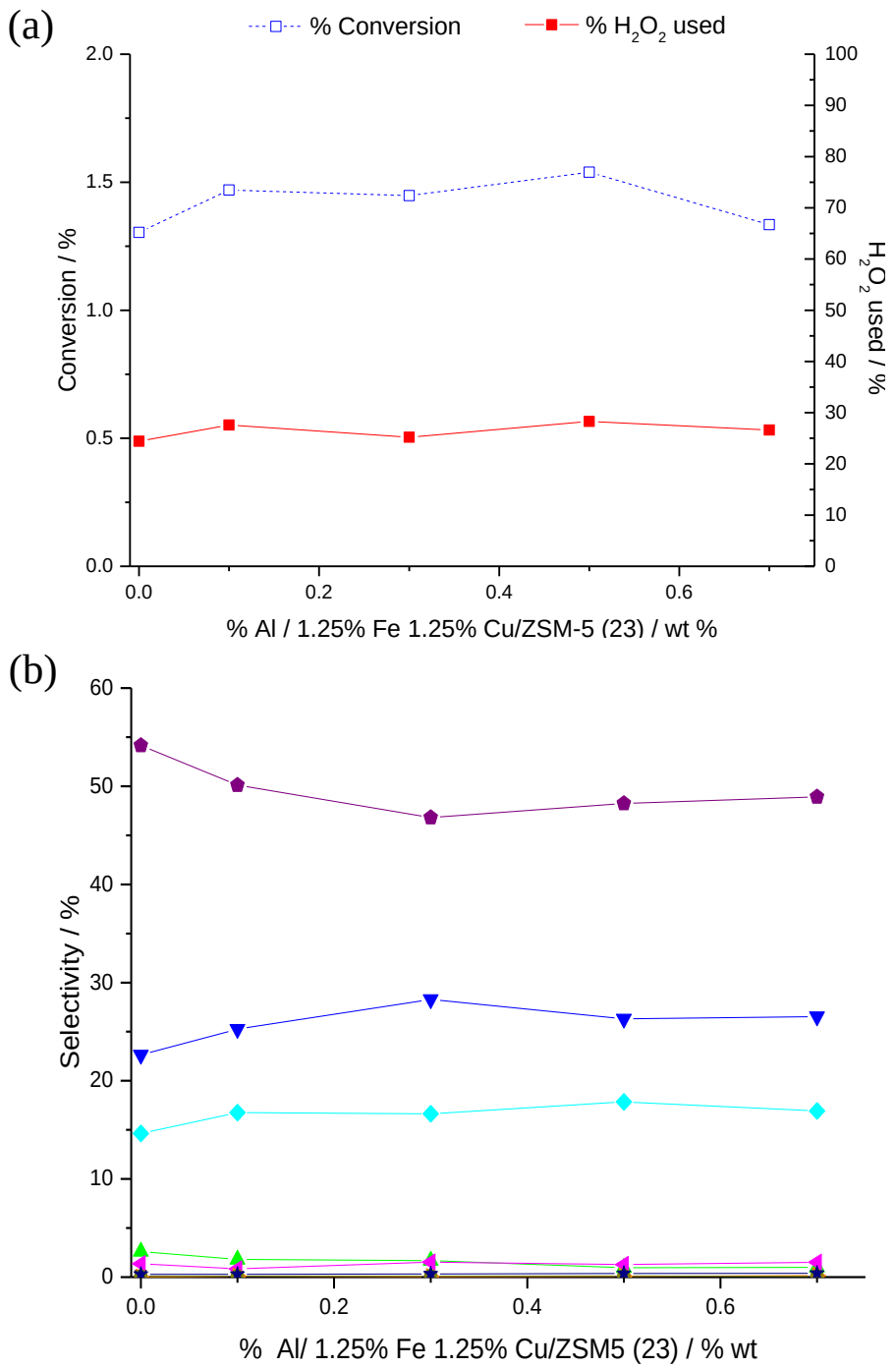

■ Black squares (CH_3OOH), ● Red Circles (CH_3OH), ♦ Aquamarine diamonds (CH_3COOH), ◀ Pink triangles (CH_3CHO), ▼ Blue triangles (C_2H_5OH), ▲ Green triangles ($HCOOH$), ● Beige circles (CH_4), ★Navy Stars (CO_2), ⬟ Purple pentagons (C_2H_4),

Test conditions; 27 mg catalyst reaction volume 10 ml, 0.5 h, [H_2O_2]= 0.5M, 50°C, P(C_2H_6) = 20 bar, 1500 rpm

Figure 5.22 Ethane conversion and H_2O_2 decomposition (a) and product selectivities for 1.25% Fe 1.25% Cu/ZSM-5 (23) catalysts following deposition of varying wt% Al

No significant trends in ethane conversion or product distributions are observed with increasing Al loading, barring the slight drop in ethene selectivity shown at low Al loadings in Figure 5.22 (b) (54.2% for 0% wt added Al and 46.8% selectivity when 0.3wt% Al was deposited). This non- promoting effect of extraframework Al sites was found to be consistent with previous studies on ZSM-5 (30) catalysed methane oxidation with H_2O_2.[2] The nature of Al species formed via CVI, whether aluminium oxides or ionic Al^{3+} species is yet to be confirmed, therefore trends cannot be conclusively attributed to Lewis acidic Al^{3+} sites.

5.4 Conclusions

Prompted by the discovery in Chapter 3 that the product distribution of ZSM-5 catalysed ethane oxidation may be controlled through variation of the zeolite's SiO_2/Al_2O_3 molar ratio, the role of framework and extraframework Al sites has been considered in this chapter. Particular emphasis has been put on the role of framework Al in the catalytic oxidative transformation of ethane to ethene, catalysed by Cu- and FeCu- ZSM-5 catalysts.

This study has epitomised the complexity which is inherent in identification of specific active sites and promoters in M/ZSM-5 (M= transition metal) catalysts, for which a number of factors including; framework metals, exchanged extraframework cations or cationic species, supported and metal oxides and extraframework Lewis acidic species (such as Al^{3+}) must be considered in addition to physical properties such as hydrophilicity/hydrophobicity.

It has been shown that through increasing the concentration of framework Al sites, and thereby increasing Brønsted acidity and hydrophilicity of catalysts, the size of copper

oxide species deposited onto ZSM-5 supports via chemical vapour impregnation, a novel vapour deposition technique, may be controlled. This might be attributed to a metal support interaction through comparison of the hydrophilicity of the zeolite support used of the organometallic transition metal precursor (copper (II) acetylacetonate). As of yet the significance of copper oxide particle size in catalytic activity/ selectivity has not yet been determined conclusively, though the increasing reducibility and deactivation of Cu/ZSM-5 catalysts which present small surface copper oxide species might indicate that copper oxide species play a role in the activation of both hydrogen peroxide and ethane. Through testing of analogous Cu/Silicalite materials, which showed higher selectivity to oxygenated products than ZSM-5 supported catalysts at a comparable level of ethane conversion, it is suggested that the presence of framework Al is integral to high ethene selectivity. Future TEM studies shall be conducted to determine the morphology of Cu species deposited on silicalite via CVI, though previous studies would suggest a likely size of *ca.* 1-3 nm.[1]

Through comparison with Cu/ZSM-5 studies within the literature, characterisation and testing data suggests a potential role of the distribution of cationic Cu^{2+} species in determining catalyst activity and selectivity, with catalytic trends suggesting that ethane conversion and ethene selectivities are favoured at Cu/Al molar ratios of < 0.5. As of yet the potential role of cationic Cu species (Cu-II and Cu-IV) in the materials tested is purely circumspect, based upon comparison with the literature. Future work shall address the presence of such species through NO adsorption IR studies, as it has been shown within the literature that NO exhibits characteristic vibrational frequencies when bound to these cationic species.

High catalyst productivities may be achieved through co deposition of Fe and Cu onto ZSM-5 via CVI, with productivities of 51.1 h^{-1} total (25.6 h^{-1} ethene productivity)

observed at the relatively low temperature of 70 ^{o}C. This chapter represents a gain in the understanding of the role of Cu in promoting ethene as a product of the catalytic oxidation of ethane with H_2O_2 over zeolite catalysts.

References

1 Forde, M. M.; Armstrong, R. D.; Hammond, C.; He, Q.; Jenkins, R. L.; Kondrat, S. A.; Dimitratos, N.; Lopez-Sanchez, J. A.; Taylor, S. H.; Willock, D.; Kiely, C. J.; Hutchings, G. J. *Journal of the American Chemical Society* **2013**, *135*, 11087.

2 Hammond, C.; Forde, M. M.; Ab Rahim, M. H.; Thetford, A.; He, Q.; Jenkins, R. L.; Dimitratos, N.; Lopez-Sanchez, J. A.; Dummer, N. F.; Murphy, D. M.; Carley, A. F.; Taylor, S. H.; Willock, D. J.; Stangland, E. E.; Kang, J.; Hagen, H.; Kiely, C. J.; Hutchings, G. J. *Angewandte Chemie International Edition* **2012**, *51*, 5129.

3 Corma, A. *Journal of Catalysis* **2003**, *216*, 298.

4 Haag, W. O. In *CATALYSIS BY ZEOLITES - SCIENCE AND TECHNOLOGY*; Elsevier Science Bv, Amsterdam, 1994; Vol. 84. pp 1375.

5 Pine, L. A.; Maher, P. J.; Wachter, W. A. *Journal of Catalysis* **1984**, *85*, 466.

6 Barthomeuf, D. *Materials Chemistry and Physics* **1987**, *17*, 49.

7 Auerbach, S. M.; Currado, K. A.; Dutta, P. K. *HANDBOOOK OF ZEOLITES SCIENCE AND TECHNOLOGY*; Marcel Dekker Inc, New York, 2003.

8 Johnson, G. R. A.; Nazhat, N. B.; Saadallanazhat, R. A. *J. Chem. Soc.-Chem. Commun.* **1985**, 407.

9 Goldstein, S.; Meyerstein, D. *Accounts of Chemical Research* **1999**, *32*, 547.

10 Perez-Benito, J. F. *Journal of Inorganic Biochemistry* **2004**, *98*, 430.

11 Jung, Y.; Park, J. Y.; Ko, S. O.; Kim, Y. H. *Chemosphere* **2013**, *90*, 812.

12 Kawai, T.; Tsutsumi, K. *Colloid Polym. Sci.* **1992**, *270*, 711.

13 Gounder, R.; Davis, M. E. *Aiche J.* **2013**, *59*, 3349.

14 Khouw, C. B.; Dartt, C. B.; Labinger, J. A.; Davis, M. E. *Journal of Catalysis* **1994**, *149*, 195.

15 Urquieta-González, E. A.; Martins, L.; Peguin, R. P. S.; Batista, M. S. *Materials Research* **2002**, *5*, 321.

16 TorreAbreu, C.; Ribeiro, M. F.; Henriques, C.; Delahay, G. *Appl. Catal. B-Environ.* **1997**, *12*, 249.

17 Sullivan, J. A.; Cunningham, J.; Morris, M. A.; Keneavey, K. *Appl. Catal. B-Environ.* **1995**, *7*, 137.

18 Torre-Abreu, C.; Ribeiro, M. E.; Henriques, C.; Delahay, G. *Appl. Catal. B-Environ.* **1997**, *14*, 261.

19 Bulanek, R.; Wichterlova, B.; Sobalik, Z.; Tichy, J. *Appl. Catal. B-Environ.* **2001**, *31*, 13.

20 Dossi, C.; Fusi, A.; Recchia, S.; Psaro, R.; Moretti, G. *Microporous and Mesoporous Materials* **1999**, *30*, 165.

21 Neylon, M. K.; Marshall, C. L.; Kropf, A. J. *Journal of the American Chemical Society* **2002**, *124*, 5457.

22 Shetti, V. N.; Manikandan, P.; Srinivas, D.; Ratnasamy, P. *Journal of Catalysis* **2003**, *216*, 461.

23 Que, L.; Tolman, W. B. *Nature* **2008**, *455*, 333.

24 Lobree, L. J.; Hwang, I. C.; Reimer, J. A.; Bell, A. T. *Journal of Catalysis* **1999**, *186*, 242.

25 Smeets, P. J.; Woertink, J. S.; Sels, B. F.; Solomon, E. I.; Schoonheydt, R. A. *Inorganic Chemistry* **2010**, *49*, 3573.

26 Wichterlova, B.; Dedecek, J.; Sobalik, Z.; Vondrova, A.; Klier, K. *Journal of Catalysis* **1997**, *169*, 194.

27 Dedecek, J.; Sobalik, Z.; Tvaruazkova, Z.; Kaucky, D.; Wichterlova, B. *The Journal of Physical Chemistry* **1995**, *99*, 16327.

28 Dedecek, J.; Sobalik, Z.; Tvaruzkova, Z.; Kaucky, D.; Wichterlova, B. *J. Phys. Chem.* **1995**, *99*, 16327.

29 Hunger, B.; Hoffmann, J.; Heitzsch, O.; Hunger, M. *J. Therm. Anal.* **1990**, *36*, 1379.

30 Schnabel, K. H.; Peuker, C.; Parlitz, B.; Loffler, E.; Kurschner, U.; Kriegsmann, H. *Zeitschrift Fur Physikalische Chemie-Leipzig* **1987**, *268*, 225.

31 Long, R. Q.; Yang, R. T. *Journal of Catalysis* **2001**, *198*, 20.

32 Iwasaki, M.; Yamazaki, K.; Banno, K.; Shinjoh, H. *J. Catal.* **2008**, *260*, 205.

33 Ivanova, II; Kolyagin, Y. G. *Chemical Society Reviews* **2010**, *39*, 5018.

6

Conclusions &Future Work

6.1 Conclusions

The overall objective of this thesis related to the selective oxidative upgrading of ethane to higher value C_2 products. As a major component of natural gas (1-10% composition)[1]the direct transformation of ethane to valorised products would circumvent current industrial processes which are operated on a global scale. Ethene is a highly versatile feedstock produced via the steam cracking of hydrocarbons, including ethane, over zeolite catalysts at an annual output of *ca.* 143 Mt/ annum.[2] This process requires temperatures of > 800 ^{o}C and accounts for around 40% of the energy consumed by the petrochemical industry, the majority of which is required for heating of the reaction furnaces.[3] Ethene itself is used in the production of; polyethylene, ethylene oxide, ethylene glycol, ethylene dichloride, ethylbenzene and α-olefins, all of which have commercial importance. Meanwhile 60% of the global acetic acid output of 7.8 Mt/ annum is met through methanol carbonylation, typically over homogeneous Rh(I) (operated by Celanese) or Ir(I) catalysts (BP Cativa Process), a highly energy intensive process which operates at high temperatures, high pressures of CO and generates corrosive iodide waste streams. Meanwhile a direct process with 30,000 t/annum acetic acid output from ethane has been developed by SABIC using a solid catalyst $Mo_1V_{0.398}$-$La_{7.08e-6,}Pd_{0.0003}Nb_{0.125}Al_{0.226}$ and showing 10% ethane conversion with 85% acetic acid selectivity at 280 ^{o}C.[4] Additionally SABIC have shown coproduction of ethene and acetic acid from ethane over $Mo_{2.5}V_{1.0}Nb_{0.32}P_x$ (x= 0.01-0.06), with 53.3% conversion to ethene (10.5%) and acetic acid (49.9%) at an operating temperature of 260 ^{o}C.[5]

Whilst a number of studies have been published concerning the partial oxidation of ethane to oxygenated products in liquid phase systems using homogeneous catalysts, these suffer additional separation steps, often require additives and concentrated acidic media and show limited reusability. Enzyme catalysts such as soluble *Methylococcus Capsulatus* (sMMO) and *Methylosinus Trichosporium* have been shown to selectively oxidise ethane to ethanol with productivities of 4.1 mol (ethanol) kg^{-1} (sMMO) h^{-1} and 30 mol (ethanol) kg^{-1} (protein) h^{-1} with O_2 as oxidant. However, the activity of such enzyme catalysts is dependent on the expensive cofactor NADH.[6, 7]

Few heterogeneous liquid phase ethane oxidation systems have been reported thus far within the literature. For comparison, the catalyst productivities and selectivities for the three such systems which have been published are shown in Table 6.1 accompanied by data pertaining to the catalysts from this thesis which showed the highest selectivity to; acetic acid, ethanol and ethene. It is clear that the catalytic system investigated in this thesis shows significantly higher productivities than previously reported TS-1 and Pd/C catalysts, to the order of 2 and 1 order of magnitude respectively, whilst the ZSM-5 catalyst system reported by Rahman *et al* showed higher productivity when tested for ethane oxidation to tests of H-ZSM-5 featured in Chapter 3 where H-ZSM-5 of SiO_2/Al_2O_3 molar ratios of 23,30, 50 and 280 showed productivities of 0.21, 0.84, 0.67 and 0.91 h^{-1} respectively. This is likely due to their use of higher temperatures (120 ^oC compared with 50 ^oC) and higher H_2O_2 concentrations (4M compared with the standard 0.5 M used in this thesis) both reaction parameters which have been shown to have a significant effect upon catalyst productivity.

Table 6.1 Product selectivities and productivities for reported heterogeneous liquid phase ethane oxidation systems

Catalyst	% Product Selectivities							Productivity[g]	ref
	CH_3COOH	CH_3CHO	CH_3CH_2OH	CH_3OH	HCOOH	C_2H_4	CO_2		
TS-1[a]	-	**94.27**	5.72	-	-	-	-	0.248	8
5% Pd/C[b]	**78.10**	21.90	-	-	-	-	-	3.40	9
H-ZSM-5 (23.7)[c]	**48.51**	2.07	1.12	0.26	36.31	-	11.93	6.81	10
1.25% Fe/ZSM-5 (30) CVI[d]	**62.66**	3.32	7.99	2.90	16.21	0.17	3.47	15.32	This work
1.25% Fe/ZSM-5 (30) CVI[e]	36.70	4.50	**43.99**	3.91	8.11	0.80	0.62	17.87	This work
1.25% Fe 1.25% Cu/ZSM-5 (23) CVI[f]	18.80	0.70	13.28	4.65	2.99	**58.63**	0.67	39.12	This Work

[a] 10 mg TS-1, 1 ml H_2O_2 (35 wt%, 11,000 µmol), 60 ^oC, 12 h, P (C_2H_6) = 30 bar (0.120 mol)
[b] 40 mg 5% Pd/Carbon, 85 ^oC, 24 h, P (C_2H_6) = 34.47 bar (0.180 mol), P (CO) = 6.89 bar P (O_1) = 6.89 bar.
[c] 1500 mg H-ZSM-5 (23.7), 120 ^oC, [H_2O_2] = 4 M (279 mmol), 5 h, P (C_2H_6) = 30 bar (0.145 mol)
[d] 27 mg 1.25% Fe/ZSM-5 (30) CVI, 50^oC, [H_2O_2] = 0.5 M (5000 µmol), 0.5 h. 1500 rpm, P(10% C_2H_6 / N_2) = 20 bar (0.02 mol)
[e] 27 mg 1.25% Fe/ZSM-5 (30) CVI, 50 ^oC, [H_2O_2] = 0.5 M, (5000 µmol), 0.5 h. 1500 rpm, P(C_2H_6) = 20 bar (0.02 mol)
[f] 27 mg 1.25% Fe 1.25% Cu/ZSM-5 (23) CVI, 60^oC, [H_2O_2] = 0.5 M, (5000 µmol), 0.5 h. 1500 rpm, P(C_2H_6) = 20 bar (0.02 mol)
[g] Productivity measured as mol (2C in products) kg^{-1} (catalyst) h^{-1}

It is clear from the work in the preceding results chapters that the selective oxidation of ethane may be carried out using Fe- and Cu- modified ZSM-5 catalysts within both batch and flow regimes using an environmentally benign oxidant and solvent (hydrogen peroxide / water) at low temperatures of < 90 ^oC. This catalyst group is bifunctional in activating not only hydrogen peroxide but also the primary C-H bond in ethane. It was shown in Chapter 3 that the post synthesis technique used in depositing iron onto ZSM-5 impacts significantly upon catalyst activity and selectivity, with 2.5% wt Fe/ZSM-5 prepared via CVI, a novel vapour deposition technique showing both higher catalyst TOFs and higher primary product selectivity than traditional impregnation and ion

exchange catalysts of equal iron loading. This was attributed to formation of a porous iron oxide film on the zeolite surface and within micropores upon deposition via CVI, whilst traditional techniques led to formation of greater population of large Fe_xO_y species which have been indicated in C-C scission and deep oxidation to CO_2. Using 1.25% Fe/ZSM-5 (30) prepared via CVI as a screening catalyst, due to its relatively high catalytic activity and primary oxidation product selectivity, reaction parameters were shown to impact significantly upon both catalytic activity and product distributions, with increased temperature, catalyst mass and hydrogen peroxide concentration associated not only with heightened ethane conversion but also a greater degree of C-C scission and deep oxidation to CO_2. A high hydrated substrate/active site/ oxidant ratio achieved at increased ethane pressures or ethane partial pressures was shown to inhibit secondary oxidation and cracking processes, which has been attributed to blocking of the active site through competitive sorption.

Through mechanistic studies a complex reaction scheme was shown to be in operation, whilst three primary products were identified as; ethanol, ethylhydroperoxide and ethene. Through deposition of Cu and FeCu onto ZSM-5 via CVI, high selectivity to ethene at 50 ^oC was achieved.

Given that C_2 products were shown in Chapter 3 to undergo facile C-C scission to yield the C_1 products; methylhydroperoxide, methanol, formic acid and CO_2 over ZSM-5 catalysts, Chapter 4 focused upon translating the catalytic system into a continuous flow regime, with the aim of minimising product- catalyst contact times and thereby minimising these processes. Optimisation of reaction parameters led to the development of a process which showed 23.4% ethane conversion at high acetic acid selectivity (73.1%), with formic acid (18.8%) and CO_2 (1.2%) additional C_1 products. A key limitation of this system was the low partial pressure of ethane used (10% C_2H_6/N_2)

which was necessitated due to safety considerations, but has been shown in Chapter 3 to enhance C-C scission processes as well as acetic acid selectivities. Nevertheless high selectivity to ethene (31.2 %) and acetic acid (43.0%) at appreciable levels of ethane conversion (8.2%) was shown for 0.4% Fe 0.4% Cu/ZSM-5 (30) at the low temperature of 50 ^{o}C.

Given that an increased concentration of framework aluminium sites was tentatively attributed in Chapter 3 to increasing primary product selectivities, Chapter 5 focussed upon elucidating the role played by framework and extraframework aluminium species in the catalysis of Cu- and FeCu- ZSM-5 materials. Studies suggest that whilst the aluminium content of ZSM-5 materials controls their hydrophilic/ hydrophobic nature, it may also direct the distribution of cationic Cu^{2+} species formed upon deposition via CVI, and that different ionic species interact differently with hydrogen peroxide. Whilst the latter effect requires future spectroscopic confirmation, a clear effect of Al content upon copper oxide particle size has been shown via TEM studies, whereby low aluminium content ZSM-5 materials directed formation of small copper oxide species of narrow particle distribution. Deactivation of monometallic Cu/ZSM-5 catalysts observed via time on line analyses might be attributed to formation of long lived $CuOOH^{+}$ species which are not directly active in the activation of ethane, and appears to increase with decreased mean copper oxide particle size. Visible inspection of used Cu/ZSM-5 materials indicates increasing reduction of copper species present at increasing SiO_2/Al_2O_3 ratios (decreasing copper oxide particle size). Reduction of Cu^{2+} to Cu^{+}/Cu^{0} has been confirmed via XPS analysis of used 2.5% Cu/ZSM-5 (280) and is associated with a higher degree of catalyst deactivation. This suggests that catalyst activity is favoured by copper being in the Cu^{2+} oxidation state, which TPR studies imply is favoured in low SiO_2/Al_2O_3 molar ratio zeolites.

6.2 Recommended Future Work

Further to the discoveries presented in this thesis, and with the aim of gaining greater understanding of the catalytic processes which are in operation, it is recommended that several studies be conducted. These are outlined below;

- It was shown in this study that ethene is a primary product of the ZSM-5 catalysed reaction of ethane with hydrogen peroxide. As of yet the mechanism by which ethene is formed has not been determined. This should be the focus of an in depth study as it could enable the design of more highly selective catalysts.
- As discussed in Chapter 5, it is possible that the trends in activity of 2.5% Cu/ZSM-5 catalyst and ZSM-5 (23 and 30) catalysts of varying wt% Cu might be due to the presence of ionic Cu^{2+} of differing coordination and reducibility. As of yet no spectroscopic evidence of the presence of such species has been provided, though previous studies have shown them to ellicit characteristic vibrational frequencies through NO- IR studies. Integration of the relative intensities at the corresponding vibrational frequencies might allow for identification of catalytically active cationic species.
- In lieu of cationic Cu^{2+} species, the most plausible explanation for catalytic trends observed for 2.5% Cu/ZSM-5 catalysts would be the differing copper oxide particle size presented upon deposition onto different ZSM-5 supports. TEM studies should be conducted on materials of varied wt% Cu to determine whether the copper oxide particle size variation corresponds to catalysis observed. Additionally TEM studies of pre heated-treatment 2.5% Cu/ZSM-5 CVI catalysts should be conducted to determine the stage at which copper oxide particle size is determined by the zeolite support, whether during impregnation or calcination.

- In light of the positive effect of aluminium content upon catalyst productivity and ethene selectivity, high aluminium zeolite supports should be investigated. These might be ZSM-5 of SiO_2/Al_2O_3 < 20 or non MFI zeolites such as Zeolite-Y or mordenite.
- Given that increased primary product selectivities were shown in batch studies to be achievable at 100% ethane composition, flow reactions should be conducted using a pure ethane feed, as opposed to the dilute 10% C_2H_6 feed used in chapter 4. This would likely lead to enhanced ethanol and ethene selectivities for Fe- and Cu or FeCu catalysts respectively, whilst increasing productivity.
- Mixed catalyst beds should be investigated within the trickle bed reactor with the aim of developing a bifunctional system which allows for formation of hydrogen peroxide *in situ* from hydrogen and oxygen in an upper catalyst later, with a second layer composed of a catalyst which activates the peroxide and substrate. For such a study H-ZSM-5 catalysts would be favoured as the lower layer given the relatively high O_2 balance observed for unmodified zeolites under flow conditions in Chapter 4.
- Finally, given that bimetallic FeCu/ZSM-5 (30) has previously been reported as highly active for the partial oxidation of methane to methanol with hydrogen peroxide,[11, 12] the trickle bed system developed in Chapter 4 should be investigated for partial methane oxidation. Results of preliminary studies on 1.25% Fe 1.25% Cu/ZSM-5 catalysts, utilising a 10% CH_4/Ar feed are shown in Figure 6.1 as proof of concept. High CO_2 selectivities observed in Figure 6.1 (b) are likely due to the low partial pressure of methane used (10%) which has been shown in this thesis to heighten deep oxidation processes. This system presents an intriguing prospect for future work.

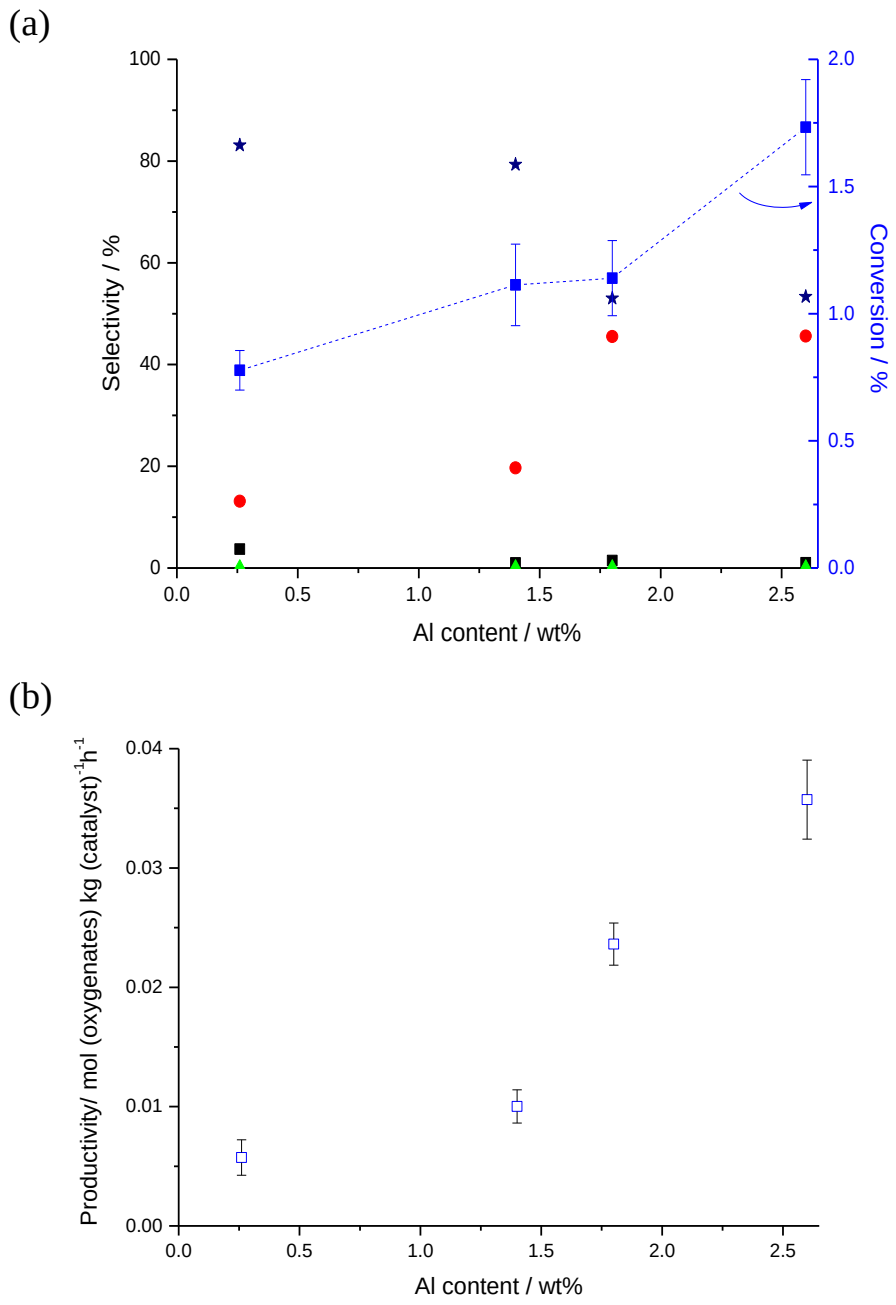

■ Black squares (CH_3OOH), ● Red Circles (CH_3OH), ▲ Green triangles ($HCOOH$), ★Navy Stars (CO_2), -■- Blue squares (% conversion based on Carbon)

Test conditions: 0.5g catalyst pelleted + SiC diluent (24 grit), 0.25 ml min^{-1} H_2O_2/H_2O flow (0.123 M, 30.6 µmol min^{-1} H_2O_2), 10 ml min^{-1} of 10% CH_4/Ar (37 µmol min^{-1} CH_4), P(CH_4/Ar) = 30 bar, Temp = 50 ^{o}C

Figure 6.1 Preliminary methane oxidation test results for 1.25% Fe 1.25% Cu/ZSM-5 catalysts of varying Al content. Product selectivities and methane conversion are shown (a) as are oxygenates productivities (b)

6.3 References

1 In *What is Natural Gas?*, http://www.naturalgas.org/overview/background.asp, 2011.

2 Zimmermann, H.; Walzl, R. In *Ethylene*; Wiley-VCH Verlag GmbH & Co. KGaA, 2000.

3 Fan, D.; Dai, D. J.; Wu, H. S. *Materials* **2013**, *6*, 101.

4 Karim, K.; Al-Hazmi, M.; Khan, A. In *Catalysts for the oxidation of ethane to acetic acid, methods of making and using the same* 2000.

5 Karim, K.; Al-Hamzi, M. H.; Mamedov, E. In *Catalysts for the oxidation of ethane to acetic acid, processes of making same and processes of using same*; Saudi Basic Industries Corp, 1999.

6 Colby, J.; Stirling, D. I.; Dalton, H. *Biochem. J.* **1977**, *165*, 395.

7 Tonge, G. M.; Harrison, D. E. F.; Higgins, I. J. *Biochem. J.* **1977**, *161*, 333.

8 Shul'pin, G. B.; Sooknoi, T.; Romakh, V. B.; Süss-Fink, G.; Shul'pina, L. S. *Tetrahedron Letters* **2006**, *47*, 3071.

9 Lin, M.; Sen, A. *Journal of the American Chemical Society* **1992**, *114*, 7307.

10 Rahman, A. K. M. L.; Indo, R.; Hagiwara, H.; Ishihara, T. *Applied Catalysis A: General* **2013**, *456*, 82.

11 Hammond, C.; Forde, M. M.; Ab Rahim, M. H.; Thetford, A.; He, Q.; Jenkins, R. L.; Dimitratos, N.; Lopez-Sanchez, J. A.; Dummer, N. F.; Murphy, D. M.; Carley, A. F.;

Taylor, S. H.; Willock, D. J.; Stangland, E. E.; Kang, J.; Hagen, H.; Kiely, C. J.; Hutchings, G. J. *Angewandte Chemie International Edition* **2012**, *51*, 5129.

12 Hammond, C.; Jenkins, R. L.; Dimitratos, N.; Lopez-Sanchez, J. A.; ab Rahim, M. H.; Forde, M. M.; Thetford, A.; Murphy, D. M.; Hagen, H.; Stangland, E. E.; Moulijn, J. M.; Taylor, S. H.; Willock, D. J.; Hutchings, G. J. *Chemistry – A European Journal* **2012**, *18*, 15735.